MgB_2 Superconductor Doped with Different Boride Compounds by High Energy Ball Milling

by

Yenny P. Cardona Quintero

A thesis submitted in partial fulfillment of the requirements for the degree of

MASTER OF SCIENCE
in
PHYSICS

UNIVERSITY OF PUERTO RICO
MAYAGÜEZ CAMPUS
2009

Approved by:

Oswald N C Uwakweh, PhD President of the Graduate Committee	Date
Yong Jihn Kim, PhD Member of the Graduate Committee	Date
Eric E. Hellstrom, PhD Member of the Graduate Committee	Date
Henri A. Radovan, PhD Member of the Graduate Committee	Date
Anand D. Sharma Ph.D Representative of Graduate Studies	Date
Hector Jiménez González, PhD Chairperson of the Department	Date

Para mi Madre que siempre ha creído en mí, que siempre ha sido mi motivación y mi apoyo. Gracias por la vida Mamita, gracias por tus plegarias, gracias por tu amor incondicional.

ABSTRACT

The study of 5 at.% MeB_2 doped MgB_2 (Me = Ta, Ti, Nb and Cr) was carried out using the High Energy Ball Milling (HEBM) technique and Hot Isostatic Press (HIP) process. Each compound was milled separately for 120 min and then they were mixed and milled at 60 min, 120 min, 180 min, 300 min and 600 min. The milled materials were HIPed at 1000°C and 30,000 psi for 24 hours. Both powder and HIPed materials were characterized in the structural properties with X-ray diffraction (XRD); crystallite size, strain, composition and lattice parameter were determined with this technique. The superconducting properties were carried out on the HIPed material with the use of the physical property measurement system (PPMS); critical temperature (T_c), critical magnetic field (Hc_2), connectivity and electron scattering were found.

In the structural properties of the powder materials, as the milling time increased, reduction in crystallite sizes and increase in strain was observed. Additionally, decomposition of MgB_2 in Mg and B elements occurred. Moreover, with the HIP process the increase in crystallite sizes, the decrease in strain and the reorganization of the structure was determined.

In the superconducting properties, the MgB_2 – 5 at.% TaB_2 material had the highest Hc_2 (25 K) value at 180 min of milling time with 7.539 T, while the T_c for the same sample was 38.48 K. These results showed that with TaB_2 at 5 at.% material, it is possible to increase Hc_2 without decreasing T_c in MgB_2.

However, the MgB_2 – 5 at.% CrB_2 material showed a decreased in Hc_2 and T_c for all milling times, which suggests that CrB_2 is not a good dopant material for MgB_2.

The residual resistivity ratio (RRR) is an indicator of the electron scattering; RRR decreased with the increase in electron scattering approaching to 1 for very high defect concentration. In this research the RRR parameter decreased with the increasing in milling time, while the Hc_2 property increased with the increase in RRR.

RESUMEN

Se llevó a cabo el estudio del dopaje de MgB_2 con 5 % at. de MeB_2 (Me = Ta, Ti, Nb and Cr) usando la técnica de molienda por alto impacto (HEBM). Cada compuesto fue molido individualmente por 120 min y posteriormente el material base y el dopante fueron mezclados y molidos por 60, 120, 180, 300 y 600 min. Los materiales molidos fueron sinterizados usando el proceso de presión isostática bajo tratamiento térmico (HIP) a 1000°C y 30000 psi por 24 horas. Las propiedades estructurales tamaño de cristal, strain, composición y parámetros de red fueron determinadas al material en polvo y al material sinterizado con la técnica de difracción de rayos-X (XRD) , mientras las propiedades superconductoras temperatura critica (T_c), campo magnético critico (Hc_2), conectividad y dispersión electrónica fueron halladas usando un sistema de medida de propiedades físicas (PPMS).

Los resultados muestran que al incrementar el tiempo de molienda se genera una reducción en el tamaño de partícula y un aumento en el strain, y ocurre además la disociación de MgB_2 en Mg y B. Además, con el proceso de HIP el tamaño de cristal aumenta, el strain disminuye y se produce la reorganización de la estructura.

El material MgB_2 dopados a 5 % at. con TaB_2 tuvo el mayor valor en Hc_2 (25 K) con 7.539 T, para 180 min de tiempo de molienda, mientras T_c para la misma muestra tuvo un valor de 38.48 K. Estos resultados demuestran que con el dopaje de MgB_2 con TaB_2 al 5 % at. es posible incrementar Hc_2 sin que se dé la disminución de T_c.

Por otra parte, el compuesto MgB_2 dopado con CrB_2 al 5 % at. mostró una disminución en Hc_2 y T_c para todos los tiempos de molienda, lo cual sugiere que CrB_2 no es un buen dopante para MgB_2.

La razón de la resistividad residual (RRR) es un indicador de la dispersión electrónica, RRR decrece con el incremento en la dispersión electrónica aproximándose a 1 para grandes defectos de concentración. En esta investigación el parámetro RRR decrece con el incremento en el tiempo de molienda, mientras Hc_2 incrementa con el aumento en RRR.

Acknowledgment

The reason of this moment and the reason of this life is God; you Father have given to me the opportunity to live this instant, thanks to be with me en every moment, thanks for the strength and the motivation.

In this stage of my life when I am concluding one of my dreams I have to include as part of this achievement to every person that helped me to be here.

Thanks to my family; to my Mom, you have always been my motivation, you taught me to dream, your love was my strength. Mamita tu siempre has sido mi motivación, tú me enseñaste a sonar, tu amor fue mi fortaleza.

Thanks to my sister, Claudia you marked my way, you set the example, you changed the perspective.

Thanks to my brother, David you taught me that the discipline is the base of the dreams; you were always my protector and my friend.

To my father that taught me the importance of believing in myself. A mi padre que me enseño la importancia de creer en mí misma.

Richard thanks for your advice, support and motivation, thanks for share your life and dreams with me. Thanks for your positivism and your unforgettable happiness.

Thanks to my friends in Colombia and Puerto Rico, the friendship is a treasure difficult to obtain. Thanks to be part of this history.

Thanks to my advisor Dr. Oswald N. C. Uwakweh, you taught me that most valuable advice is for the life.

Thanks to Dr Eric Hellstrom, for your help in the experiments in Tallahassee, your advice and unconditional disposition.

Thanks to Dr Yong Jihn Kim, for your humility in all your lessons, for share your immense knowledge.

Thanks to Dr Henri Radovan, for your corrections and your suggestion in this research.

Thanks to Dr Alfonso Devia (RIP), for the unconditional help to your students, for taught me the discipline in research.

Thanks to Ms. Clarita to Mr. Billy and Charon, you made me part of your family.

Thanks to the persons who always helped me unconditionally, who always have a smile, Aracelis, Nancy, Sory, Carlos…

Thanks to University of Puerto Rico Mayaguez, for this amazing opportunity, for letting me know wonderful researchers, and better persons. Thanks to the teaching in Physics and in Life.

Thanks to Florida State University, to National High Magnetic Field Laboratory and the Applied Superconductivity Center for allowing me to carry out the synthesis process and the characterization and thanks to the persons who helped me in that process.

Thanks to Synergistic Partnership for Research and Education on Functional and Nanostructured Materials (PREM), National Science Foundation (NSF) Award number 0351449 and Focused Research Group on Magnesium Diboride (FRG): two-gap superconductivity in magnesium diboride and its implications for applications, DMR- 0514592, for the support and for this opportunity.

Table of Contents

Abstract i
Resumen ii
Acknowledgement iii
Table of Contents v
Table List vii
Figure List ix
Symbols xiv

1. Introduction 1
2. Theoretical Background 3
2.1 Superconductivity 3
2.1.1. Classification of Superconducting Materials 5
2.1.2. Characteristic of the Superconducting State 7
2.1.2.1. Critical Temperature (T_c) 7
2.1.2.2. Critical current (J_c) 7
2.1.2.3. Critical Magnetic Field (H_c) 7
2.1.2.4. Penetration Depth (λ) 10
2.1.2.5. Coherence Length (ξ) 11
2.1.2.6. The Ginzbur – Landau Parameter (κ) 12
2.1.2.7. Order Parameter (Ψ) 13
2.1.2.8. Vortex 14
2.2. Magnesium Diboride 14
2.2.1. Resistivity Measurements for MgB_2 17
2.3. Literature Review 18
3. Experimental Procedure 24
3.1. Synthesis and Sample Preparation 24
3.1.1. Sample Preparation 24
3.2. Ball Milling Process 27
3.2.1. SPEX 8000D 28
3.2.2. Ball Milling Parameters 28
3.3. Cold Isostatic Press (CIP) 30
3.4. Hot Isostatic Press (HIP) 33
3.5. Preparation of Samples to Characterization 34
3.6. Characterization 34
3.6.1. Physical Property Measurement System (PPMS) - Resistivity 35
3.6.2. X-ray Diffraction (XRD) 41
3.6.3. Scanning Electron Microscopy (SEM) 43
4. Effect of 5 at.% TaB_2 in the Structural and Superconducting Properties of MgB_2 44
4.1. Structural Properties 44
4.2. Superconducting Properties 61
4.2.1. Critical Temperature (T_c) 61

4.2.2. Critical Magnetic Field (Hc_2) 63
4.2.3. Resistivity Analysis 66
5. Effect of 5 at.% NbB_2 in the Superconducting and Structural Properties of MgB_2 72
5.1. Structural Properties 72
5.2. Superconducting Properties: Resistivity Measurements 84
5.2.1. Critical Temperature (T_c) 84
5.2.2. Critical Magnetic Field (Hc_2) 87
5.2.3. Resistivity analysis 90
6. Effect of 5 at.% TiB_2 doped MgB_2 Premilled on Superconducting Properties 98
6.1. Structural Properties 98
6.2. Superconducting Properties 111
6.2.1. Critical Temperature (T_c) 111
6.2.2. Critical Magnetic Field (Hc_2) 113
6.2.3. Resistivity Analysis 117
7. Effect of 5 at.% CrB_2 in the Superconducting and Structural Properties of MgB_2 124
7.1. General Characteristics 124
7.2. Structural Properties 125
7.3. Superconducting Properties: Resistivity Measurements 140
7.3.1. Critical Temperature (T_c) 140
7.3.2. Critical Magnetic Field (Hc_2) 143
7.3.3. Resistivity Analysis 146
8. Comparison in Structural and Superconducting Properties for TaB_2, TiB_2, NbB_2 and CrB_2 doped MgB_2 155
8.1. Structural Properties 155
8.2. Superconducting Properties 159
9. Conclusions 167
9.1. Suggestions for Future Works 169
References 170

Table List

Table	Description	Page
Chapter 2		
Table 2.I.	Properties of MgB_2 in bulk, crystallites, thin films, single crystal and powders.	15
Chapter 3		
Table 3.I	Samples synthesis in this investigation	29
Chapter 4		
Table 4.I	Processing parameters, designations, and properties [26].	48
Table 4.II.	Composition, lattice parameters, crystallite size and strain of ball milled samples at different milling times	59
Table 4.III.	Composition, lattice parameters, crystallite size and strain of ball milled samples at different milling times.	60
Table 4.IV.	T_c and Hc_2 values for TaB_2 doped MgB_2 material and MgB_2 undoped sample.	66
Table 4.V.	Resistivity measurements for TaB_2 samples.	67
Chapter 5		
Table 5.I.	Composition, lattice parameters, crystallite size and strain of NbB_2 5 at.% material in powder ball milled at different milling times.	82
Table 5.II.	Composition, lattice parameters, crystallite size and strain of NbB_2 5 at.% material in pellet ball milled at different milling times	83
Table 5.III.	T_c and Hc_2 values for NbB_2 doped MgB_2 material and MgB_2 undoped sample.	84
Table 5.IV.	Resistivity measurements for NbB_2 5 at.% ball milled at different times samples.	90
Chapter 6		
Table 6.I.	Composition, lattice parameters, crystallite size and strain of MgB_2 - TiB_2 5 at.% doped material in powder ball milled at different times.	109
Table 6.II.	Composition, lattice parameters, crystallite size and strain of MgB_2 - TiB_2 5 at.% doped materials post HIP ball milled at different times.	110
Table 6.III.	T_c and Hc_2 values for 5 at.% TiB_2 doped MgB_2 material and MgB_2 undoped sample	117
Table 6.IV.	Resistivity measurements for MgB_2 - 5 at.% TiB_2 doped materials	119
Chapter 7		
Table 7.I.	Composition, lattice parameters, crystallite size and strain of CrB_2 5 at.% material in powder ball milled at different milling times.	138
Table 7.II.	Composition, lattice parameters, crystallite size and strain of CrB_2 5 at.% material in pellet ball milled at different milling times.	139
Table 7.III.	T_c and Hc_2 values for CrB_2 doped MgB_2 material and MgB_2 undoped sample.	140
Table 7.IV.	Resistivity measurements for CrB_2 5 at.% ball milled at different times samples.	148
Chapter 8		
Table 8.I	Crystallite Size for MeB_2 phase after the HIP process.	156
Table 8.II.	Crystallite Size for MgB_2 phase after the HIP process.	156

Table 8.III. Comparison of T_c for the different MgB_2 – 5 at.% doped MeB_2 materials as a function of ball milling times. Me: Ta, Ti, Nb, and Cr. 162

Table 8.IV. Hc_2 of doped MeB_2 (Me = Ta, Ti, Nb and Cr) – MgB_2 materials as a function of ball milling time after HIP process 164

Figure List

Figure	Description	Page
Chapter 2		
Figure 2.1	Superconducting State for Mercury	3
Figure 2.2	Meissner Effect	4
Figure 2.3	Behavior of the magnetization for the type I and type II superconductors in function of the applied magnetic field.	5
Figure 2.4	Hc (T) dependence for a type-I superconductor [1]	8
Figure 2.5	H_{c1} (T) and H_{c2} (T) dependences for a type-II superconductor [1]	8
Figure 2.6	Normal-state vortices in the mixed state of a type-II superconductor	9
Figure 2.7	Penetration of the magnetic field into a superconducting sample. [1].	10
Figure 2.8	Temperature dependence of penetration depth, $\boldsymbol{\lambda(T)}$ [1]	11
Figure 2.9	The hexagonal crystal structure of MgB_2 [9].	16
Figure 2.10	The structure of mercury-based high-T_c superconducting (HTSC) cuprates [9].	16
Figure 2.11	The Fermi surface of MgB_2 [14].	17
Figure 2.12	Critical temperature versus doping content for diversal elements [9].	19
Chapter 3		
Figure 3.1	Jar and balls used in the ball milling process	25
Figure 3.2	Rubber tube used to save the powder during the CIP and impermeable balloon which protect the material from the water and air	31
Figure 3.3	Mechanism to protect the sample and connect it with the vacuum system	32
Figure 3.4	Cycle used in HIP	33
Figure 3.5	Physical Property Measurement System (PPMS)	35
Figure 3.6	Sample puck used to resistivity measurement	36
Figure 3.7	Dimensions and connections for resistivity sample	37
Figure 3.8	Trend resistivity versus temperature at 0 T	38
Figure 3.9	Trend of resistivity versus temperature at constant field, 1 T for this case	39
Figure 3.10	Example of T_c Versus Applied Magnetic Field Graph	40
Figure 3.11	Example of Hc_2 versus Temperature graph	41
Chapter 4		
Figure 4.1	X–ray diffraction of the powder MgB_2 - 5 at.% TaB_2 premilled.	45
Figure 4.2	X–ray diffraction of the powder MgB_2 - 5 at.% TaB_2 material [29].	46
Figure 4.3	X–ray diffraction of the HIP MgB_2 - 5 at.% TaB_2 as a function of ball milling time.	46
Figure 4.4	XRD measurements for the SPEX-8000D for the 5 at.% TaB2 doped MgB2: 60, 120, 300, 600 and 2400 minutes.	47
Figure 4.5	X-ray diffraction patterns of heat treated samples (Cu-Kα) [26]	48
Figure 4.6	EDS of TaB_2 5 at.% 2 hours ball milling sample.	49
Figure 4.7	SEM of TaB_2 5 at.% 2 hours ball milling sample.	49
Figure 4.8	Composition of TaB_2, MgB_2, MgO and B phases for powder material in	50

function of milling time.
Figure 4.9 Composition of TaB_2, MgB_2, MgO and B phases, for pellet post HIP material in function of milling time. 51
Figure 4.10 Crystallite size of TaB_2 phase for powder and pellet material in function of milling time. 53
Figure 4.11 Crystallite size of MgB_2 phase for powder and pellet material in function of milling time. 54
Figure 4.12 Strain of TaB_2 phase for powder and pellet material in function of milling time. 55
Figure 4.13 Strain of MgB_2 phase for powder and pellet material in function of milling time. 56
Figure 4.14 Lattice Parameter for MgB_2 – 5 at.% TaB_2 pelletized material pre-milled and milled at different milling times. 57
Figure 4.15 Lattice Parameter for MgB_2 – 5 at.% TaB_2 pelletized material ball milled at different times [29]. 58
Figure 4.16 T_c Vs Applied Magnetic Field for TaB_2 5 at.% samples at different milling times and MgB_2 undoped. 61
Figure 4.17 T_c Vs milling time for TaB_2 5 at.% 62
Figure 4.18 Hc_2 Vs Temperature for TaB_2 5 at.% samples at different milling times. 64
Figure 4.19 Hc_2 at 25K Vs milling time for TaB_2 5 at.%. 65
Figure 4.20 A_F Vs milling time for TaB_2 5 at.% 68
Figure 4.21 Hc_2 Vs A_F for TaB_2 5 at.%. 68
Figure 4.22 RRR Vs milling time for TaB_2 5 at.% 69
Figure 4.23 Hc_2 at 25 K Vs RRR for TaB_2 5 at.% samples at different milling times 70
Chapter 5
Figure 5.1 X ray diffraction spectra of 5 at.% NbB_2 doped MgB_2 as a function of increasing ball milling times. 73
Figure 5.2 X ray diffraction spectra of 5 at.% NbB_2 doped MgB_2 as a function of increasing ball milling times. Zoom of 2θ between 35° and 70°. 74
Figure 5.3 MgB_2 – 5 at.% NbB_2 doped sample corresponding to 2 hours of ball milling. 75
Figure 5.4 Scanning Electron Micrograph (SEM) of two hours ball milled 5 at.% NbB_2 doped MgB_2 material after HIPing 75
Figure 5.5 Composition of NbB_2, MgB_2, MgO and B phases for powder material as a function of ball milling time 77
Figure 5.6 Composition of NbB_2, MgB_2, MgO and B phases, for pellet post HIP material in function of milling time. 77
Figure 5.7 Crystallite size variation of NbB_2 phase for the powder and pellet form as a function of milling time. 78
Figure 5.8 Crystallite size variation of MgB_2 phase for the powder and pellet form as 79

a function of milling time.
Figure 5.9 Comparison of the average strain of NbB_2 phase in the powder and pellet forms. 80
Figure 5.10 Comparison of the average strain of MgB_2 phase in the powder and pellet forms. 81
Figure 5.11 T_c Vs Applied Magnetic Field for the MgB_2 undoped and MgB_2 - 5 at.% NbB_2 doped materials. 85
Figure 5.12 T_c Vs milling time for MgB_2 - NbB_2 5 at.% material. 86
Figure 5.13 Hc_2 Vs Temperature for MgB_2 - NbB_2 5 at.% samples at different milling times. 88
Figure 5.14 Hc_2 at 25K Vs milling time for MgB_2 - NbB_2 5 at.%. 89
Figure 5.15 Resistivity Vs Temperature for MgB_2 - NbB_2 5 at.% ball milled at different times 91
Figure 5.16 A_F Vs milling time for MgB_2 - NbB_2 5 at.% material. 92
Figure 5.17 Hc_2 (25 K) Vs A_F for MgB_2 - NbB_2 5 at.% doped material for different milling times 93
Figure 5.18 ρ_A Vs milling time for MgB_2 - NbB_2 5 at.% doped material. 94
Figure 5.19 Hc_2 (25) Vs ρ_A for MgB_2 - NbB_2 5 at.% doped material. 95
Figure 5.20 RRR Vs milling time for MgB_2 - NbB_2 5 at.% doped material. 96
Figure 5.21 Hc_2 (25 K) Vs RRR for MgB_2 - NbB_2 5 at.% doped material. 97
Chapter 6
Figure 6.1 XRD analysis for MgB_2 - 5 at.% TiB_2 doped materials at different milling times 100
Figure 6.2 XRD analysis for MgB_2 - 5 a.% TiB_2 doped maerials at different milling times. Zoom of 2θ between 35 and 70 grades. 101
Figure 6.3 EDS of MgB_2 -TiB_2 5a.% doped materials 2 hours ball milling sample. 102
Figure 6.4 SEM of MgB_2 - TiB_2 5 at.% doped materials 2 hours ball milling sample 102
Figure 6.5 Composition of TiB_2, MgB_2, MgO and B phases for powder material in function of milling time. 104
Figure 6.6 Composition of TiB_2, MgB_2, MgO and B phases for post HIP material in function of milling time. 104
Figure 6.7 Crystallite size of TiB_2 phase for powder and pellet material Vs milling time. 105
Figure 6.8 Crystallite size of MgB_2 phase for powder and pellet samples Vs milling time 106
Figure 6.9 Strain of TiB_2 phase for powder and pellet material in function of milling time. 107
Figure 6.10 Strain of MgB_2 phase for powder and pellet material in function of milling time. 108
Figure 6.11 T_c Vs Applied Magnetic Field for MgB_2 - TiB_2 5 at.% doped materials at 112

different milling times and MgB_2 undoped.
Figure 6.12 T_c Vs milling time for MgB_2 - TiB_2 5 at.% doped materials 113
Figure 6.13 Hc_2 Vs Temperature for MgB_2 - TiB_2 5 at.% doped materials at different milling times. 115
Figure 6.14 Hc_2 at 25 K Vs milling time for MgB_2 - 5 at.% TiB_2 doped materials 116
Figure 6.15 Resistivity graph for MgB_2 - TiB_2 5 at.% doped materials milled at different times versus Temperature. 118
Figure 6.16 A_F Vs milling time for MgB_2 - 5 at.% TiB_2 doped materials. 120
Figure 6.17 Hc_2 Vs A_F for MgB_2 - TiB_2 5 at.% doped materials 121
Figure 6.18 RRR Vs milling time for MgB_2 - TiB_2 5 at.% doped materials 122
Figure 6.19 Hc_2 at 25 K Vs RRR for MgB_2 - TiB_2 5 at.% doped materials at different milling times 123

Chapter 7

Figure 7.1 X ray diffraction spectra of 5 at.% CrB_2 doped MgB_2 as a function of increasing ball milling times. 126
Figure 7.2 X-ray diffraction patterns of $Mg_{1\_x}Cr_xB_2$ samples with different Cr content. (a) x = 0; (b) x = 0.01; (c) x = 0.02; (d) x = 0.03; (e) x = 0.05. The impurities were marked by: ‘‘•’’ MgO; ‘‘+’’ CrB2; ‘‘*’’ CrB. Zhang *et al* [52] 127
Figure 7.3 MgB_2 – 5 at.% CrB_2 doped sample corresponding to 2 hours of ball milling. 128
Figure 7.4 Scanning Electron Micrograph (SEM) of two hours ball milled 5 at.% CrB_2 doped MgB_2 material after HIPing. 128
Figure 7.5 Composition of CrB_2, MgB_2, MgO and B phases for powder material as a function of ball milling time. 129
Figure 7.6 Composition of CrB_2, MgB_2, MgO and B phases, for pellet post HIP material in function of milling time. 130
Figure 7.7 Crystallite size variation of CrB_2 phase for the powder and pellet form as a function of milling time. 132
Figure 7.8 The crystallite size change of MgB_2 phase as with milling time in the powder and pellet forms. 134
Figure 7.9 Comparison of the average strain of CrB_2 phase in the powder and pellet forms. 135
Figure 7.10 Comparison of the average strain of MgB_2 phase in the powder and pellet forms. 135
Figure 7.11 Lattice parameter variation in MgB_2 phase as a function of milling time. 136
Figure 7.12 Variation of the lattice parameters of a-axis and c-axis with Cr content in $Mg_{1\_x}Cr_xB_2$ [52]. 137
Figure 7.13 T_c Vs Applied Magnetic Field for the MgB_2 undoped and MgB_2 - 5 at.% 141

CrB_2 doped materials.
Figure 7.14 T_c Vs milling time for MgB_2 - 5 at.% CrB_2 material. 142
Figure 7.15 Dependence of superconducting transition temperature T_c on Cr content for $Mg_{1\_x}Cr_xB_2$ [52]. 143
Figure 7.16 Hc_2 Vs Temperature for MgB_2 - CrB_2 5 at.% samples at different milling times. 144
Figure 7.17 Hc_2 at 25K Vs milling time for MgB_2 - 5 at.% CrB_2. 145
Figure 7.18 Resistivity Vs Temperature for MgB_2 - CrB_2 5 at.% ball milled at different times 146
Figure 7.19 Temperature dependence of the resistivity for Cr doped MgB_2 with different Cr content [52] 147
Figure 7.20 A_F Vs milling time for MgB_2 – 5 at.% CrB_2 material 149
Figure 7.21 Hc_2 (25 K) Vs A_F for MgB_2 - 5 at.% CrB_2 doped material for different milling times 150
Figure 7.22 ρ_A Vs milling time for MgB_2 - 5 at.% CrB_2 doped material. 151
Figure 7.23 Hc_2 Vs ρ_A for MgB_2 - 5 at.% CrB_2 doped material. 152
Figure 7.24 RRR Vs milling time for MgB_2 - 5 at.% CrB_2 doped material. 153
Figure 7.25 Hc_2 (25 K) Vs RRR for MgB_2 - CrB_2 5 at.% doped material. 153
Chapter 8
Figure 8.1 Crystallite size evolution of the MeB_2 phase for the dopant material with ball milling. 157
Figure 8.2 Crystallite size evolution of the MgB_2 phase for the dopant material with ball milling 158
Figure 8.3 Strain for MeB_2 phase for the doped materials in function of milling time 159
Figure 8.4 T_c of MeB_2 5 at.% doped samples in function of the applied magnetic field. 160
Figure 8.5 Comparison of the T_c values of MgB_2 – 5 at.% MeB_2 doped materials as a function of milling times. 161
Figure 8.6 Hc_2 of MeB_2 5 at.% doped samples in function of the temperature. 163
Figure 8.7 Hc_2 (25 K) of MeB_2 5 at.% doped samples at different milling times. 163
Figure 8.8 Resistivity of MeB_2 5 at.% doped MgB_2 samples in function of the temperature. 164
Figure 8.9 RRR Vs Milling time of MeB_2 5 at.% doped MgB_2 samples. 165

Symbols

Å	Angstroms [$1 \times 10^{-10} m$]
σ	Sigma band, or conductivity [$(\mu\Omega.cm)^{-1}$]
σ_0	Low temperature conductivity [$(\mu\Omega.cm)^{-1}$]
π	3.14159 or pi band
ξ	Superconducting coherence length [Å]
ξ_0	Superconducting coherence length in clean limit [Å]
ξ_{GL}	Superconducting coherence length in the Ginzburg – Landau theory [Å]
ξ_{GL}^{c}	Superconducting coherence length in clean superconductors [Å]
ξ_{GL}^{d}	Superconducting coherence length in dirty superconductors [Å]
λ	Penetration depth [nm] or wavelength [m]
θ	Bragg angle
Φ	Magnetic flux [Wb]
ρ	Resistivity [$\mu\Omega$.cm]
ρ_A	Adjusted resistivity [$\mu\Omega$.cm]
$\Delta\rho$	ρ(300 K) – ρ(40 K) [$\mu\Omega$.cm]
$\Delta\rho_{ideal}$	Ideal $\Delta\rho$ [$\mu\Omega$.cm]
ρ_{def}	Defect component of resistivity [$\mu\Omega$.cm]
ρ_{Ph}	Phonon component of resistivity [$\mu\Omega$.cm]
Ψ	Wavefunction
Ψ^*	Complex conjugate of Ψ
//c	Parallel to c-axis
//ab	Parallel to ab-plane
A	Area, cross section [m^2]
A_F	Active area fraction
a	a-axis lattice parameter
B	Magnetic field [T] or constant
c	c-axis lattice parameter
CIP	Cold isostatic press
d	Sample dimension [mm]

e	Exponent, charge of an electron [$1.602 \text{ x } 10^{-19}\ C$]
F_P	Pinning force [GN/m^3]
h	Planck's constant [$6.626 \text{ x } 10^{-34}\ Js$]
H	Magnetic field [T]
H*	Irreversibility field [T]
Hc_1	Critical magnetic field [mT]
Hc_2	Upper critical field [T]
$Hc_{2\parallel}$	Upper critical field parallel to the plane [T]
$Hc_{2\perp}$	Upper critical field perpendicular to the plane [T]
HIP	Hot isostatic press
I	Current [k.A/cm^2]
J	Current density [k.A/cm^2]
J_c	Critical current density [k.A/cm^2]
k	Ginzbur – Landau parameter or kilo
K	Kelvin units
l	Length [m] or mean free path [nm]
M	Atomic mass [amu] or Magnetization [A.m^2/kg]
m	magnetic moment [A.m^2]
n	Number of free conduction electrons
n_n	Number of non-superconducting electrons
n_s	Number of superconducting electrons
P	Pressure [Pa]
r	Radius [m]
R	Electrical resistance [Ω]
RRR	Residual resistivity ratio
T	Temperature [K] or Tesla units
T_c	Critical temperature [K]
T_{HIP}	Temperature of hot isostatic press [K]
Tm	Melting temperature [K]
t	Time [s]
V	Volume [m^3] or voltage [V]

w	Sample dimension [mm]
CrB_2	Chromium diboride
NbB_2	Niobium diboride
MgB_2	Magnesium diboride
MeB_2	Metal diboride
TaB_2	Tantalum diboride
TiB_2	Titanium diboride
PPMS	Physical property measurement system
SEM	Scanning electron microscope
SQUID	Supercondcuting Quantum Interferometer Device
TEM	Transmission electron microscope
XRD	X-ray diffraction
VSM	Vibrating sample magnetometer

1. INTRODUCTION

Superconductivity is a state in certain materials characterized by the absence of electrical resistance to the flow of current usually at low temperatures. This state has been widely studied in many elements and compounds when in the search for materials that would permit necessary applications in technology and science fields.

The applications of superconductor materials include superconducting magnets, which are used in magnetic resonance imaging, nuclear magnetic resonance equipments and mass spectrometers. Superconductors are also used to make digital circuits, microwave filters, and Josephson junctions which form the base of the superconducting quantum interference devices (SQUIDs). One of the most known applications of the superconductors is the magnetic levitation train which uses the Meissner effect, while future applications include magnet levitation devices, power storage devices, and electric motors.

The superconducting properties such as critical temperature (T_c), upper critical magnetic field (Hc_2), and critical current density (J_c) form the base of decision to establish the applicability of a superconductor, however, these superconducting properties are the result of conditions predicated by structural and compositional characteristics, and are reflected in the enhancement or deterioration of one or several of the superconducting properties.

The MgB_2 material was discovered as superconducting in 2001 with a T_c of 39 K which was considered a high value for a binary compound. Since then, this material has been the subject of numerous studies by many scientists with great expectation not only in the understanding of fundamental science of superconductivity, but also for prospective technological applications. Besides the medium T_c, the MgB_2 has shown values in Hc_2 which can make this material potentially applicable in diverse areas, and also, it is a material that is considered to be of low economic inversion thereby making it more viable in terms of future applications.

The MgB_2 doping has occupied many of the current researches focused on enhancement of some of the superconducting properties to extend the range of applications. It is for this purpose that different synthesis methods and diverse elements and compounds have been used as dopant materials including metal diborides. The introduction of a dopant in the B or Mg site in MgB_2

lattice could introduce effective pinning centers to enhance the flux pinning increasing J_c , Hc_2 and H*.

The diboride material has interesting properties such as the hexagonal structure C32-type, the same as the MgB_2 with similar c/a ratio which could represent an easier replacement of Me for Mg in the MgB_2 lattice, thus offering an easier doping process that will change not only the structural properties in the MgB_2 material but also the superconducting properties.

The use of diborides MeB_2 as dopant materials has been studied with interesting results, however there are many diboride materials which are yet to be studied with potential to give remarkable results.

Among the different techniques that have been reported for the synthesis of MgB_2, the high energy ball milling (HEBM) process has unique advantage that the reactions could be initiated in the solid state to effectuate the doping and synthesis processes. This technique uses balls to mill the material through high energy impacts resulting in the decreasing in particle and grain sizes and the creation of both structural defects (vacancies, grain boundaries, etc) and disorders such as internal microscopic strains.

In this thesis four different diborides TaB_2, TiB_2, NbB_2 and CrB_2 at 5 at.% were used as dopant for the MgB_2 material using HEBM technique in the synthesis process. The characterization was carried out using scanning electron microscope (SEM), X-ray diffractometer (XRD), and physical property measurement system (PPMS) to determine phase composition, structural properties such as crystallite size, strain, lattice parameter and the superconducting properties such as Hc_2, T_c, electron scattering and connectivity.

The objective of this research was to determine the material properties enhancement due to the effect of the dopant material MeB_2 and the HEBM technique on the structural and superconducting properties of MgB_2 in order to determine the viability of these materials in future applications.

2. THEORETICAL BACKGROUND

2.1. Superconductivity

Superconductivity was discovered in 1911 by the Dutch physicist H. Kamerlingh Onnes and Gilles Holst in Leiden, who found that the resistivity of metal mercury suddenly dropped to zero when the material was cooled down below its critical temperature T_c (**Figure 2.1**). A year later, Onnes and Holst discovered that a sufficiently strong magnetic field restored the resistivity in the sample [1].

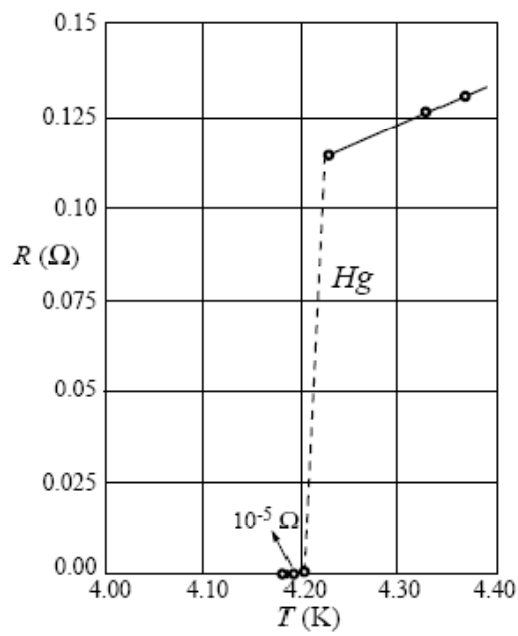

Figure 2.1. Superconducting State for Mercury [1].

In 1933, W. Meissner and R. Ochsenfeld discovered the perfect diamagnetism; they found that the magnetic flux was expelled from the material when it was cooled down below its critical temperature in weak external magnetic fields. Thus, they found that no applied magnetic field was allowed inside a metal when it became superconducting. This phenomenon is known as the Meissner effect [1], and is depicted in **Figure 2.2**.

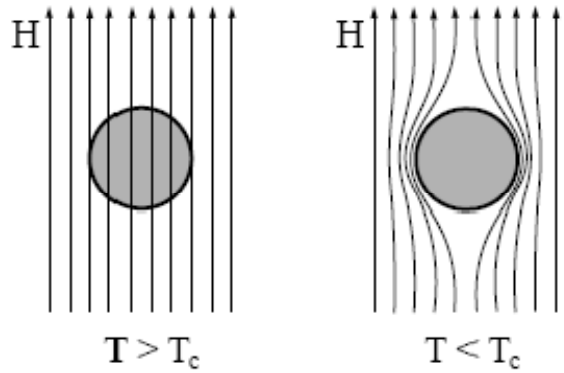

Figure 2.2. Meissner Effect [1].

The materials that expels the magnetic field $H < H_c$ completely outside from the material due to the Meissner effect are called type I superconductor, most of the type I superconductor are pure elements, some examples of type I superconductors are: Ta, Al, and Hg [2]. Shubnikov, in 1937 described the properties of type II superconductivity. In a type II superconductor the magnetic field is not totally expelled from the interior of a superconductor material, except for very low fields. In the type II superconductor there are three states; the superconducting state, the mixed state, and the normal state. In the superconducting state there is a complete expulsion of the field from the interior of the material and, in this way the type II superconductor behaves as a type I superconductor. In the mixed state there is a partial penetration of the flux into the sample creating some regions that are superconducting and some that are in the normal state with the field in which there is a penetration of flux in the material known as the lower critical field (Hc_1). Complete penetration of the flux takes place at the upper critical field Hc_2. After the applied magnetic field reaches the Hc_2 point, the material is in the normal state and behaves as a normal conductor [2]. The behaviors of the type I and type II superconductors are shown in **Figure 2.3.**

After Shubnikov described the behavior of the type II superconductor in 1956, Leon Cooper [3] showed that two conducting electrons were capable of forming a stable paired when the temperature of the material is lower than its critical temperature and in the presence of a very weak electron-phonon interaction. These electron pairing were described or called the Cooper pair. On this basis, Cooper showed that a Cooper pair can move in a crystal without resistance.

Consequently to this, Bardeen, Cooper, and Schrieffer [4] reported in 1957 the first successful microscopic theory of superconductivity (BCS theory). The central concept of the BCS theory is a weak electron-phonon interaction which leads to the appearance of an attractive potential between two electrons that is the basis to form the Cooper pairs. [1].

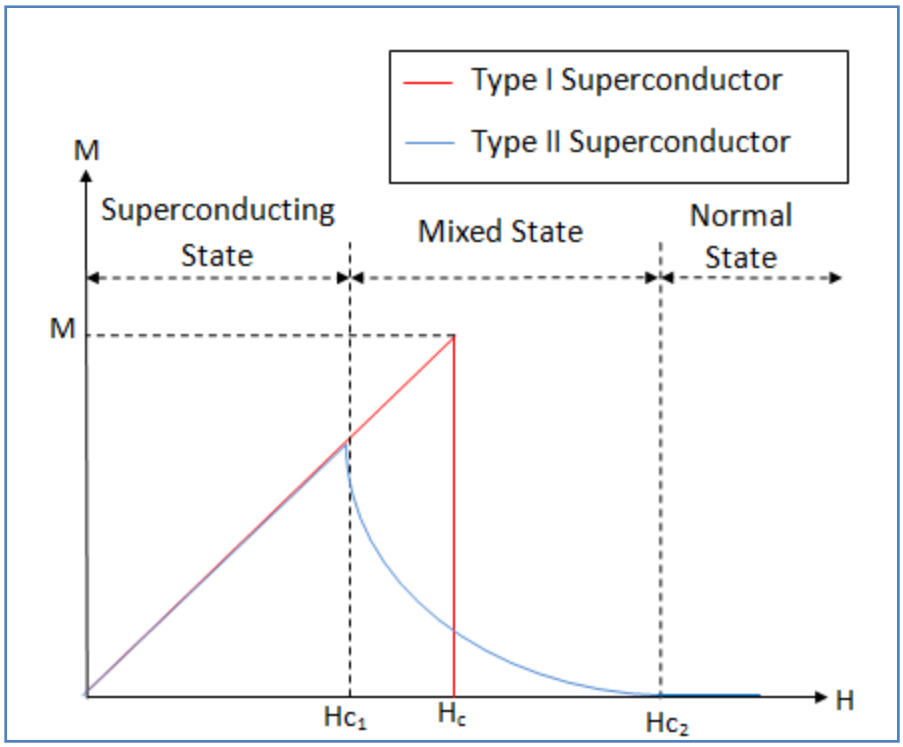

Figure 2.3. Behavior of the magnetization for the type I and type II superconductors in function of the applied magnetic field.

2.1.1 Classification of Superconducting Materials.

Superconducting materials can be classified in three groups according to the mechanism of superconductivity operating in the compound. The materials which are included in these three groups are:

a. Metals and some of other alloys
b. Low dimensional, non magnetic compounds
c. Low dimensional, magnetic compounds.

The first group includes all classical conventional superconductors. The critical temperature of these superconductors does not exceed 10 K and most of them are type I superconductor [1, 5]. The critical temperature of some elements is raised dramatically by preparing them in thin films, however, the number of superconductors in this group is very small, and they are not suitable for applications.

The superconducting state of the second group of low dimensional, non magnetic compounds is characterized by the presence of two interacting superconducting subsystems. The critical temperature of these superconductors is limited by ~ 40 K. All of them are type II superconductors with an upper critical magnetic field usually exceeding 10 T. Many superconductors from this group are suitable for different applications. Some examples of this group are the superconductors with the structure A_3B, (A= Nb, V, Ta, Zr and B = Sn, Ge, Al, Ga, Si) and are usually called the A-15 superconductors. Other superconductors that pertain to the second group are $sBa_{1-x}K_xBiO_3$, MgB_2, nitrides and carbides [1].

The third group incorporates unconventional superconductors which are low dimensional and magnetic and have a low density of charge carriers. In all superconductors belonging to this group, the coherence length (ξ_{GL}) is very short, while the penetration depth (λ) is very large; which indicates that all superconductors of this group are type-II. The coherence length (ξ_{GL}) refers to the characteristic scale over which variations of the order parameter (Ψ) occurs, while the penetration depth (λ) is the layer of thickness inside a superconductor in which is established a persistent supercurrent that cancels the applied field, these terms will be expanded further in section 2.1.2. The low dimensional, magnetic compounds have a very large upper critical magnetic field, whence many superconductors from this group are used for practical applications. As examples of compounds that pertain to this group are the Chevrel; that are generally designed as $M_xMo_6S_8$ (where M refers to a large number of metals and rare earths) exhibited the highest upper critical magnetic field (Hc_2) values. Another group referred to as the copper oxides based superconductors are known as the high temperature superconductors. As example is the $YBa_2Cu_3O_{6+x}$, otherwise designed as YBCO (where the Y refers to Yttrium, B to Barium, C to Copper and O to Oxygen).The YBCO was the first superconductor found to have T_c higher than 77 K [1].

2.1.2. Characteristics of the Superconducting State

The superconducting state can be described in terms of its basic characteristic features. As part of the characteristics of the superconducting state are: critical temperature (T_c), critical magnetic field (Hc_2), critical current density (J_c), Cooper pair wavefunction, order parameter, penetration depth, and coherence length [1].

2.1.2.1. Critical Temperature (T_c)

The maximum temperature below which a superconductor exhibits superconductivity at zero magnetic field and current is defined as the **critical temperature (T_c)** [2]**.** Each material has a characteristic T_c which is determined experimentally as it is also difficult to predict the T_c for a material. In the framework of the BCS theory, there is a formula to estimate the T_c value, however it is a general formula which does not take into account any specific features of a given material. Moreover, T_c is a macroscopic quantity while, the Cooper – pair wavefunction is a quantum one [1].

2.1.2.2. Critical Current Density (J_c)

The critical current density J_c is the maximum current that a superconductor can support without loss of superconductivity. For a current higher than J_c, the Cooper pairs are broken, and thus, superconducting state is destroyed. In other words, J_c is the minimum pair-breaking current. The temperature dependence of the critical current density is similar to the temperature dependence of H_c [1]. J_c can also be expressed as a function of the critical magnetic field ($H_c(0)$) as described by **Equation 2.1.**

$$\boldsymbol{J_c = \frac{c\, H_c(0)}{4\pi\sqrt{3}\,\lambda(0)}} \tag{2.1}$$

With $c = 3 \text{ x } 10^8 \text{m/s}$, $\pi = 3.1416$, and λ (0) as the penetration depth.

2.1.2.3. Critical Magnetic Field (H_c)

The critical magnetic field (H_c) is defined as the maximum magnetic field below which a superconductor exhibits superconductivity at zero current and temperature. The superconducting

state can be destroyed by a sufficiently strong magnetic field. The variation of the critical field H_c with temperature for a type I superconductor is approximately parabolic:

$$H_c(T) \cong H_c(0)[1 - (T/T_c)^2] \tag{2.2}$$

Where $H_c(0)$ is the value of the critical field at absolute zero [1]. This is shown in **Figure 2.4.**

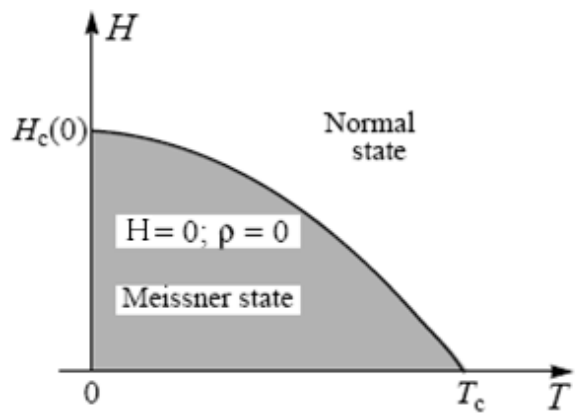

Figure 2.4. $H_c(T)$ dependence for a type-I superconductor [1].

For a type-II superconductor, there are two critical fields, the lower critical field H_{c1} and the upper critical field H_{c2}, as shown in **Figure 2.5**.

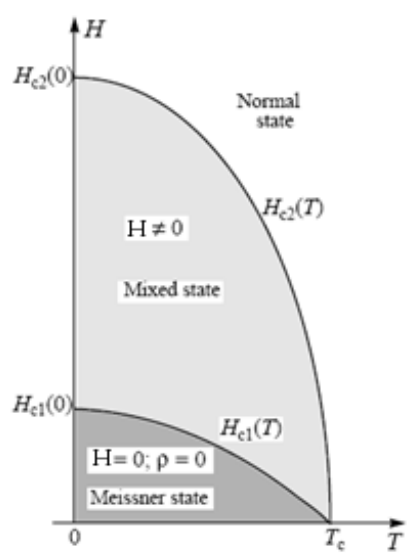

Figure 2.5. $H_{c1}(T)$ and $H_{c2}(T)$ dependences for a type-II superconductor [1]

In applied fields less than H_{c1}, the superconductor completely expels the field outside from the material and then behaves as a type-I superconductor does below H_c. At fields just above H_{c1}, flux begins to penetrate the superconductor in microscopic filaments named vortex. Each vortex consists of a normal core in which the magnetic field is large, surrounded by a superconducting region. **Figure 2.6** shows the vortices forming a regular triangular lattice. Arrows show the supercurrent circulating around the vortices at a distance from the centers of vortices of approximately the penetration depth (λ) (See section 2.1.2.4). The radius of the vortices is about the coherence length ξ_{GL}.

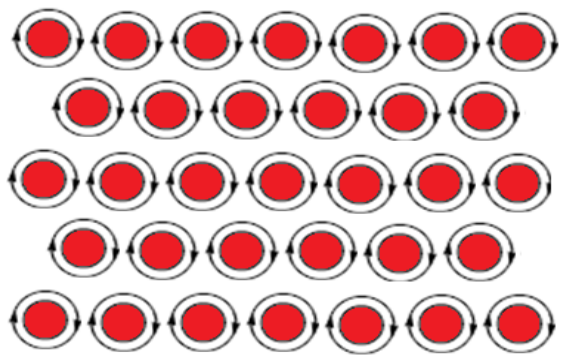

Figure 2.6. Normal-state vortices in the mixed state of a type-II superconductor

In type II superconductors, the values of the critical magnetic field Hc_1 and Hc_2 as well as λ and ξ_{GL}, are anisotropic. Being anisotropic, these properties are dependent on crystallographic orientation of the material. The upper critical field applied perpendicular to the layers $Hc_{2\perp}$ is determined by vortices whose screening currents flow parallel to the planes, while $Hc_{2\parallel}$ is determined by vortices whose screening currents flow perpendiular to the planes. A chracteristic paremeter known as the anisotropy ratio for a layered type II superconductor is defined thus:

$$\frac{Hc_{2\parallel}}{Hc_{2\perp}} = \frac{\xi_{GL,ab}}{\xi_{GL,c}} \tag{2.3}$$

2.1.2.4. Penetration Depth (λ)

The way in which a superconductor expels from its interior an applied magnetic field with the small magnitude is by establishing a persistent supercurrent on its surface which exactly cancels the applied field inside the superconductor. This surface current flows in a very thin layer of thickness, which is called the penetration depth λ. The existence of a penetration depth was predicted by the London brothers and it was later confirmed by experiments [1].

A magnetic field is exponentially screened from the interior of a sample with penetration depth λ, as shown in **Figure 2.7.**

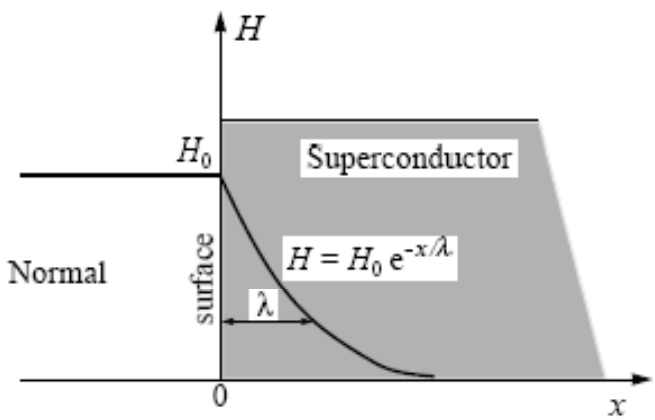

Figure 2.7. Penetration of the magnetic field into a superconducting sample. [1].

The penetration depth is associated with the number of superconducting electrons (n_s) which are temperature dependent; subsequently λ depends also of the temperature [1]. In conventional superconductors the empirical formula to determine the penetration is given by:

$$\lambda(T) = \frac{\lambda(0)}{[1-(T/T_c)^4]^{1/2}} \tag{2.4}$$

This dependence is shown in **Figure 2.8** and exhibits an asymptotic behavior.

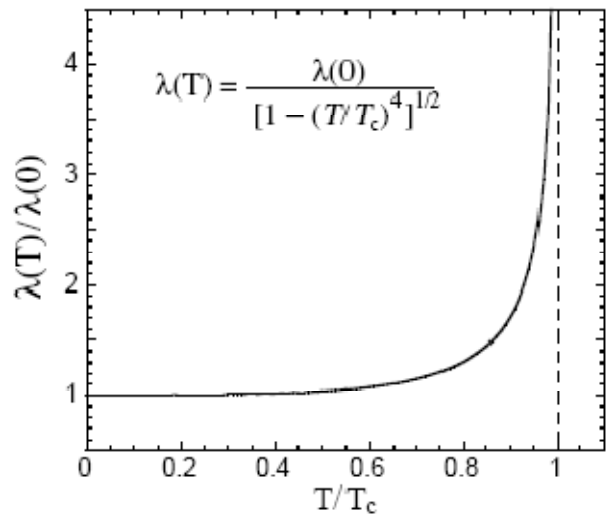

Figure 2.8. Temperature dependence of penetration depth, $\boldsymbol{\lambda(T)}$ [1]

2.1.2.5. Coherence Length (ξ)

The term coherence length has been used to describe two concepts. The coherence length (ξ) defined in the BCS theory which refers to the size of the Cooper pair and that is temperature independent, while in the framework of the Ginzburg – Landau theory the coherence length ξ_{GL} is the characteristic scale over which variations of the order parameter Ψ occurs (referring wave function to be explained in section 2.1.2.7), ξ_{GL} varies with temperature.

In conventional superconductors at zero temperature $\xi_{GL}(0) = \xi$, at $0 < T < T_c$. The value of the coherence length in "clean" conventional superconductors is always larger than the average size of Cooper pairs, $\xi < \xi_{GL}(T)$ [1]. ξ_0 is the coherent length determined by the energy gap at zero temperature, while the temperature dependence of coherence length in "clean" superconductors ($\ell \gg \xi_0$, where ℓ refers to the mean free path; the average distance covered by a particle between subsequent impacts) at temperatures close to T_c is given by:

$$\xi_{GL}^{c}(T) = 0.74\xi_0\left(1 - \frac{T}{T_c}\right)^{-1/2} \tag{2.5}$$

For "dirty" superconductors ($\ell \ll \xi_0$), the Ginzburg-Landau temperature dependence of coherence length at temperatures close to T_c is described by **Equation 2.6.**

$$\xi_{GL}^{d}(T) = 0.85(\xi_0 \ell)^{1/2}\left(1 - \frac{T}{T_c}\right)^{-1/2} \tag{2.6}$$

In conventional superconductors, the intrinsic coherence length can be extremely large reaching ~ 1000 Å [1].

A very useful relation used to obtain the coherence ξ_{GL} length in type-II superconductor is:

$$\Phi = 2\pi\xi_{GL}^{2}H_{c2} \tag{2.7}$$

where the magnetic flux quantized is given by:

$$\Phi = \frac{h}{2e} = 2.0679 \times 10^{-15} \tag{2.8}$$

The quantum nature of the superconducting state manifests itself in *quantization of magnetic flux.* Since the superconducting state is a quantum state occurring in a macroscopic scale, some superconducting properties are quantized too [1]. This can depend on the material microstructure. If a magnetic field is applied parallel to the pores of a material at $T_1 > T_c$, then, with cooling to $T_2 < T_c$, some magnetic flux will remain frozen within the pores as a result of the supercurrents generated at the internal surfaces. On the other hand, the wave function Ψ, will go through the internal number of oscillation around the pore. This explains the quantization of the magnetic flux inside the pore [1].

2.1.2.6. The Ginzbur – Landau Parameter (κ)

The Ginzbur – Landau Parameter (κ) is defined as ratio between the penetration depth λ and the coherence length ξ_{GL}:

$$k = \frac{\lambda}{\xi_{GL}} \tag{2.9}$$

Close to T_c, this dimensionless ratio is approximately independent of temperature, and allows one to distinguish between type-I and type-II superconductors.

As defined by Abrikosov, a superconductor is of type-I if, $k < 1/\sqrt{2}$. If, $k > 1/\sqrt{2}$, then the material is a superconductor is type II [1].

2.1.2.7. Order Parameter (Ψ)

The wavefunction of the superconducting condensate is called the Order Parameter Ψ. The wavefunction can be represented as:

$$\Psi\,(r) = |\Psi\,(r)|e^{i\theta(r)} \tag{2.10}$$

Where $\theta(r)$ is the phase.

Between the properties of the order parameter are:

Ψ is a complex scalar which is continuous in real space,

$\Psi^*(r)\Psi(r)$ can only have one value, where $\Psi^*(r)$ is the complex conjugate of $\Psi(r)$.

In the absence of magnetic field, $\Psi \neq 0$ at $T < T_c$.

$\Psi = 0$ when the temperature is higher than the critical temperature, i.e., $T \geq T_c$, and also outside a superconductor [1].

The order parameter is usually normalized such that $|\Psi(\mathrm{r})|^2$ gives the number density of Cooper pairs at a point **r**:

$$|\Psi(\mathrm{r})|^2 \equiv \Psi^*(r)\Psi(r) = n_s/2 \tag{2.11}$$

Where n_s is the number of superconducting electrons and, $n_s \equiv n - n_n$, where n is the total number of free conduction electrons, and n_n is the number of non-superconducting electrons. If the total number of the free electrons is, $n = n_s + n_n$, then n_s decreases from n to 0, as the temperature increases from 0 to T_c.

In conventional superconductors each electron of a Cooper pair has opposite momentum and spin compared to the other. The order parameter in conventional superconductors has an s-wave symmetry, which means that $|\Psi| \neq 0$ everywhere in real space. When $|\Psi|$ is constant, the s-wave symmetry of the order parameter is called *isotropic*. If $|\Psi|$ varies slightly in real space, the s-wave symmetry of the order parameter is called *anisotropic* [1].

2.1.2.8. Vortex

The vortex pinning is usually related to the defect structure of a material. There is a difference between the elementary pinning force at the level of andividual flux line and the bulk pinning force density. A pore which generates a elementary pinning interaction between a flux line and a crystal lattice. When a vortex passes through the pore, the energy is lowered. In superconductors there are different lattice defects which act as pinning centers, some examples are grain boundaries and dislocations.

The pinning force density, F_p, is the pinning force per unit volume of a pinning centre, this is a product of the critical current density and the magnetic flux: $F_p = J_c B$ [2].

When the vortices are pinned near the defects or the grain boundaries, the Cooper pair will rotate around the vortices leading to a quantized flux. If the magnetic flux moves transversely through the material, the Cooper pair can be destroyed and a resistence or scattering of electrons will be reflected in J_c. One way to increase the magnetic flux line by introducing normal or superconducting phase to the superconducting material is known as artificial pinning center (APC).

The coherence length is a key parameter for the performance of superconductors for applications, because this parameter determines the size of the normally conducting core of the flux lines. In order to control the motion of flux lines one needs a microstructure with defects as small as the coherence length [7]. When the thickness and/or spacing of the different phases are of the order of the ξ, the proximity effect will induce superconductivity in those regions which will transform in the internal defects as superconducting phases. This generates magnetic flux pinning which is highly efficient at increasing the critical current density [8].

2.2. Magnesium Diboride

In January 2001, magnesium diboride (MgB_2) was found to superconduct at T_c = 39 K by Akimitsu [6]. MgB_2 thus become a very much studied superconductor because of its features that include a high T_c for a binary compound having simple crystal structure, (**Figure 2.9**) large coherence lengths, high critical current density and fields, and transparency of grain boundary to current [9]. Moreover, the MgB_2 has other properties like isotope effect [10, 11], and a linear *T*-dependence of the upper critical field with a positive curvature near T_c [12] that indicates unconventional superconductivity.

The MgB_2 compound has been studied by many groups in different forms: bulks, thin films, powders, wires, tapes and single crystal. The reported values of the superconducting properties showed a high dependence of material behavior as a function of synthesis and processing techniques. **Table 2.I** shows some reported values in Hc_2, ξ, and γ for the different forms. The values in Hc_1 are situated between 25 and 48 mT. J_c has also been studied in different materials. For instance, in bulks for applied magnetic fields of 6 T, J_c maintains a value above 10^4 A/cm^2, while in 10 T, J_c is about 10^2 A/cm^2.

Table 2.I. Properties of MgB_2 in bulk, crystallites, thin films, single crystal and powders [9].

Form	Reference	$H_{c2}^{\parallel ab}(0)$ [T]	$H_{c2}^{\parallel c}(0)$ [T]	$\xi_{ab}(0)$ [nm]	$\xi_c(0)$ [nm]	γ
Textured bulk	Handstein *et al* (2001)	12	11	5.5	5.0	1.1
Aligned crystallites	de Lima *et al* (2001b)	11	6.5	7.0	4.1	1.7
	de Lima *et al* (2001a)	12.5	7.8	6.5	4.0	1.6
Films	Jung *et al* (2001c)	30	24	3.7	3.0	1.25
	Ferdeghini *et al* (2001)	26.4	14.6	4.7	2.6	1.8
	Patnaik *et al* (2001)	22.5	12.5	5.0	2.8	1.8
	Patnaik *et al* (2001)	24.1	12.7	5.0	2.6	1.9
	Patnaik *et al* (2001)	39	19.5	4.0	2.0	2
Single crystals	Jung *et al* (2001f)	14.5	8.6	6.1	3.7	1.7
	Xu *et al* (2001)	25.5	9.2	6.5	2.5	2.6
	Lee *et al* (2001b)					2.7
Powders	Bud'ko *et al* (2001a)	20	2.5	11.4	1.7	5–8
	Simon *et al* (2001)	16	2	12.8	1.6	6–9

Note: $H_{c2}^{\parallel ab}(0)$ and $H_{c2}^{\parallel c}(0)$ are the upper critical magnetic field parallel and perpendicular to the ab-plane respectively; $\xi_{ab}(0)$ and $\xi_c(0)$ are the coherence length parallel and perpendicular to the ab-plane respectively; and γ is the anisotropy ratio $H_{c2}^{\parallel ab}/H_{c2}^{\parallel c}$.

Although T_c in MgB_2 is only 39 K, which is much less than 134 K found in the mercury-based high-T_c superconducting (HTSC) cuprates (**Figure 2.10**), the high cost of HTSC wires that are 70% silver [13] make them very expensive. This explains one of the major interest in develop MgB_2 based superconducting material.

MgB_2 possesses the simple hexagonal AlB_2-type structure (space group P6/*mmm*), which is common among borides. It contains graphite-type boron layers which are separated by hexagonal close-packed layer of magnesium. The magnesium atoms are located at the centre of hexagons

formed by borons and donate their electrons to the boron planes. Similar to graphite, MgB_2 exhibits a strong anisotropy in the B–B lengths: the distance between the boron planes is significantly longer than the inplane B–B distance [9]. In MgB_2, superconductivity occurs in the boron layers, according to Buzea and Yamashita [9], the electron-phonon interaction seems to be responsible for the occurrence of superconductivity in MgB_2 [9] .

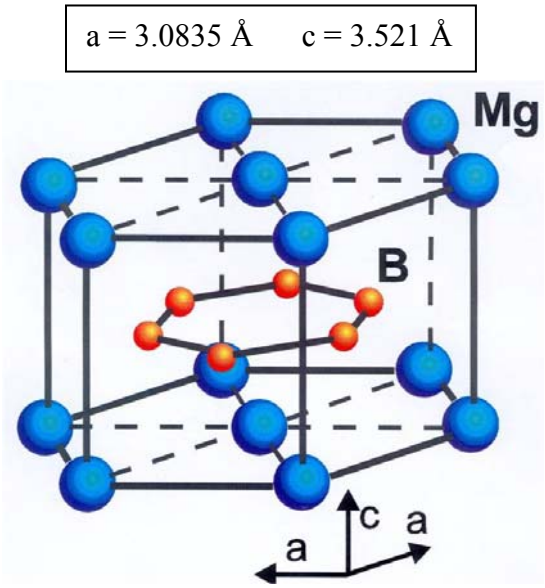

Figure 2.9. The hexagonal crystal structure of MgB_2 [9].

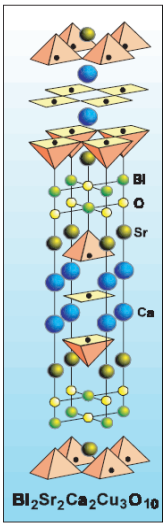

Figure 2.10. The structure of mercury-based high-T_c superconducting (HTSC) cuprates [9].

MgB_2 has a strong covalent B-B bonding (the bonding-antibonding splitting due to in-plane B-B hopping is about 6 eV) and thus exhibits strong electron-phonon interactions. Mg s-states are pushed up by the B pz orbitals and fully donate their electrons to the boron-derived conduction bands. Borons form a primitive honeycomb lattice, consisting of graphite-type sheets stacked with no displacement. The borons form hexagonal prisms with the base diameter of 3.5 Å nearly equal to the height. As in graphite, the intraplanar B-B bonds are much shorter than the distance between the planes, and hence the B-B bonding is strongly anisotropic. However, the interplane bonds are only twice as long as the intraplane ones, as compared to the ratio of 2.4 in graphite, thereby allowing for a significant interplane hopping [14].

There is almost no valence charge inside the Mg sphere as about half of the total valence charge resides inside the B spheres, and about the same amount in the interstitials. Band-structure calculations of MgB_2 show that there are at least two types of bands at the Fermi surface: the first one is a heavy hole band, built up of boron σ orbitals. The second one is a broader band with a smaller effective mass, built up mainly of π boron orbitals. The larger energy gap Δ_L occurs in the σ-orbital band, while Δ_s in the π-orbital band [14].

In **Figure 2.11** the character of the bands is observed (showing only the B p-character, since contributions from other orbitals near the Fermi level are very small). It is observed to have two B bands system: two bands are derived from B p_z states and four from B $p_{x,y}$. In **Figure 2.11** green and blue cylinders (hole-like) come from the bonding $p_{x,y}$ bands, the blue tubular network (hole-like) from the bonding p_z bands, and the red (electron-like) tubular network from the antibonding p_z band. The last two surfaces touch at the K-point [14].

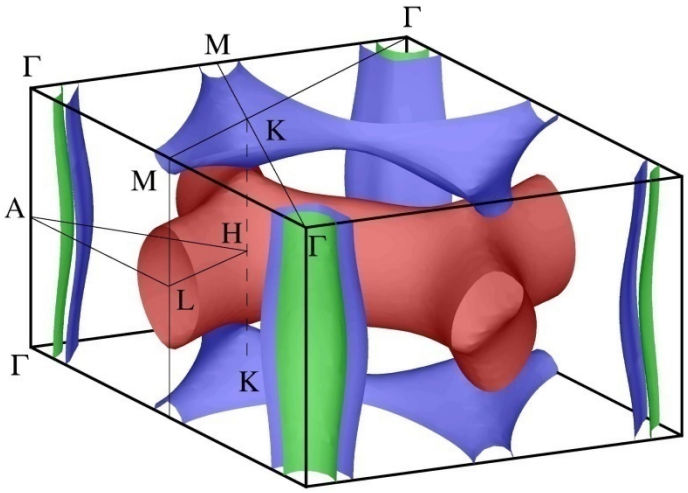

Figure 2.11. The Fermi surface of MgB_2 [14].

2.2.1. Resistivity Measurements for MgB_2

The Rowell theory [15] permits the possibility to estimate the connectivity in a material, using resistivity measurements. The basis for the Rowell analysis is that MgB_2 dense samples completely connect, have an electronic dispersion dependent of time that defines a characteristic change in the resistivity ($\Delta\rho_{ideal}$) between 300 K and 40 K. This resistivity is given by

$$\Delta\rho_{ideal} = \rho_{ideal}(300K) - \rho_{ideal}(40K) \quad (2.12)$$

The best experimental approximation for ρ_{ideal} is deduced from a totally dense and connected sample, made with material of high purity, which could be a monocrystal or a dense filament made by chemical vapor deposition (CVD) for which ρ_{ideal} = 7.3 μΩ.cm [15, 16].
An active area fraction A_F, of current transport is given by:

$$A_F = \rho_{ideal}/[\rho(300K) - \rho(40K)] \quad (2.13)$$

With the A_F known, it is possible to estimate the real resistivity for the sample, defined as the adjusted resistivity ρ_A (T) given by:

$$\rho_A(T) = A_F\rho(T) \quad (2.14)$$

2.3. Literature Review

The substitutions are important from several points of view. First, it may increase the critical temperature of one compound. Second, it may suggest the existence of a related compound with higher T_c, and last the dopant elements may act as pinning centers and increase the critical current density [9].

Substitution has been made and repored in MgB_2 with different elements such as carbon, aluminium, lithium, silicon, beryllium, zinc, copper, manganese, niobium, itanium, iron, cobalt, nickel, sodium and zirconium [9].

The T_c versus doping content for substitution with Al, C, Co, Fe, Li, Mn, Ni, Si and Zn is shown in **Figure 2.12.** The critical temperature decreases at various rates for different substitution [17-21].

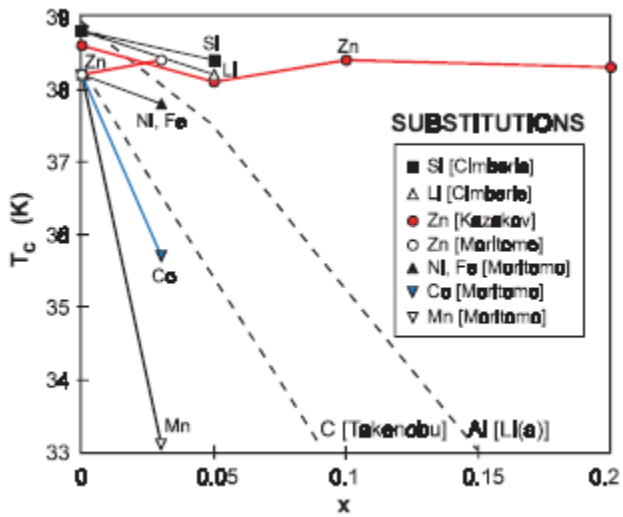

Figure 2.12. Critical temperature versus doping content for diversal elements [9].

Other studies were made in dense pure and doped $(Mg_{1-x}A_x)B_2$ samples with A = Na, Ca, Cu, Ag, Zn and Al synthesized at high pressure – high temperature in a multi-anvil press (3.5-6 GPa, 900-1000°C) for $0 < x < 0.20$. Only Al was confirmed to have substituted on the Mg site. The other elements formed secondary phases with B or Mg. No large effect was observed on the superconducting properties such as T_c, J_c, H_{irr} and H_{c2} [22, 23]

The effect of C, Cu, and Be substitution in Superconductivity of MgB_2 was studied by Mehl *et al.* [24]. They investigated the effects of partial substitution alloying of the B site in MgB_2 with C and Be alone, and combined with alloying of the Mg site with Cu, including band structure, lattice stiffness, and electron-phonon calculations. It was found that Be substitution for B is unfavorable for superconductivity as it led to a softer lattice and weaker electron-phonon couplings. Replacement of Mg by Cu leads to an increase in the stiffness and doping level at the same time, while the carrier concentration could be controlled by partial replacement of B by C. The authors estimated that with full replacement of Mg by Cu and fractional substitution of B by C, T_c values of 50 K could be attainable.

Next, one of the most studied dopants in MgB_2 is carbon. There have been several studies to determine the conditions which could lead to the enhancement of the superconducting properties in MgB_2. Different synthesis methods have been used to carbon dope MgB_2 [25, 26].

Using a solid state reaction route with ingredients of Mg, B, n-SiC and C powder, Awana, *et al.* [25] fabricated $MgB_{2-x}C_x$ and Mg_2Si, with C incorporated into the lattice of MgB_2 on the B sites. For $MgB_{2-x}C_x$ system, the T_c values of 34.5 and 32 K for which x = 0.10 and 0.20 were obtained. For the case of MgB_2 with *n*-SiC added, T_c was 36 K, and 35 K for 5 wt.% and 10 wt% *n*-SiC added samples respectively. For J_c results they found an enhancement in C doped MgB_2 which they attributed to two factors principally; first a contribution to flux pinning originating from the disorder in the σ-band superconducting condensate, that serve as weakly superconducting pins, and secondarily the introduction of SiC nano-particles that served as normal pin centers.

It is important to mention that breaking of doped *nano*-Carbon derivatives and ensuing substitution at B site in MgB_2 depends upon both the nature of the dopant and the heat treatment applied [27-30]. For example, *n*-SiC is more susceptible to react than *n*-Diamond [27-30] at common MgB_2 synthesis temperatures.

An important factor that can influence the superconducting properties in MgB_2 is the annealing temperature. It was reported in a study by Ribeiro *et al.* [31] doping MgB_2 with B_4C and latter heated to 750, 950, 1100 and 1200°C, they found that nearly single phase material could be formed by reaction of nominal $Mg(B_{0.8}C_{0.2})_2$ for 24 h at 1200°C. Correspondingly the T_c for this composition was between 21.9 and 22.7 K (depending on criterion used for T_c).

Senkowicz *et al.* [32] studied ball milled and heat treated MgB_2 samples exposure to different amounts of air. The results showed increase in resistivity, depressed in T_c and enhance in Hc_2 as a result of increased contact with air. The authors explained how the exposure to air could be considered as a doping process, and the posibility of this as a cause for the wide variability of the MgB_2 properties found in the literature, thus sustituing the air control as an important practice in the doping process in way to study the real influence of the element or compound in the superconduting properties.

MgB_2 is a material capable of being synthesized in different forms (bulk, thin film, wires and tapes), with the view of all of these looking for the enhancement in its superconducting properties.

The most successful method reported to grow single crystal of MgB_2 was at high pressure and high temperature from a precursor containing Mg, B and BN. For investigations for a P-T phase

diagram, Karpinski *et al* [33] found that the MgB_2 phase is stable up to 2200°C at high hydrostatic pressure. They explained the spcific band structure of MgB_2 with two bands (π and σ) involved in superconductivity which is strongly influenced by chemical substitutions, and summarized many studies substituting Al for Mg and C for B which lead to increases of scattering within both the π and σ bands; however, with different rates for both dopants. They found different changes of the upper critical field, H_{c2}, and its anisotropy, for $Mg_{1-x}Al_xB_2$ and $MgB_{2-x}C_x$. For $Mg_{1-x}Al_xB_2$ crystals, they observed decrease of T_c until 32 K for $x = 0.092$ and, simultaneously, significant reduction of H_{c2} and its anisotropy at lower temperatures, as compared to the value for unsubstituted crystals.

Moreover Karpinski, *et al.* [33] explained the properties obtained for diverse substitution: $MgB_{2-x}C_x$ crystals exhibit only slight reduction of T_c with substitution and, a significant increase of H_{c2} for an applied field oriented both parallel, $H_{c2\parallel}ab$, and perpendicular, $H_{c2\parallel}c$, to the ab-plane. For the single crystal with x = 0.13, $H_{c2\parallel}c(0) \approx 8.5$ T was more than twice as large as that for an unsubstituted compound. The anisotropy of Hc_2 decreases from 6 (MgB_2) to about 4 (x = 0.13) at low temperatures. The corresponding $Hc_{2\parallel}ab(0) \approx 34$ T was close to the maximum possible enhancement of H_{c2} due to the chemical substitutions. Hole doping with Li decreased T_c, but in much slower rate than electron doping with C and Al. For MgB_2 crystals with simultaneously substituted Li for Mg and C for B, T_c decreased more rapidly than in the case when only C was substituted. The T_c reduction in co-doped crystals was a sum of T_c reductions for separate C and Li doping. This meant that holes introduced with Li could not counterbalance electrons added with C. The possible reason of this could be that holes coming from Li occupied π band and did not compensate the addition of electrons which, coming from C, filled the σ band. Substitution of magnetic Mn for Mg strongly suppressed T_c and H_{c2} due to the magnetic pair breaking. However, this was not the case for the substitution of Fe for Mg, at least for low Fe concentration [33].

Senkowicz [34] studied MgB_2 doped with Carbon at different concentrations using ball milling process by varying the milling times. Between the conclusions he found were: the optimum milling time was around 1200 min, C-doping was the most effective way to increase H*(4.2K) beyond 10 T, maximum J_c (12 T) could be achieved by X = 0.04 - 0.07, grain size was very important to J_c because fine grains increased H*.

Studies were done on MgB_2 doping with MeB_2 compounds that have the AlB_2-type crystalline structure to maintain the MgB_2 crystalline structure of the phases and the efficient mixture of the superconductor with the doping compound. The experiments were designed to substitute metal Me on the Mg site. In this case, the ball milling will positively influence the final crystal structure, probably maintaining the AlB_2-type hexagonal structure, while generating intragranular and intergranular pinning centers [8].

In the case of ZrB_2 doped MgB_2, the samples syntheses were made by adding 7.5at.% of ZrB_2 in a mechanical alloing process with ball milling followed by heat treatment that was carried out between 700 - 900°C for 0.5 hours. Si-C samples were prepared in a similar way to facilitate comparison. The resistivity transition, $\mu_0 H_{irr}$ and H_{c2}values were determined at 4.2K. The authors found an enhancement in H_{c2} from 20.5 T to 28.6 T as well as $\mu_0 H_{irr}$ from 16 T to 24 T. J_c was also found to increase in all temperatures between 4.2 K and 35 K [35].

Rodrigues [8] studied the doping of MgB_2 with diboride materials which had AlB_2-type structure. The doping materials were ZrB_2, TaB_2, VB_2 and AlB_2. He analyzed materials that were balled milled for different times (300, 600, 1000, 1200, 3000 and 4000 minutes) for all the dopants, with a heat treatment at 1000°C under a pressure of 200 MPa for 24 hours under vacuum. He found J_c values around 6800 A/cm^2 at 8 T, 4.2 K for pure MgB_2 milled at 300 minutes, in comparison to the values of 8 A/cm^2 for the initial material (unmilled, HIP sample). At low fields it was found that the sample doped with 5at. % TaB_2 milled for 300 minutes had an increase in J_c to 9.7x 10^5 A/cm^2 at 1 T, 4.2 K, in comparison to the value of 4.8 x 10^5 A/cm^2 for the MgB_2 unmilled HIPed MgB_2 sample.

Following close with Rodrigues, Perez Moyet [36] investigated the MgB_2 doping with TaB_2 at 2 and 5 at.% to compare two processes of milling based on SPEX and pulverisette-4 machines. He found that material processed at 5 at. % showed higher superconductivity properties compared with the 2 at.% TaB_2 doped one, due to higher amount of TaB_2 that penetrated in the material. The highest J_c (2 T, 4.2 K) 474.1 kA/cm^2 was for 5 at.% TaB_2 corresponding to the 600 minutes ball milled material. Its T_c at 10% of the crest had value of 37.332 K. The second best value in J_c (2 T, 4.2 K) for 5 at.% TaB_2 was for 120 minute ball milled sample that showed 390.9 kA/cm^2 and T_c of 37.56 K. In general, SPEX milling exhibited higher J_c, F_p, and H_{irr} values than the Puleverisette-4 processed material for their investigation.

Based on these considerations, the ball milling of the dopant materials prior to further ball milling with MgB2 was conceived. This was judged necessary in order to enhance the alloying/doping process. Thus, the main difference in the work carried out in the present study was the pre-milling of the dopant materials prior to the doping of the MgB_2.

3. EXPERIMENTAL PROCEDURE

The first phase of the synthesis was made at the University of Puerto Rico – Mayaguez campus and the second phase was made at Florida State University – Tallahassee campus. This thesis was developed with the supporting of NSF to PREM group.

The elements, alloy, compression, heat treatment, and synthesis in general will be described in this chapter. The characterization and equipment used will be introduced, along with techniques needed to obtain the data and finally the superconducting and structural properties.

3.1. Synthesis and Sample Preparation

Ball milling was the technique used in this investigation for mechanical alloying. The compounds (base material and dopant material) were mixed and ball milled for different milling times to determine the best alloy conditions. The reaction expected to be achieved is:

$$(1-x)MgB_2 + xMeB_2 \rightarrow Mg_{(1-x)}Me_xB_2 \tag{3.1}$$

Where MeB_2 represents the dopant materials, which in this case are the compounds titanium diboride; TiB_2 (-325 mesh, typ. 10 microns average or less, 99.5% pure), tantalum diboride; TaB_2 (-325 mesh, typical 10 microns average or less, 99.5% pure), niobium diboride; NbB_2 (-325 mesh, typ. 10 microns average or less, 99.5% pure), and chromium diboride; CrB_2 (-325 mesh, 99% pure)

Magnesium diboride (MgB_2) is the base material. Its powder size is -325 mesh, and average particle size reported by the supplier (Alfa Aesar) is 4 µm.

3.1.1. Sample Preparation

The implications in the superconducting properties, given by the powder materials exposure to air have been highly studied. The formation of MgO and MgB_4, and the decomposition of CO_2 resulted in the unintentional C-doping of the MgB_2 with the exposure to air. The formation of MgO during ball milling and material handling result in the changes in T_c and H_{c2} values. [34], [36, 32]. The use of a glove box with a controlled atmosphere avoids the exposure to air for a powder sample.

All samples synthesized in this investigation were prepared inside a glove box in a nitrogen atmosphere. The glove box has an exterior chamber in which a vacuum process is performed to remove the air; the elements that will be taken to the interior of the glove box will be placed in that chamber first, once the chamber is closed the purge process begins generating a vacuum inside it, after have -100 psi the chamber is full with nitrogen precedent for the interior of the glove box. This process is repeated three times to liberate the air from the chamber as much as possible and in that way keep the glove box free from oxygen.

Once the chamber is full with nitrogen the elements keep inside are available to place in the glove box. All the powders, the jars, and the tools needed in the synthesis are keeping inside the glove box.

Equipment used to mill the powder consisted of one external basket, one internal jar, four balls and two gaskets. The external basket was used to avoid the contamination from exposure to air mention above, since the ball milling machine was placed outside the glove box and the transport of the sample from the inside of the globe box to the outside should be with high protection to keep the sample free of oxygen. The external basket is made from aluminum and the cap has eight screws which keep the basket hermetically closed; the internal jar fixes inside the gasket with some space in case of thermal expansion. A gasket was placed between the cap and the body of the milling jar to seal the internal jar and avoid loss of powder during milling. The internal jar contains the powder and the milling balls. **Figure 3.1.**

Figure 3.1. Jar and balls used in the ball milling process.

The material used for the milling balls and the internal jars was tungsten carbide (W_3C). Four milling balls were used for each synthesis; one ball measures $^1/_2$", two $^3/_8$" and one $^1/_4$" in diameter. The ball to powder mass ratio (BPR) was set at 3:1 for this study, therefore the powder mass is estimated from Equation 3.2 and 3.3

$$Ball\ to\ Powder\ Ratio = Balls\ mass : Powder\ mass \tag{3.2}$$

$$Total\ Powder\ Mass = \frac{Balls\ mass}{3} \tag{3.3}$$

The quantity of doping powder was selected based on the results obtained by Perez Moyet [36]. That work investigaed 2 atomic percent (at.%) and 5 at. % for different milling times, getting the best results in all cases for 5 at. %, due to higher amount of TaB_2 that penetrates in the material. Therefore 5 at.% TaB_2 was selected for the present study.

There are various ways to specify composition. It is often useful to specify composition in terms of atomic percentages or atomic fractions. On the other hand, in many practical situations, weight percent or weight fraction of a given component is used to specify the composition. Therefore, it is sometimes necessary to convert back and forth between weight percent and atomic percent [37].

The relation between at.% and wt.% is described in the Equations 3.4 – 3.7

We begin to define some terms:

M = Atomic mass of each element or compound. (g/mol)

W = wt. % of the element or compound

A = at. % of the element or compound.

If we consider the Equation 3.4., we can defined

M_1 = Atomic mass of MgB_2

M_2 = Atomic mass of MeB_2

x = quantity of dopant material

As of the terms define above, the relation can be expressed as follow:

$$W_1 = \frac{(1-x)M_1}{(1-x)M_1+xM_2} x\ 100 = wt.\%\ for\ MgB_2 \tag{3.4}$$

$$W_2 = \frac{xM_2}{(1-x)M_1+xM_2} x\ 100 = wt.\%\ for\ MeB_2 \tag{3.5}$$

Having the equation for wt. %, it is possible to define the term of at. % in function of wt. % as follow:

$$A_1 = \frac{W_1M_2}{W_1M_2+W_2M_1} x\ 100 = at.\%\ for\ MgB_2 \tag{3.6}$$

$$A_2 = \frac{W_2M_1}{W_1M_2+W_2M_1} x\ 100 = at.\%\ for\ MeB_2 \tag{3.7}$$

Consequently, the powder mass of each compound is determined multiplying the total powder mass given by Equation 3.6 – 3.7, by the wt. % of the compound.

3.2. Ball Milling Process

Ball milling process is a technique uses in bulk material to reduce the particle size with the employ of grinding balls. The powder and the balls are deposit inside a jar, which is place in the SPEX 8000D. The movement made in the machine makes the balls strike with the walls in the jars, grinding the powder.

3.2.1. SPEX 8000D

The SPEX 8000D has two symmetrical arms each one with a support for the sample holder which sustains one jar. Each arm generates the shaking of the jar which contains the balls and the powder with movements in horizontal and vertical directions. The movements in horizontal directions makes the balls strike from the top to bottom of the jar and conversely, the movement in vertical direction makes the balls strike with the walls of the jar, and the combination of both movements generates a tangential direction that displace the balls through the walls. These movements are made by several shakes per second, generating high energy impacts which milling the powder and reduce the particle size. In MgB_2 the particle size reduction is from 325 mesh to 10 nm in 20 hours approximately [34].

3.2.2. Ball Milling Parameters

The first ball milling process was made from each compound separately for 120 minutes (process we will name from now on pre-milled), that is to say, the MgB_2 powder was pre-milled for 120 minutes and all the MeB_2 were also pre-milled at the same time. This process was made with the principal objective to reduce the particle size and in this way get a more homogeneous material when the two compounds were mix. The assumption is that this process could help to increase the superconducting properties. To corroborate this; it was synthesized for each dopant one sample without the pre-milling process which works as a comparison sample.

Once the compounds were pre-milled, it was mixed MgB_2 with each dopant at 5 at. % and ball milled at different milling times, to investigate at what time the superconducting properties present the better values. The milling times were 60 min, 120 min, 180 min, 300 min and 600 min. In **Table 3.I** is shown the samples studied in this thesis.

Table 3-I. Samples synthesis in this investigation

Pre-milling Time	Milling Time/	SAMPLE			
		95 at. % MgB_2 + 5 at. % TiB_2	**95 at. % MgB_2 + 5 at. % TaB_2**	**95 at. % MgB_2 + 5 at. % NbB_2**	**95 at. % MgB_2 + 5 at. % CrB_2**
0 min	120 min	TIB22H	TAB22H	NBB22H	CRB22H
120 min	60 min	PTIB21H	PTAB21H	PNBB21H	PCRB21H
120 min	120 min	PTIB22H	PTAB22H	PNBB22H	PCRB22H
120 min	180 min	PTIB23H	PTAB23H	PNBB23H	PCRB23H
120 min	300 min	PTIB25H	PTAB25H	PNBB25H	PCRB25H
120 min	600 min	PTIB210H	PTAB210H	PNBB210H	PCRB210H

The jars with the compounds were taken inside the glove box, there the powder was taken away from the jar and save in a glass vial. Each vial was labeled and put in a vacuum container. When the powder is taken away from the jar, some of the material remains adhered to the walls because of the high energy that is get involved in the process and that makes difficult to remove the powder with a spatula in first place. To clean the jars it is necessary to take them away from the glove box and wash them as well as the balls with water, soap and a hard sponge that is used just for this propos, in most of the times it is needed to use some hard spatula or sand paper to remove all of the material on the walls. After washing all the materials with water and soap again, they are dry and some of the Isopropanol 99.99% is apply and dry again with hot air, trying to keep the material free of humidity and water before to turn back to the glove box. The cleaning process was made carefully to avoid contamination and the presence of different materials in the samples. Because in this thesis it was used different dopants, it was run all the samples of each dopant before to continue with the next one to avoid contamination of multiple materials in the samples.

Once all the samples were ball milled it was taken 0.5 gr approximately of each vial to analyze the powder by X-ray diffraction. The vials with the sample remaining were surrounded with aluminum foil, and saved in a plastic container which keep the vacuum inside. The samples were taken away from the glove box and sent to Florida State University where the synthesis process continues.

The ball milling process besides to reduce the particle size generates in the powder a metastable state because of the high energy impact. The balls strike the powder with high force generating strain and other defects in the atomic structure. As reported by Schultz, amorphous powder can be formed by mechanical alloying in a high energy ball mill. Milling leads an ultrafine composite in which amorphization by solid state reactions takes place. Measurement of intrinsic physical properties such as the crystallization or the superconducting transition temperature and of extrinsic physical properties such as the saturation magnetization or the crystallization enthalpy allows an accurate determination of the homogeneity range of the amorphous phase and of the metastable phase diagram. He conclude that amorphization by mechanical alloying is based on a solid-state reaction and occurs under a metastable thermodynamic equilibrium neglecting the existence of intermetallic phases [38]

This metastable state generated during the ball milling can be reduced in the compression and heat treatment processes. The small and instable particles can find an equilibrium state during the heat treatment.

In Florida State University is located the Applied Superconductivity Center where was carry out the second phase of the synthesis; they have the equipments needed to carry out the Cold Isostatic Press (CIP), Hot Isostatic Press (HIP) processes and the characterization of the samples.

3.3. Cold Isostatic Press (CIP)

Cold Isostatic Press is a technique used to compact the material with high pressure using water with oil has the pressing material. The force is applying for all the places with the same pressure on the sample for few seconds getting finally a compress material.

To apply the CIP to each sample it was needed to take one rubber tube with a hall in the middle and two compact rubber cylinders with equal diameter as the hall of the tube. It was placed one of the cylinder inside the rubber tube as base, 3 gr approximately of one sample were placed inside the tube, after that was closed with the other cylinder and pressing for both sides looking that the sample were compact inside the tube.

As the sample has to be immersed inside the pressing liquid it is needed to protect it with an impermeable material, for that the tube which contains the sample is put inside a balloon of enough thickness and sealed with a strong node. Every container which saves a sample is labeled to avoid confusion. The sample with the impermeable material is protected from the liquid in the CIP and also from the air which can contaminate it with a minimum exposure; with the sample protected it can be taken away from the globe box.

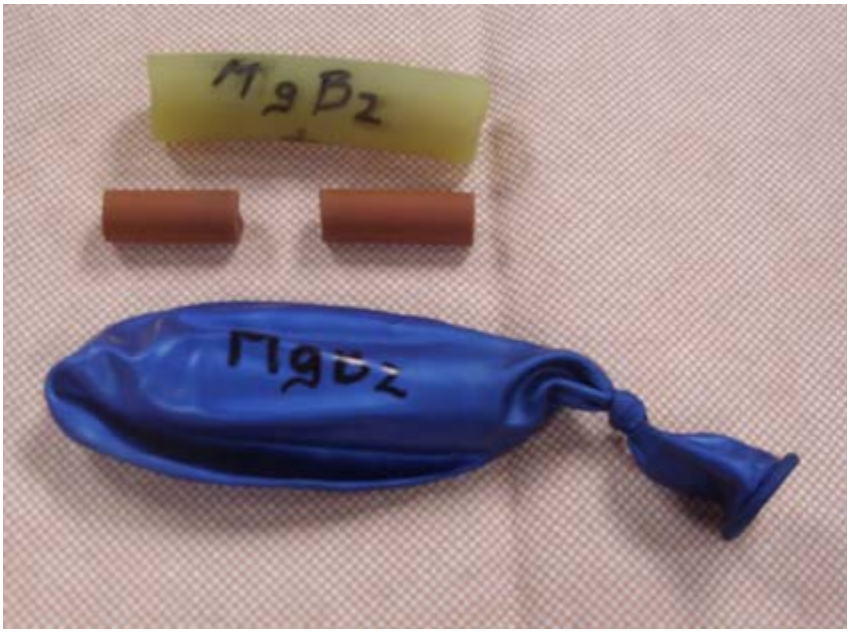

Figure 3.2. Rubber tube used to save the powder during the CIP and impermeable balloon which protect the material from the water and aire.

Before introducing the sample in the equipment to initiate the CIP process it were putting inside a mesh since in this way it is getting back easily. Once the equipment is closed by hydrostatic press, the pressure begins to increase until it reaches 30,000 psi, the value stipulated for all

samples prepared in this thesis. The force is applied from the liquid en each point of the sample with the same pressure.

The sample is taken away from the liquid and the plastic has to be cleaned with water and soap and after with alcohol and dry with air, in this way we are getting the sample free for humidity to be able to return it in to the glove box.

In the glove box the plastic is cut and the sample, now compressed in a pellet, is taken out of the rubber tube. The sample compress is put inside a stainless steel tube of 10 cm approximately which was closed in one side, welded and cleaned before to bring into the glove box. The stainless steel tube is inserted in a mechanism made of rubber canals and valves that connects the tube with a vacuum system, and which permits removing the tube with the sample out of the glove box without submit the sample to the atmospheric contamination. (**Figure 3.3**)

Figure 3.3. Mechanism to protect the sample and connect it with the vacuum system.

Initially the vacuum is made in the tube, it is filled with argon and made the vacuum again, this purge process is repeated three times until to have the system in vacuum. The valve is closed in the connection mechanism when the system completes the vacuum, and the tube is flat in the other side with a manual press as much as possible to avoid the entrance of air when the tube be

cut and welded. The higher length allow for the tube to fix in the crucible use for the Hot Isostatic Press is 4”. To verify that the tube is well welded and the sample is free of oxygen it is made another CIP process to the tube welded, if it has a leak or if it is expanded with liquid inside, the sample has to be repeated. If the tube is well closed it can be made the Hot Isostatic Press.

3.4. Hot Isostatic Press (HIP)

The Hot Isostatic Press (HIP) is a process which applies heat besides pressure. For all samples made in this thesis the conditions for the HIP were 29,500 psi, 1000°C for 24 hours. The tube has to have a maximum length of 4” to fix in the crucible which holds and retains the samples in the HIP unit, the maximum number of samples run at each time were 12 placed in all the volume of the crucible. Each cycle needs an appropriate flow of water and argon to decrease the temperature and increase the pressure. The HIP uses an automated system to control the cycle; it is necessary to describe the cycle needed for each sample in accordance with the parameters of each one. The cycle used is observed in **Figure 3.4**.

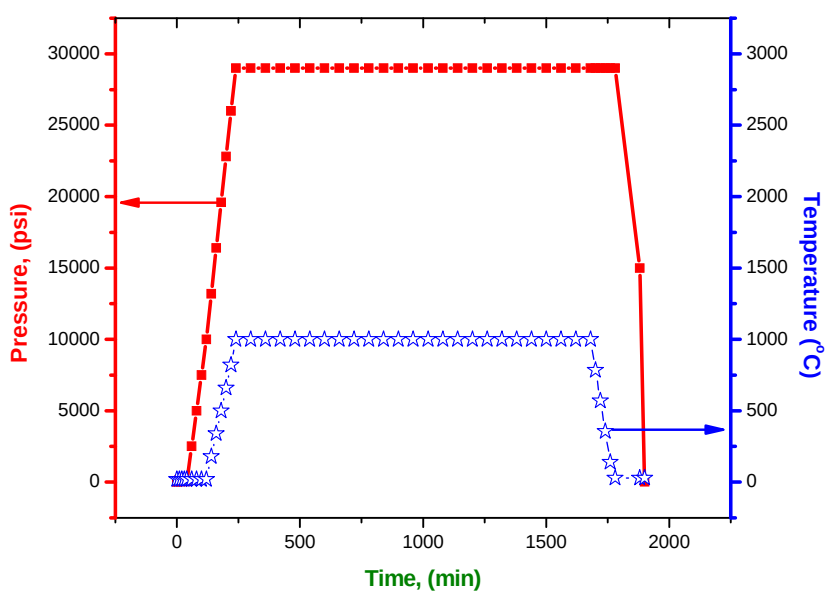

Figure 3.4. Cycle used in HIP.

The HIP is a heat treatment process follow of pressure which permits the reorganization of the atomic structure from a metastable state going through a stable state. The ball milling process bring to the sample a reduction in particle size accompanied from a disorganization in the atomic structure and many structural defects as strain, vacancies, and others. The pressure permits the grain connectivity in the sample, the fill of spaces, and the formation of a more homogeneous sample facilitating the alloy process, that is to say, the dopant could be introduced itself into the structure of MgB_2 helped for the HIP process.

3.5. Preparation of Samples to Characterization

Once the sample finishes the HIP process it is needed to be cut in slides to make the different characterizations. The samples were cut with a diamond blade of dimensions 4" of extern diameter, 0.0012" of tick and 0.5" of intern diameter, the lubricant used to cut them was vacuum pump oil; water was not used because the sample at contact with it, experiments an alteration of the surface characteristics and very probably of the structure and superconducting characteristics. The thickness of the slice was between 1.0 and 2.0 mm. Once the slice was cut it was formed for a flat slice of the sample with shape similar to an oval and surrounded for a metallic band which is simply the tube added to the sample as result of the HIP, this band was cut with pliers and taken away from the sample.

3.6. Characterization

The samples were characterized by different methods and processes; they included superconducting properties characterization and surface properties characterization.

In superconducting characterizations, resistivity characterization was carried out to obtain data in resistivity, critical magnetic field, and critical temperature, while the magnetization was developed to get data in critical current density.

For structural characterization it was analyzed x- ray diffraction to determine the composition of the samples, the changed in the structure with the synthesis process, the strain and particle size.

Moreover, Scanning Electron Microscopy was performed to analyze the particle and grain arrangement and to observe the different phases.

3.6.1. Physical Property Measurement System (PPMS) - Resistivity

Physical Property Measurement System (PPMS) of Quantum Design Model 6000 (**Figure 3.5**) localized in the Florida State University in Tallahassee campus has the capability of measure normal state resistivity, magnetic moment, heat capacity and applications for heat transport. The PPMS can generate a field from 0 to 16 T, a current from 0.01 to 5000 μA, a power from 0.001 to 1000 μW and a voltage from 1 to 95 mV.

Figure 3.5. Physical Property Measurement System.

In the MgB_2 doped with MeB_2 samples the PPMS was used in the resistivity option from which we can find some of the superconducting properties as resistivity (ρ), critical magnetic field (H_{c2}), critical temperature (T_c) and the analysis of connectivity.

To perform the measure it is used a resistivity sample puck (**Figure 3.6**) which have the availability to mount up to three samples; for each sample there is a set of four labeled contact pads, one positive and one negative contact for current and voltage, the sample has to be mounted near of the contact pads and fix to a sapphire substrate place in the bottom of the puck with GE varnish.

Figure 3.6. Sample puck used to resistivity measurement.

To connect the contact pads with the sample, it is used Cu wire which is fixed to the sample with silver paint and to the pads with welding. Each sample is distinguish with a number positioned in the top of the contact pads, this method is the only use to label each sample once they are place in the PPMS.

To carry out the measurement in the sample it is insert the puck inside the PPMS and set all the parameters for the measurement. The parameters used were 5000 μA, 1000 μW and 95 mV as constant values. In the sequence the field was swept from 0 T to 15 T in step of 1 T. The temperature was scanning from 300 K to 20 K in 0 T and from 40 K to 20 K from 1T to 15 T.

They were used two different steps; from 300 K to 40 K it was used steps of 20 K and from 40 K to 20 K the steps were of 0.5 K.

To carry out the resistivity measurement, it was necessary to know some geometric characteristic in the sample.

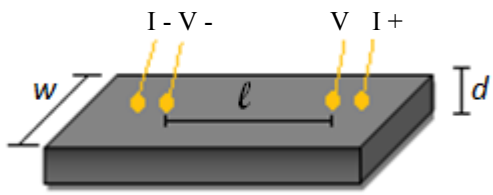

Figure 3.7. Dimensions and connections for resistivity sample.

From **Figure 3.7** we define *w* as the width of the sample, *d* as the depth and l as the distance between the voltage tap separation, from this terminology we can define *A* as the cross section area (**Equation 3.8**)

$$A = wd \tag{3.8}$$

Looking at the leads, it is observed that the outer points are for current supply and the inner points are for voltage sensing. A 5 mA current was applied on the circuit generating a potential difference which can be measure, from these two knowing values we can obtain the resistance from Ohm's law (**Equation 3.9**)

$$R = \frac{V_{sensing}}{I_{supply}} \tag{3.9}$$

Once *A* and *R* are calculated, the resistivity can be obtain from the Equation 3.10

$$\rho = R\frac{A}{\ell} \tag{3.10}$$

The values of *A* and *ℓ* were measured for each sample and they were included in the PPMS information before the measurement, in this way the equipment calculated ρ giving the final information in function of this variable.

The equipment gives the resistivity of each sample in 0 T from 300 K to 20 K, and between 1 T and 15 T from 40 K to 20 K.

With the behavior information of the resistivity in 0 T between 300 K and 20 K, we can analyze the connectivity in the sample using the Rowell [39, 40] model and the Residual Resistivity Radio (RRR). Electron scattering is observable as increase normal state resistivity, electron scattering can be observed either by lattice defects or by interactions with phonons. The resistivity contributions will be given by the Matthiesen's rule represented by the Equation 3.11

$$\rho = \rho_{def} + \rho_{ph}(T) \tag{3.11}$$

As the phonon contribution to resistivity is a function of temperature, near to 0 K the phonon contribution is close to 0, the resistivity is $\rho \sim \rho_{def}$ and the measure value is the residual resistivity.

The trend in the resistivity versus temperature graph at 0 T is shown in **Figure 3.8**, which give information about the influence of the phonon contribution while the temperature increases, this contribution generates a lineal tendency in the graph with the increasing of temperature.

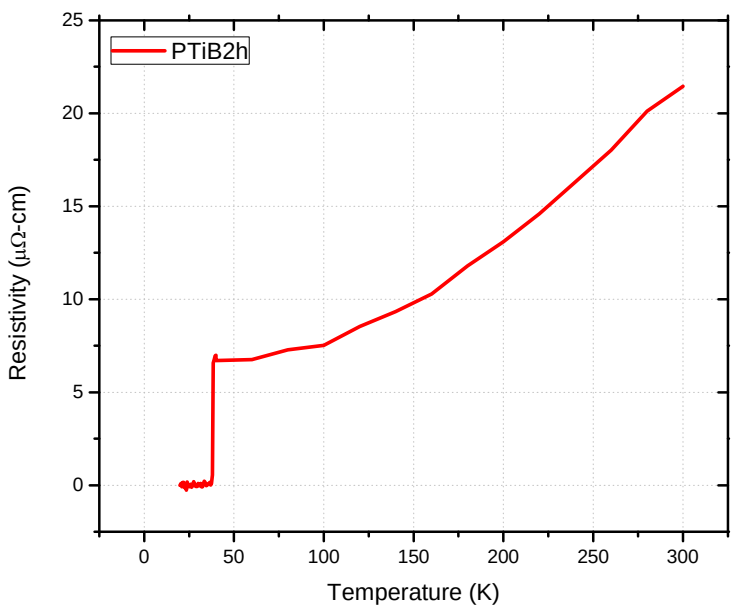

Figure 3.8. Trend resistivity versus temperature at 0 T.

The graph of resistivity versus temperature at some specific field gives the information about the increasing of the resistivity with temperature. A representative graph of resistivity versus temperature at constant field is shown in **Figure 3.9**. The trend of resistivity versus temperature at different fields let us obtain the values of T_c.

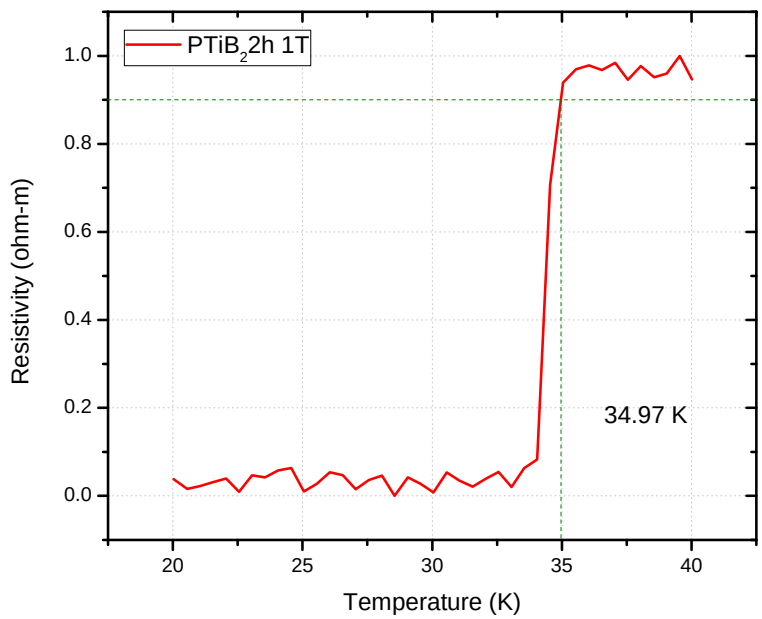

Figure 3.9. Trend of resistivity versus temperature at constant field, 1 T for this case.

To obtain the critical temperature (T_c) from this graph, it is applied the 90% criterion which will determined the critical temperature at the 90 % of the maximum value, considering some factor as the noise and the difficult of measure a point at 100% with high accurately, this criterion allow us to have a more real value and compare with other works that use the same criterion in the literature.

To apply the 90 % criterion the values of resistivity are normalized from 0 to 1, obtaining a graph of normalize resistivity vs temperature. In the 0.9 resistivity point is searching the value of the respective temperature at a establish field and this graphs are repeated at different fields to get finally a graph of critical temperature Vs field. **Figure 3.10**

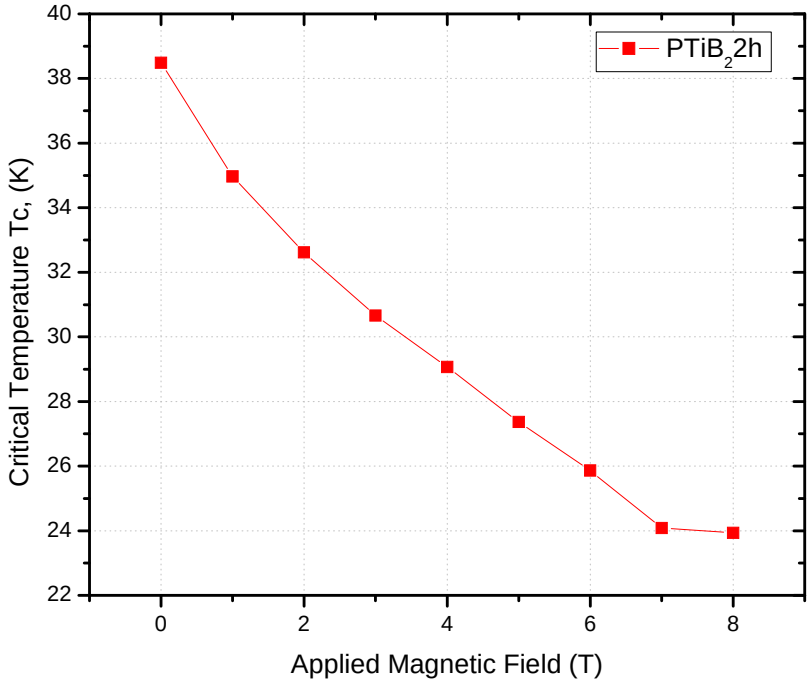

Figure 3.10. Example of Tc Versus Applied Magnetic Field Graph.

To obtain the critical field (H_{c2}) the procedure is similar to critical temperature, however the graph created is from resistivity versus field at a fix temperature, and the process is repeated at different temperatures. It is apply the 90 % criterion also and finally is construct a H_{c2} versus temperature graph. **Figure 3.11**

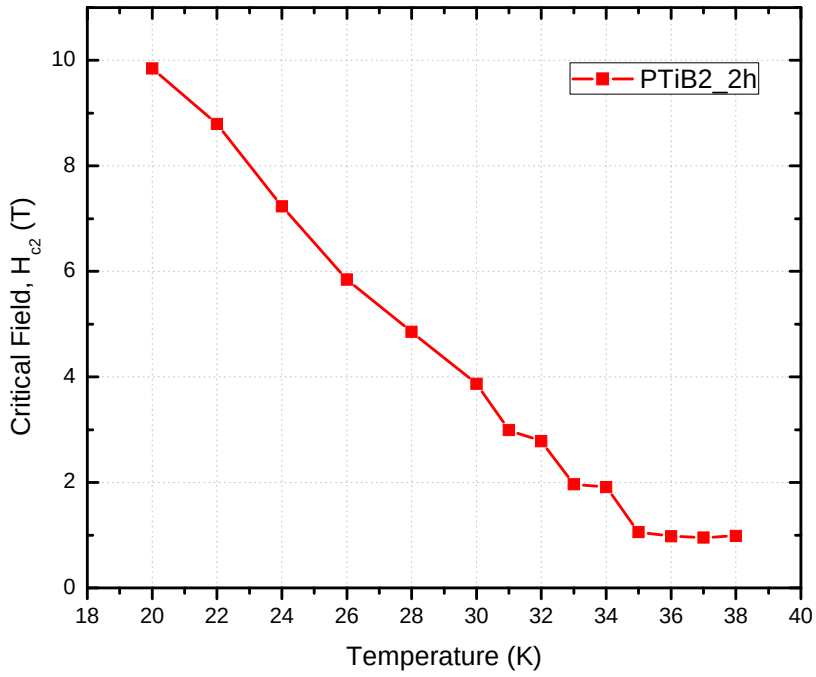

Figure 3.11. Example of Hc_2 versus Temperature graph.

This process is repeated for each sample which permits to compare the samples of the same dopant, but also the samples at the same ball milling time for different dopants. The analysis of these parameters will show important relations between the samples.

3.6.2. X-ray Diffraction (XRD)

The X-ray diffraction (XRD) is a characterization technique used to analyze the structural properties. The XRD is a tool which is useful to determine the lattice parameters, the strain and the grain size; moreover it can identify the phases present each sample.

The x-ray is generating by irradiation of the Cu metal with high energy electrons. The electrons generate that the Cu atoms expel electrons out of their orbits but because of the tendency to keep the lowest energy state, electrons in the Cu atom fill the vacancies in lower levels, generating liberation of energy in form of x-ray. The x-ray beam pass through a slit with a establish aperture to limit the wavelength beam, this x-ray inside on the sample and strikes with the atoms depending of the atomic structure and the type of atom. Once the beam strikes a plane of atoms

with an angle θ with respect to the normal, the x-ray direction changes and a path length difference proportional to sin θ arises for x-ray reflected by each plane. When the path length difference between reflections from adjacent planes is an integer multiple *n* of the wavelength λ, then constructive interference occurs and the angle between the diffracted beam and the transmitted beam is 2θ, and *d* is the interplanar spacing. The condition for diffraction in any observable angle is then expressed for the Bragg equation (Equation 3.12)

$$n\lambda = 2d\ sin\theta \tag{3.12}$$

Using the XRD pattern it is possible to determine important characteristics in the sample as the average size of the grain (*t*) using the Scherrer formula (Equation 3.13):

$$t = \frac{0.9\lambda}{B\ cos\theta_B} \tag{3.13}$$

Where B is the line broadening by reference to a standard, so that:

$$B^2 = B_M^2 - B_S^2 \tag{3.14}$$

Where B_s is the halfwidth of the standard material in radians.

A method of interpreting particle size broadening and strain broadening is using the Williamson-Hall's analysis (Equation 3.15)

$$\beta cos\theta = 4e(sin\theta) + \frac{\lambda}{\varepsilon} \tag{3.15}$$

Where β is the integral width in radians (crystallite size plus non uniform distortion), θ is the Braggs' angle of diffracted rays, ε is the crystallite size and *e* is the average lattice strain.

The XRD diffractometer used is a Siemens D 500 model with a CuK(α) source and (β)Ni filter. The wavelength of the CuK(α) source is 1.5406 nm.

The parameters used in this thesis to effect the x-ray characterization are: voltage 30 KV, current 35 mA, range from 10 to 90 grades in steps of 0.03 in 1 second.

3.6.3. Scanning Electron Microscopy (SEM)

The Scanning Electron Microscopy (SEM) was used to analyze the microstructure, second phases and estimation of grain size.

The sample surface is scanned with an electron beam, and the back-scattered beam of electrons is collected and displayed at the same scanning rate on a cathode ray tube, the image on the screen represents the surface of the specimen. The surface must be electrically conductive.

The samples are introduced in a vacuum column, the air is pumped out and the electron gun emits a beam of high energy electrons. This beam travels through a series of magnetic lenses which direct the beam toward a fine spot and finally in direction to the sample. When the beam hits the sample, secondary electrons are expelled from the surface; they are collected in a detector, sent to an amplifier and the image is built up from the number of electrons emitted from each spot on the sample.

4. Effect of 5 at.% TaB_2 in the Structural and Superconducting Properties of MgB_2

MgB_2 doped with TaB_2 material has been studied before by Rodrigues [8] and Perez [36] and determined some important properties for this material at different conditions.

Rodrigues [8] determined the critical properties of 5 at.% TaB_2 doped MgB_2 that were ball milled for 300 and 4000 minutes respectively. The values determined for the 300 min ball milled material were 18.6 T for Hc_2 (0 K), 37.6 for T_c, while 9.7 x 10^5 A/cm^2 for J_c (1 T, 4.2 K). In then, the structural characteristics for the same sample were such, that the materials exhibited a crystallite size of 14.41 nm for MgB_2 phase, 43.89 nm for TaB_2 phase, and 38.25 nm for MgO phase, while strain of 0.002285 for MgB_2 phase, 0.000286 for TaB_2 phase, and 0.001764 for MgO phase was obtained.

Perez [36] determined the superconductive properties J_c, T_c, F_p and H* and the structural properties crystallite size and strain for TaB_2 samples doped at 2 at.% and 5 at.% ball milled in SPEX 8000D and Pulverisette 4. The values obtained for 300 min TaB_2 at 5 at.% sample, ball milled in SPEX 8000D were 3.12 x 10^5 KA/cm^2 for J_c (2 T, 4.2 K), 37.20 K for T_c ,6.24 GN/m^3 for F_p (2 T, 4.2 K), and 6.69 T for H* (4.2 K).

In this chapter the analyses of MgB_2 materials doped with 5 at.% TaB_2 will be presented. Both the MgB_2 and TaB_2 were premilled for 120 minutes separately and later mixed and milled at 60, 120, 180, 300 and 600 minutes. This was followed by electrical superconductivity properties such as Hc_2, T_c, resistivity were determined in addition to their structural characterization.

4.1. Structural Properties

Each sample was analyzed using XRD technique to determine composition, crystallite size and strain. The MgB_2 and TaB_2 compounds were pre-milled for 120 min prior to the mixing. Next, the pre-milled materials were mixed to yield the overall composition corresponding to MgB_2 – 5 at.% TaB_2 that were eventually ball milled for the different times shown in **Figure 4.1**. Perez [36] characterized the MgB_2 – 5 at.% TaB_2 materials in powder, ball milled at 60, 120, 300 and 600 min using the XRD technique, the XRD patter is shown in **Figure 4.2** [36]. The peaks of the XRD pattern from Perez [36] were sharp, while the peaks found in this research were broader.

The MgB_2, TaB_2 and MgO peaks were identified in both studies, however Perez [36] did not report the B element.

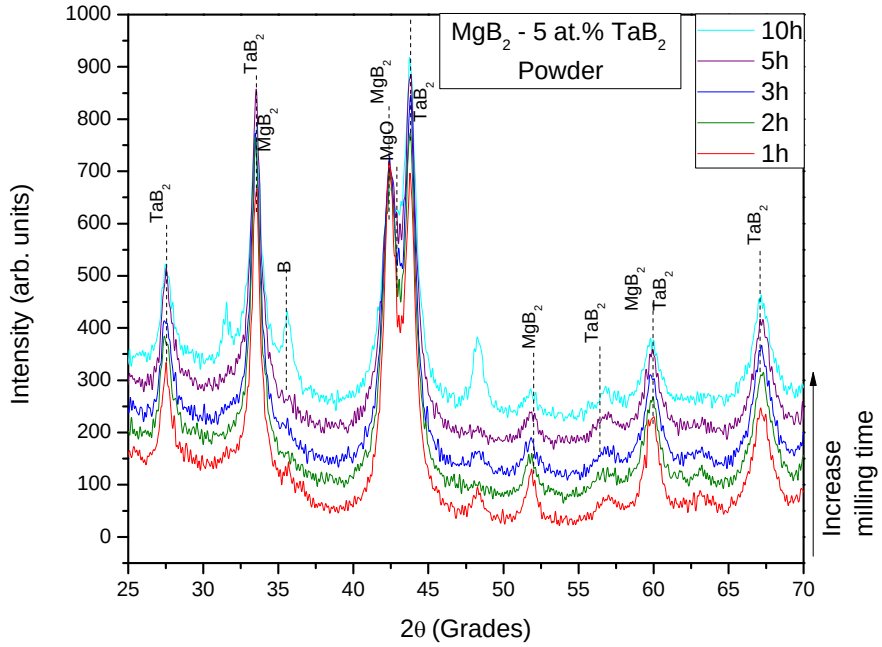

Figure 4.1. X–ray diffraction of the powder MgB_2 - 5 at.% TaB_2 premilled.

After the pre-milled and the ball milling process, the MgB_2 – 5 at.% TaB_2 materials were subjected to cold isostatic and hot isostatic pressing respectively (CIP and HIP) before investigating their unique proportion. In addition to the peaks corresponding to the single phases MgB_2 and TaB_2, there were other peaks corresponding to B, Si and MgO as shown in **Figure 4.3**, for all the materials investigated.

Perez [36] used the same pressure and temperature conditions in the CIP and HIP process for the MgB_2 – 5 at.% TaB_2 materials that the ones described for this research. The XRD pattern for the pelletized material reported by Perez [36] is shown in **Figure 4.4.** He found the TaB_2, MgB_2, MgO compound and additionally the WC and MgB_4 phases, however he did not reported Si. The peaks observed for the materials no pre-milled [36] are sharper than the peaks of the material synthesized in this research, which imply bigger crystallite sizes.

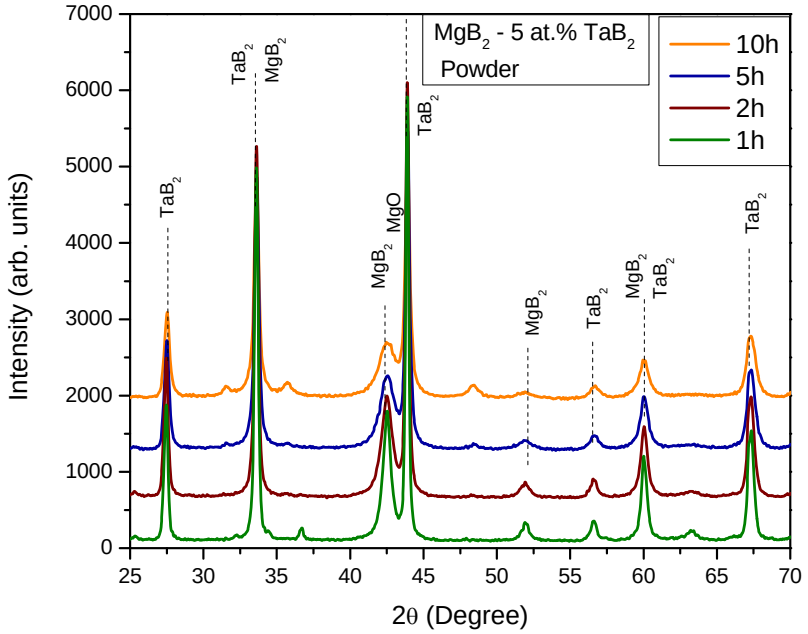

Figure 4.2. X–ray diffraction of the powder MgB_2 - 5 at.% TaB_2 material [36].

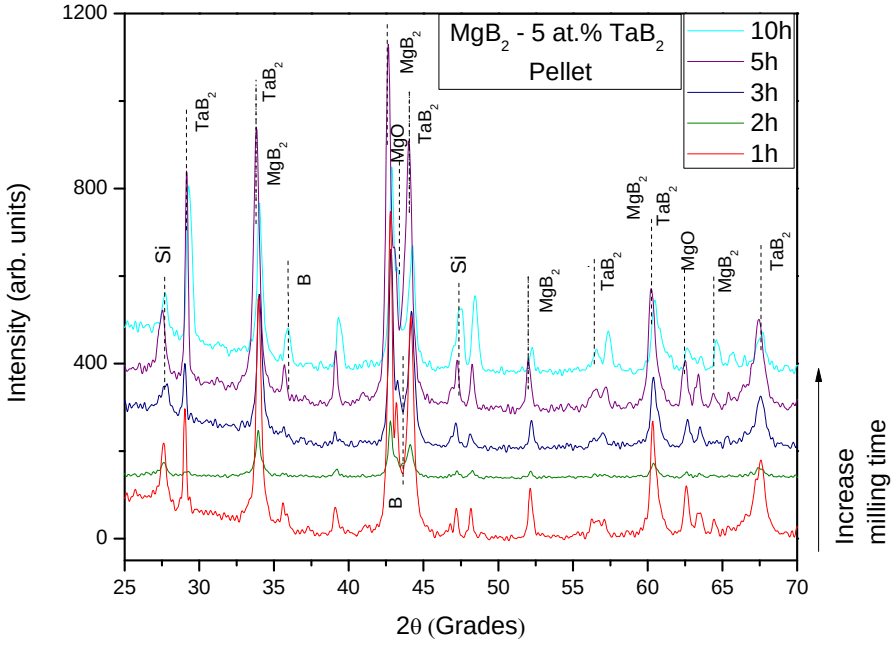

Figure 4.3. X–ray diffraction of the HIP MgB_2 - 5 at.% TaB_2 as a function of ball milling time.

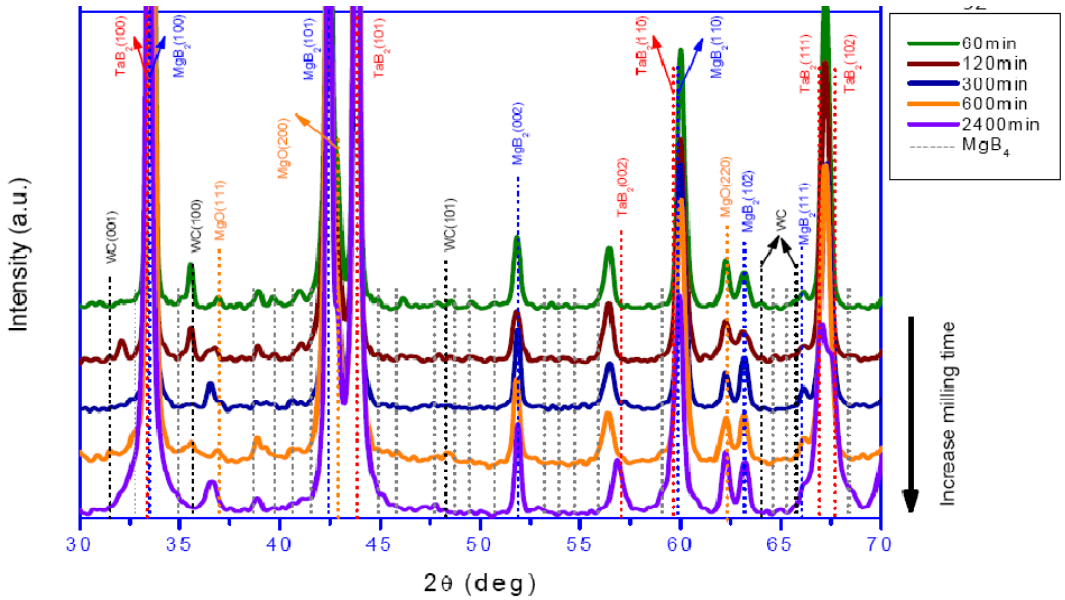

Figure 4.4. XRD measurements for the SPEX-8000D for the 5 at.% TaB2 doped MgB2: 60, 120, 300, 600 and 2400 minutes.

The MgO component in the samples shows the presence of Oxygen in any stage of the synthesis. The presence of Oxygen and it influence in superconductivity was studied by Senkowicks *et al*. [32], although it is consider that the high level of oxygen can decrease the superconductivity in the sample, it is extremely difficult to avoid the complete presence of this element, because there are several steps in the synthesis process including pre-milling, milling, CIP, tube welding and HIP, which are develop outside the glove box.

Senkowicks *et al*. [32] studied different amounts of exposure to air, for four different environments; glove box, glove bag, air (sealed) and air (valve); the XRD pattern for the different samples is shown in **Figure 4.5**. The increased electron scattering including increased resistivity, depressed T_c, and enhanced Hc_2 of the milled and heat treated samples were observed as a result of increased contact with air; in **Table 4.I** is shown the values in superconducting and resistivity properties for the samples with different exposure to air reported by Senkowicks *et al*. [32]. Although Senkowicks *et al*. [32] reported the increase in Hc_2 as a result of increased contact with air; they argued that this result is caused for the introduction of CO_2 in the sample that could be considered as a doping with C, moreover, they reported that the formation of MgO

in MgB_2 could block current flow. In addition, Eisterer *et al.* [41] reported the decrease in J_c with the increase in MgO.

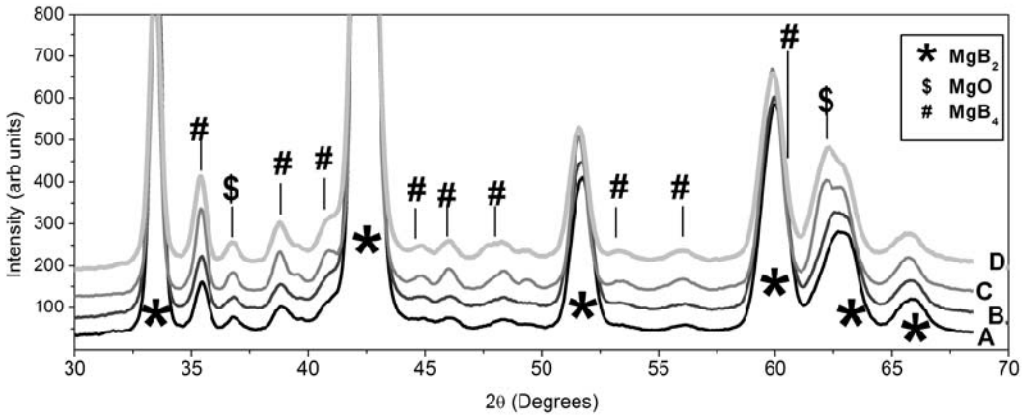

Figure 4.5. X-ray diffraction patterns of heat treated samples (Cu-Kα) [34].

Table 4.I – Processing parameters, designations, and properties [34].

Sample	Atmosphere	T_c (SQUID 90%) (K)	H_{c2}(24K) (T)	ρ(40) μΩ-cm	ρ(300) μΩ-cm	RRR	Δρ μΩ-cm	A_F	$ρ_A$(40) μΩ-cm
A	Glove Box	38.0	7.0	8.44	30.53	3.62	22	0.33	2.8
B	Glove Bag	37.9	7.2	10.23	35.37	3.46	25	0.29	3.0
C	Air (sealed)	37.8	7.3	17.58	56.73	3.23	39	0.19	3.3
D	Air (valve)	37.5	7.9	14.91	41.26	2.77	26	0.28	4.1

The presence of elemental B peaks suggests that the ball milling process resulted in the partial decomposition of the boron bearing phases; MgB_2 or TaB_2. However the peaks corresponding to either the Mg or Ta following the possible decomposition were not recorded or observed, which suggest that MgB_2 was decomposed in Mg and B with the subsequent formation of MgO.

The EDS analysis of the MgB_2 – 5 at.% TaB_2 material ball milled for 120 minutes is shown in **Figure 4.6** where the peaks corresponding to Si are shown to non-negligible.

Figure 4.7 shows the SEM of one phase corresponding to the based material (MgB_2) and a second phase which could correspond to Si, TaB_2 or B. The grains observed of the second phase presented small sizes, even though the resolution of the equipment does not permit to observe the MgB_2 crystallite in detail.

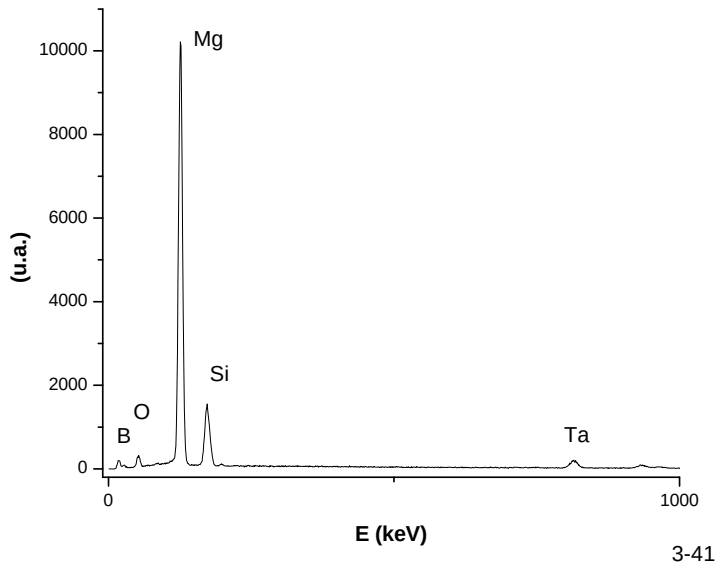

Figure 4.6. EDS of TaB_2 5 at.% 2 hours ball milling sample.

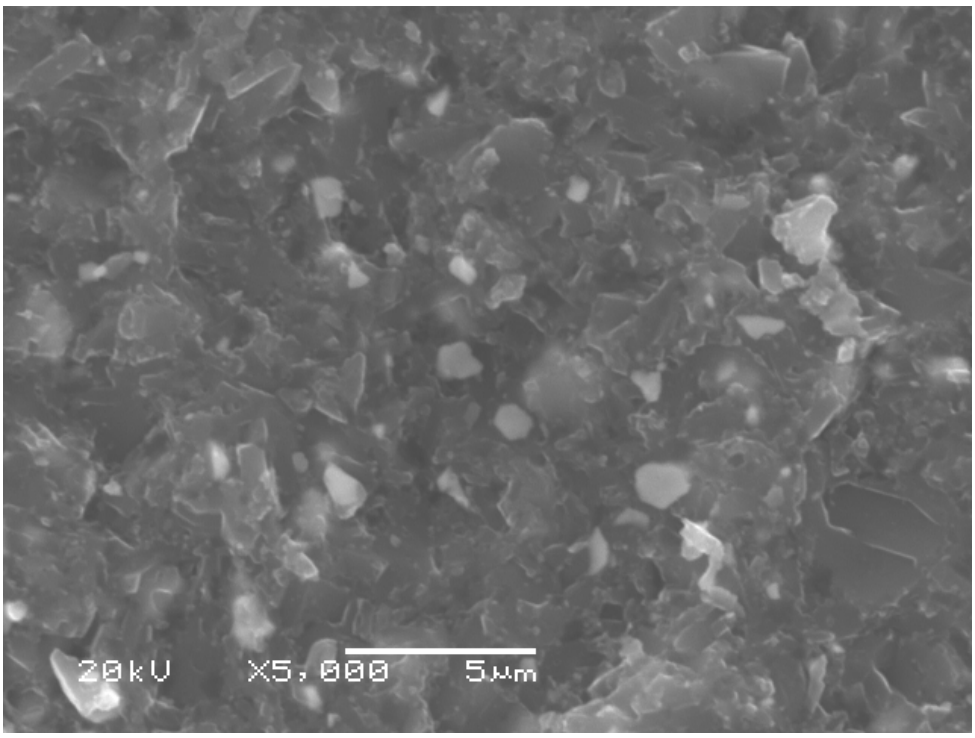

Figure 4.7. SEM of TaB_2 5 at.% 2 hours ball milling sample.

By considering the possibility of the decomposition of the MgB_2 and TaB_2 during the ball milling stage, together with the unavoidable exposure of oxygen, the presence of Mg, B, O and

Ta were suspected. However, only TaB_2, MgB_2, MgO and B were observed as shown in **Figure 4.8.** The phases Ta, Mg, MgB_4 and WC were not observed during the analyses of the doped materials.

The 5 at.% TaB_2 corresponded to 18.84% in weight, which compared to 6.2 - 9.3 wt.% determined in the ball milled materials could implicated that more that 50% or there about was dissolved in the MgB_2 phase with the ball milling.

The amount of TaB_2 phase determined after the HIP process of the materials was between 1.2 wt.% to 5.4 wt.% as shown in **Figure 4.9**. These results indicate that during the annealing, the dissolution process of TaB_2 continued leading the overall decrease in the amount of TaB_2 after HIP.

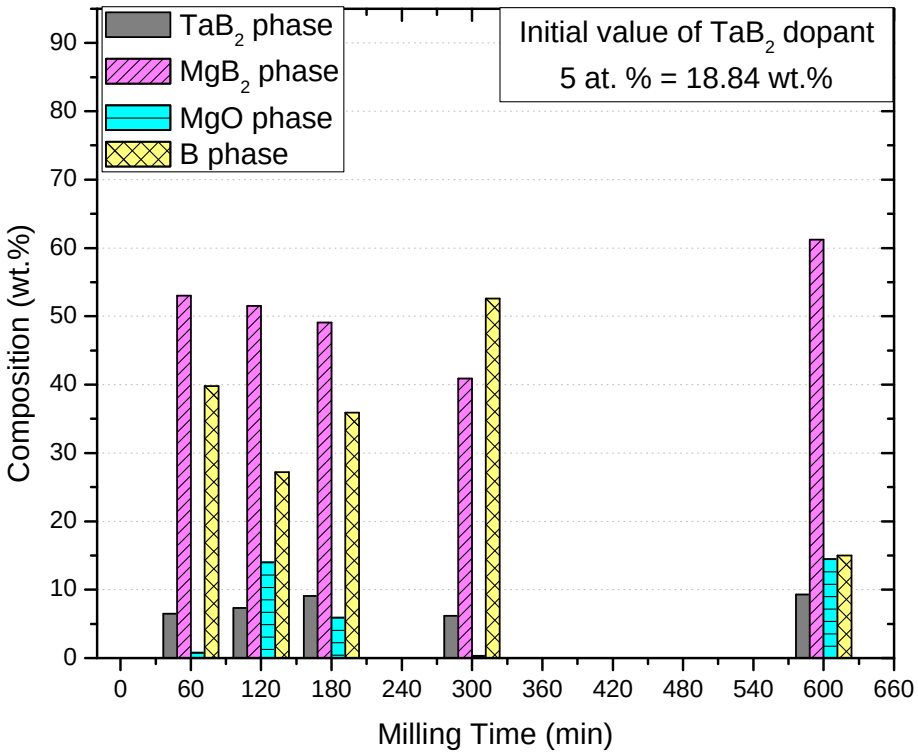

Figure 4.8. Composition of TaB_2, MgB_2, MgO and B phases for powder material in function of milling time.

The decomposition of MgB_2, TaB_2 or both compounds were established because of the low composition percentage in TaB_2 and MgB_2 contrasted with the high presence of B in powder and pellet materials, however there was not observed the Ta and Mg elements individually in the XRD, which suggest the possibility of formation of a new phase between Ta and other elements or compounds. The composition of samples at different milling times is described in **Table 4.II**.

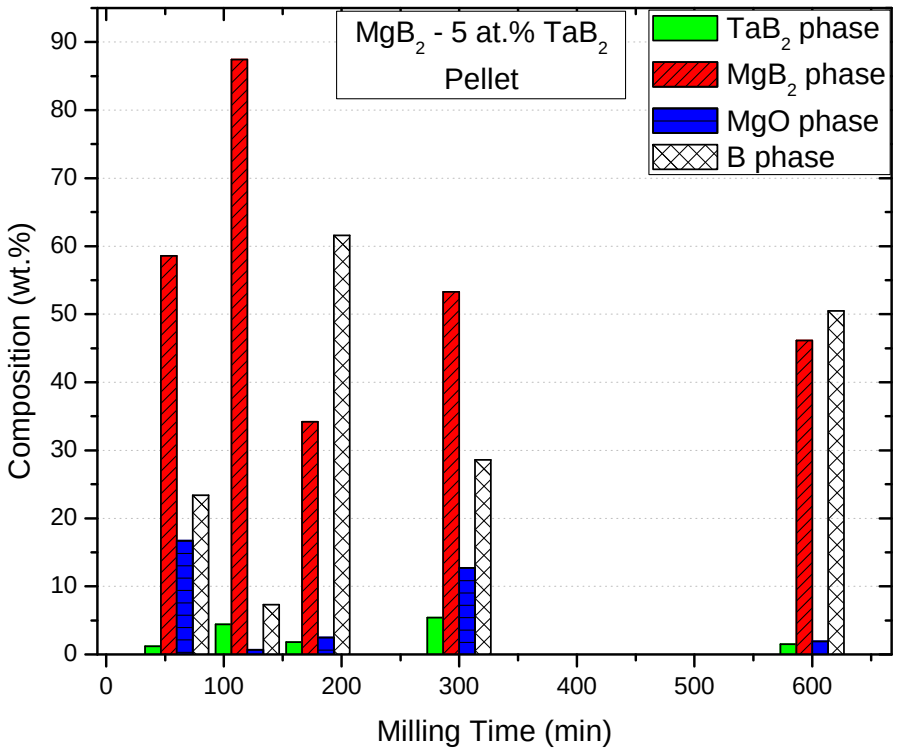

Figure 4.9. Composition of TaB_2, MgB_2, MgO and B phases, for pellet post HIP material in function of milling time.

Senkowicz [34] and Perez [36] reported MgB_4 and WC between the components of the MgB_2 doped ball milled materials, however they did not informed about presence of B phase in the ball milled compounds in powder or pellet. As was suggested by Senkowicz [34] the possible reactions when it is perceived MgB_4 between the components are:

$$2\,MgB_2 + \tfrac{1}{2}O_2 \rightarrow MgO + MgB_4 \quad (4.1)$$

$$2\,MgB_2 + H_2O \rightarrow MgO + MgB_4 + H_2 \quad (4.2)$$

The results observed in this thesis with the presence of the B phase and the absence of Ta and Mg suggest the reactions:

$$MgB_2 + \tfrac{1}{2}O_2 \rightarrow MgO + 2B \quad (4.3)$$

$$MgB_2 \rightarrow Mg + 2B \quad (4.4)$$

It TaB_2 decomposed as is shown in Equation (4.5), the absence of Ta and the possible reaction represents in Equation (4.4), could imply the formation of a new phase similar as is represent in Equation (4.6)

$$TaB_2 \rightarrow Ta + 2B \quad (4.5)$$

$$XTa + YMg + 2B \rightarrow (Ta_X\,Mg_Y)B_2 \quad (4.6)$$

The crystallite size of the TaB_2 phase in the powered material was in the 6.49 – 8.75 nm range, and showed very slight changes with ball milling.

Following the HIP process, the average crystallite size of the TaB_2 phase was bigger than the Pre-HIP or powdered state size in general. Given that high energy ball milling resulted in crystallite size reduction, together with the generation of a lot of structural defects, therefore it is expected that the metastable material would experience some amount of crystallite growth with the high temperature used in the HIP process. The difference of the crystallite size between the powder material and the pellet material is observed in the XRD patter of the samples; the powder material have peaks more broadening (**Figure 4.1**) while the pellet materials have peaks sharper (**Figure 4.3**).

The overall variations of the crystallite size of TaB_2 following initial ball milling and after the ball milling that accompanied the doping process are shown in **Figure 4.10**. The 300 min ball milled material exhibited the lowest crystallite size while the size reduction tendency with initial increasing ball milling time is evident.

For MgB_2 – 5 at.% TaB_2 powder material ball milled at 300 min Perez [36] reported crystallite size of 20.98 nm for MgB_2 and 10.1 nm for TaB_2. The crystallite size for the pre-milled and milled material at 300 min in powder for this research was 6.53 nm for MgB_2 phase and 8.75 nm for TaB_2 phase. The results describe before could suggest that the pre-milling process decreased the crystallite size in a more representative way for MgB_2 than for TaB_2.

For MgB_2 – 5 at.% TaB_2 material ball milled at 300 min and HIP at 1000°C Rodrigues [8], reported a crystallite size of 14.41 nm for MgB_2 phase and 43.89 nm for TaB_2 phase. For MgB_2 – 5 at.% TaB_2 material ball milled and HIPed with similar conditions, Perez [36] reported a crystallite size of 33.58 nm for MgB_2 phase and a crystallite size of 34.77 nm for TaB_2 phase. The crystallite sizes reported before for MgB_2 phase were similar than the value found in this work with 20.48 nm, however, the crystallite size of the TaB_2 phase showed a reduction until 15.89 nm compare with the values reported in [8] and [36].

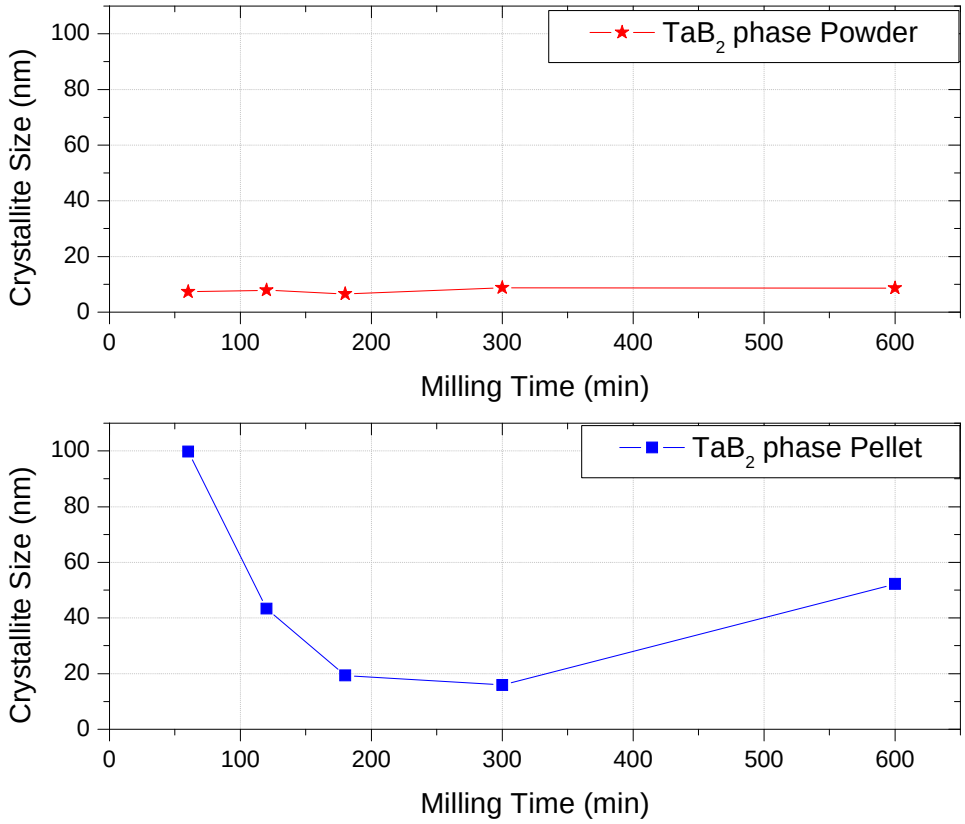

Figure 4.10. Crystallite size of TaB_2 phase for powder and pellet material in function of milling time.

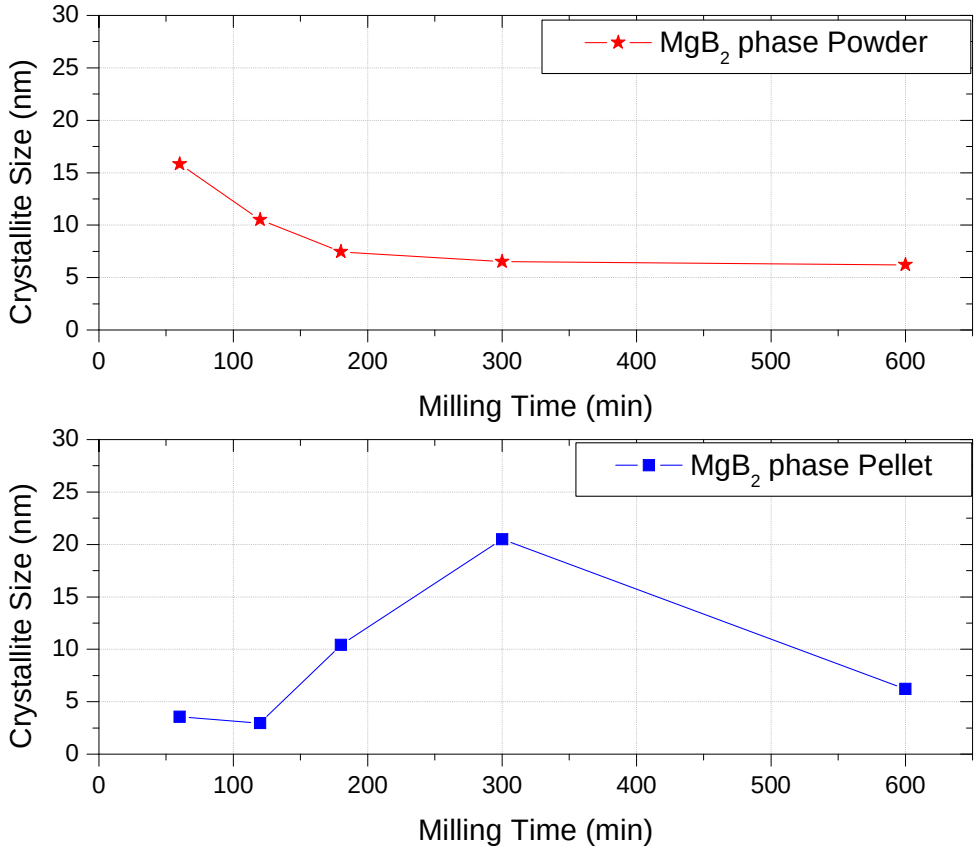

Figure 4.11. Crystallite size of MgB_2 phase for powder and pellet material in function of milling time.

In general, the crystallite size for the MgB_2 phase in powder material was smaller than for the post HIP one, following a similar tendency describe for the TaB_2 phase. (**Figure 4.11**).

Figure 4.12 shows the strain Vs milling time for TaB_2 phase. The values in strain were higher for the powder samples than for pellet samples, the decreasing in strain is a result of the HIP process which converts the sample from a metastable state to a stable state, reorganizing the structure.

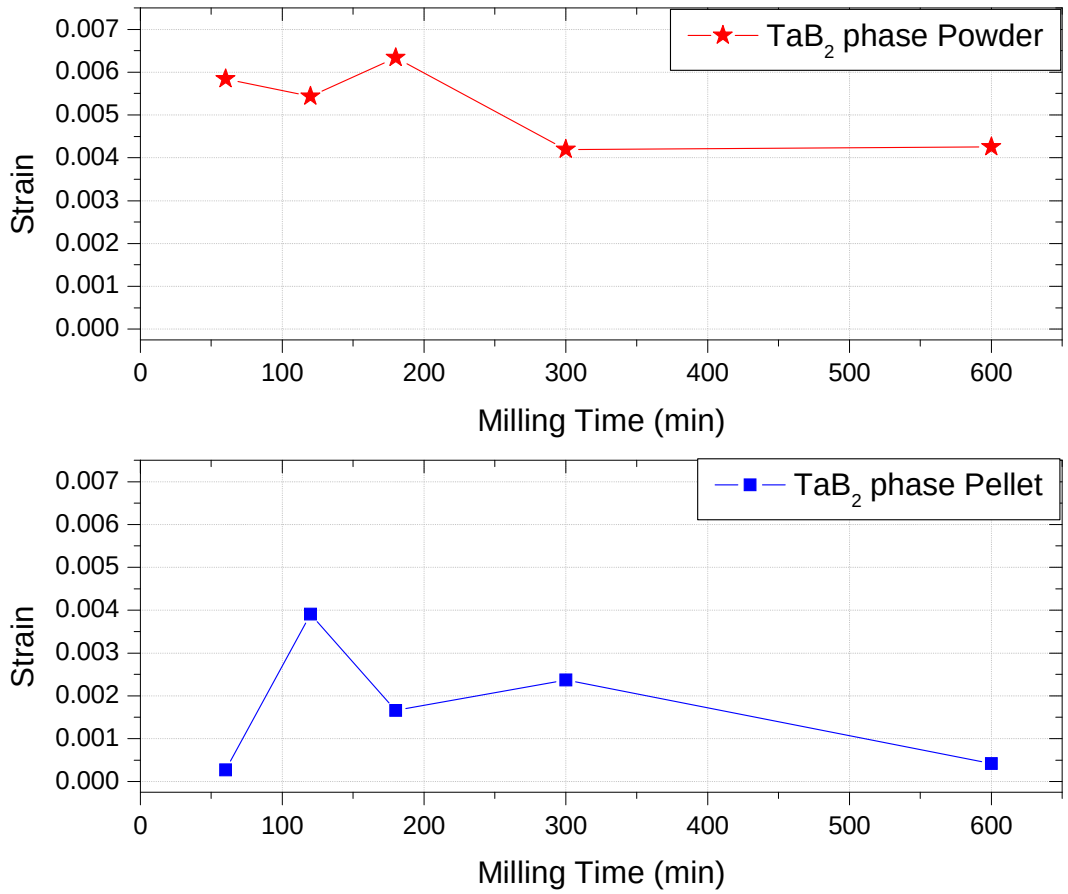

Figure 4.12. Strain of TaB_2 phase for powder and pellet material in function of milling time.

Figure 4.13 shows the Strain Vs milling time for the MgB_2 phase for the powder and the post HIP sample. For 60 and 12 minutes of ball milling, the post HIP samples had higher values in strain compare with the powder sample. Between 180 minutes and 600 minutes the powder material had higher values for strain than the post HIP material.

Strain broadening can be caused by any type of lattice defect, such as, vacancies, interstitials, substitution, and stacking faults [42]. Serquis *et al.* [42] related the content of MgO and the content of Mg vacancies with the increase in strain for MgB_2 material. Zhu *et al.* [44] reported that MgO particles presented as a second phase in MgB_2 can generate dislocations. Serquis *et al.* [42] also establish a relation between the increasing in strain and the decrease in T_c in MgB_2

material, however in accordance with the results in strain and content of MgO for this work observed in **Table 4.III**, is not possible to establish a relation between those two properties.

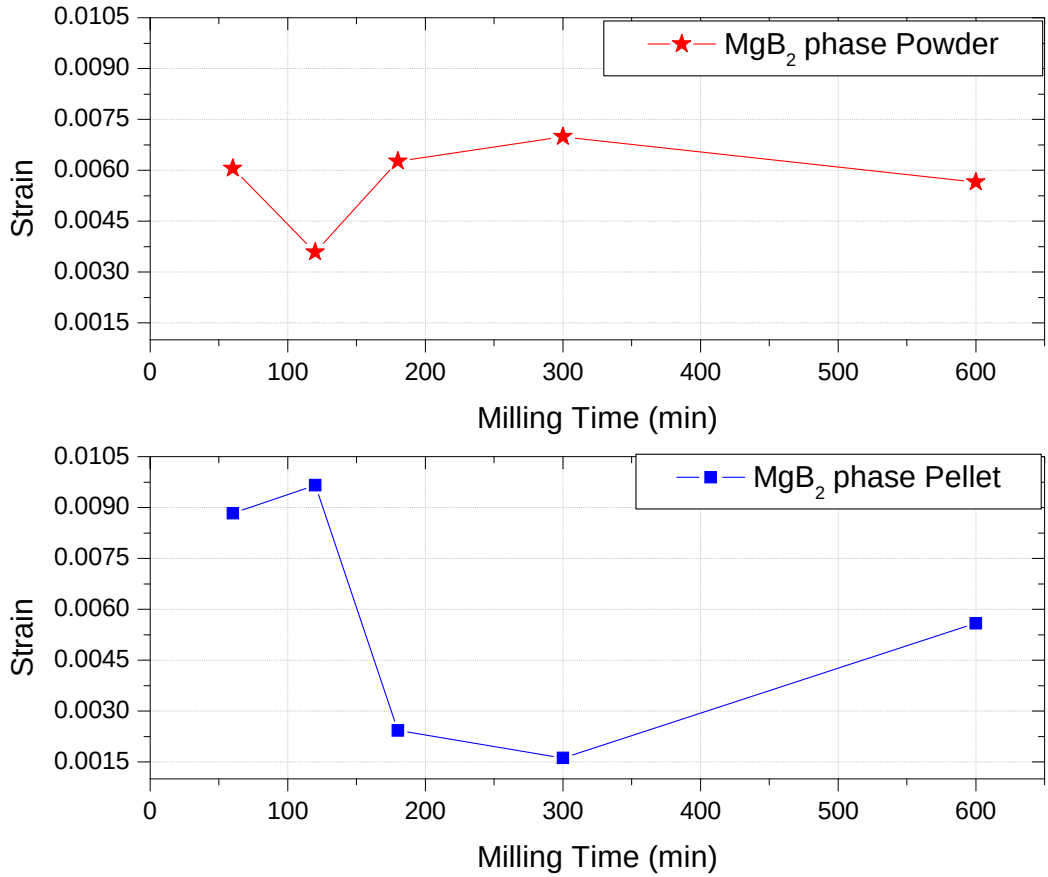

Figure 4.13. Strain of MgB_2 phase for powder and pellet material in function of milling time.

The lattice parameters for MgB_2 – 5 at.% TaB_2 material pre-milled, milled and pelletized is shown in **Figure 4.14**. The a-axis lattice parameter increased from 0 to 60 min of milling time and after decreased in 120 min showing an almost constant value between 120 and 600 min. The final value in a-axis was smaller than the initial value. The c-axis decreased between 0 and 60 min of milling time and in 120 min reached almost the initial value, having a low increase until 600 min of milling time.

The lattice parameter for MgB_2 – 5 at.% TaB_2 material milled and pelletized reported by [36] is shown in **Figure 4.15.** The a-axis decreased from 0 to 60 min of milling time, between 60 and

300 min the a-axis increased and between 300 min and 600 min the a-axis remain constant, with a smaller value than the initial one. The c-axis increased between 0 and 120 min of milling time, and decreased between 120 min and 600 min. The final value in c-axis was smaller than the initial.

The high variation in the lattice parameter for both cases could be associated with the increase in the strain that is caused during the ball milling; however the HIP process decreased the strain with the reorganization of the structure and should take the material to the initial state or close to it.

The material reported in [36] and the studied in this thesis showed a high difference respect to the initial value, which besides to be associated with the strain related with the milling process, could also imply that there was an introduction of Ta in the MgB_2 lattice.

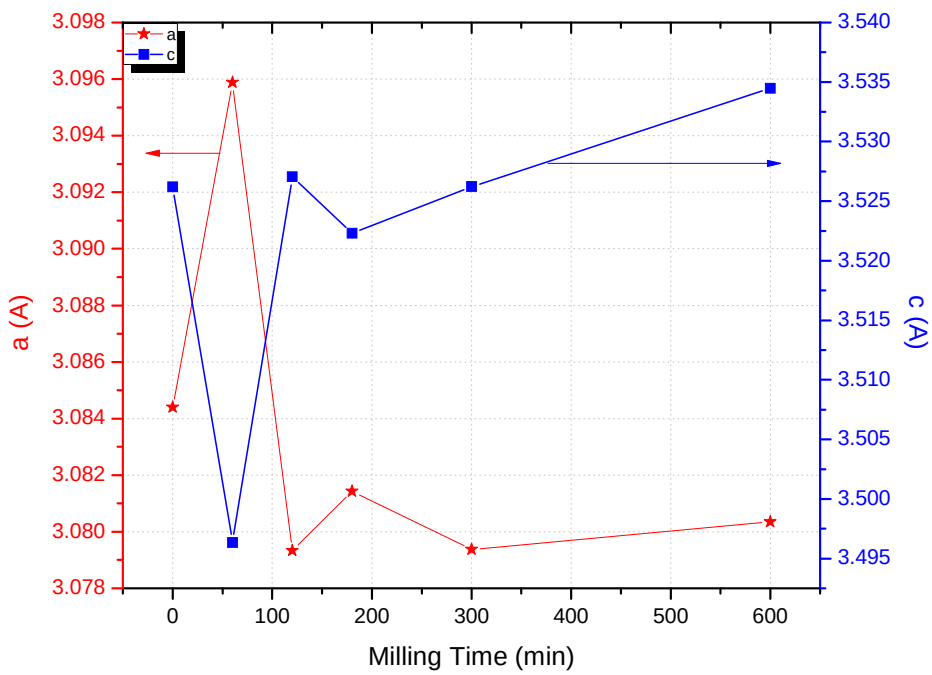

Figure 4.14. Lattice Parameter for MgB_2 – 5 at.% TaB_2 pelletized material pre-milled and milled at different milling times.

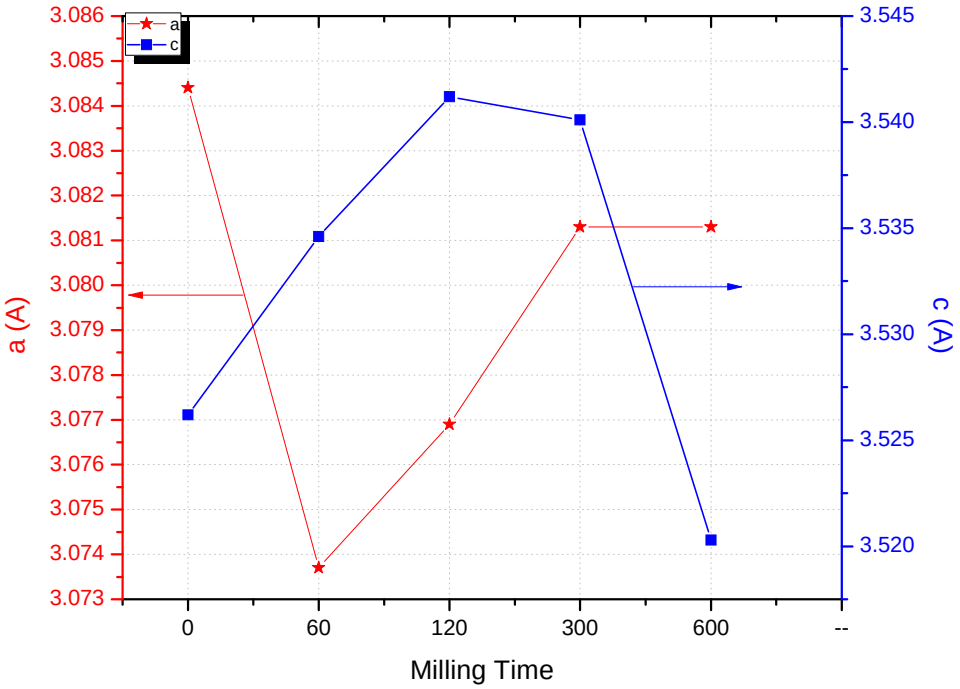

Figure 4.15. Lattice Parameter for MgB_2 – 5 at.% TaB_2 pelletized material ball milled at different times [36].

Table 4-II. Composition, lattice parameters, crystallite size and strain of ball milled samples at different milling times

Structural Characteristic for 5 at.% TaB_2 samples in Powder							
Sample	**Compound**	**Composition (wt. %)**	**Lattice Parameters**			**Crystallite Size (nm)**	**Strain**
			a(Å)	c(Å)	c/a		
60 min	TaB_2	6.5	3.096047	3.236487	1.045361	7.24	0.005839
	MgB_2	53.0	3.079238	3.521175	1.143522	15.83	0.006058
	MgO	0.8	4.234236	4.234236	1	4.74	0.004682
	B	39.8	4.810000	12.48439	2.595507	3.50	0.012507
120 min	TaB_2	7.3	3.103969	3.242780	1.04472	7.94	0.005432
	MgB_2	51.5	3.081755	3.537897	1.148014	10.53	0.003588
	MgO	14.0	4.158583	4.158583	1	3.50	0.009901
	B	27.2	4.863098	12.50477	2.571359	3.62	0.010673
180 min	TaB_2	9.1	3.094211	3.236556	1.046004	6.49	0.006337
	MgB_2	49.1	3.072461	3.535904	1.150838	7.47	0.006264
	MgO	5.9	4.211000	4.211000	1	25.74	0.008864
	B	35.9	4.855042	12.47000	2.568464	3.49	0.012134
300 min	TaB_2	6.2	3.096684	3.238975	1.045949	8.75	0.004197
	MgB_2	40.9	3.065891	3.539221	1.154386	6.53	0.006988
	MgO	0.3	4.111000	4.111000	1	3.46	0.008013
	B	52.6	4.889762	12.63786	2.584555	3.09	0.006892
600 min	TaB_2	9.3	3.098849	3.238589	1.045094	8.65	0.004250
	MgB_2	61.2	3.069480	3.530503	1.150196	6.21	0.005652
	MgO	14.5	4.212717	4.212717	1	3.57	0.010086
	B	15	4.872780	12.48153	2.56148	3.65	0.012224

Table 4-IIII. Composition, lattice parameters, crystallite size and strain of ball milled samples at different milling times.

Structural Characteristic for 5 at.% TaB_2 samples in Pellets							
Sample	**Compound**	**Composition (wt. %)**	**Lattice Parameters**			**Crystallite Size (nm)**	**Strain**
			a(Å)	**c(Å)**	**c/a**		
MgB2 raw unmilled HIP*	MgB_2	92.2	3.0844	3.5262	1.143237	73.03	0.001098
	MgO	7.8	4.2242	-		19.47	0.001600
MgB_2 undoped premilled HIP	MgB_2	79.2	3.085226	3.526575	1.143052	32.76	0.001316
	MgO	17.5	4.215603	-	-	3.77	0.009647
	B	3.2	4.932873	12.57649	2.549526	5.10	0.006819
60 min	TaB_2	1.2	3.097877	3.227024	1.041689	99.76	0.000273
	MgB_2	58.6	3.095882	3.496332	1.129349	3.56	0.008833
	MgO	16.7	4.117762	-	-	3.71	0.007453
	B	23.4	4.981397	12.47000	2.503314	3.59	0.013719
120 min	TaB_2	4.4	3.095380	3.283962	1.060924	43.39	0.003904
	MgB_2	87.4	3.079336	3.527056	1.145395	2.96	0.009661
	MgO	0.7	4.245050	-	-	12.85	0.005554
	Ta	0.2	3.293305	-	-	179.60	0.002740
	B	7.3	4.8100	12.50458	2.599705	2.98	0.009345
180 min	TaB_2	1.8	3.097881	3.229879	1.042609	19.36	0.001663
	MgB_2	34.2	3.081426	3.522296	1.143073	10.4	0.002423
	MgO	2.5	4.207085	-	-	27.94	0.000427
	B	61.6	4.819302	12.64754	2.624351	3.59	0.013657
300 min	TaB_2	5.4	3.073953	3.269979	1.06377	15.89	0.002374
	MgB_2	53.3	3.079377	3.526212	1.145106	20.48	0.001618
	MgO	12.7	4.160959	-	-	2.91	0.008836
	B	28.6	4.824685	12.65128	2.622198	3.16	0.010854
600 min	TaB_2	1.5	3.099292	3.225579	1.040747	52.29	0.000422
	MgB_2	46.1	3.080345	3.534473	1.147428	6.22	0.005588
	MgO	1.9	4.211034	-	-	45.34	0.000303
	B	50.5	4.900554	12.47772	2.546186	3.60	0.013576

* Sample processed by Rodrigues Junior, D. [8]

4.2. Superconducting Properties

The superconducting properties studied in this thesis were Hc_2, ρ and T_c.

The 5 at.% TaB_2 samples ball milled at different times are compare with the MgB_2 undoped Post-HIP material.

4.2.1. Critical Temperature (T_c)

The T_c variable is analyzed comparing the behavior of all doped materials with the undoped one. It is important to define if there is an increase or decrease in the critical temperature of the doped material and the subsequent analysis of Hc_2 to determine the changes in the superconducting and structural properties.

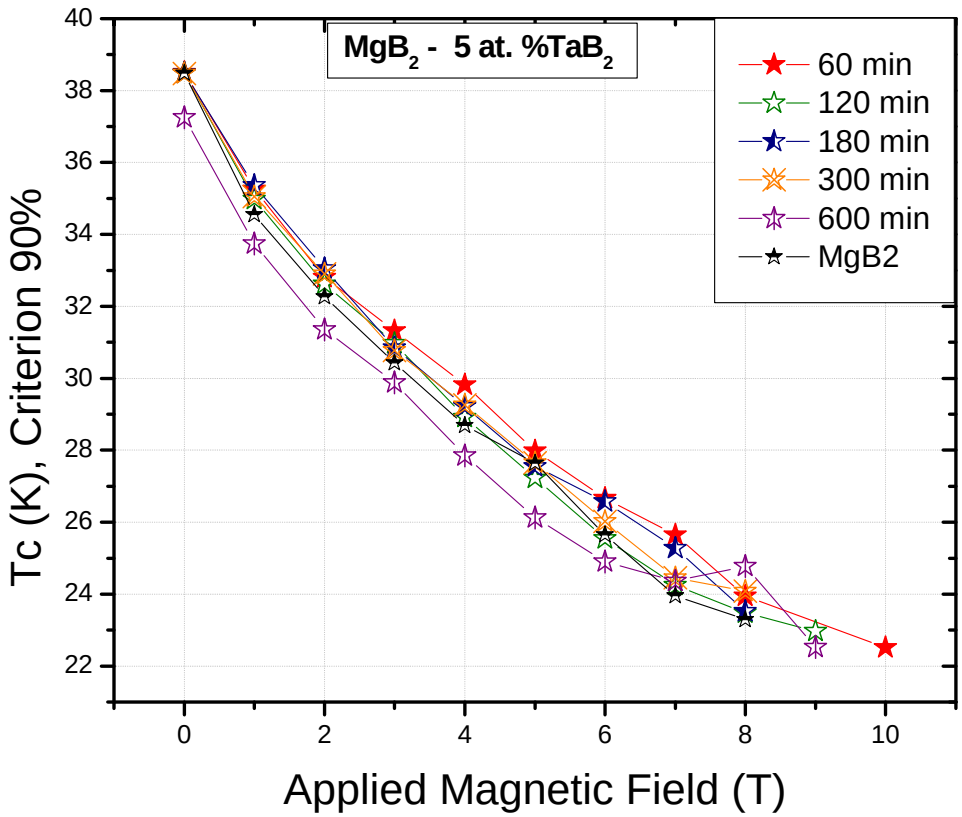

Figure 4.16. T_c Vs Applied Magnetic Field for TaB_2 5 at.% samples at different milling times and MgB_2 undoped.

In **Figure 4.16** is observed the closeness in cero field for T_c values in most of the samples, except for 600 min ball milled sample which has the lowest value between the milled materials. The T_c value at cero field is the maximum temperature which can be applied to the sample before it lost the superconducting state, the T_c values in function of milling time is shown in **Figure 4.17**. For the analyzed samples T_c is in the range between 38.47 K and 38.51 K for 60, 120, 180 and 300 min of milling time sample. These values are very close to the T_c of the MgB_2 undoped sample (38.49 K). The proximity of T_c values for 5 at.% TaB_2 samples and MgB_2 undoped Post-HIP sample shows that the dopant fraction and the experimental procedure applied to the described samples does not affect negatively the T_c in MgB_2 based materials.

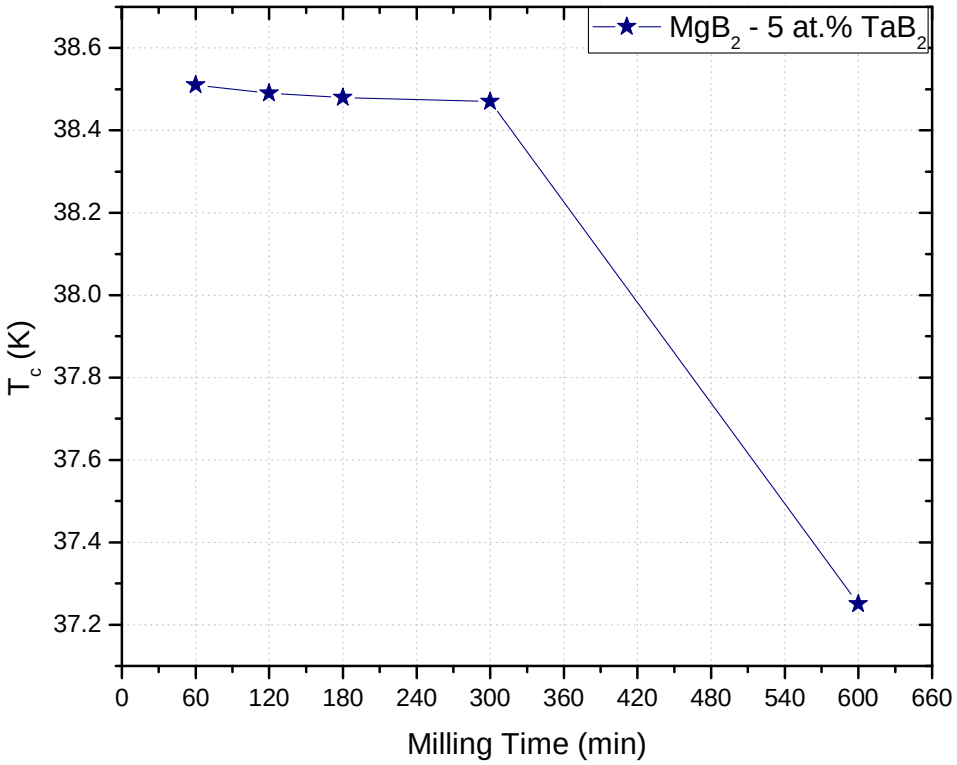

Figure 4.17. T_c Vs milling time for TaB_2 5 at.%

In researches previously reported, the T_c of the MgB_2 based material was decrease and in some cases significantly as result of the compounds used as dopants or because the experimental techniques. Senkowicz [34] used ball milled technique to doped MgB_2 based material with 4 at.% Carbon, he varies some conditions in his samples to compare the results; these variations were made in milling time, HIP time and HIP temperature. The undoped material shows a value for T_c of 36.2 K while the 4 at.% doped samples present reduction in T_c with all values less than 32.8 K. Karpinski *et al.* [33] conclude that the substitution of Al for Mg and C for B dope electrons to MgB_2, and that the decrease of T_c with C and Al doping has been attributed to σ hole-band filling. Carbon and aluminum electron dopants reduce the number of holes at the top of the σ band and both decrease T_c with a similar rate. The hole doping with Li also decrease T_c, but in much slower rate. Rodrigues [8] and Perez [36] obtained decreasing in T_c for the MgB_2 – 5 at.% TaB_2 300 min ball milled material with values of 37.5 K and 37.2 K respectively.

The T_c value for the MgB_2 undoped material in this work was lower than the theoretical reported (39 K), the reason could be the pre-milling applied on the sample or the contaminants found in it; Senkowicz *et al.* [32], conclude that MgB_2 is highly sensitive to atmospheric O_2 and CO_2 and that reaction with oxygen results in the formation of MgO and MgB_4 that could block current. However the value gets in this thesis for T_c in the MgB_2 undoped Post-HIP is in the range of the experimental material reported (38.49 K).

The T_c values for different milling time samples as well as the MgB_2 undoped sample are found in **Table 4.IV**

4.2.2. Critical Magnetic Field (Hc_2)

The Hc_2 variable represents the maximum field which can be applied to a material before it lost the superconducting state.

The Hc_2 was analyzed using the criterion of 90%. In **Figure 4.18** is shown the Hc_2 graph for different milling times (60, 120, 180, 300 and 600 minutes), compare with MgB_2 sample (Post-HIP, without milling).

The higher values in Hc_2 for low temperature were for 60 and 180 minutes milling times samples. The 600 minutes ball milled sample showed the smallest value for the Hc_2 in low temperature.

In middle temperature (25 K), the 180 minutes ball milled sample presented the highest value in Hc_2 (7.5 T) close to 60 minutes ball milled sample (7.09 T), these two samples showed higher values than the Hc_2 for the MgB_2 undoped Post-HIP sample (6.75 T).

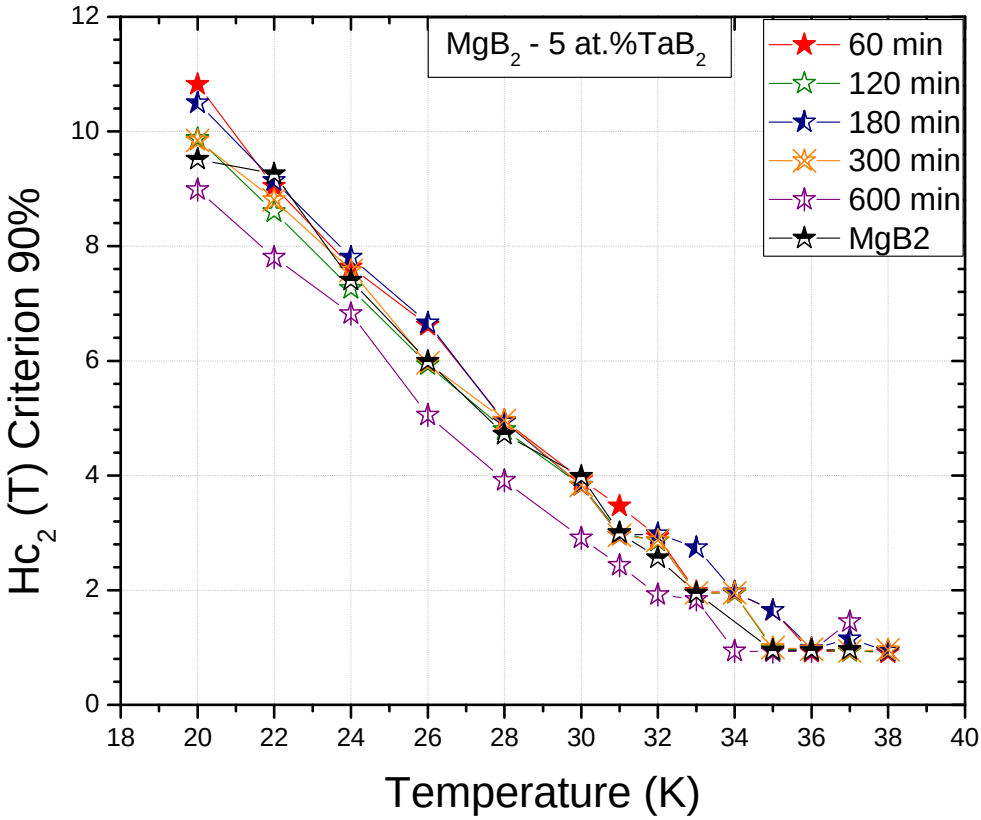

Figure 4.18. Hc_2 Vs Temperature for TaB_2 5 at.% samples at different milling times.

For higher temperatures (38 K) all samples showed similar values for Hc_2 between 0.91 T and 0.96 T with the higher for 300 minutes ball milled sample. The MgB_2 undoped Post-HIP material had a value of 0.99 T.

In **Figure 4.19** is graphed the Hc_2 values at 25 K Vs milling time, in this graph is observed the decreasing in Hc_2 when the milling time is increase until 10 hours, getting the smallest value for this variable. Between 1 hour and 5 hours of milling time, the values were close, but it was an important pick in three hours ball milling time which presents the higher value for Hc_2 between the milling samples. Moreover the three hours ball milled sample showed an increase in Hc_2 compare with the MgB_2 undoped material.

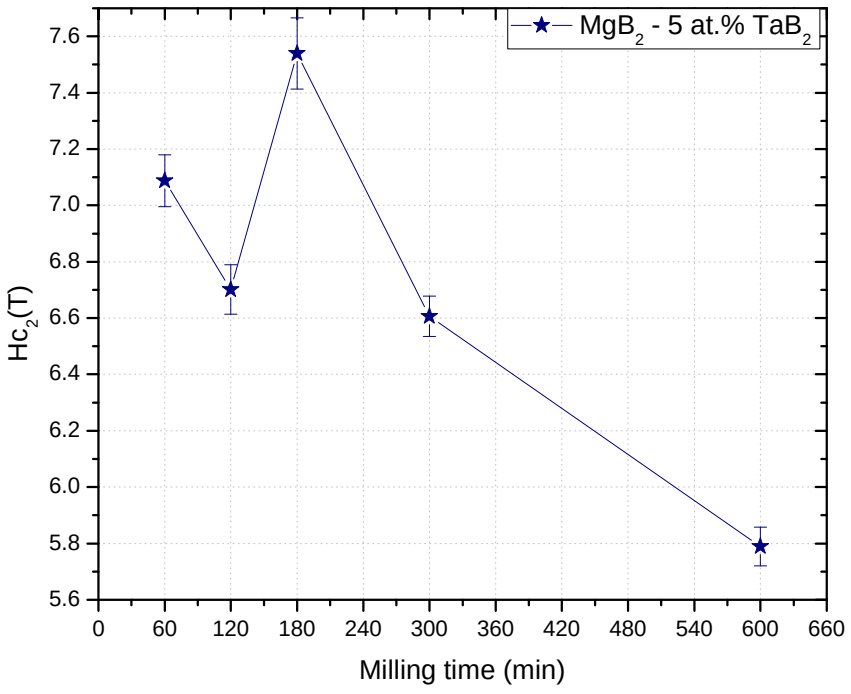

Figure 4.19. Hc_2 at 25K Vs milling time for TaB_2 5 at.%.

The 180 minutes ball milled sample had important results not only for the increase in Hc_2 (7.539 T) compare with the MgB_2 undoped Post-HIP sample (6.752 T), but also because the T_c (38.48 K) value remains constant and had not a decrease in this variable, which could amplify the range of applications in which this material could be used.

In similar experiments made before, the Hc_2 value had similar or less values than the found here, but they presented reduction in T_c. Senkowickz [34] doped MgB_2 based material with 4 at.% Carbon using high energy ball milling, the best result in Hc_2 (25 K) 7.37 T he found was to 1200 minutes of milling time, 900° of HIP temperature and 300 minutes of HIP time, and although this value in Hc_2 represents an increase compare with the undoped material which had a Hc_2 (25 K) value of 6.60 T, this sample shows a drastic decrease in T_c from 36.2 K (undoped sample) to 32.74 K. The Hc_2 values for different milling time samples as well as the MgB_2 undoped sample are found in **Table 4.IV**.

Table 4.IV. T_c and Hc_2 values for TaB_2 doped MgB_2 material and MgB_2 undoped sample.

Sample	T_c (K)	H_{c2} (25K) (T)
MgB_2 undoped	38.49	6.7518
60 min	38.51	7.0874
120 min	38.49	6.7012
180 min	38.48	7.539
300 min	38.47	6.6062
600 min	37.25	5.7895

4.2.3. Resistivity Analysis

Using the Rowell theory, it is possible to determine the connectivity in the sample, using an ideal resistivity value as a comparison ρ_{ideal} = 7.3 μΩ.cm, based on empirical measurements of MgB_2 undoped samples thought to be fully connected.With this theoretical value is possible to find the experimental value,

$$A_F = \rho_{ideal}/[\rho(300K) - \rho(40K)] \tag{4.8}$$

The A_F value indicates the percentage of the transversal area for which the current pass and that is effectively connected in the sample. Then, the adjust resistivity ρ_A (T) is given by:

$$\rho_A(T) = A_F\rho(T) \tag{4.9}$$

Which represents the true residual resistivity of the fully connected portion of the sample.

The 5 at.% TaB_2 samples were analyzed using the Rowell theory. The ρ(300K), ρ(40K), A_F, ρ_A and RRR are shown in **Table 4.V**.

Table 4.V. Resistivity measurements for TaB_2 samples.

Sample	ρ_{300K} (μΩ.cm)	ρ_{40K} (μΩ.cm)	RRR (ρ_{300K}/ ρ_{40K})	ρ_{300K} - ρ_{40K} (μΩ.cm)	A_F	ρ_A (40K) (μΩ.cm)
MgB_2 undoped	15.48	4.01	3.86	11.48	0.64	2.55
60 min	41.85	13.97	3.00	27.88	0.26	3.66
120 min	27.70	8.93	3.10	18.77	0.39	3.47
180 min	28.59	9.57	2.99	19.02	0.38	3.67
300 min	25.11	9.10	2.76	16.00	0.46	4.15
600 min	27.69	13.48	2.05	14.21	0.51	6.93

In **Figure 4.20** is graphed the A_F values Vs milling time for 5 at.% TaB_2 samples. The highest A_F value was for MgB_2 undoped material (0.64), the lowest values was for 1 hour ball milled sample with 0.26. The A_F values increase while the milling time increase, the highest value for the milled samples was for 10 hours with 0.51, which following the Rowell's theory indicates that this sample is connected in a more effective way than the others, but in **Figure 4.21** is observed the decreasing of Hc_2 with the increasing in A_F, however, the Hc_2 property is directly related with the connectivity in the sample; this result could indicate then, that for TaB_2 5 at.% doped this theory could not be applied. Analyzing the effect of the applied field in the sample, it is known that the field can penetrates some areas where exists impurities or big particles, areas which lose the superconducting state before the rest of the sample creating a flux which decrease the conductivity. For a well connected sample this areas are smaller and the critical magnetic field supported for the sample is higher than for not well connected samples. Moreover, for a well connected sample there will be more areas to flow electrons with less scattering and the resistivity will be then smaller. The critical magnetic field will increase its value for a well connected sample which will generates an internal magnetic field bigger for a bigger current flowing inside the superconductor. The Rowell could not be the appropriate model to be applied in this doping, considering that this model was made for MgB_2 pure dense sample and could require some adaptations to apply in doped samples.

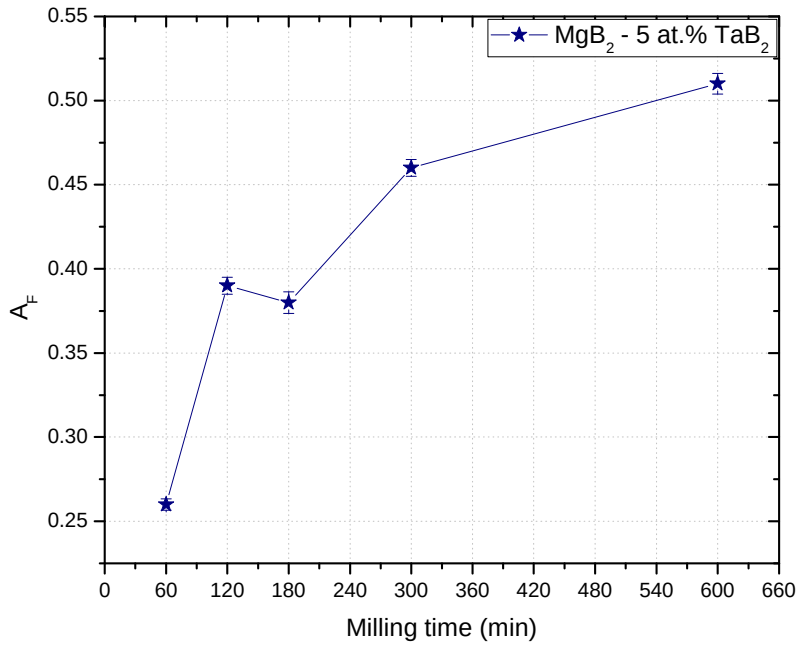

Figure 4.20. A_F Vs milling time for TaB_2 5 at.%

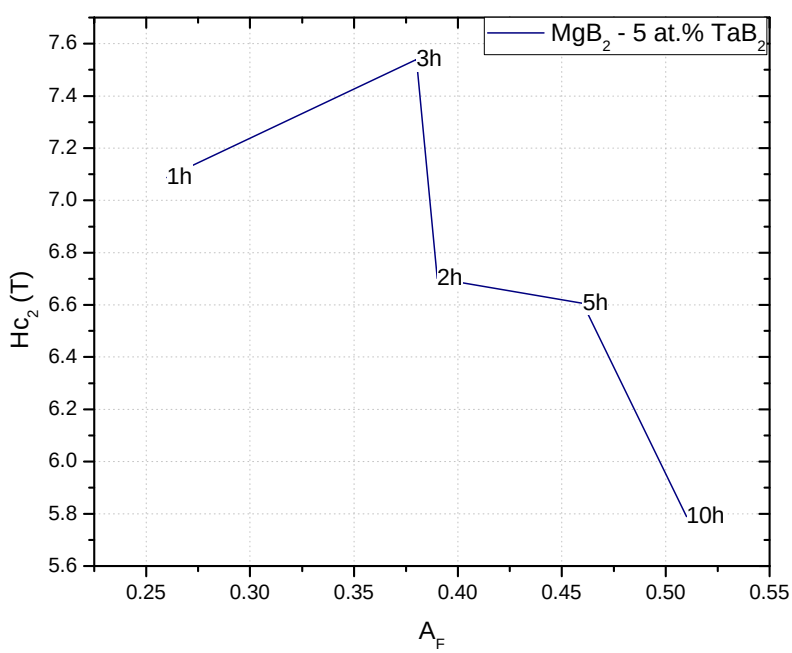

Figure 4.21. Hc_2 Vs A_F for TaB_2 5 at.%.

The residual resistivity ratio (RRR) is a measure of the defect scattering, while defect scattering increase, the RRR decreases, approaching to 1 for very high defect concentrations [34].

Increase in RRR is generally taken to signify less electron scattering from compositional and microstructural sources, independent of connectivity.

It is important to consider that RRR of nanoparticles appears to be much smaller than the measure for the high density bulk polycrystalline MgB_2. It is likely that the small size of the nanoparticles with more crystallite boundaries and the existence of the remaining Mg impurity at grain boundaries will deteriorate the inter-grain connectivity. So the corresponding resistance force during the current transport process will be increased, whereas the overall critical current density (J_c) cannot be decreased [43].

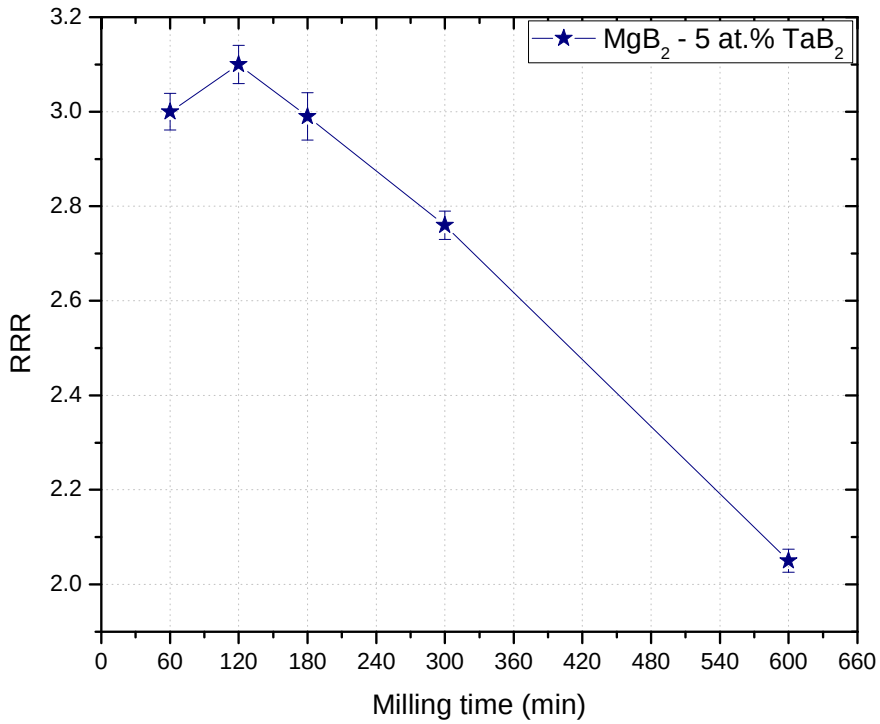

Figure 4.22. RRR Vs milling time for TaB_2 5 at.%

The RRR in TaB_2 doped MgB_2 samples showed a tendency to decrease with the increase in the milling time (**Figure 4.22**); however between one hour and three hours the RRR values were almost constant; between 2.99 and 3.10. The higher value in RRR was shown for MgB_2 undoped with 3.86.

In **Figure 4.23** is shown the relation between Hc_2 and RRR; with the increase in RRR is observed an increase in Hc_2 until reach a maximum value which corresponds to three hours ball milling. After this pick, the Hc_2 values decrease for 1 and 2 hours ball milling, although the 1, 2 and 3 hours ball milling present close values in RRR.

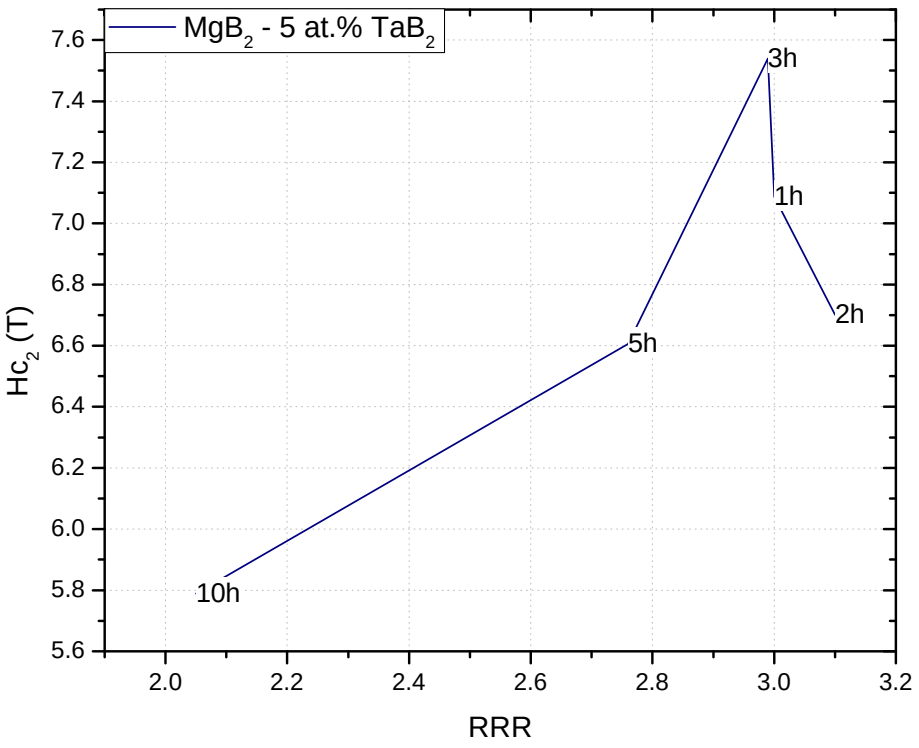

Figure 4.23. Hc_2 at 25 K Vs RRR for TaB_2 5 at.% samples at different milling times

The values reported by Senkowicz *et al.* [26] in RRR for MgB_2 – 4 at.% C in samples between 1 and 3000 min of milling, varied from 2.36 to 1.15, decreasing with the increasing of milling time, the value in RRR for the 300 min ball milled sample was 1.44. Rodrigues [8] obtained in the RRR property a value of 2.34 for the MgB_2 – 5 at.% TaB_2 ball milled at 300 min. The value obtained in this work for the MgB_2 – 5 at.% TaB_2 300 min ball milled sample was 2.76, which indicates a higher value than the reported by Senkowicz *et al.* [26] and Rodrigues [8], which indicates that the sample studied in this thesis had less electron scattering for compositional and microestructural sources.

5. Effect of 5 at.% NbB_2 in the Superconducting and Structural Properties of MgB_2

The superconducting properties of doped MgB_2 materials have widely studied using different synthesis techniques.

NbB_2 shows the hexagonal C32-type structure. Some of the thermal properties include formation enthalpy ($-\Delta H^0_{f298}$) of 41.9 kcal/mole, melting enthalpy ($\Delta H_{melting}$) of 22.84 kcal/mole and melting temperature of 3000°C.

To effectuate the doping of MgB_2 with NbB_2, HEBM was used to carry out pre-milling of the two compounds first. This was necessary to ensure that they were equally reduced to similar crystallite sizes, and activated similarly which would subsequently ensure better dissolution or inter-mixing with further ball milling of their appropriate mixtures. The MgB_2 - 5 at.% NbB_2 mixture were then ball milled for 60, 120, 180, 300 and 600 min respectively.

The milled powder mixtures were annealed at a temperature of 1000°C and a pressure of 30000 psi, after which the pellet samples were characterized.

To help verify the doping process and eventual contribution to properties enhancement, both the powder materials and the corresponding pelletized counterparts were characterized similar with XRD, resistivity, and SQUID measurement.

5.1. Structural Properties

In **Figure 5.1** is shown the XRD spectrum of MgB_2 5 at.% NbB_2 samples milled at different times. The peaks found corresponded with NbB_2 and MgB_2 single phases in addition to the characteristic peaks of B, MgO, and Si phases. The presence of B element in the samples indicated that either one or both compounds, i.e., MgB_2 and NbB_2, decomposed to Mg and B or Nb and B. Moreover, the presence of MgO showed that the MgB_2 compound reactsed with Oxygen to form MgO.

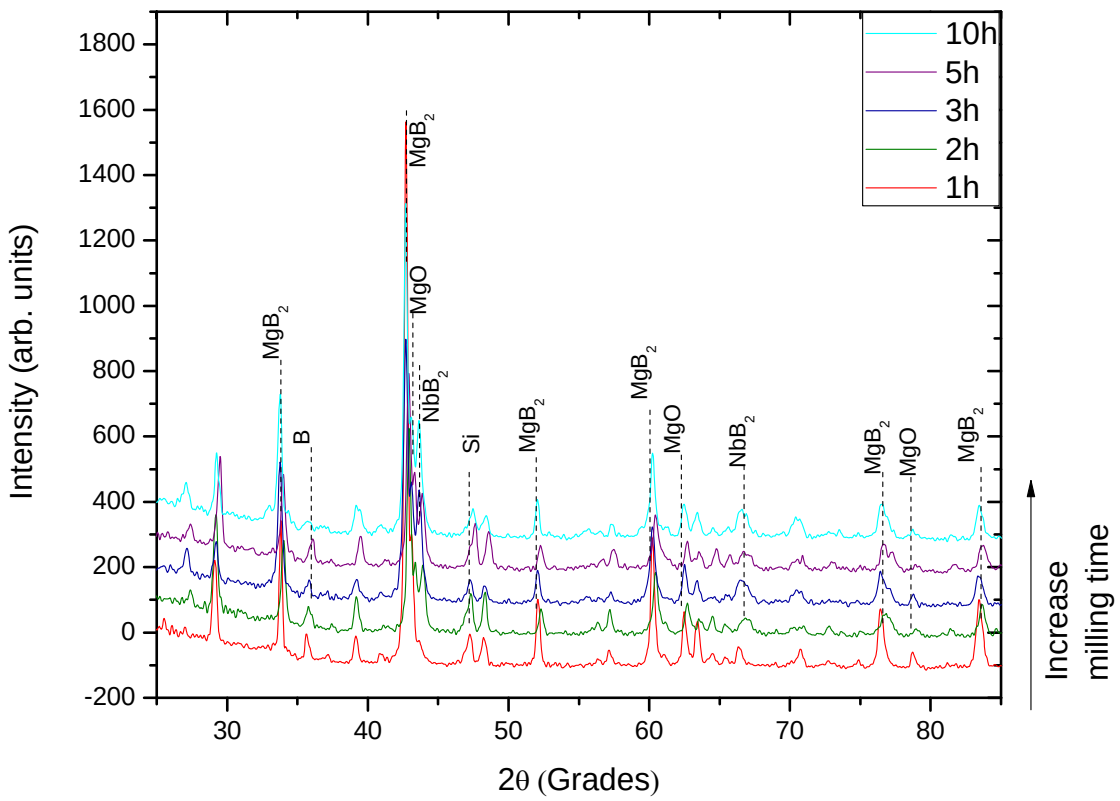

Figure 5.1. X ray diffraction spectra of 5 at.% NbB_2 doped MgB_2 as a function of increasing ball milling times.

The presence of Si peaks was observed as indicated in **Figure 5.1** and **Figure 5.2**. It is possible that Si contamination occurred during the hot isostatic process possibly with the welding and cutting operation associated with the stainless steel tube handing.

The analysis focused in the identification of MgB_2, NbB_2, B, MgO, WC, Mg, Nb and MgB_4 phases, however, only the last four phases were not observed in the spectra.

The spectra of the ball milled materials displayed the presence of peaks that would not be attributed to either MgB_2 or NbB_2, or their others derivative of them. These unidentified peaks were marked "UNK" in the corresponding spectra.

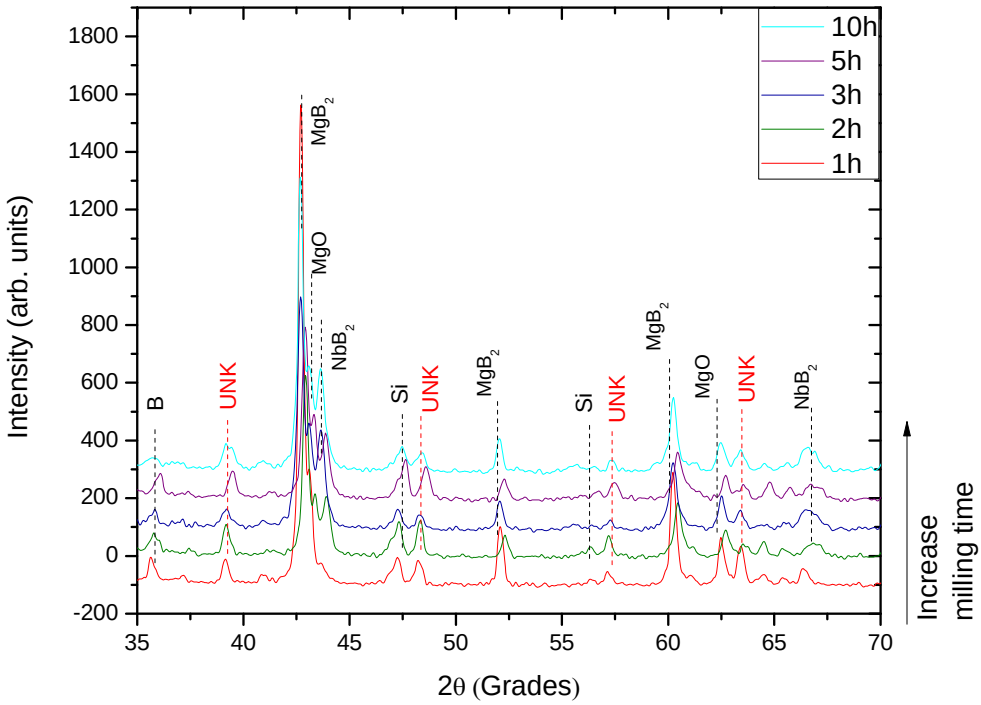

Figure 5.2. X ray diffraction spectra of 5 at.% NbB_2 doped MgB_2 as a function of increasing ball milling times. Zoom of 2θ between 35° and 70°.

Figure 5.3 shows the EDS of the MgB_2 - NbB_2 5 at.% doped material after two hours of ball milled. The presence of peaks corresponding to Nb, Mg, B, O and C showed that there were contaminations. The presence of the first four elements were found also in the XRD spectra except for the C element. It is possible that the small fraction of C observed could have originated from WC grinding materials used in the ball milling.

The SEM of the powder materials MgB_2 – NbB_2 5 at.% corresponding to two hours of ball milling is shown in **Figure 5.4.**

The micrograph shows the evidence of two contrasts corresponding to the base compound, MgB_2 and the NbB_2 dopant compound respectively. The bright contrast regions correspond to the dopant phase NbB_2 while the dark contrast regions correspond to the matrix MgB_2 phase.

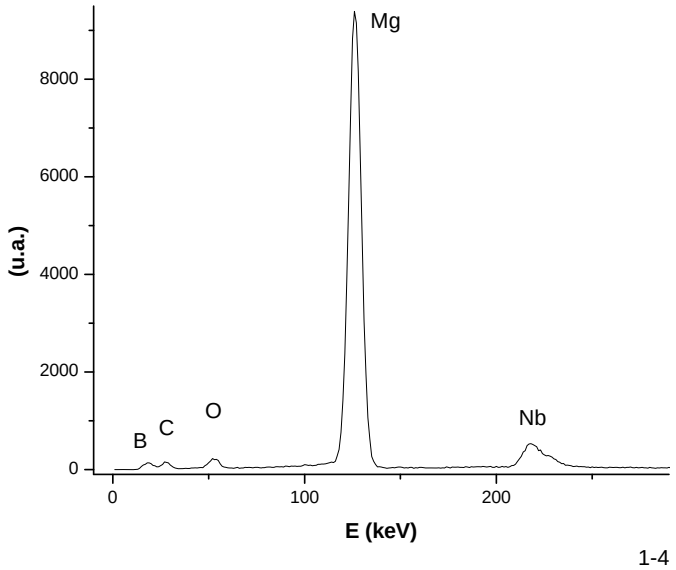

Figure 5.3. MgB_2 – 5 at.% NbB_2 doped sample corresponding to 2 hours of ball milling.

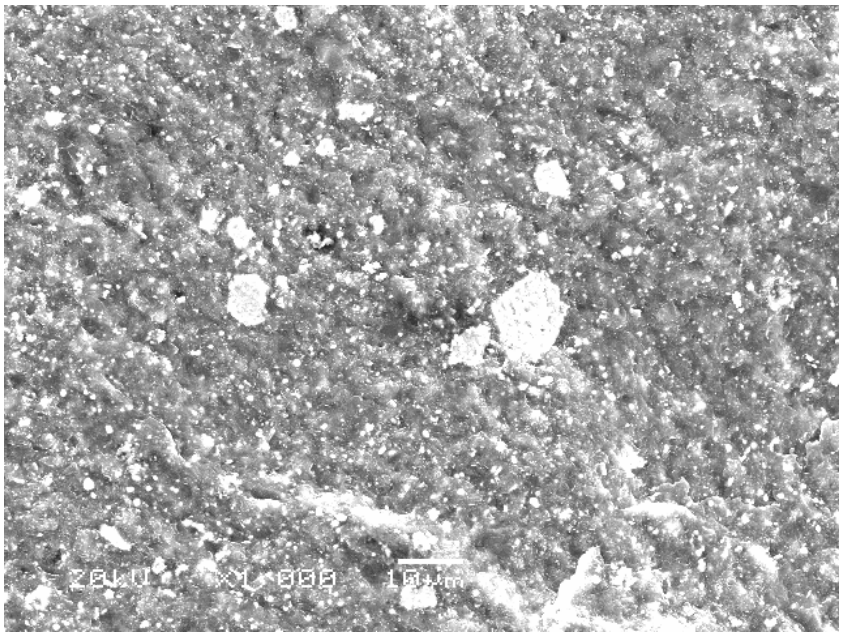

Figure 5.4. Scanning Electron Micrograph (SEM) of two hours ball milled 5 at.% NbB_2 doped MgB_2 material after HIPing

The detailed analysis for the composition, crystallite size, strain and lattice parameters for he powder materials are shown in **Table 5.I**, in comparison to the corresponding values for the pelletized materials in **Table 5.II**.

The compositional analyses of the powder and pelletized material are shown in **Figure 5.5** and **Figure 5.6** respectively as a function of different milling times. The composition in both cases presents some differences that could show the effect of the pressure and temperature in the final state of the sample.

The analyses of the powder material revealed a composition of MgB_2 between 57.1 wt.% and 73 wt.%. In pellet material the composition for MgB_2 was smaller, with values ranging between 35.6 wt.% and 71.5 wt.%. The values for B in powder material were between 15.9 wt.% and 28.8 wt.%, while the composition of B in pellets was higher with values between 16.0 wt.% and 53.2 wt.%. These results indicate the possibility of a higher decomposition of MgB_2 in Mg and B during the HIP process, which would be the reason for the decreased amount of MgB_2 phase with the increase of the B phase present in the samples.

Even though the decomposition of MgB_2 was perceived, Mg was not found as element in the powder or pellet samples, and the further percentage of MgO did not change significantly between powder and pellet samples, which could indicate the possibility of formation of a new phase that could have contained Mg and other elements as Nb, giving as result new peaks in the XRD spectrum as we found in the samples.

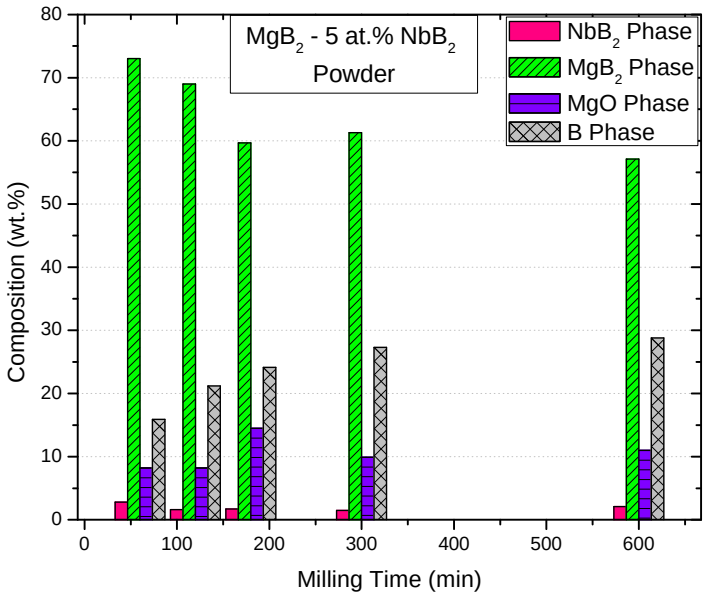

Figure 5.5. Composition of NbB_2, MgB_2, MgO and B phases for powder material as a function of ball milling time

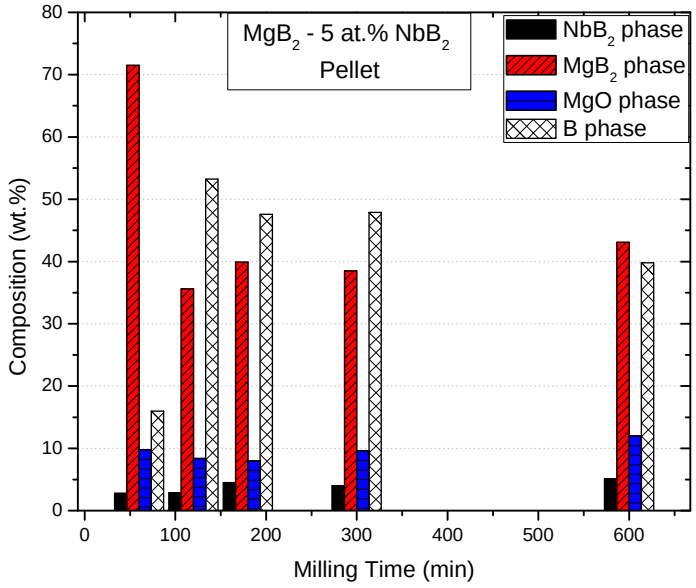

Figure 5.6. Composition of NbB_2, MgB_2, MgO and B phases, for pellet post HIP material in function of milling time.

Between the characteristics of ball milling process is the significant reduction in crystallite and particle size. The crystallite size of MgB_2 as received from Alfa Aesar was 97 nm, reported by Senkowicz. For the MgB_2 - NbB_2 5 at.% doped material, the smallest crystallite size reached with the HEBM technique, for the MgB_2 phase powder was 6.98 nm after 10 hours of ball milling. The higher crystallite size between the milled samples for the powder materials was 12.26 nm corresponding to the 1 hour ball milled materials. For the NbB_2 phase the range in the crystallite size for the powder materials was between 2.95 nm and 12.24 nm.

Figure 5.7 shows the graph of crystallite size for the different milling times in the NbB_2 phase for powder and pellet materials. For the powder material between 60 and 180 min of milling time the crystallite sizes increased, while between 180 and 600 min of milling time the crystallite size decreased. Comparing the crystallite size for powder and pellet materials, the further showed increasing compared with its powder counterpart between 4 nm and 27 nm.

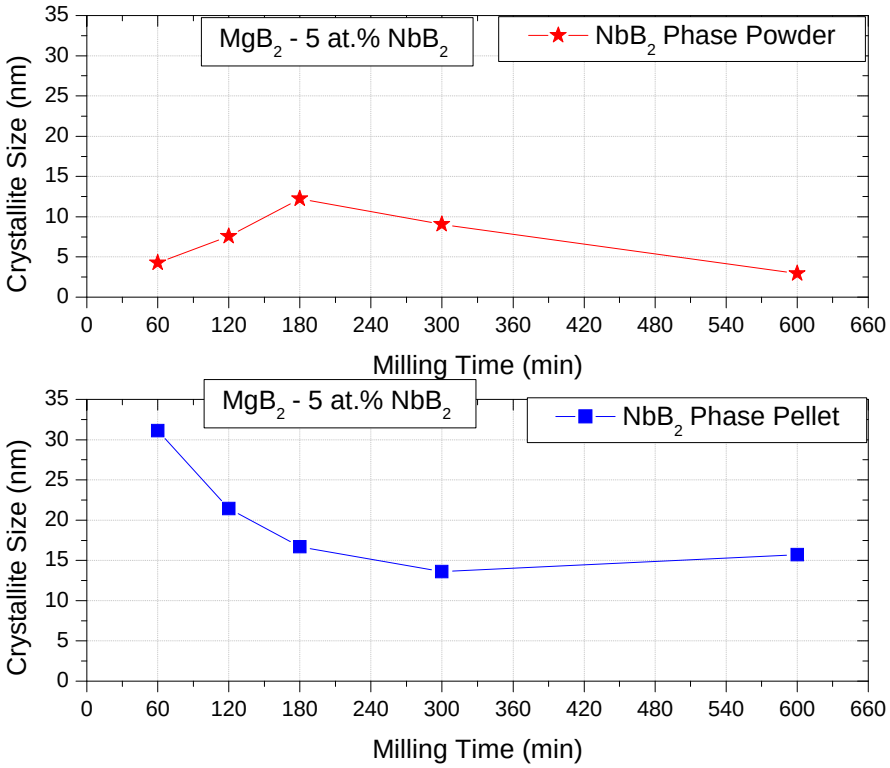

Figure 5.7. Crystallite size variation of NbB_2 phase for the powder and pellet form as a function of milling time.

The crystallite size for MgB_2 phase in MgB_2 - 5 at.% NbB_2 material in powder and pellet is shown in **Figure 5.8**. For powder material the crystallite sizes values were close between the different samples, with values smaller than 13 nm. The smallest crystallite size was for 10 hours ball milled sample.

For the case of the pellet material it was observed an increasing tendency in crystallite sizes compared with its powder counterpart; the crystallite size was in a range between 20.35 nm and 61.58 nm, the range of crystallite size increasing from powder to pellet was between 11 nm and 49 nm.

During the HIPing process, pressure and temperature were applied to the MgB_2 – 5 at.% NbB_2 doped material which cause the increment in crystallite size observed for MgB_2 and NbB_2 phases.

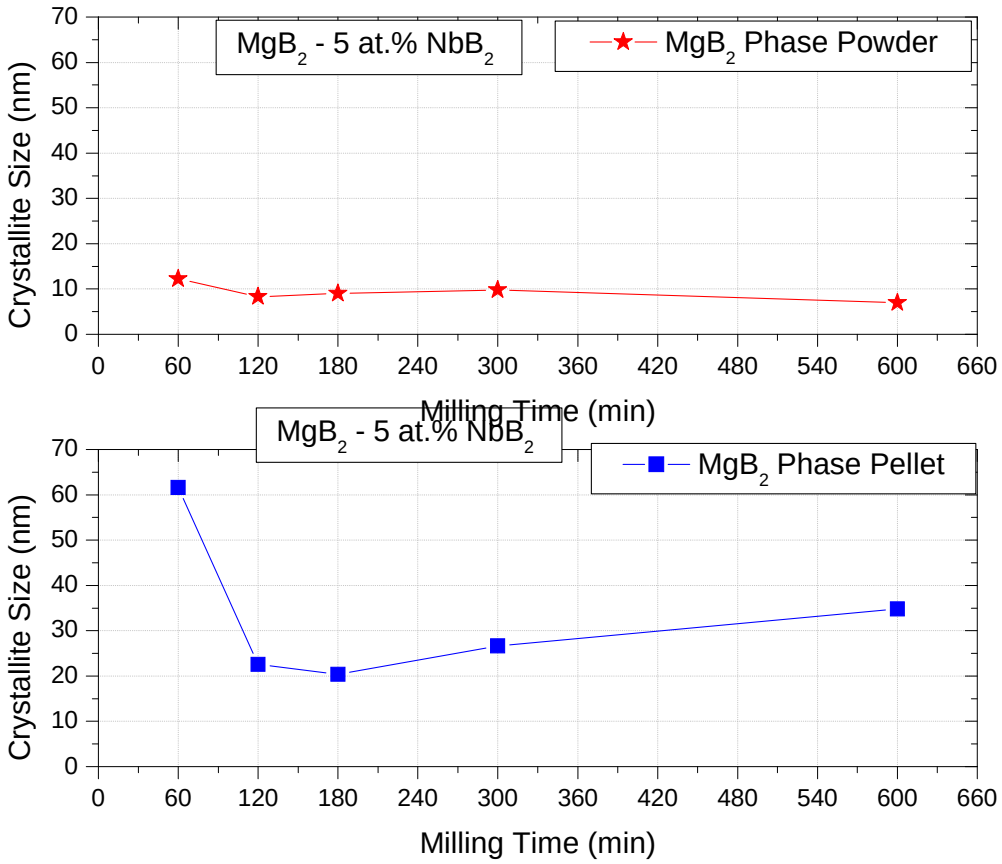

Figure 5.8. Crystallite size variation of MgB_2 phase for the powder and pellet form as a function of milling time.

The samples after the milling process were in a metastable state because of the high milling energy that decreased the crystallite size and increased the strain. The pressure and temperature applied to the sample in the HIPing process generated the changing from the metastable state to a stable with the agglomeration of the crystallites.

The strain for NbB_2 phase in MgB_2 – 5 at.% NbB_2 material at different milling times for powder and pellets is observed in **Figure 5.9**. The strain values for powder were between 0.0030 and 0.0094 with a tendency to increase between 120 min and 600 min. The values in strain for all milling time samples decrease with the HIP process, for which the pellet materials had smallest values in strain than their respective powder material, although the decreasing range is not constant for the different samples.

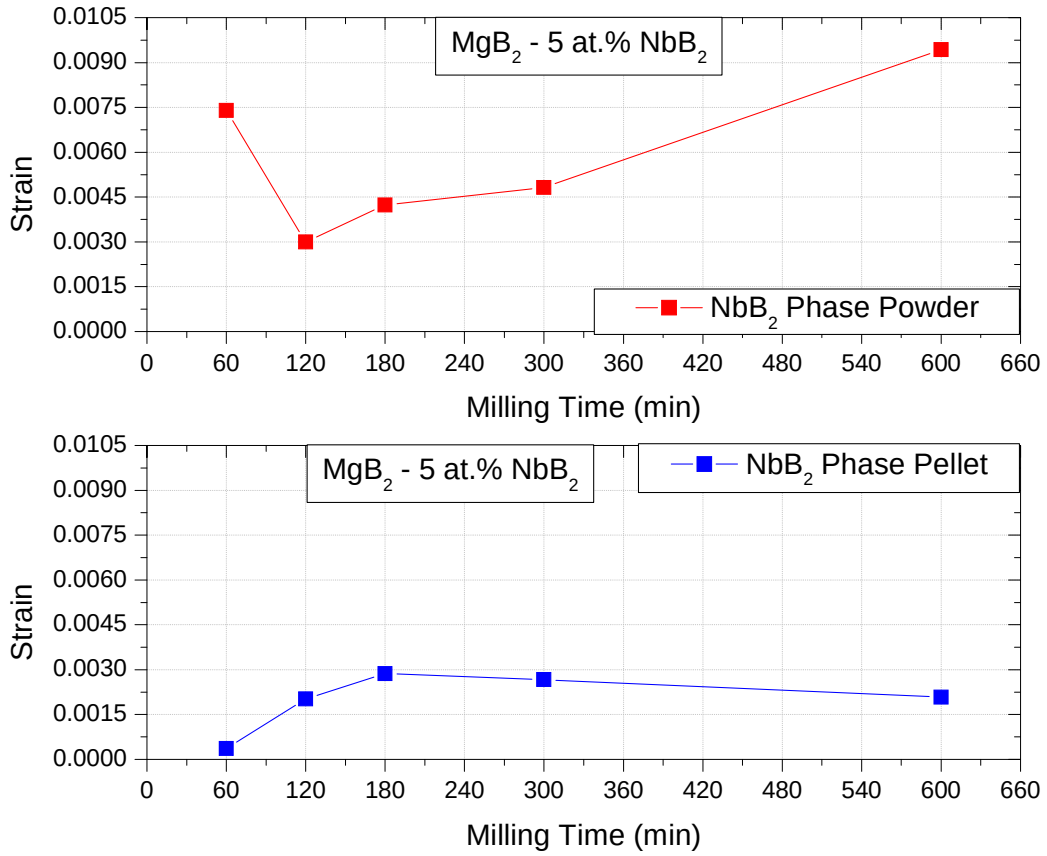

Figure 5.9. Comparison of the average strain of NbB_2 phase in the powder and pellet forms.

For the MgB_2 phase in the MgB_2 - 5 at.% NbB_2 material, the strain values decreased from powder to pellet with a similar tendency between 60 and 300 min which can be observed in **Figure 5.10**. The values in strain for powder material were between 0.0011 and 0.0060, while the respective values in strain for pellet material were between 0.000511 and 0.002044. Although in all cases the values in pellet were smaller than in powder, the range of decreasing was very variable between the different samples.

The higher strain in powder materials and the lower strain in pellet materials were a consequence of the synthesis process. The high energy impacts that were applied to the powder during the ball milling caused in the sample the change in the structure generating an increase in the strain, then after the HEBM process the poweder was in a metastable state. The temperature applied during the HIPing process reorganized the structure decreasing the strain and reaches a stable state.

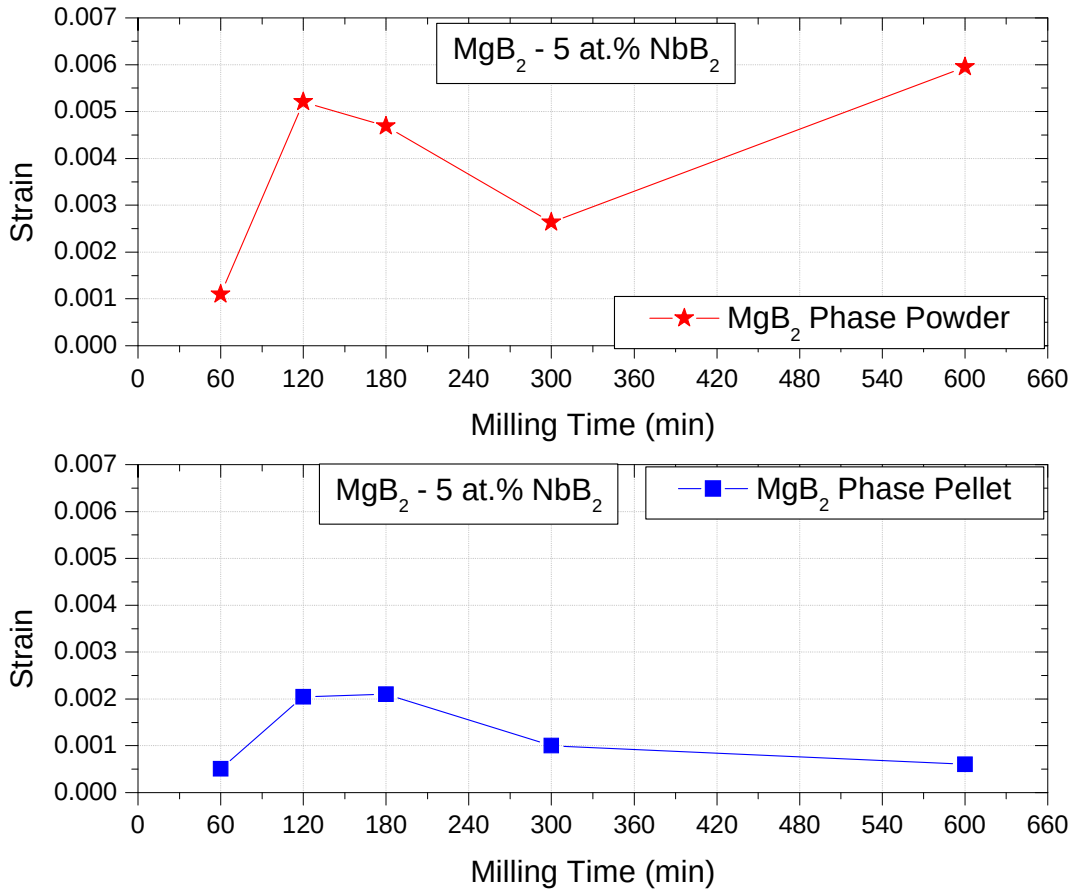

Figure 5.10. Comparison of the average strain of MgB_2 phase in the powder and pellet forms.

Table 5.I. Composition, lattice parameters, crystallite size and strain of NbB_2 5 at.% material in powder ball milled at different milling times.

NbB_2 5 at.% Powder Samples at Different Milling Times							
Sample	**Compound**	**Composition (wt. %)**	**Lattice Parameters**			**Crystallite Size (nm)**	**Strain**
			a(Å)	**c(Å)**	**c/a**		
60 min	NbB_2	2.8	3.084347	3.420614	1.109024	4.29	0.007398
	MgB_2	73.0	3.085491	3.527700	1.143319	12.26	0.001097
	MgO	8.2	4.229028		1	5.03	0.007133
	B	15.9	4.909272	12.49468	2.545119	3.94	0.012703
120 min	NbB_2	1.6	3.044941	3.421000	1.123503	7.56	0.003001
	MgB_2	69	3.081835	3.524569	1.143659	8.32	0.005206
	MgO	8.2	4.214833	4.214833	1	9.53	0.002357
	B	21.2	4.861851	12.61885	2.595483	3.48	0.012532
180 min	NbB_2	1.7	3.075054	3.421000	1.112501	12.24	0.004233
	MgB_2	59.7	3.084110	3.521249	1.141739	9.02	0.004688
	MgO	14.5	4.238409	4.238409	1	5.49	0.005878
	B	24.1	4.810000	12.47000	2.592516	3.79	0.012876
300 min	NbB_2	1.5	3.067899	3.421000	1.115095	9.05	0.004818
	MgB_2	61.3	3.085108	3.530445	1.144351	9.77	0.002637
	MgO	9.9	4.226015	4.226015	1	10.22	0.004776
	B	27.3	4.816941	12.56656	2.608826	3.62	0.013486
600 min	NbB_2	2.1	3.058786	3.409898	1.114788	2.95	0.009435
	MgB_2	58.1	3.084570	3.532965	1.145367	6.98	0.005950
	MgO	11.0	4.230742	4.230742	1	4.36	0.006278
	B	28.8	4.886127	12.61487	2.581773	2.98	0.009941

Table 5.II. Composition, lattice parameters, crystallite size and strain of NbB_2 5 at.% material in pellet ball milled at different milling times

NbB_2 5 at.% Pellet Samples at Different Milling Times							
Sample	**Compound**	**Composition (wt. %)**	**Lattice Parameters**			**Crystallite Size (nm)**	**Strain**
			a(Å)	**c(Å)**	**c/a**		
MgB2 raw unmilled HIP*	MgB_2	92.2	3.0844	3.5262	1.143237	73.03	0.001098
	MgO	7.8	4.2242	4.2242	1	19.47	0.001600
MgB_2 undoped premilled HIP	MgB_2	79.2	3.085226	3.526575	1.143052	32.76	0.001316
	MgO	17.5	4.215603	4.215603	1	3.77	0.009647
	B	3.2	4.932873	12.57649	2.549526	5.10	0.006819
60 min	NbB_2	2.8	3.108508	3.310121	1.064858	31.13	0.000361
	MgB_2	71.5	3.083603	3.519419	1.141333	61.58	0.000511
	MgO	9.8	4.220410	4.220410	1	20.67	0.004175
	B	16.0	4.910000	12.57000	2.560081	3.52	0.012309
120 min	NbB_2	2.9	3.096413	3.316938	1.07122	21.43	0.002021
	MgB_2	35.6	3.086186	3.532845	1.144728	22.59	0.002044
	MgO	8.4	4.220362	4.220362	1	20.27	0.000386
	B	53.2	4.810000	12.47000	2.592516	3.52	0.009023
180 min	NbB_2	4.5	3.088814	3.315223	1.0733	16.69	0.002871
	MgB_2	39.9	3.080162	3.525449	1.144566	20.35	0.002103
	MgO	8.0	4.213311	4.213311	1	43.10	0.002345
	B	47.6	4.810000	12.47000	2.592516	2.98	0.009816
300 min	NbB_2	4.0	3.094925	3.328151	1.075358	13.60	0.002670
	MgB_2	38.5	3.081704	3.525287	1.143941	26.68	0.001004
	MgO	9.6	4.232568	4.232568	1	4.35	0.008462
	B	47.9	4.888026	12.55064	2.56763	2.98	0.009924
600 min	NbB_2	5.1	3.093710	3.321228	1.073542	15.72	0.002082
	MgB_2	43.1	3.079944	3.524339	1.144287	34.83	0.000606
	MgO	12.0	4.215665	4.215665	1	4.34	0.008435
	B	39.8	4.854836	12.47000	2.568573	2.98	0.009253

5.2. Superconducting Properties: Resistivity Measurements

The superconducting properties T_c and Hc_2 were determined for the MgB_2 - 5 at.% NbB_2 doped material compound at different milling times. The analysis of superconducting properties in the ball milled NbB_2 doped materials was used to establish the influence of the processing (milling and HIPing) of the doped material in the superconducting behavior of the MgB_2 materials, which could indicate the viability of this dopant for future considerations in the enhancement of MgB_2 superconducting properties.

Table 5.III has the values of T_c and Hc_2 (25 K) for NbB_2 5 at.% samples at different milling times.

Table 5.III. T_c and Hc_2 values for NbB_2 doped MgB_2 material and MgB_2 undoped sample.

Sample	T_c (K)	H_{c2} (25K) (T)
MgB_2 Undoped	38.49	6.7518
60 min	38.47	6.775
120 min	38.47	6.7476
180 min	38.19	6.4458
300 min	38.45	6.8193
600 min	37.48	5.9583

5.2.1. Critical Temperature (T_c)

The critical temperature is the value below which a material maintains its superconducting behavior. The T_c of NbB_2 5 at.% samples were determined using the resistivity measurement.

The graph of T_c versus applied magnetic field for the MgB_2 - 5 at.% NbB_2 doped samples ball milled at different times, are shown in **Figure 5.11** as compared comparing with the MgB_2 undoped premilled sample. The criterion of 90% was used to determine the T_c of MgB_2 - 5 at.% NbB_2 materials ball milled at the different times.

At zero field the T_c values for all samples were very similar, except for the 600 minutes ball milled sample, with a lower T_c value up to a field of 6 T approximately. After 7 T the T_c of the 10 hours ball milled sample had similar values to the other samples.

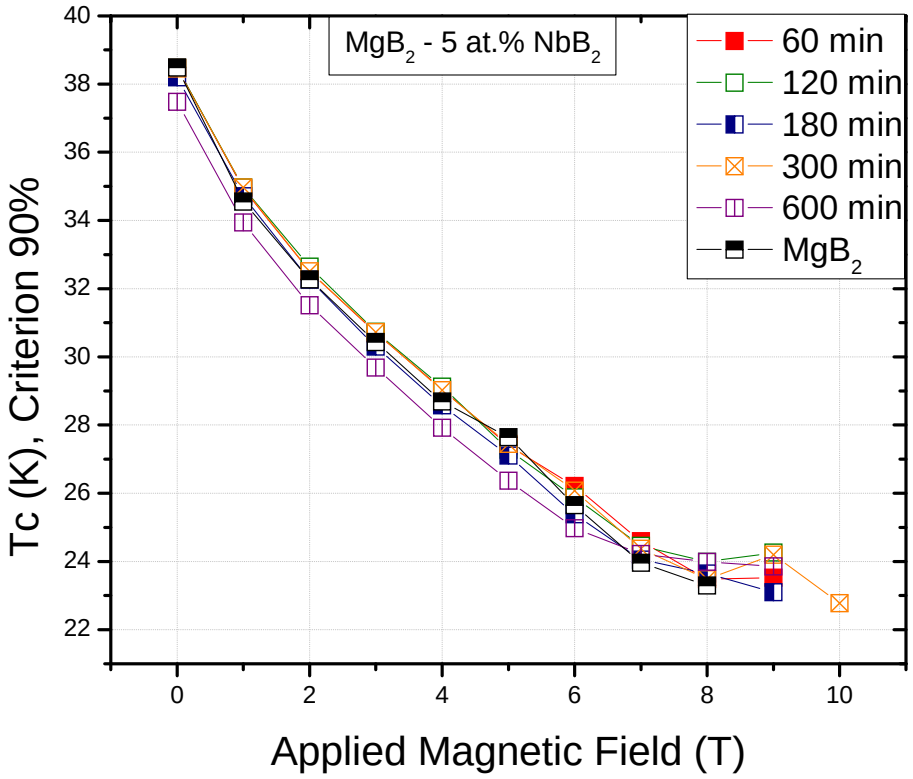

Figure 5.11. T_c Vs Applied Magnetic Field for the MgB_2 undoped and MgB_2 - 5 at.% NbB_2 doped materials.

T_c values for MgB_2 – 5 at.% NbB_2 materials as function of milling time are shown in **Figure 5.12.** The values were in the range between 37.48 K and 38.47 K, the maximum value was for 60 and 120 min of milling time. There was a decreasing of T_c for 600 min of ball milling until 37.48 K, which is practically 1 K comparing with the higher value. The MgB_2 undoped sample had a higher T_c value than the doped materials with 38.49 K, even thought the difference was just of 0.02 K compare with the higher value for the MgB_2 – 5 at.% NbB_2 doped materials.

The T_c property of the MgB_2 doped 5 at.% NbB_2 material could be affected by diverse factors such as the milling time and composition. Relating both factors it is observed that the sample milled for longest time corresponds to the sample with the highest composition in MgO and also the sample with the lowest T_c. From these results it is possible to conclude that increase in MgO implies a decrease in T_c. The MgO material acts as a non-superconducting dopant phase affecting the superconducting properties T_c, Hc_2 and J_c.

Similar results were reported by Senkowick and Perez [32, 34, 36] who concluded that MgB_2 is highly sensitive to atmospheric O_2 and CO_2. They explained that the reaction of MgB_2 with oxygen results in the formation of MgO and MgB_4 that could block current flow, and also that the reaction of MgB_2 with CO_2 increased electron scattering having strong effect on T_c, Hc_2 and H*.

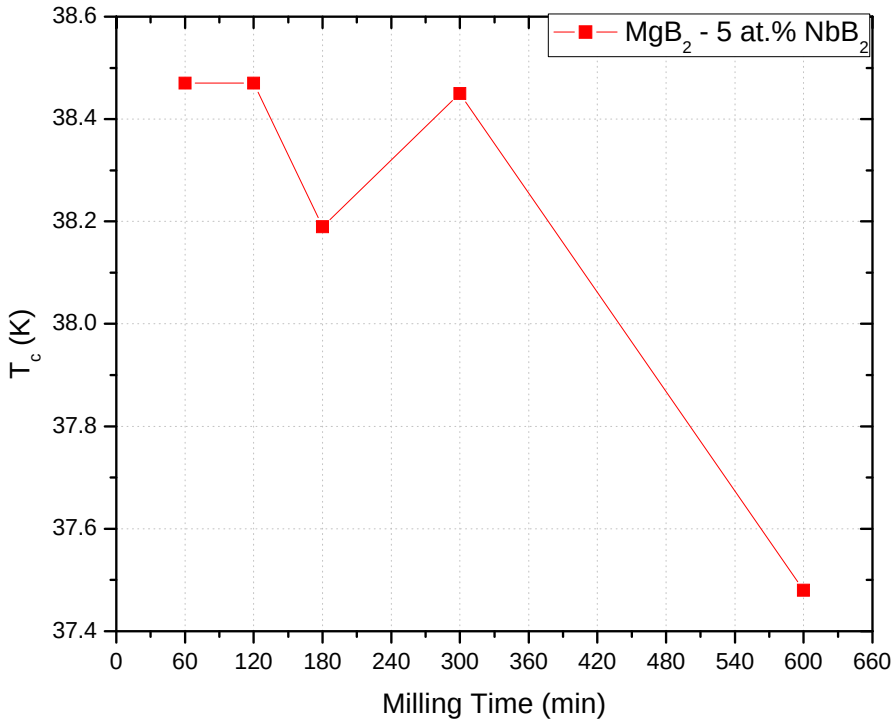

Figure 5.12. T_c Vs milling time for MgB_2 - NbB_2 5 at.% material.

5.2.2. Critical Magnetic Field (Hc_2)

Critical Magnetic Field (Hc_2) is the maximum field that can be applied to a material before it lost the superconducting state.

The Hc_2 for MgB_2 - 5 at.% NbB_2 materials were found between 20 K and 40 K, however the reported value was selected at 25 K because some authors before have used this value in their publications, which permits to compare this work with the found in the literature.

Hc_2 versus temperature for MgB_2 - 5 at.% NbB_2 materials milled at different times is shown in **Figure 5.13**. The MgB_2 undoped sample is also shown in the graph as comparison.

The samples exhibited similar behavior for the 20 K measurement, while differences emerged from the 22 K measurements. For instance, the Hc_2 values of the 180 min and 600 min ball milled materials were smaller compared to the preceding 20 K values. In addition, the 600 min ball milled samples showed the same decreasing in values of Hc_2 with increasing T_c values until 34 K which remained unchanged with further increase in temperature.

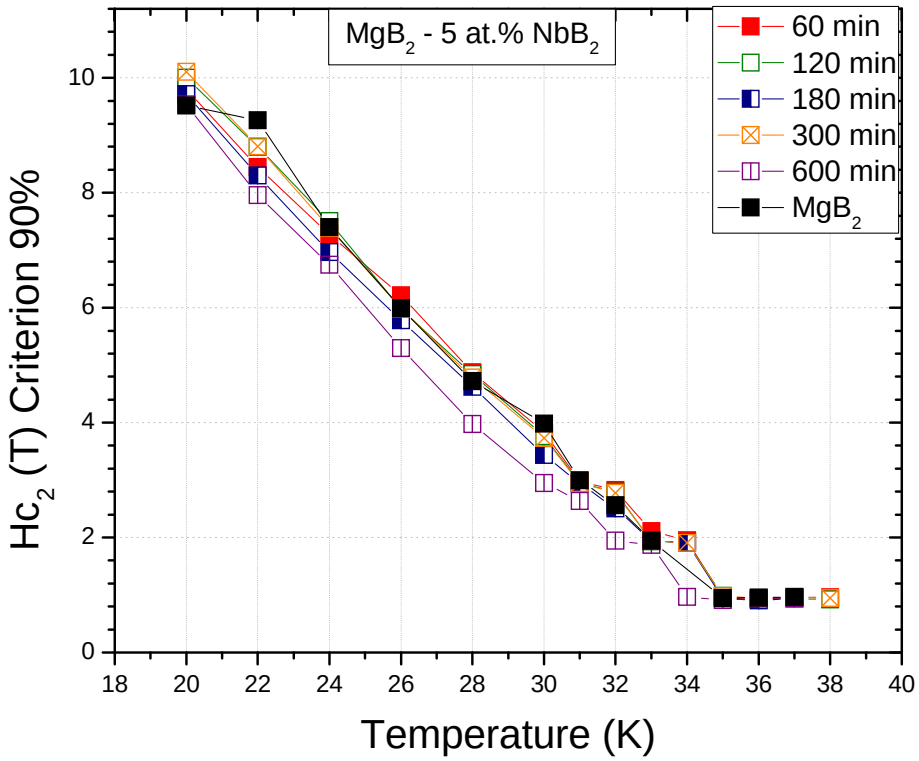

Figure 5.13. Hc_2 Vs Temperature for MgB_2 - NbB_2 5 at.% samples at different milling times.

Figure 5.14 shows the Hc_2 values at 25 K versus milling time. The range in Hc_2 (25 K) values for NbB_2 5 at.% milled samples was between 5.9583 T and 6.8193 T. The highest value obtained was for the 300 min sample (6.8193 T), very close to the second value for 60 min sample (6.775 T). The MgB_2 undoped sample had a value of 6.7518T that was lower than for the 60 min and 300 min ball milled sample, which indicates that there was an increase in Hc_2 for two samples.

The Hc_2 (25 K) for the 600 min ball milled sample decreased compared with the other milled samples and with the MgB_2 undoped, until the value of 5.958 T.

The 60 min and 300 min ball milled samples, in addition of having the highest values for Hc_2, had values in T_c very close to the MgB_2 undoped material, which indicated a good behavior of these two superconducting properties for both materials. The tendency observed in T_c versus

milling time (**Figure 5.12**) was very similar to the trend observed for **Figure 5.14** in Hc_2 (25 K) versus milling time.

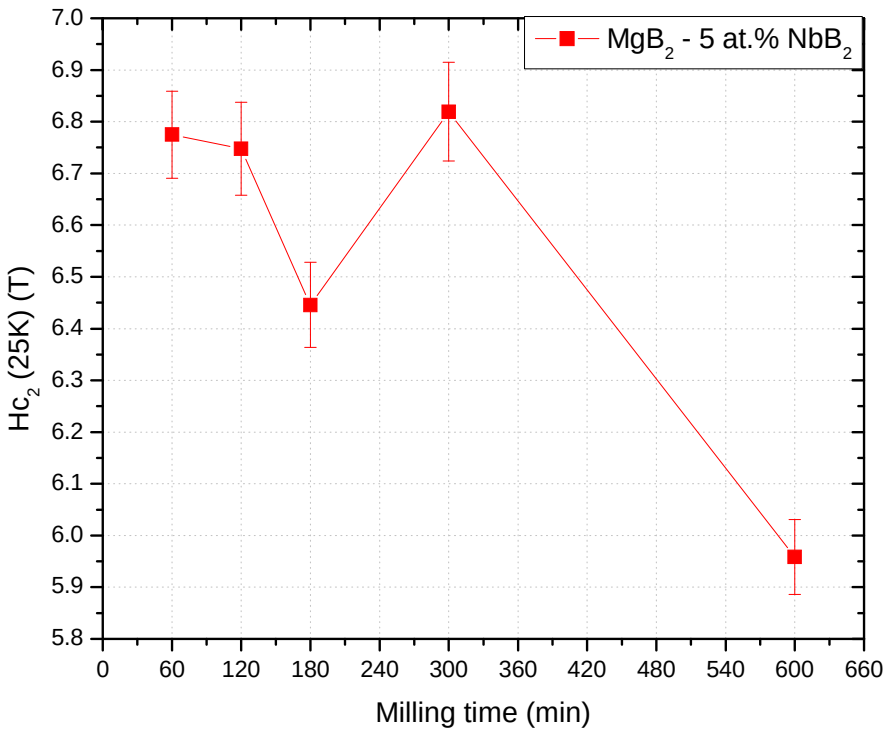

Figure 5.14. Hc_2 at 25K Vs milling time for MgB_2 - NbB_2 5 at.%.

The behavior of the Hc_2 property is influenced by different factors, composition is one of them. The influence of MgO in the decreasing of T_c property had been explained before, in similar way the trend observed for Hc_2 (25 K) in **Figure 5.14** permits conclude that the oxygen could also cause a decrease in Hc_2. Senkowicz reported an increase in Hc_2 with the exposure to air, however he suggested that this increment was caused for the reaction between MgB_2 and CO_2 that produce a C dopant in MgB_2, in this way the principal responsible in the Hc_2 increased will be C element and O could be a secondary factor.

The MgO phase in a relative high composition (12 wt.%) will imply a higher flux penetration through this insulating phase. The flux crossing the material could be non-localized and then will

be moving through the sample, which could destroy the superconducting state in a lower field than a sample with a lower composition of MgO.

Eisterer *et al.* [41] studied the implications of MgO content in the superconducting properties of MgB_2, they reported that T_c, and J_c decreases with the augment of MgO content, where the decrease in J_c was associated with the fast reduction in effective cross section.

5.2.3. Resistivity analysis

The resistivity measurement provides useful information to determine some important properties in the samples such as connectivity (A_F), resistivity of the well connected sample (ρ_A), and the defect scattering (RRR). **Table 5.IV** had the values for the resistivity properties RRR, A_F and ρ_A.

Table 5.IV. Resistivity measurements for NbB_2 5 at.% ball milled at different times samples.

Sample	**ρ_{300K} (μΩ.cm)**	**ρ_{40K} (μΩ.cm)**	**RRR (ρ_{300K}/ ρ_{40K})**	**ρ_{300K} - ρ_{40K} (μΩ.cm)**	**A_F $\left(\frac{\rho_{ideal}}{\rho_{(300K)} - \rho_{(40K)}}\right)$**	**ρ_A (40K) (μΩ.cm)**
MgB_2 Undoped	15.48	4.01	3.86	11.48	0.64	2.55
60 min	18.66	5.30	3.52	13.36	0.55	2.89
120 min	33.89	11.57	2.93	22.32	0.33	3.79
180 min	25.52	9.88	2.58	15.64	0.47	4.61
300 min	40.40	13.81	2.93	26.59	0.27	3.79
600 min	37.23	18.09	2.06	19.14	0.38	6.90

The plot of resistivity as a function of temperature for the doped MgB2 – 5 at.% NbB2 together with the undoped MgB_2 are shown in **Figure 5.15,** with the later displaying the least value.

Among the doped samples, the material corresponding to the 60 min ball milling yielded the least resistivity value, while the 600 min one had the highest value.

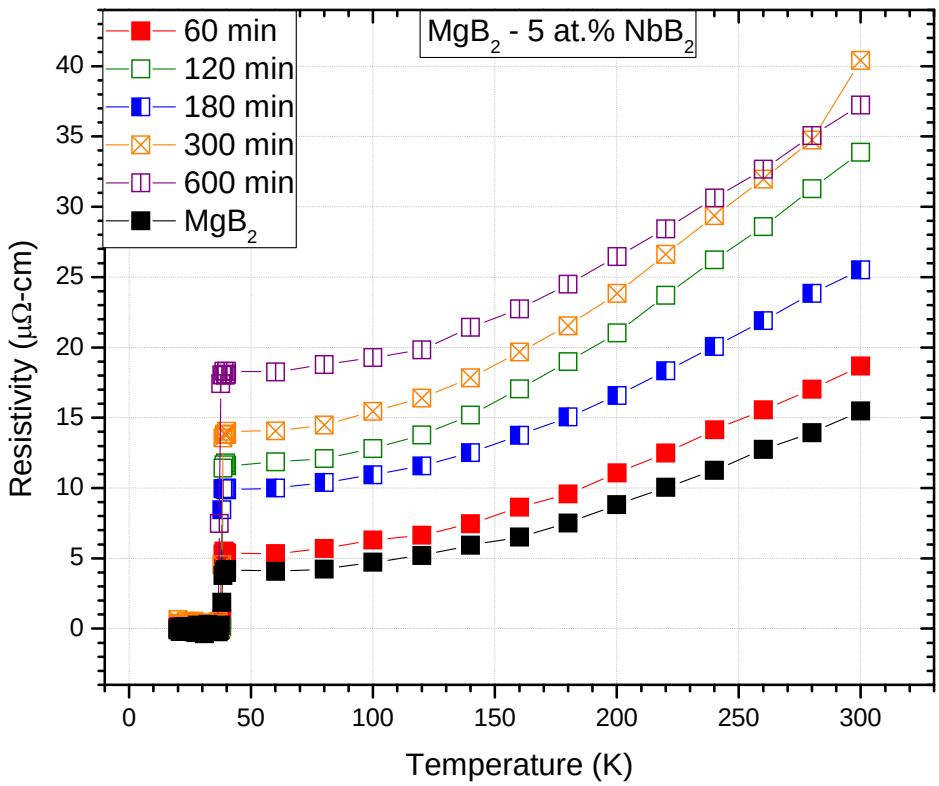

Figure 5.15. Resistivity Vs Temperature for MgB_2 - NbB_2 5 at.% ball milled at different times

The active area fraction (A_F) parameter determines the percentage of the area effectively connected in the sample.

The higher value obtained in A_F was for the MgB_2 undoped sample with a value of 0.64.s

The A_F parameter for the MgB_2 – 5 at.% NbB_2 materials did not have a defined trend as a function of the milling time. The highest value was for 60 min (0.55), followed by 180 min (0.47) and 600 min (0.38). The 120 and 300 min had the smallest values of 0.33 and 0.27 respectively as shown in **Figure 5.16**.

The A_F property indicated that the sample with the highest value was the sample that had the larger path by which the current passed. This property is directly related with the critical current

density (J_c). The results found here could predict the behavior of J_c since the higher A_F will be imply the higher the J_c. Based on this the 60 min sample could have a high J_c value, in contrast to the 300 min material that could have a small J_c value .

Moreover, the results also suggest that for these materials the connectivity is not a variable depending on the milling time or the crystallite size, but could be related with other parameters as the distribution of the phases in the material.

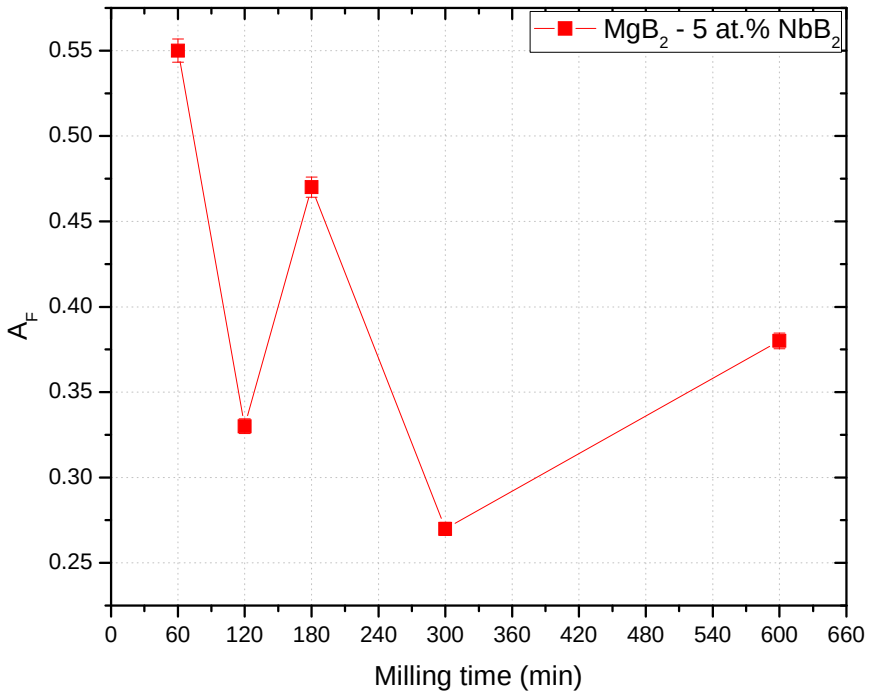

Figure 5.16. A_F Vs milling time for MgB_2 - NbB_2 5 at.% material

If they are observed **Table 5.II** and **Table 5.IV,** it would be found a similar tendency in MgB_2 phase composition with A_F parameter. NbB_2 have been reported to be non-superconducting material by Gasprov et al. [45] and Kackzorowski et al. [46], however other authors reported NbB_2 as superconductor material [47-51], while Mudgela *et al.* [52] reported the non superconductivity of pure NbB_2 and the achieved of the superconductivity in NbB_2 with variation of the Nb/B ratios. If NbB_2 and MgO phases acted as non-superconducting materials

and break the connectivity in the sample, then the increase in MgB_2 phase would determine an increase in A_F parameter and subsequently in J_c. For MgB_2 doped MgO at different compositions, it was reported by Eisterer *et al.* [41] the decreased in J_c values with the decreased of MgB_2 and the increase in MgO contents. However is important to observe that although the content of MgB_2 is an important factor in the A_F parameter, also the MgO, NbB_2 and B content could have an influence in the connectivity.

Hc_2 as function of A_F is shown in **Figure 5.17,** the tendency observed has not a clear patron and the trend is very variable, the initial tendency is to decrease finishing in a valley with a change in the trend of Hc_2 to increase with the increase in A_F.

The highest Hc_2 (25 K) correspond to 300 min that had the smallest A_F, and the second value in Hc_2 (25 K) had the highest A_F, which probes clearly that is difficult establish a relation between the two properties and that accord with other authors [34] A_F could have more influence on J_c than on Hc_2, because it relation with the materials connectivity.

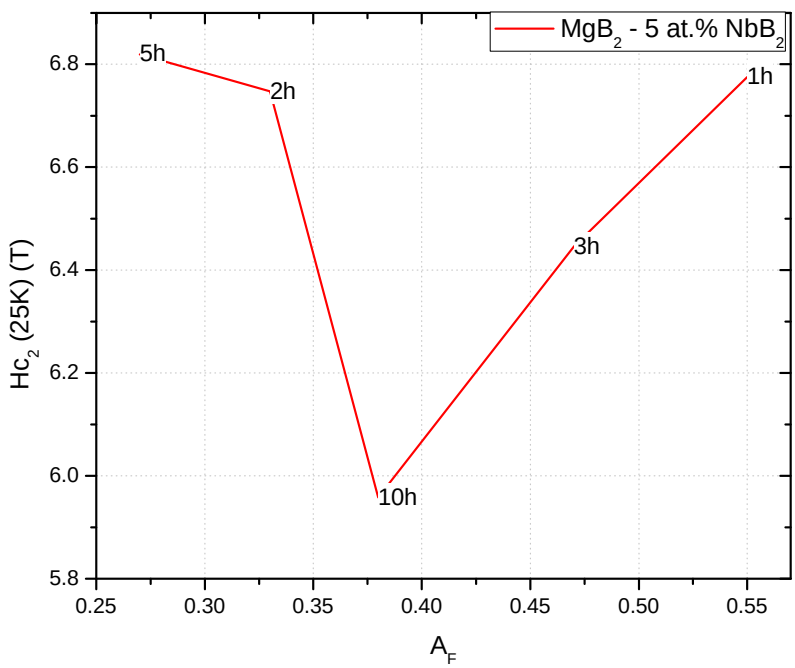

Figure 5.17. Hc_2 (25 K) Vs A_F for MgB_2 - NbB_2 5 at.% doped material for different milling times

The ρ_A parameter represents the real resistivity of tshe well connected area in the samples, this is, the resistivity of the portion of the sample given by A_F.

The MgB_2 undoped sample showed the smallest value in ρ_A with 2.55 μΩ.cm. For the MgB_2 - 5 at.% NbB_2 doped materiales The smallest value in ρ_A was for 60 min ball milled sample (2.89 μΩ.cm) while the highest was for the 600 min (6.90 μΩ.cm).

The ρ_A parameter for MgB_2 - 5 at.%NbB_2 showed a tendency to increase with increasing milling time however, the 300 min ball milled sample has a change in the trend, decreasing respect to 180 min samples, and presenting the same value in ρ_A than the 120 min sample (3.79 μΩ.cm) The behavior of ρ_A as function of milling time is shown in **Figure 5.18**.

If NbB_2 is consider as a non-superconducting phase [45, 46] the increasing of this insulating phase in the sample could imply the increasing in the resistivity. The increasing tendency for ρ_A with the increasing of milling time and the change in this tendency for the 300 min of milling time could be then related with the increasing in the content of NbB_2 and the subsequent decreasing for 300 min of milling time.

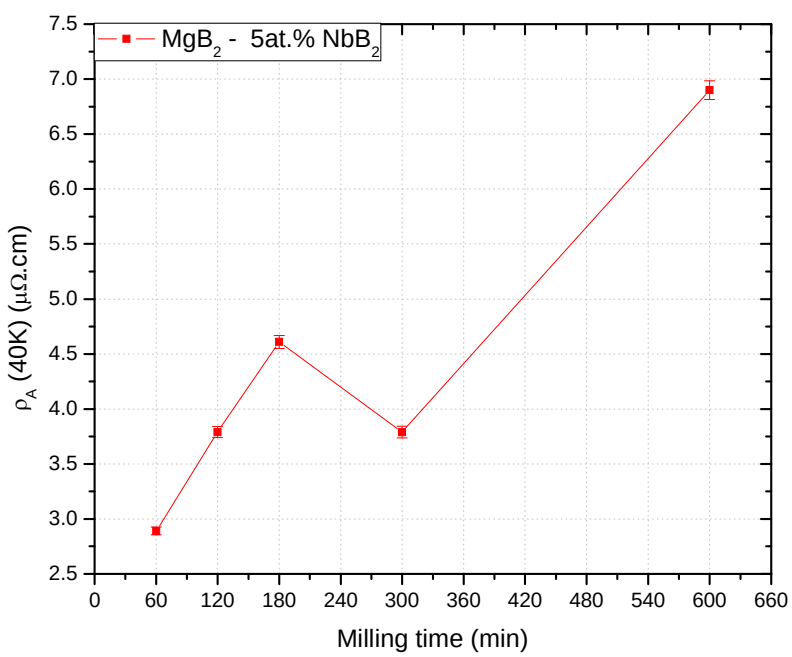

Figure 5.18. ρ_A Vs milling time for MgB_2 - NbB_2 5 at.% doped material.

Figure 5.19 shows the relation between Hc_2 (25 K) and the ρ_A parameter, the tendency in Hc_2 is to decrease with the increasing in ρ_A. These results indicates that the increment in real resistivity, influence the value of Hc_2 negatively generating a decreasing in the superconducting property.

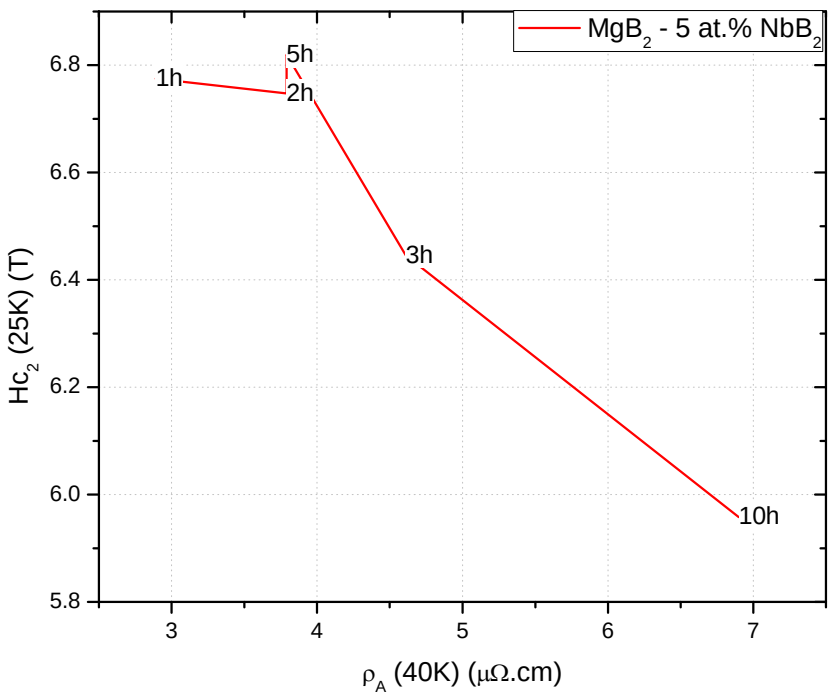

Figure 5.19. Hc_2 (25) Vs ρ_A for MgB_2 - NbB_2 5 at.% doped material.

The Residual Resistivity Radio (RRR) is a measure of the defect scattering, while defect scattering increase, the RRR decreases, approaching to 1 for very high defect concentrations [34].

The higher value in RRR was found for the MgB_2 undoped sample with 3.86. Between the doped milled samples the higher values was for 60 min with 3.52, the smallest value was for 600 min milled sample with 2.06. The results show a tendency of the RRR to decrease with the increasing in milling time, even thought the 300 ball milled sample had an increase presenting the same value than the 120 min sample (2.93). The graph of RRR for MgB_2 – 5 at.% NbB_2 as function of the milling time is found in **Figure 5.20**.

The tendency of decrease of RRR with ball milling time indicated that defect scattering increased with longer milling times which could indicate a resistance saturation effect, which could be attributed to the substitution microscopic defects acting as electron scattering centers [53].

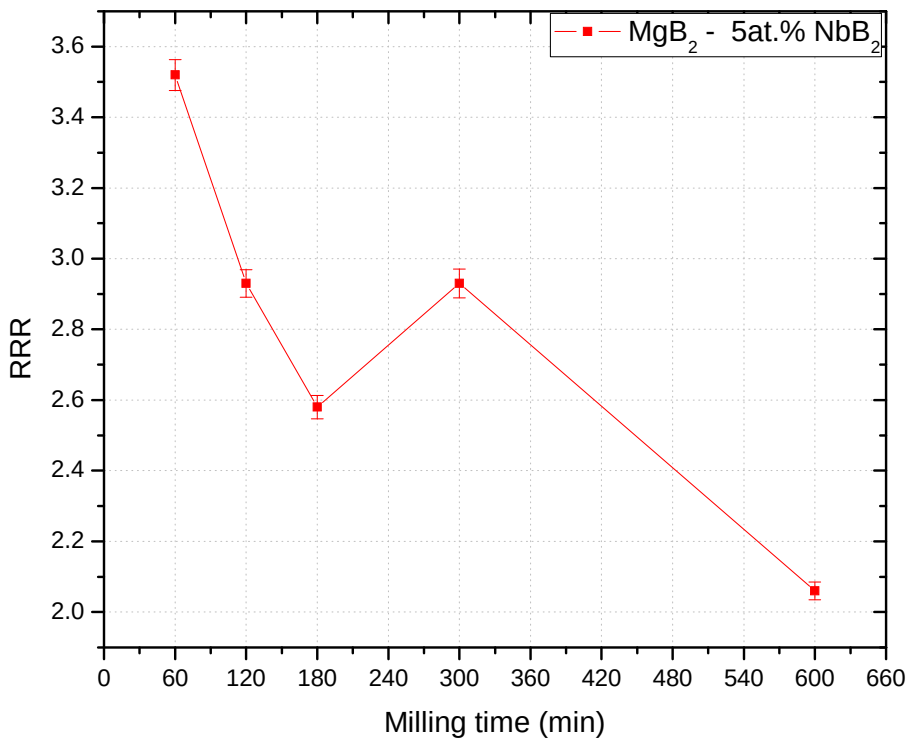

Figure 5.20. RRR Vs milling time for MgB_2 - NbB_2 5 at.% doped material.

The relation between the Hc_2 (25 K) property and the RRR parameter in MgB_2 – 5 at.% NbB_2 material is shown in **Figure 5.21**. In the graph is observed the tendency of increasing Hc_2 (25 K) with the increasing in RRR, the highest value in Hc_2 (25 K) shows the second value in RRR; while the second value in Hc_2 (25 K) had the first value in RRR.

The Hc_2 increase in MgB_2 – 5 at.% NbB_2 material with the increasing of RRR indicates that Hc_2 increases for less electron scattering. The increasing in RRR implies the decreasing in electron scattering for compositional and microstructural sources [34]. The compositional sources could be related with the content of NbB_2, MgO as well as the Si as secondary phases in the material.

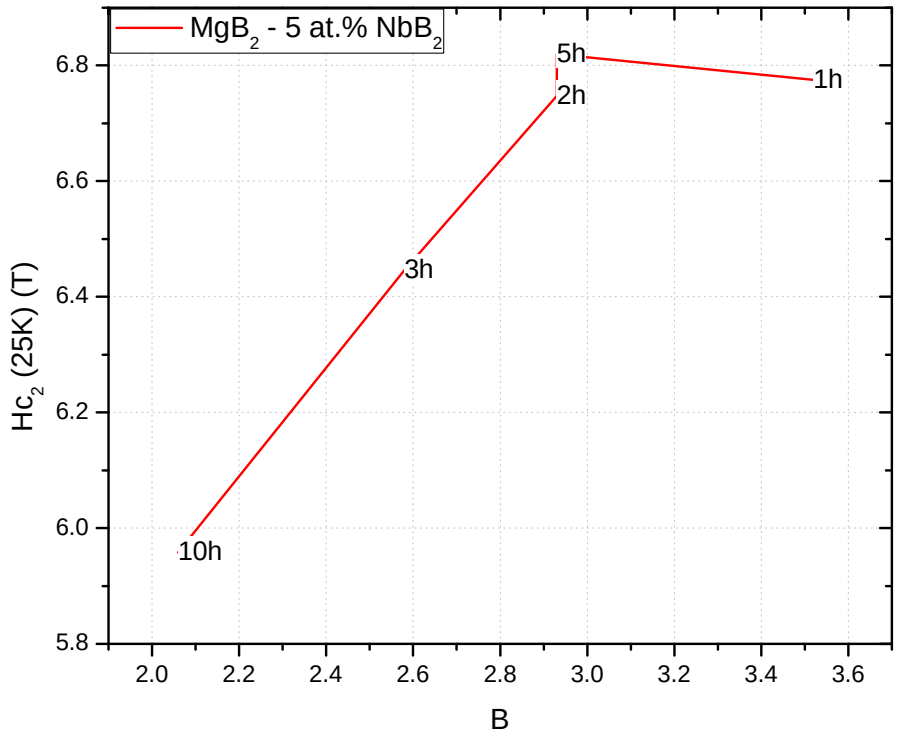

Figure 5.21. Hc_2 (25 K) Vs RRR for MgB_2 - NbB_2 5 at.% doped material.

6. Effect of 5 at.% TiB_2 doped MgB_2 Premilled on Superconducting Properties

This chapter describes the results found in the MgB_2 doped 5 at.% TiB_2 in the structural and superconducting properties.

TiB_2 and MgB_2 are both hexagonal compounds. TiB_2 is a transition metal diboride stable down to room temperature which pertains to group IV diborides, these diborides evaporate congruently at high temperature with possibly a slight tendency towards larger boron pressure. TiB_2 has a high melting temperature at 2920°C and a standard formation enthalpy ($-\Delta H^0_{f298}$) of 66.8 kcal/mole.

The doping of MgB_2 with TiB_2 using the high energy ball milling technique was made with the objective to analyze the results in the structural properties and the creation of defects, and the effect in superconducting properties which will determine the viability of future studies and applications of this material.

6.1. Structural Properties

The XRD analysis was made to 5 at.% TiB_2 doped MgB_2 to determine the components formed in the process. This analysis was carry out to the powder samples after the ball milling and to pellet samples after the HIP process to analyze the effect of the milling and the annealing processes in the structural properties of the samples.

Table 6.I show the values for composition, lattice parameters, crystallite size and strain for MgB_2 - 5 at.% TiB_2 in powder at different milling times. **Table 6.II** show the values for composition, lattice parameters, crystallite size and strain for MgB_2 - 5 at.% TiB_2 post HIP samples at different milling times and the comparison with the undoped material.

Figure 6.1 shows the XRD spectrum of MgB_2 doped 5 at.% TiB_2 post HIP samples at different milling times. The peaks found for these samples indicate the presence of MgB_2, TiB_2, MgO and B, some of the peaks however, don't correspond to any of the analyzed compounds, and could represent either a contamination or an additional phase formed after the synthesis, the peaks are identify in **Figure 6.2**.

The presence of MgO indicates that was an introduction of oxygen in one or several stages of the synthesis were the sample was extract of the glove box for the ball milling, the CIP or the HIP process. The MgO composition percentage in powder samples are smaller compare to the post HIP material; for the powder samples the composition percentages for MgO were between 1.1 wt.% and 6.2 wt.%, for the pellet material the values were between 7.1 wt.% and 9.4 wt.%.

As part of the elements found in the post HIP samples are Silicon and Carbon. Carbon element was identified in the EDS analysis (**Figure 6.3**) with a small contribution, however it was not found in the XRD spectrum. This element accesses in the sample as contamination in any phase of the process. Because of the different phases that sample go through in the synthesis and during preparation to the characterization, the contamination could ingress to the sample. Studying each stage, it could be identified specifically the cutting phase when was used oil as lubricant of the blade, which could be the reason for Carbon. In the XRD of the powder material after the ball milling was not found the Silicon contamination which indicates that this stage was not the origin of this element. The powder samples don't show additional peaks to MgO, B, MgB_2 and TiB_2.

The XRD analysis of both powder and post HIP materials showed the B element. The B element was in the samples as the result of the decomposing of the MgB_2 in Mg and B or the decomposing of TiB_2 in Ti and B, Serebryakova *et al.* [54] reported that MgB_2 is thermally unstable and decomposes at 800°C with the liberation of Mg and formation of higher borides. However the Mg or Ti elements were not in the XRD patterns, but the MgO compound was found in it. If MgB_2 decompose in Mg and B, probably the Mg resultant reacts with O to form the MgO. If TiB_2 on the other hand decompose in Ti and B, Ti could form another phase more stable with other elements or compounds.

For the post HIP material the ten hours ball milled sample doesn't show any presence of the compounds analyzed. The MgB_2, TiB_2, MgO and B phases are absent in this sample, however, the same sample in powder material had all the phases mentioned before and also a WC phase in a very small composition. Even though the composition of the ten hours post HIP sample is not clear, the presence of some peaks (**Figure 6.1**) is evident which could correspond to a new phase.

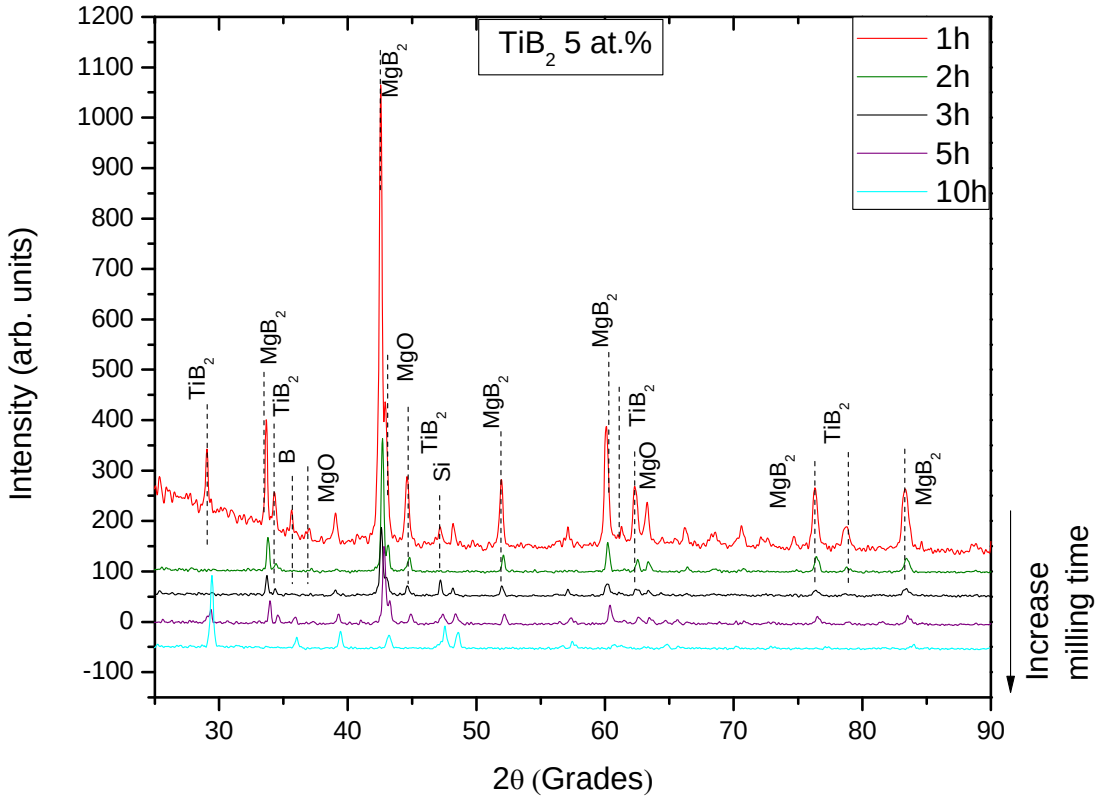

Figure 6.1. XRD analysis for MgB_2 - 5 at.% TiB_2 doped materials at different milling times

In Figure 2 are identify the impurities found for MgB_2 - 5 at.% TiB_2 doped materials. Some of the peaks are not identify with known compounds or impurities, which could indicate the presence of a new phase related with the base and the doping compounds.

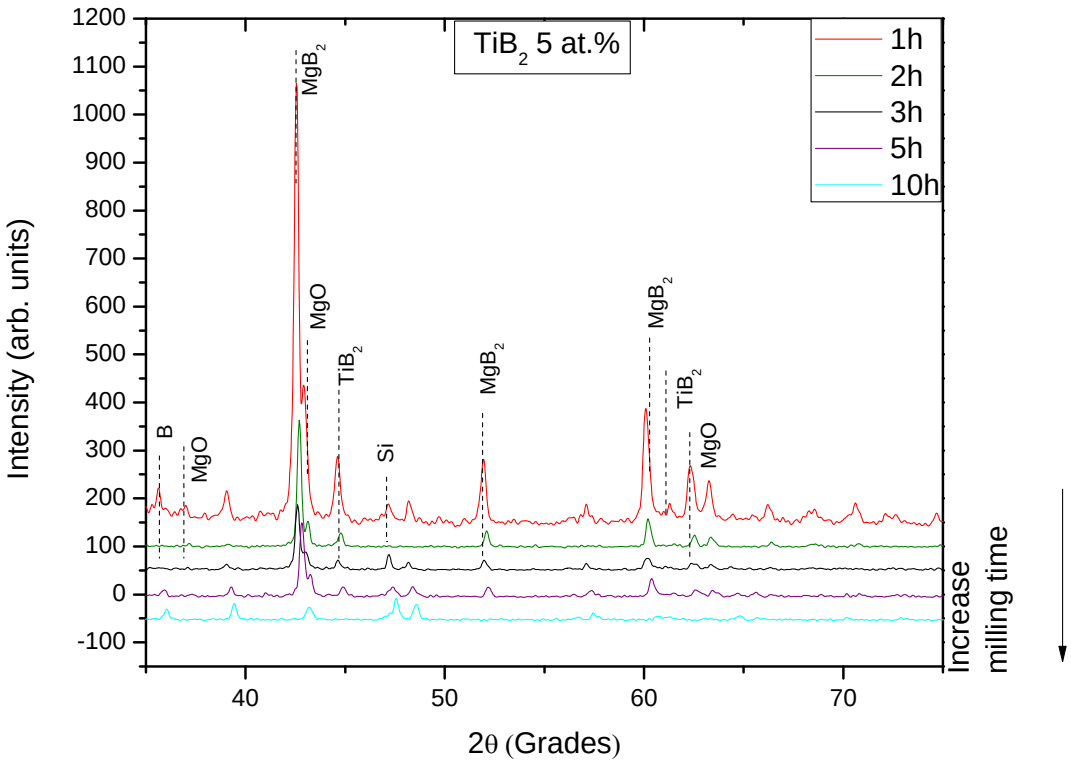

Figure 6.2. XRD analysis for MgB_2 - 5 a.% TiB_2 doped maerials at different milling times. Zoom of 2θ between 35 and 70 grades.

Figure 6.3 corresponds to the EDS of the two hours ball milled sample. This graph shows the composition of the sample with peaks related to the elements B, Mg and Ti and one additional peak representing Carbon whicsh is a contamination that ingress in the sample in one of the experimental phases.

The SEM image (**Figure 6.4**), show the presence of two phases in the sample, the base material MgB_2 is observed in obscure color and correspond to the predominant material, the small brilliant points correspond to the dopant material. The crystallites are observed very small although the definition of the equipment doesn't allow the observation in a more defined scale.

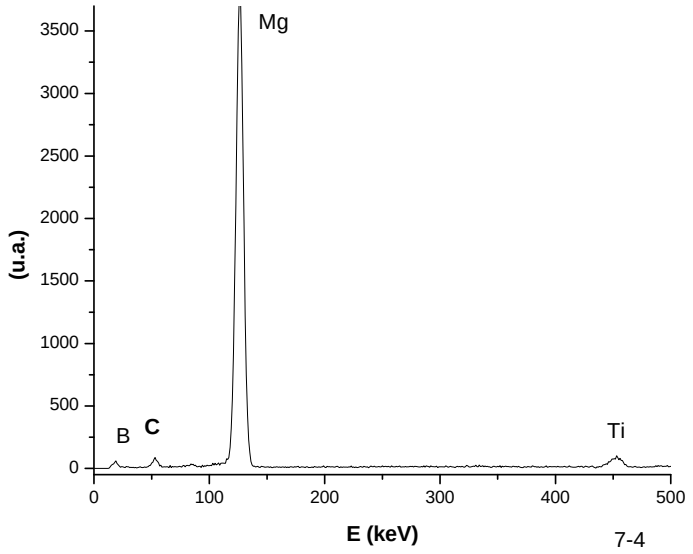

Figure 6.3. EDS of MgB_2 -TiB_2 5a.% doped materials 2 hours ball milling sample.

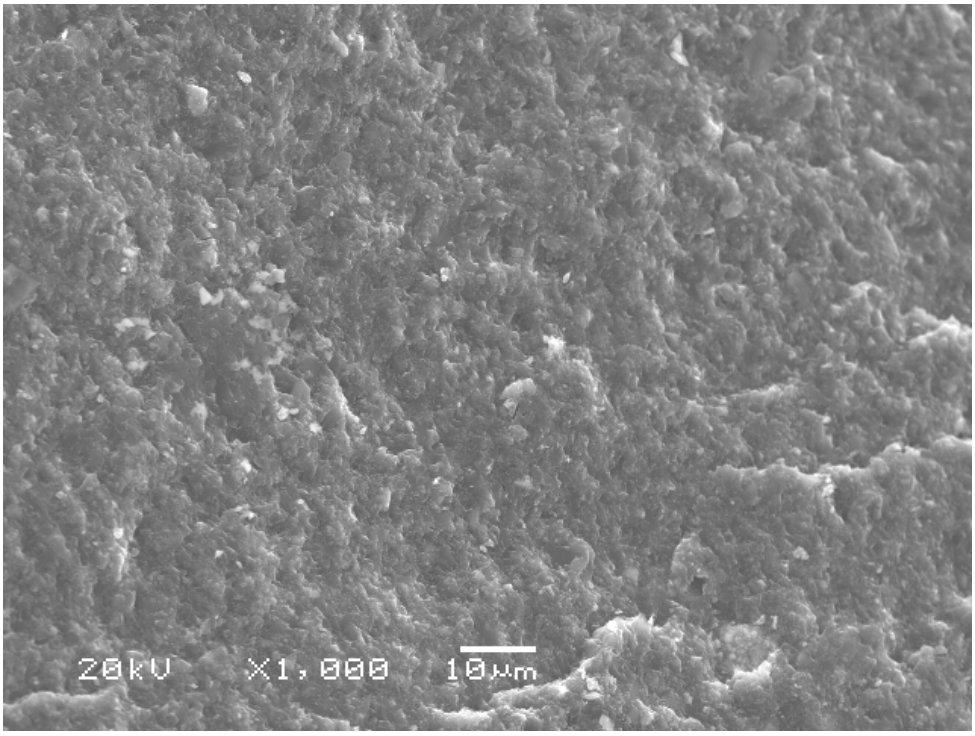

Figure 6.4. SEM of MgB_2 - TiB_2 5 at.% doped materials 2 hours ball milling sample

The composition of the powder (**Figure 6.5**) and pellet (**Figure 6.6**) samples were graph in function of milling time to establish the changes occurred in the sample with the CIP and HIP process.

The TiB_2 percentage for powder and pellet samples did not show a significant difference; for powder material the range was between 4.1 wt.% and 5.6 wt.%, for pellet material the values were between 3.4 wt.% and 5.5 wt.%. The percentage of composition didn't show a specific trend with the increasing of milling time for powder or post HIP material.

The MgO percentage of composition had smaller values for the powder material compare with the post HIP material; this result probe that there was an introduction of oxygen in the milling phase but also was a contribution of oxygen in other phases of the synthesis, probably during the welding. Analyzing the composition values is not possible to establish a relation between the milling time and the percentage of MgO.

For MgB_2 and B phases the percentage of composition varies in powder and pellet, but in all cases there is a relation between both components; if the percentage of MgB_2 is higher for pellet compare to powder, the percentage in B will be smaller for pellet compare to powder and vice versa, which indicates the relation between both phases, for the same sample and the same stage (powder or pellet) if the percentage of one phase (MgB_2 or B) increases in pellet, the percentage of the other phase (B or MgB_2) decreases for pellet.

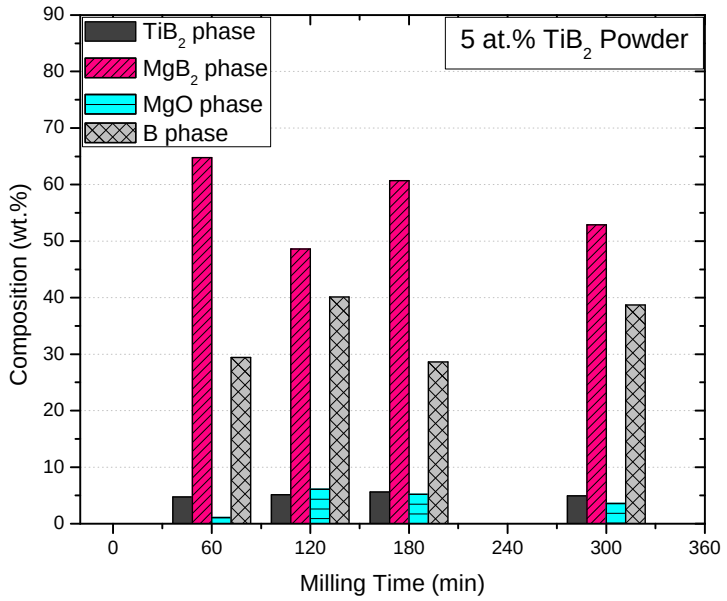

Figure 6.5. Composition of TiB_2, MgB_2, MgO and B phases for powder material in function of milling time.

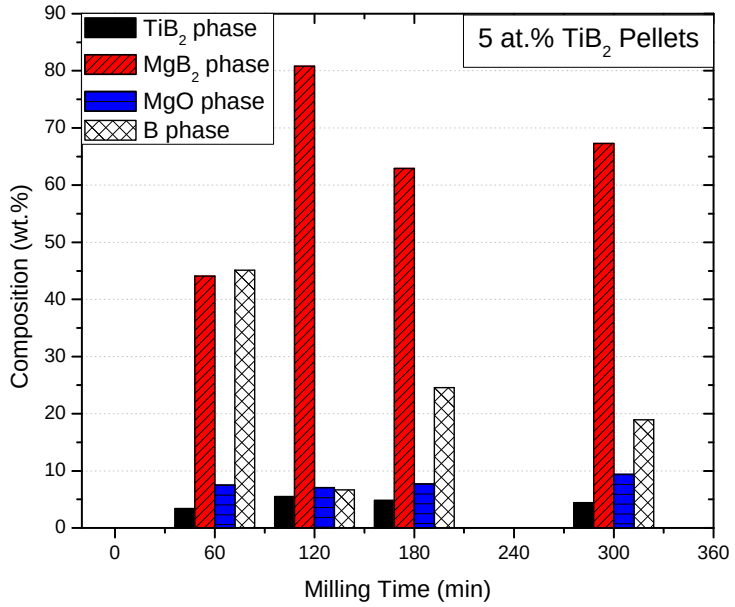

Figure 6.6. Composition of TiB_2, MgB_2, MgO and B phases for post HIP material in function of milling time.

Figure 6.7 shows the crystallite size for TiB_2 phase comparing the powder material with the post HIP material. In all cases the powder material had smaller crystallite size than the post HIP material. The increasing in crystallite size in the post HIP material is a direct effect of the temperature which generates a grain boundary migration in the sample. The growth of the crystallite size however was less significant to 60 min and 120 min ball milled sample, whereas for the 180 min and 300 min the effect of the temperature was more evident in the growth of the crystallite size.

For MgB_2 phase in powder the crystallite size shows a decreasing trend with the milling time; the highest value was for 60 min (11.93 nm) and the smallest value for 600 min (7.86 nm). The MgB_2 from Alfa Aesar has a crystallite size of 97 nm reported by Senkowicz [34] which indicates that in the first 60 minutes of milling time there was a considerable reduction in particle size and this tendency continue until the last time tested of 600 minutes.

For the MgB_2 phase, comparing the powder with the post HIP samples (**Figure 6.8**), the post HIP presented higher crystallite size. The growth of crystallite size with temperature didn't show a tendency with milling time, but the values were close for all samples; between 24.36 nm and 39.70 nm.

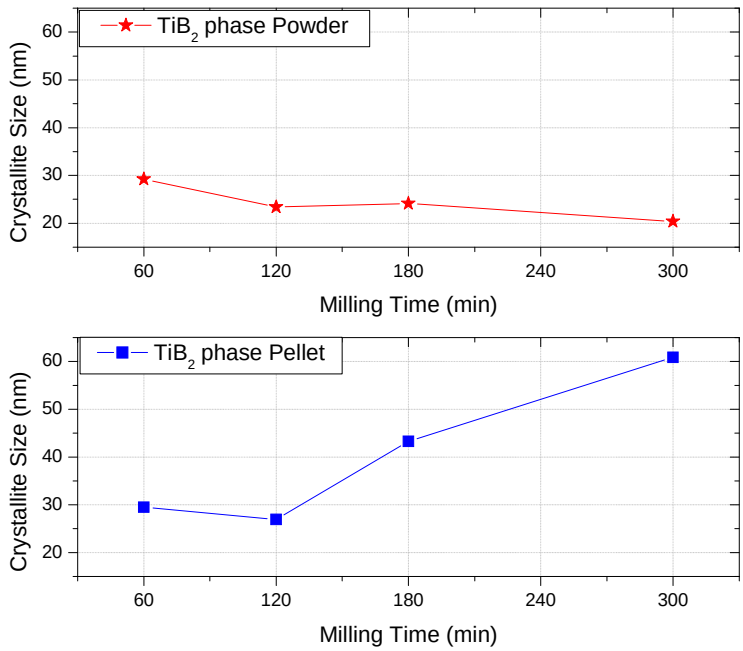

Figure 6.7. Crystallite size of TiB_2 phase for powder and pellet material Vs milling time.

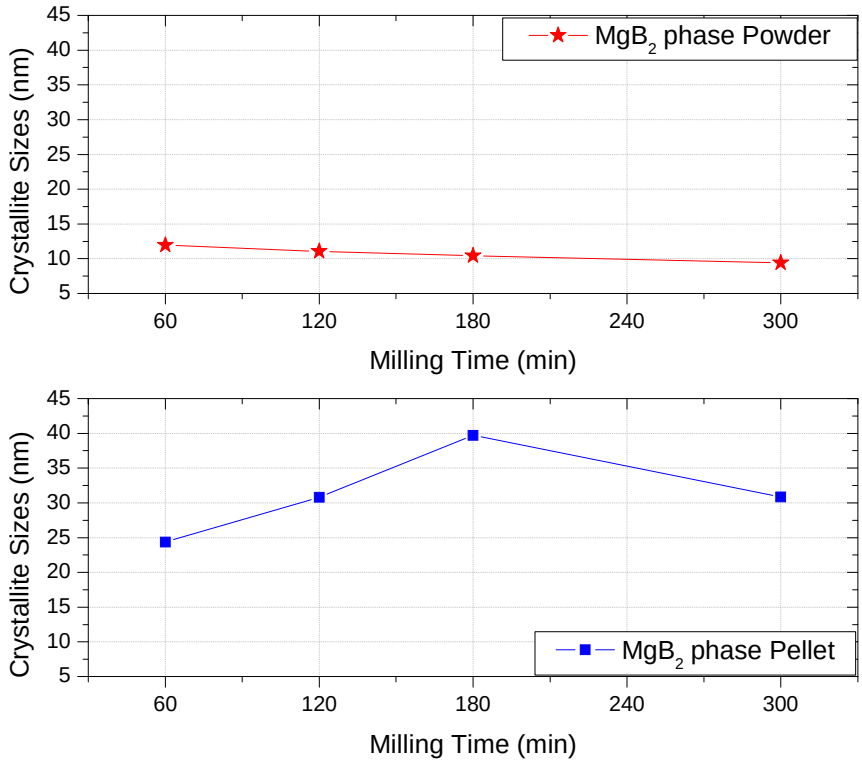

Figure 6.8. Crystallite size of MgB_2 phase for powder and pellet samples Vs milling time.

Figure 6.9 shows the Strain of TiB_2 phase in powder and pellet samples. For the powder material the strain had a tendency to increase with the increasing in milling time, for 60 min of milling time the strain was 0.000530 while for 300 min de value was 0.002125.

In the pellet sample the strain had not a clear tendency with the milling time, which could be the result of the annealing process in the sample. For the pellet sample the smallest strain was for 180 min (0.000541) the highest value was for 120 min (0.01549).

Comparing the powder and pellet materials, for 60 min and 120 min there was an increasing in the strain from powder to pellet, the range of increasing for the two samples were very close with a mean value of 0.00086 ± 0.00002. For 180 min and 300 min there was a decreasing in the strain for powder to pellet, this range of decreasing was similar for both cases, with a mean value of 0.00067 ±0.00007.

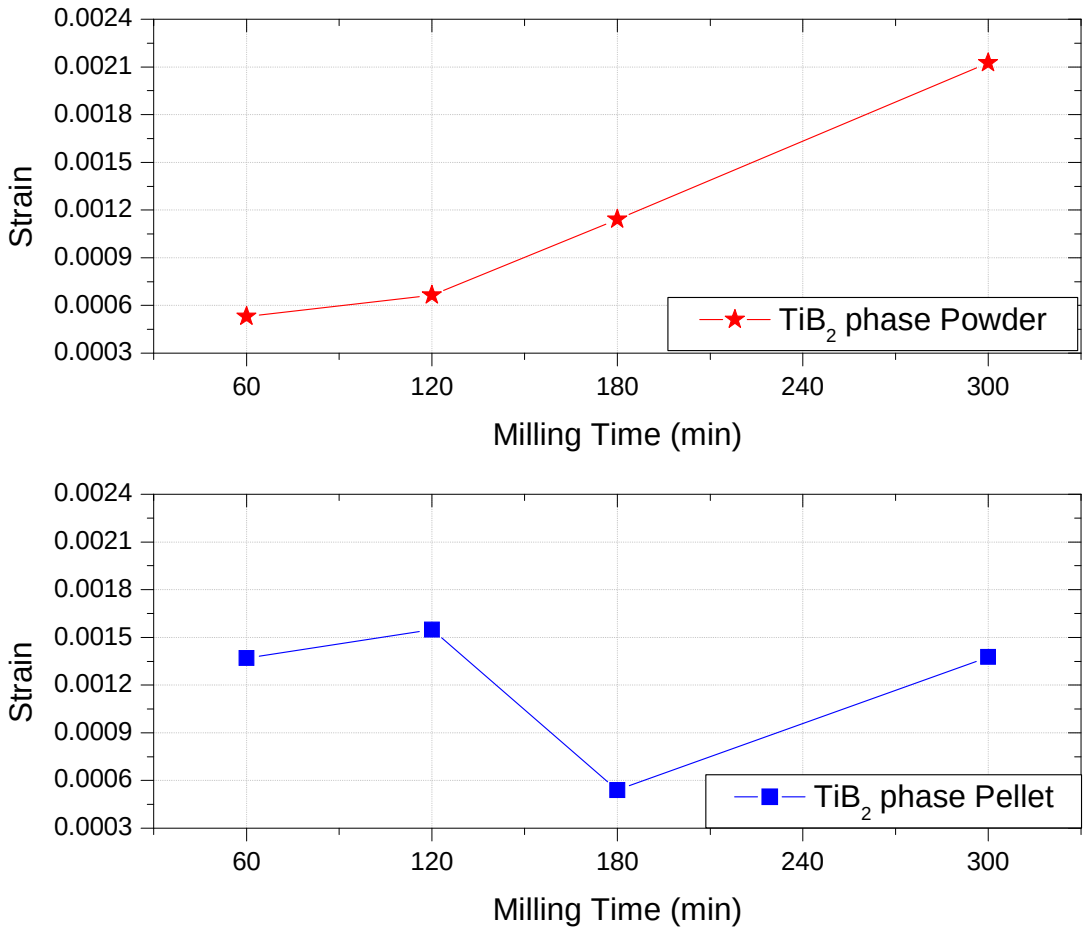

Figure 6.9. Strain of TiB_2 phase for powder and pellet material in function of milling time.

Figure 6.10 shows the strain in MgB_2 phase for powder and pellet material. The maximum value in strain for powder material was at 60 min of milling time, in 120 min there was a minimum value, following for an increasing tendency until 300 minutes. For post HIP material the strain had a tendency to decrease with the increasing in milling time, the strain values for pellets were between 0.001905 and 0.001049.

Comparing the strain in powder and pellet material for MgB_2 phase, in 60, 180 and 300 the strain values were higher for powder material than for pellet, however in 120 min was a minimum for the powder material and for this time the strain in pellet sample had a higher value.

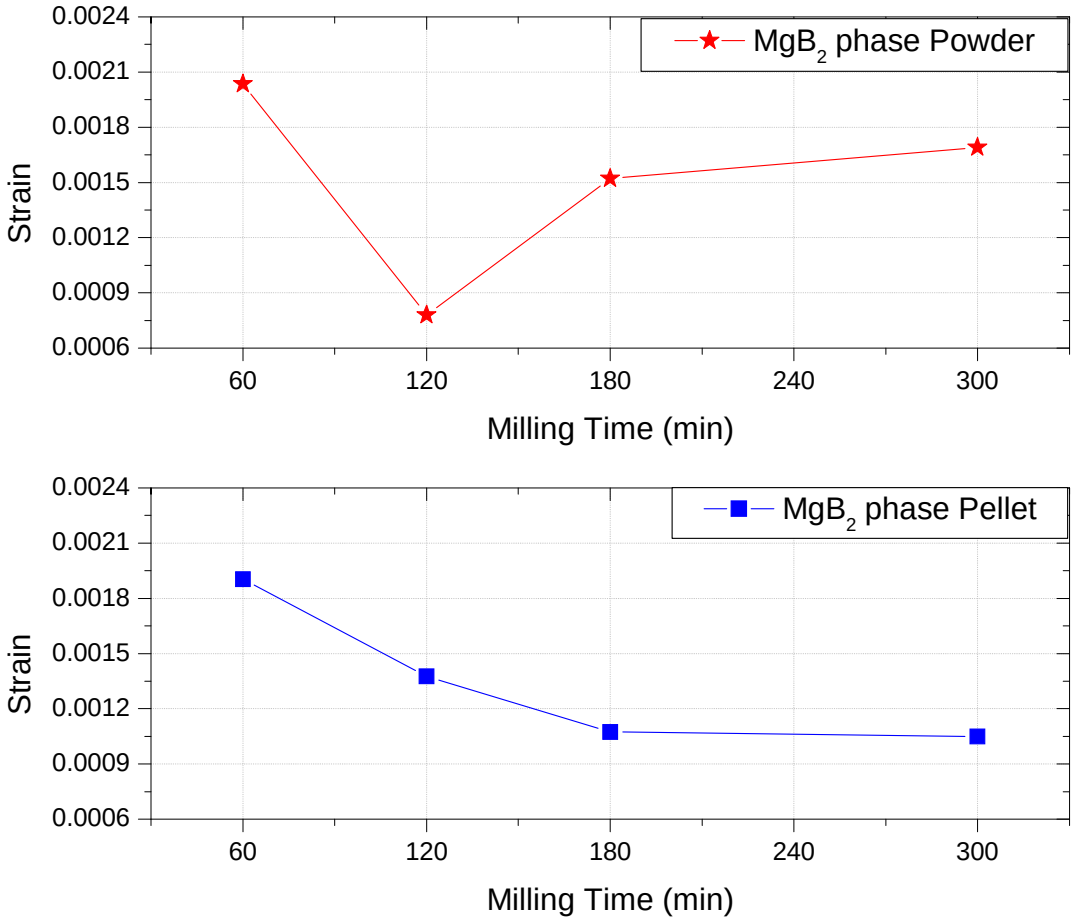

Figure 6.10. Strain of MgB_2 phase for powder and pellet material in function of milling time.

Table 6.I. Composition, lattice parameters, crystallite size and strain of MgB_2 - TiB_2 5 at.% doped material in powder ball milled at different times.

TiB_2 5 at.% Powder Samples at Different Milling Times							
Sample	**Compound**	**Composition (wt. %)**	**a(Å)**	**c(Å)**	**c/a**	**Crystallite Size (nm)**	**Strain**
60 min	TiB_2	4.7	3.026232	3.226820	1.066283	29.23	0.000530
	MgB_2	64.8	3.080902	3.524002	1.143822	11.93	0.002036
	MgO	1.1	4.199864	4.199864	1	21.38	0.001803
	B	29.4	4.894487	12.48642	2.551119	3.52	0.008763
120 min	TiB_2	5.1	3.019898	3.218929	1.065907	23.40	0.000665
	MgB_2	48.6	3.077585	3.510107	1.140539	11.05	0.000779
	MgO	6.1	4.219294	4.219294	1	3.56	0.010542
	B	40.1	4.893385	12.60508	2.575943	3.04	0.009963
180 min	TiB_2	5.6	3.020236	3.222990	1.067132	24.14	0.001142
	MgB_2	60.7	3.077465	3.518404	1.14328	10.40	0.001522
	MgO	5.2	4.206866	4.206866	1	3.72	0.007172
	B	28.6	4.872036	12.47000	2.559505	3.53	0.008737
300 min	TiB_2	4.9	3.019041	3.220120	1.066604	20.37	0.002125
	MgB_2	52.9	3.074644	3.511927	1.142222	9.37	0.001691
	MgO	3.6	4.195514	4.195514	1	2.87	0.007752
	B	38.7	4.865924	12.54336	2.577796	2.98	0.009374
600 min	TiB_2	4.1	3.022980	3.220372	1.065297	25.85	0.000627
	MgB_2	41.9	3.078267	3.512507	1.141066	7.86	0.003499
	MgO	6.2	4.208051	4.208051	1	4.03	0.005518
	B	46.8	4.864005	12.66002	2.602797	2.98	0.009356
	WC	1.1	2.897367	2.834897	0.978439	11.45	0.003562

Table 6.II. Composition, lattice parameters, crystallite size and strain of MgB_2 - TiB_2 5 at.% doped materials post HIP ball milled at different times.

TiB_2 5 at.% Post HIP Samples at Different Milling Times							
Sample	Compound	Composition (wt. %)	a(Å)	c(Å)	c/a	Crystallite Size (nm)	Strain
MgB2 raw unmilled HIP*	MgB_2	92.2	3.0844	3.5262	1.143237	73.03	0.001098
	MgO	7.8	4.2242	-	-	19.47	0.001600
MgB_2 undoped premilled HIP	MgB_2	79.2	3.085226	3.526575	1.143052	32.76	0.001316
	MgO	17.5	4.215603	4.215603	1	3.77	0.009647
	B	3.2	4.932873	12.57649	2.549526	5.10	0.006819
60 min	TiB_2	3.4	3.026272	3.227816	1.066598	29.52	0.001370
	MgB_2	44.1	3.082792	3.526254	1.143851	24.35	0.001905
	MgO	7.5	4.218093	4.218093	1	30.21	0.001034
	B	45.1	4.851529	12.47000	2.570324	3.52	0.009076
120 min	TiB_2	5.5	3.022964	3.224213	1.066573	26.92	0.001549
	MgB_2	80.8	3.081246	3.521919	1.143018	30.78	0.001376
	MgO	7.1	4.211806	4.211806	1	53.44	0.000139
	B	6.7	4.824799	12.55523	2.602229	3.94	0.008977
180 min	TiB_2	4.8	3.028823	3.224539	1.064618	43.29	0.000541
	MgB_2	62.9	3.080147	3.524950	1.14441	39.70	0.001074
	MgO	7.7	4.212582	4.212582	1	73.63	0.000914
	B	24.6	4.810000	12.47000	2.592516	3.52	0.009023
300 min	TiB_2	4.4	3.026781	3.230043	1.067155	60.84	0.001376
	MgB_2	67.3	3.082914	3.528884	1.144659	30.85	0.001049
	MgO	9.4	4.213638	4.213638	1	44.77	0.000908
	B	18.9	4.810000	12.47000	2.592516	3.52	0.009023

*Sample processed by Rodrigues Junior, D. [8]

The 600 min sample was not possible to process, because the peaks observed in the spectrum didn't correspond with the materials analyzes.

6.2. Superconducting Properties

The MgB_2 - TiB_2 5 at.% doped materials post HIP were characterized to determined the superconducting properties using the resistivity measure, the superconducting properties T_c an Hc_2 were obtain using the information of this measure applied to samples at different milling times.

The T_c and Hc_2 (25 K) values for MgB_2 - TiB_2 5 at.% doped materials premilled at 2 hours and milled at different times and for the MgB_2 undoped material premilled at 2 hours, are found in **Table 6.III**.

6.2.1. Critical Temperature

The critical temperature indicates the maximum temperature that can reach the material before it lost the superconducting state.

The results of T_c graphs versus applied magnetic field at different milling times are in **Figure 6.11**. It was used the two hours premilled undoped material as a comparison sample for the two hours premilled samples milling at different times. To determine the T_c property was used the criterion of 90%.

In general, the T_c values are very close for the different samples at cero field, however is observed that for 600 minutes ball milled sample was a decrease respect to the other sample and to the undoped material also.

In middle field at 4 T, the values continue close, even though is observed a very small difference in T_c between samples, decreasing the value with the increase in milling time. The smaller value was for 600 minutes ball milled sample and the undoped sample had a T_c value smaller than 60, 120 and 180 min ball milled samples but higher than 300 and 600 min samples.

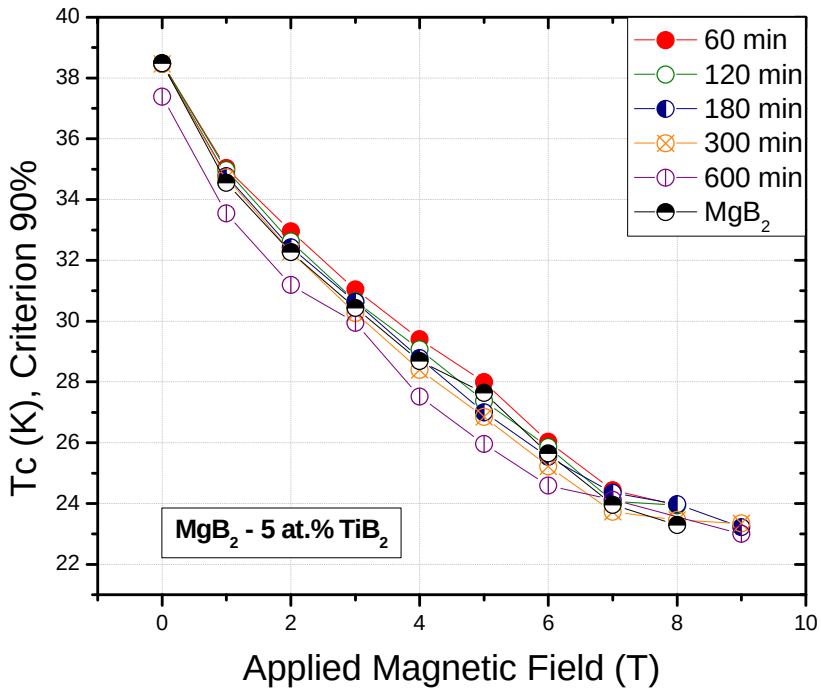

Figure 6.11. T_c Vs Applied Magnetic Field for MgB_2 - TiB_2 5 at.% doped materials at different milling times and MgB_2 undoped

In **Figure 6.12** is graphed the T_c values at cero field vs milling time. The values remain very close from 60 min to 300 min ball milled sample with a mean value of 38.47 K ± 0.02. For the 600 min the T_c value decreases until 37.39 K.

The undoped sample had a T_c value of 38.49 K which indicates that even thought there was not an increase in the T_c value respect to MgB_2 undoped, for the samples between 60 min and 300 min the T_c values didn't show a significant difference and the mean differ only in 0.02 K, while the 60 min ball milled sample reach the same value as the undoped.

The results in T_c indicate that the high energy ball milling process did not affect negatively the critical temperature for the MgB_2 - TiB_2 5 at.% doped materials for milling times lower than 300 minutes.

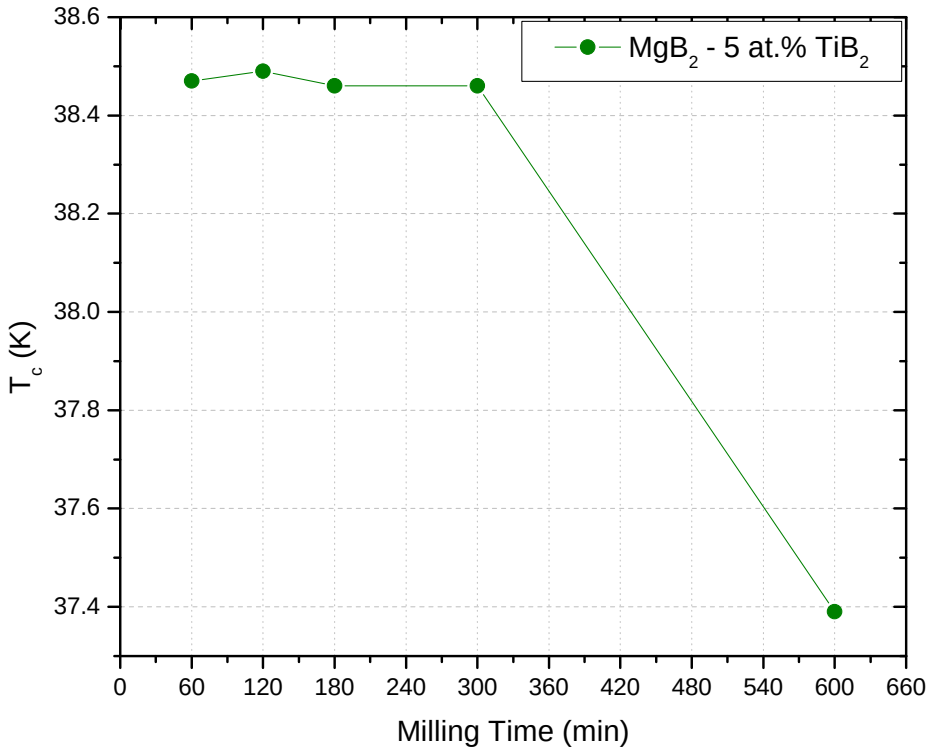

Figure 6.12. T_c Vs milling time for MgB_2 - TiB_2 5 at.% doped materials.

6.2.2. Critical Magnetic Field (Hc_2)

The critical magnetic field Hc_2 is defined as the maximum field that can be applied to a material before it lost the superconducting state.

Figure 6.13 shows the graph of Hc_2 versus Temperature for MgB_2 - TiB_2 5 at.% doped materials at different milling times in a range from 18 K to 40 K.

The Hc_2 at 20 K showed very similar values for all samples (between 9.25 T and 9.95 T), however there is a tendency of Hc_2 to decrease with the increasing in the milling time; the maximum Hc_2 value was for 60 min and the minimum for 600 min.

The MgB_2 undoped sample had the Hc_2 (20 K) value of 9.51 T, which shows that the Hc_2 values for small fields remain practically constant with a small increase between 60 min and 300 min.

At 30 K the Hc_2 of the MgB_2 - TiB_2 5 at.% doped materials were between 2.88 T and 3.87 T, with the smallest value for the 600 min ball milled sample; the tendency observed for Hc_2 is to decrease with the increasing in the milling time. The MgB_2 undoped sample had a value for Hc_2 at 30 K of 3.98 T which indicates that the Hc_2 parameter decrease in small quantity for the milled material at middle temperature.

For higher temperature, 37 K, the milled material presented values between 1.35 T and 0.92 T, the Hc_2 values showed the tendency to decrease with the increasing in milling time between 60 and 300 minutes, but for 600 minutes there was an increase until 0.99 T.

The Hc_2 (37 K) for 60 min ball milled sample had a value of 1.35 T, which was higher than the Hc_2 (37 K) for the undoped material that showed a value of 0.96 T. The Hc_2 for 120, 180 and 300 min ball milled material had smaller values than the undoped and the higher difference was with 300 min ball milled material for 0.04 T.

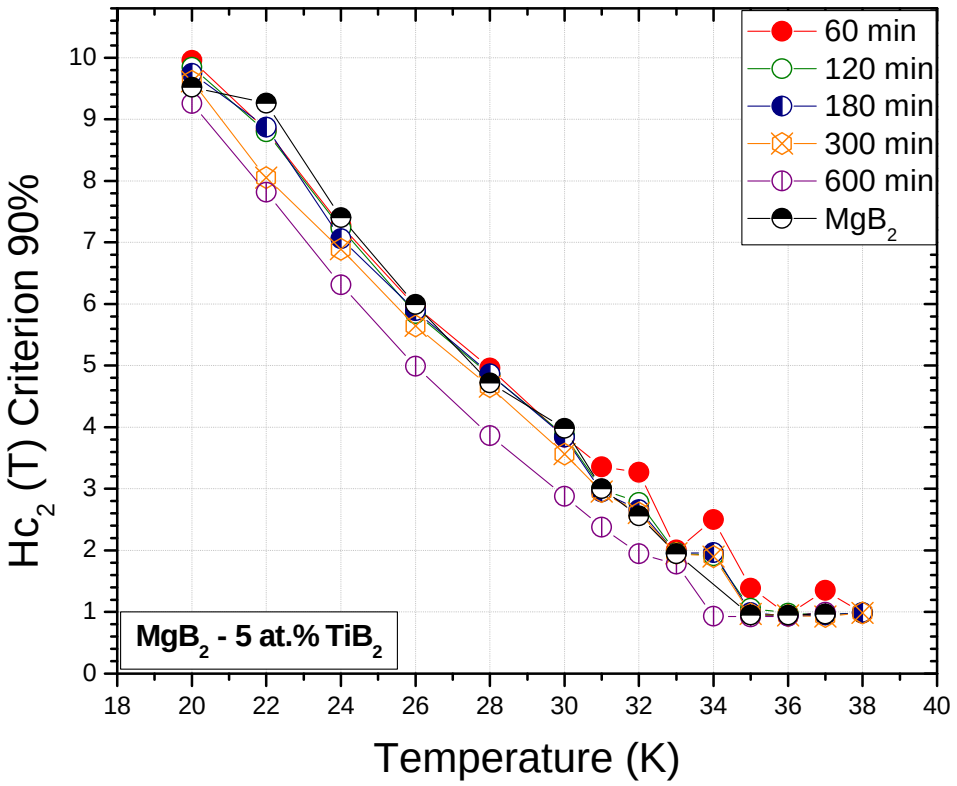

Figure 6.13. Hc_2 Vs Temperature for MgB_2 - TiB_2 5 at.% doped materials at different milling times.

In **Figure 6.14** is observed the Hc_2 (25 K) in function of milling time for MgB_2 - TiB_2 5 at.% doped materials. The tendency observed is the decreasing of Hc_2 with the increasing in milling time between 120 min and 600 min, with the maximum value for the 120 min ball milling time (6.832 T). The second value was for 60 min (6.754 T) very close to the higher value. Between 60 min and 300 min the Hc_2 (25 K) values were very close between 6.437 T and 6.754 T, however for 600 min there was a big decreasing in Hc_2 (25 K) with 5.692 T.

The reference material, the MgB_2 undoped, had an Hc_2 (25 K) of 6.752 T. The MgB_2 - TiB_2 5 at.% doped materials ball milled at 60 min and 120 min had higher values than the undoped, and between 180 min and 600 min ball milled the values for Hc_2 (25 K) were smaller.

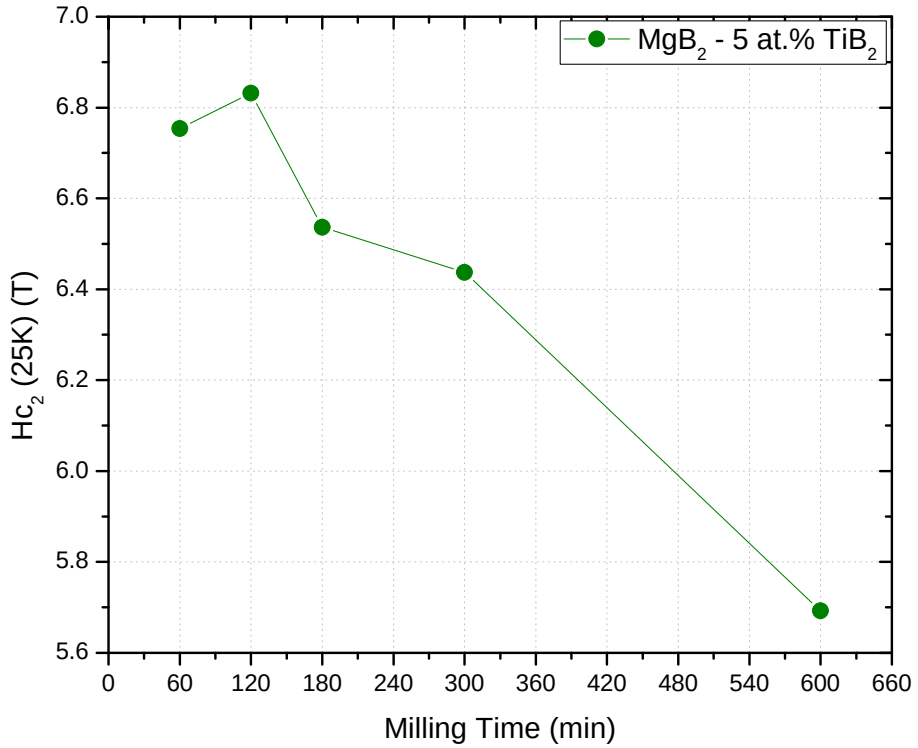

Figure 6.14. Hc_2 at 25 K Vs milling time for MgB_2 - 5 at.% TiB_2 doped materials.

The values found in Hc_2 and T_c for MgB_2 - TiB_2 5 at.% doped materials indicates that the high energy ball milling process didn't decrease the T_c and Hc_2 in significant values for milling times between 60 min and 300 min, and in some cases the Hc_2 values increase between 60 min and 120 min, without reduction in T_c which represents a good result since with this process has been demonstrated that can be enhanced one of the superconducting properties without sacrifice the other, as has occurred for other dopants. Moreover an additional property was obtained with this technique by decreasing the crystallite size with values in TiB_2 phase smaller than 61 nm and in MgB_2 phase smaller than 40 nm.

Table 6.III. T_c and Hc_2 values for 5 at.% TiB_2 doped MgB_2 material and MgB_2 undoped sample

Sample	T_c (K)	H_{c2} (25K) (T)
MgB_2 Undoped	38.49	6.7518
60 min	38.47	6.7539
120 min	38.49	6.832
180 min	38.46	6.5365
300 min	38.46	6.4374
600 min	37.39	5.6924

6.2.3. Resistivity Analysis

The resistivity graphs in function of temperature for MgB_2 - TiB_2 5 at.% doped materials at different milling times is shown in **Figure 6.15**.

The smallest resistivity is observed for MgB_2 undoped sample premilled at two hours. For the doped samples the 60, 120 and 180 minutes ball milled samples had very close resistivity graphs with smaller values than the 300 and 600 minutes. The 600 min ball milled material had the biggest resistivity. With these results is possible to outline a tendency between the resistivity and the milling time, the increasing in milling time produces an increasing in resistivity, although this tendency is more evident for the 300 and 600 min ball milled samples which exhibit a bigger increment in resistivity than the other samples.

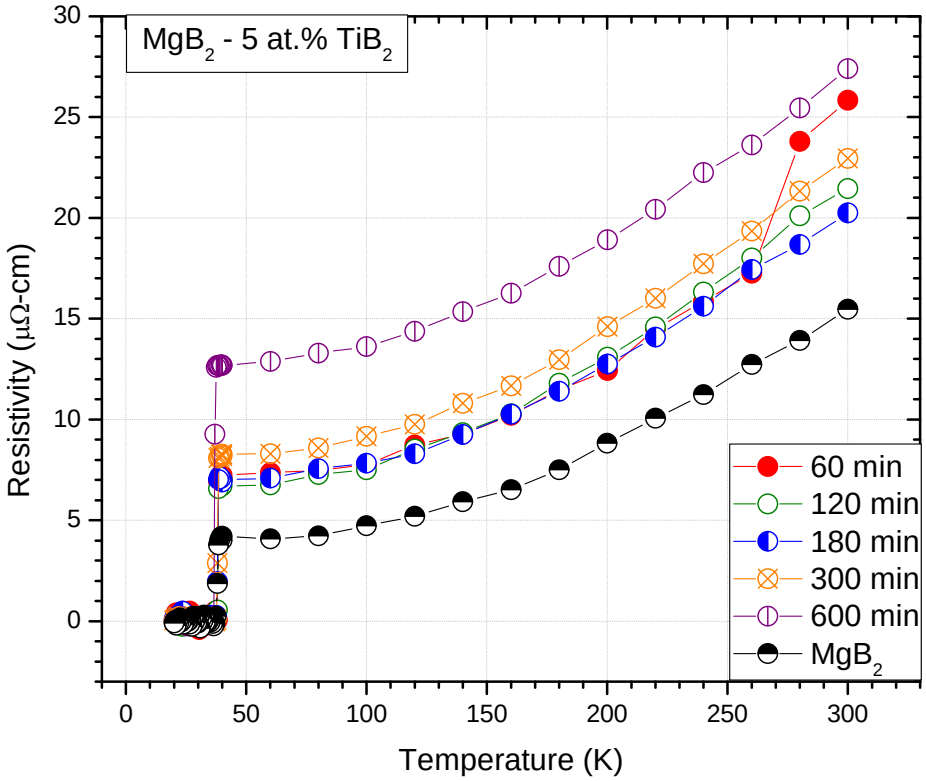

Figure 6.15. Resistivity graph for MgB_2 - TiB_2 5 at.% doped materials milled at different times versus Temperature.

Table 6.IV had the values of RRR, A_F and ρ_A properties found from resistivity measure. These properties are develop using the Rowell model which define a comparison value of resistivity for MgB_2 undoped, based in experimental results obtained for a fully connected sample (ρ_{ideal} = 7.3 μΩ.cm).

Table 6.IV. Resistivity measurements for MgB_2 - 5 at.% TiB_2 doped materials

Sample	ρ_{300K} (μΩ.cm)	ρ_{40K} (μΩ.cm)	**RRR** (ρ_{300K}/ρ_{40K})	$\rho_{300K} - \rho_{40K}$ (μΩ.cm)	A_F $\left(\frac{\rho_{ideal}}{\rho_{(300K)} - \rho_{(40K)}}\right)$	ρ_A (40K) (μΩ.cm)
MgB_2 undoped	15.48	4.01	3.86	11.48	0.64	2.55
60 min	25.84	7.07	3.66	18.77	0.39	2.75
120 min	21.45	6.70	3.20	14.75	0.49	3.32
180 min	20.24	6.90	2.94	13.35	0.55	3.77
300 min	22.95	8.19	2.80	14.76	0.49	4.05
600 min	27.40	12.68	2.16	14.71	0.50	6.29

The A_F value indicates the percentage of the transversal area for which the current pass and that is effectively connected in the sample.

The higher A_F was found for the MgB_2 undoped material with a value of 0.64, representing the percentage of the effectively connected area.

In **Figure 6.16** is graphed the A_F values for MgB_2 - 5 at.% TiB_2 doped materials at different milling times. The higher A_F is observed for 180 minutes ball milled sample with a value of 0.55, representing this value a 55% of effective connected area in the sample. For 120, 300 and 600 min ball milled samples the values were almost constant with 0.49, 0.49 and 0.5 respectively. The smallest A_F was for 60 min with 0.39, indicating a sample connected effectively in a 39% of the total area.

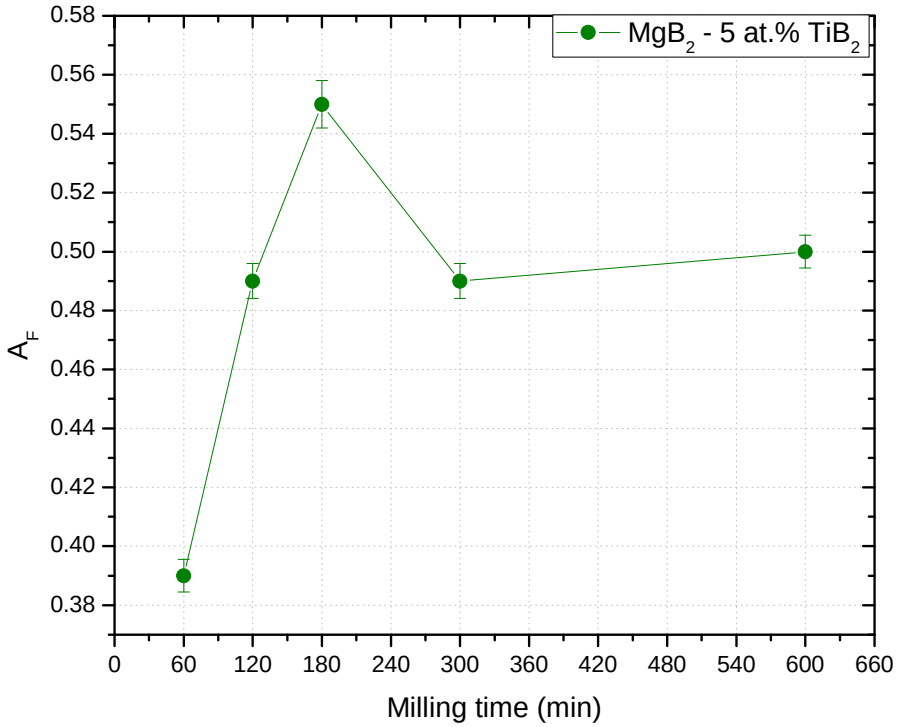

Figure 6.16. A_F Vs milling time for MgB_2 - 5 at.% TiB_2 doped materials.

Figure 6.17 shows the critical magnetic field Hc_2 in function of A_F. There is not a defined trend between the Hc_2 and A_F. The highest value in A_F corresponds to a sample which had the third value in Hc_2 between the milled samples, while the higher value in Hc_2 had a medium value in A_F. There is not a clear relation between A_F and Hc_2 specifically for these samples, because even though the 600 min ball milled sample had the lowest value in Hc_2 between the milled materials, the A_F for this sample had almost the same value than the sample with the highest Hc_2 (120 min).

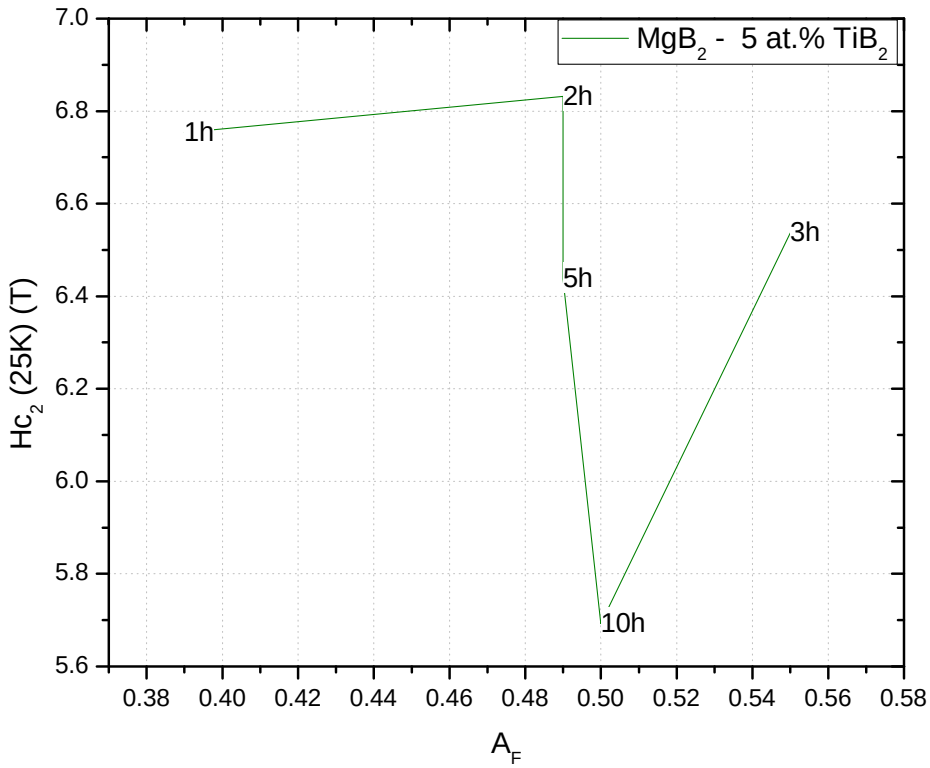

Figure 6.17. Hc_2 Vs A_F for MgB_2 - TiB_2 5 at.% doped materials

The A_F value indicates the percentage of the transversal area for which the current pass and that is effectively connected in the sample. However the definition of A_F uses as reference the ideal value for resistivity in the MgB_2 pure sample without dopant, for this reason the Rowell theory could not reflect the real connectivity in these components which have as dopant material TiB_2 at 5 at.% and probably will need a modification to have a complete validity of the results.

The residual resistivity radio (RRR) is a measure of the defect scattering, while the defect scattering increases, the RRR decreases, approaching to 1 for high defect concentrations.

The higher value in RRR was for MgB_2 undoped premilled sample with 3.86.

Figure 6.18 shows RRR in function of milling time for MgB_2 - TiB_2 5 at.% doped materials, the trend observed shows that RRR decreases with the increasing in milling time. The range in RRR for the doped material was between 2.16 and 3.66.

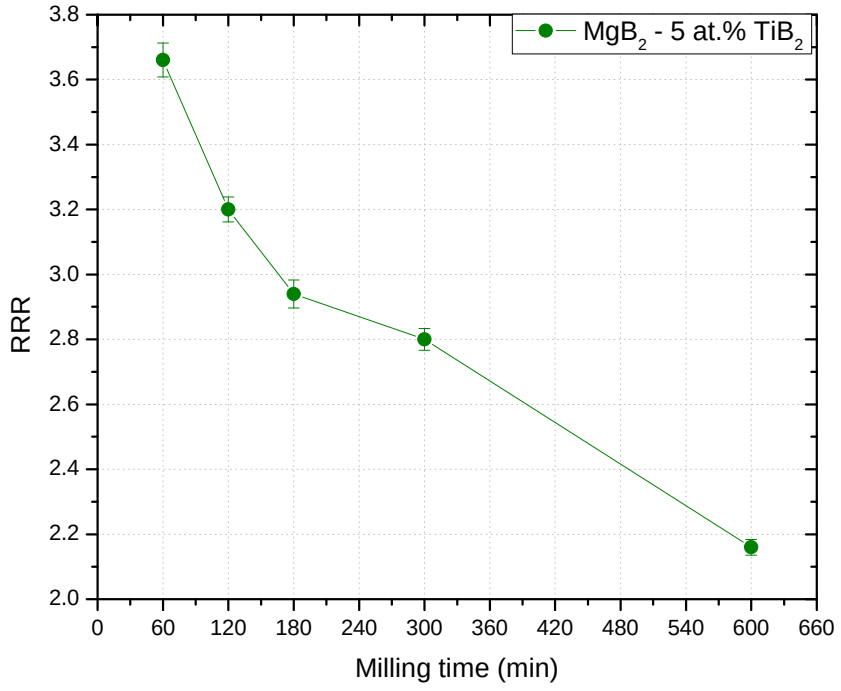

Figure 6.18. RRR Vs milling time for MgB_2 - TiB_2 5 at.% doped materials.

Figure 6.19 showed the graph of Hc_2 (25 K) versus RRR for MgB_2 - TiB_2 5 at.% doped materials for different milling times. The tendency of the Hc_2 is to increase with the increase in the RRR. The highest value in RRR was for the 60 min ball milled sample which has the second value in Hc_2, the second value in RRR was for 120 min sample which had the maximum value in Hc_2 between the doped materials. Both samples had very close values in RRR and Hc_2. The minimum value in RRR was for 600 min sample that presents also the minimum value in Hc_2.

The tendency of increase the Hc_2 with the increasing in RRR, shows that Hc_2 value can be decrease with the presence of high scattering defect. The scattering defects decrease the property of the superconducting material to generate an internal field sufficiently strong to avoid the

partial or total penetration of external field in the material, which will deteriorate the superconducting properties.

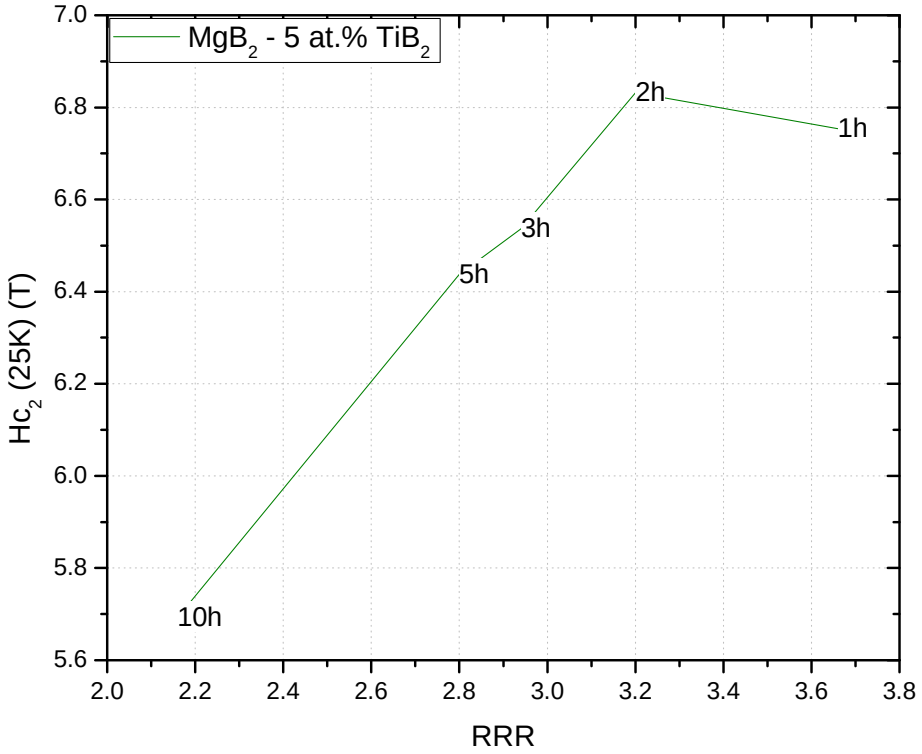

Figure 6.19. Hc_2 at 25 K Vs RRR for MgB_2 - TiB_2 5 at.% doped materials at different milling times

7. Effect of 5 at.% CrB_2 in the Superconducting and Structural Properties of MgB_2

This chapter describes the results in superconducting and structural properties of MgB_2 - 5 at.% CrB_2 material. The values of Hc_2 and T_c for CrB_2 5 at.% doped MgB_2 material were smaller compared with the MgB_2 undoped material. Moreover, the resistivity in the doped samples at different milling times were higher compared to the undoped material and the parameters extracted from the resistivity values as ρ_A, A_F, and RRR did not show an improvement compared with the MgB_2 undoped premilled material. Comparing the result obtained here with the studied reported by Zhang *et al.* [55], it is possible that the reduction in T_c and Hc_2 and the increasing in resistivity could be associated with the introduction of Cr in the Mg-layer. Due to the reduction in the superconducting properties it is possible to conclude that CrB_2 material is not a good candidate for the doping of MgB_2 material at 5 at.% with the ball milling technique.

7.1. General Characteristics

CrB_2 and MgB_2 have hexagonal C32-type structure. The lattice parameters of CrB_2 are a = 2.969 Å and c =3.066 Å, while for MgB_2 the lattice parameters are a = 3.0835 Å and c = 3.521 Å; the standard formation enthalpy ($-\Delta H^0_{f298}$) for the CrB_2 is 33 Kcal/mole and for the MgB_2 is 22 Kcal/mole and the melting temperature for CrB2 is 2280 ± 20.

The superconducting properties of MgB_2 have been widely studied, with the T_c found to be 39 K which is considered a high critical temperature for a binary compound. A lot of studies have been conducted with the purpose of increasing the J_c and Hc_2 properties, based on diverse synthesis and dopants. C and SiC dopants are between the most studied dopants for MgB_2 obtaining important results in J_c and Hc_2; Matsumoto *et al.*[56] doped MgB_2 bulk with SiC at 10% reaching an enhancement of Hc_2 (10 K) with a value higher than 33 T and extrapolated to zero temperature, exceeds 40 T. Senkowicz *et al.*[26] studied MgB_2 in bulk doped with C at 5 at.% ball milled at 1, 15, 60, 300, 600, 1200, and 3000 min and HIP at 1000°C and 30 Kpsi for 200 min. The results showed that the 60, 300 and 1200 min ball milled samples had Hc_2 (4.2 K) values very similar and close to 33 T, the higher J_c (8 T, 4.2 K) was at 80.000 A/cm^2 for the 1200 min of milling. Diborides have also been used to doped MgB_2, Bathia et al. [35] doped MgB_2

with ZrB_2 at 7.5at.% and ball milled with SPEX for 48 min, after that they formed pellets and HIP from 700-900°C at 0.5 hours. They compare the ZrB_2 7.5 at.% sample with the MgB_2 undoped sample. The results showed an increased in Hc_2 (4.2 K) from 20.5 T (MgB_2 undoped) to 28.6 T (ZrB_2 doped), while the values for $\mu_0 H_{irr}$ had an enhancement from 16 T (MgB_2 doped) to 24 T (ZrB_2 doped). The T_c property showed a decreasing compare to the MgB_2 undoped sample from 38.2 K to 35.7 K.

For the purpose of doping MgB_2 with 5 at.% CrB_2, the high energy ball milling technique (HEBM) was employed by first undertaking a pre-milling of the dopant and host materials, followed by milling of appropriate amounts as a function of ball milling time.

7.2. Structural Properties

The structural properties of CrB_2 5 at.% doped material was analyzed using the XRD characterization technique. The composition, crystallite size, strain and lattice parameters were found for the samples.

The XRD technique was used to analyze the powder material after the ball milling process as well as the pellet material after the HIP process. The comparison of both results will define the effect of the HIP on the structural properties.

The analysis of each sample was carried out based in the recognition that there was possibility of having unreacted dopant material, oxide contamination associated with the MgB_2 material, MgB4, grinding balls and containers materials (WC) and also the elemental constituents such as Mg, Cr and B. In addition, the presence of Si probably from the HIP stages was identified.

Figure 7.1 shows the graph of the MgB_2 doped CrB_2 5 at.% for different milling times identifying the peaks related with each component.

The presence of B in the XRD spectra showed that one or both of the initial compounds decomposed, thereby freeing elemental B, however the absent of Cr suggested that the compound decomposed was MgB_2, theory that was supported by the MgO content found. The presence of MgO is understood because it is known that Mg reacts with O to form MgO, and if MgB_2 decomposed it generated Mg and B. The free Mg reacted with the Oxygen that ingress in the sample during the synthesis process to form MgO.

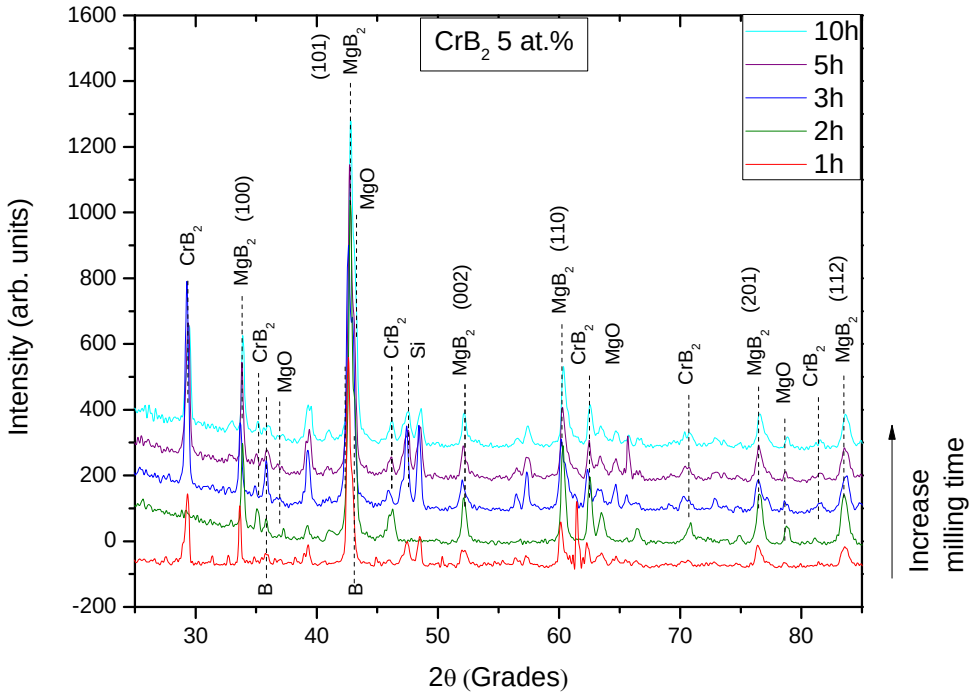

Figure 7.1. X ray diffraction spectra of 5 at.% CrB_2 doped MgB_2 as a function of increasing ball milling times.

The ingress of Si in the sample could have occurred during the polishing phase. The Si element could have remained in some pores formed in the sample during the polishing even though it was cleaned after the polishing process.

Zhang *et al.* [55] doped MgB_2 with Cr between 1 and 5 at.%; they used Mg, B, and Cr as starting materials, mixed them and pressed into pellets that were heat treated a 950°C for 10 hours. In the XRD analysis they found that the main phase was MgB_2, CrB and the CrB_2 phase appeared as the Cr doping levels reached 5 at.%. The MgO phase was presented in all their samples. The XRD pattern reported by Zhang *et al.* [55] is shown in **Figure 7.2.** The peaks for MgB_2, CrB_2 and MgO reported by Zhang *et al.* correspond with the peaks for **Figure 7.1** found in this work,

however, the peaks in the XRD pattern of Zhang *et al.* [55] are sharper than the observed for this research, which indicates bigger crystallite for their samples.

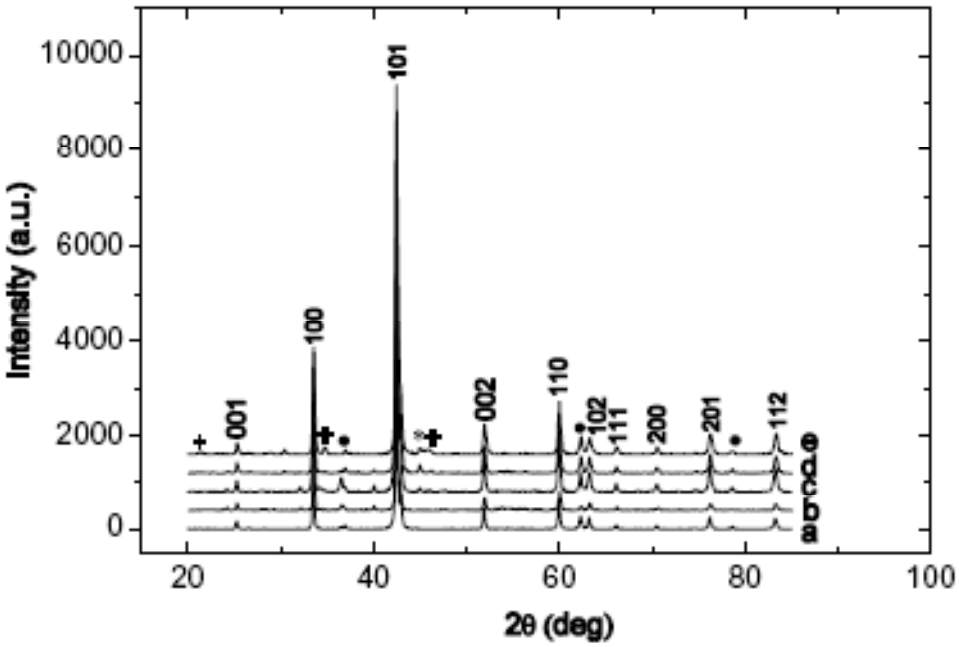

Figure 7.2. X-ray diffraction patterns of $Mg_{1\_x}Cr_xB_2$ samples with different Cr content. (a) x = 0; (b) x = 0.01; (c) x = 0.02; (d) x = 0.03; (e) x = 0.05. The impurities were marked by: ‘‘•’’ MgO; ‘‘+’’ CrB2; ‘‘*’’ CrB. Zhang *et al* [55].

The EDX analysis for the two hours ball milled material (i.e. MgB_2 – 5 at.% CrB_2) was shown in **Figure 7.3**.The results showed the presence of Fe in the sample, even though this element was not identifying in XRD, which suggested low composition percentage in the sample. The Fe can be a result of a reaction between the sample and the stainless steel tube. Some of the cut HIPed samples revealed two concentric pattern contrasts which indicated possible formation of an undesired phase between the doped material and the stainless tube material used for the HIP process.

Figure 7.4 shows the SEM of the 120 minutes ball milled sample. Two phases were identified on the image. The MgB_2 phase would correspond to the gray crystallites; while the CrB_2 would be represented by the white crystallites.

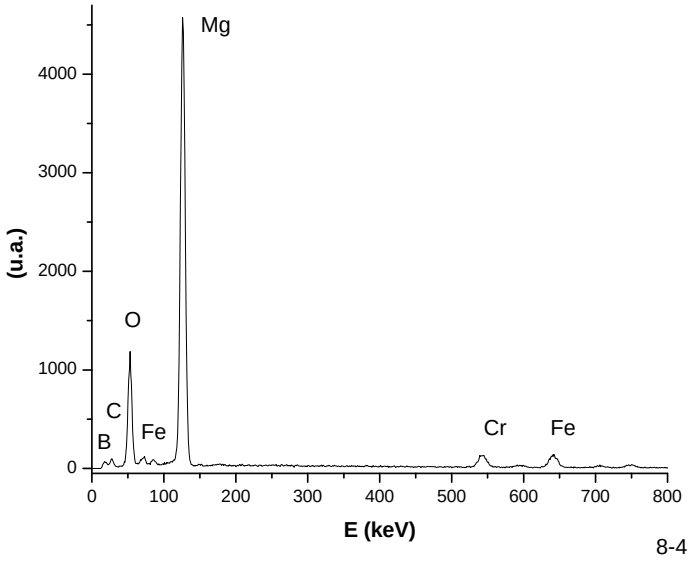

Figure 7.3. MgB_2 – 5 at.% CrB_2 doped sample corresponding to 2 hours of ball milling.

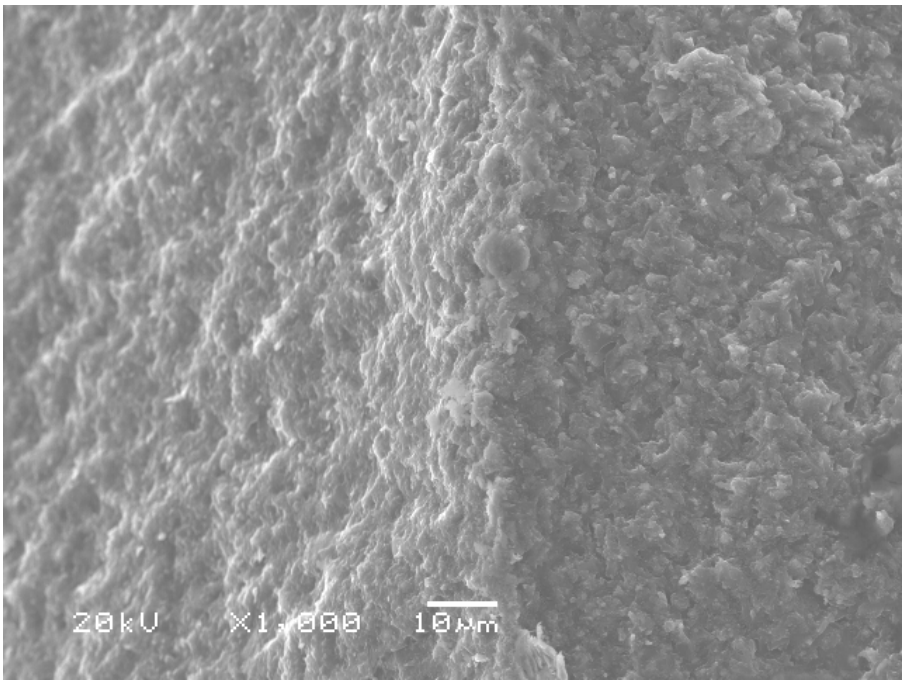

Figure 7.4. Scanning Electron Micrograph (SEM) of two hours ball milled 5 at.% CrB_2 doped MgB_2 material after HIPing.

Figure 7.5 shows the compositional analysis of the material after pre-milling and milling before the eventual consolidation to obtain the superconducting with hot isostatic pressing.

Comparing the compositional analyses of the doped MgB_2 powder materials at different milling times, a tendency to decrease with the increasing of milling time from 74 wt.% at 60 min ball milled to 62 wt.% at 600 min ball milled was observed. The decreasing in MgB_2 composition contrasted with the increasing in B from 16 wt.% at 60 min of milling time to 26 wt.% at 600 min of milling time. The compositional decreasing tendency of MgB_2 suggests the decomposition of this compound in Mg and B elements during the ball milling process, hypothesis that is supported by the increasing observed in the composition of B.

The percentages of MgO and CrB_2 for powder material did not show a significant change between the milling times.

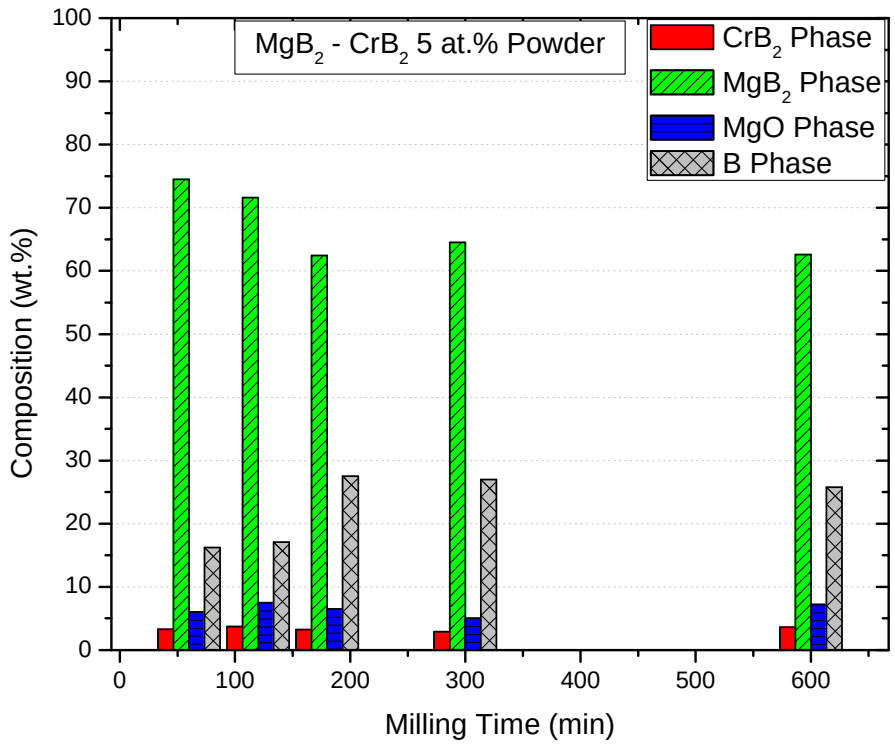

Figure 7.5. Composition of CrB_2, MgB_2, MgO and B phases for powder material as a function of ball milling time.

Figure 7.6 showed the composition of the phases for the 5 at.% CrB_2 doped MgB_2 pelletized forms as a function of ball milling time.

Comparing the 60 min ball milled sample with the other pellet samples, it was clear that there was a reduction in MgB_2 phase with corresponding increase in B phase. This behavior was similar to the described for powder material; the composition of the MgB_2 phase decreased respect to the 60 min ball milling material, which suggests the possibility of decomposition of this phase in Mg and B.

The percentage for MgO phase showed a small increase for the 600 minutes compared with the other milling times. The CrB_2 percentage didn't show significant changes between the milling times for the samples.

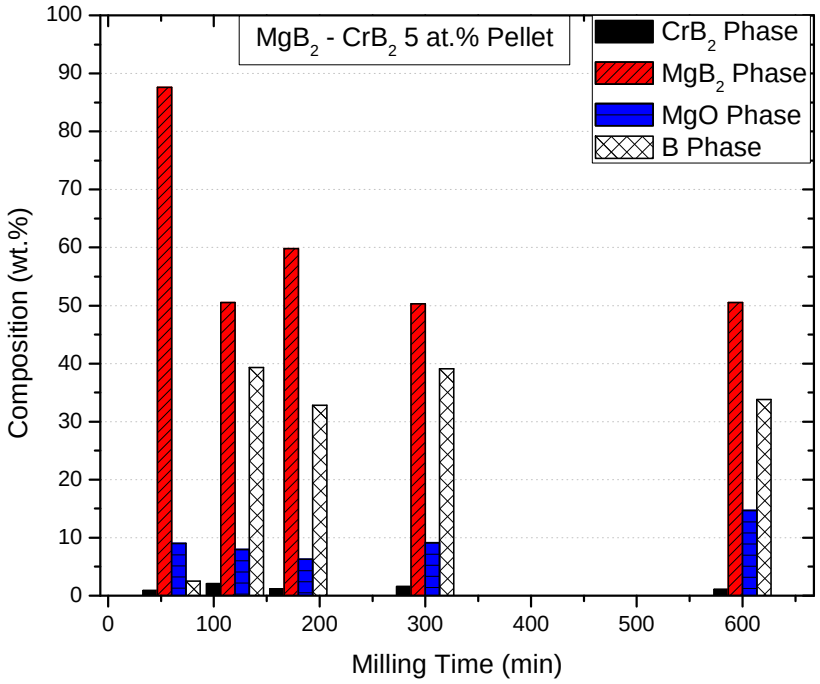

Figure 7.6. Composition of CrB_2, MgB_2, MgO and B phases, for pellet post HIP material in function of milling time.

Comparing the powder materials in the pellet form, it was observed that most of the sample showed a higher percentage for the MgB_2 phase in powder form than in the pellet form for the same composition with the exception of the one hour ball milled one. For the B phase, the powder material had a smaller percentage compared with the pellet material, except for the one hour ball milled sample. These results showed that during the HIP process the MgB_2 decomposed in Mg and B for which decreased the percentage of MgB_2 and with the increase of the percentage of B and MgO from powder to pellet.

The composition values for MgB_2, CrB_2, B, and MgO phases in powder material are observed in **Table 7.I**, the composition of the same phases in pellet material are observed in **Table 7.II.**

The crystallite size in the powder and the pellet material for the CrB_2 phase are shown in **Figure 7.7**. The crystallite size for powder material within CrB_2 phase was between 8.87 nm and 11.72 nm without showing significant variations with the milling time. For the pellet material the crystallite size was between 61.99 nm and 122.45 nm; the initial value decreased within the 60 min to 120 min ball milling, which was followed by an increase between the 120 and 600 min milling. **Figure 7.7** showed the observed increase in the crystallite size with the HIP process; for the dopant CrB_2 which didn't follow a specific pattern.

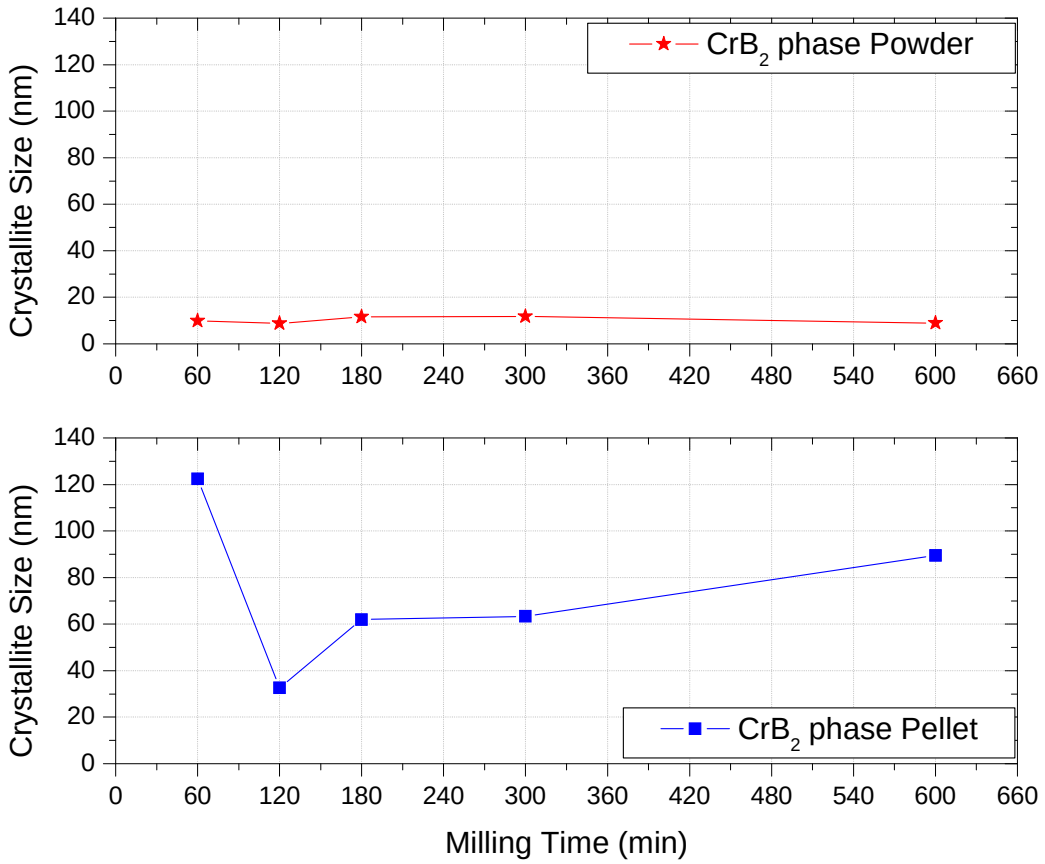

Figure 7.7. Crystallite size variation of CrB_2 phase for the powder and pellet form as a function of milling time.

The corresponding crystallite size of MgB_2 phase for CrB_2 5 at.% material in powder and pellet were shown in **Figure 7.8**. The crystallite size variation of the MgB_2 phase in the 5 at.% CrB_2 doped material was shown in **Figure 7.8**, which showed that it varied from 6.98 nm to 11.01 nm. The general tendency in the crystallite size for powder material was to decrease with the increase in milling time. For pellet samples the variation in crystallite size was between 13.85 nm and 32.59 nm. Some changes in the tendency of the crystallite size with the milling time were observed for the HIPed material; in some ranges there was a decreasing trend in the crystallite size with the increasing of the milling time, while in other there was an increasing tendency.

The crystallite size values for powder material are observed in **Table 7.I**, and for pellet material in **Table 7.II**

By comparing the powder and pellet materials it is evident that the crystallite size increased from the powder to pellet samples, indicating that during the HIP process the MgB_2 crystallites increased its size, even though there is not a clear pattern in this increment.

Based on the values of the structural properties deduced from XRD measurements which are observed in **Table 7.I** and **Table 7.II**, it is possible to conclude that with the ball milling process the crystallite size for the CrB_2 phase decreased attaining values less than 9.0 nm, contrary to the same sample after the HIP process which showed increases in the crystallite size reaching a value of 122 nm. In the case of the MgB_2 phase, the crystallite size was reduced with the ball milling to values of 11 nm or less, contrary to the increasing of the crystallite size with the HIP process which attained a maximum value close to 32 nm, even thought to a lesser degree than the case of CrB_2 phase.

Zhang *et al.* [55] determined the grain size of MgB_2 doped with Cr between 1 and 5 at.% using SEM technique, they found that grain size increased apparently with Cr dopping concentration increase; the grain size for the pure sample was about 50 nm, while the grain size became to about 1 μm for Cr 3 at.% doped MgB_2. In **Figure 7.2** sharper peaks are observed compare with the ones in **Figure 7.1** for this work, which indicated bigger crystallites for Zhang *et al.* [55].

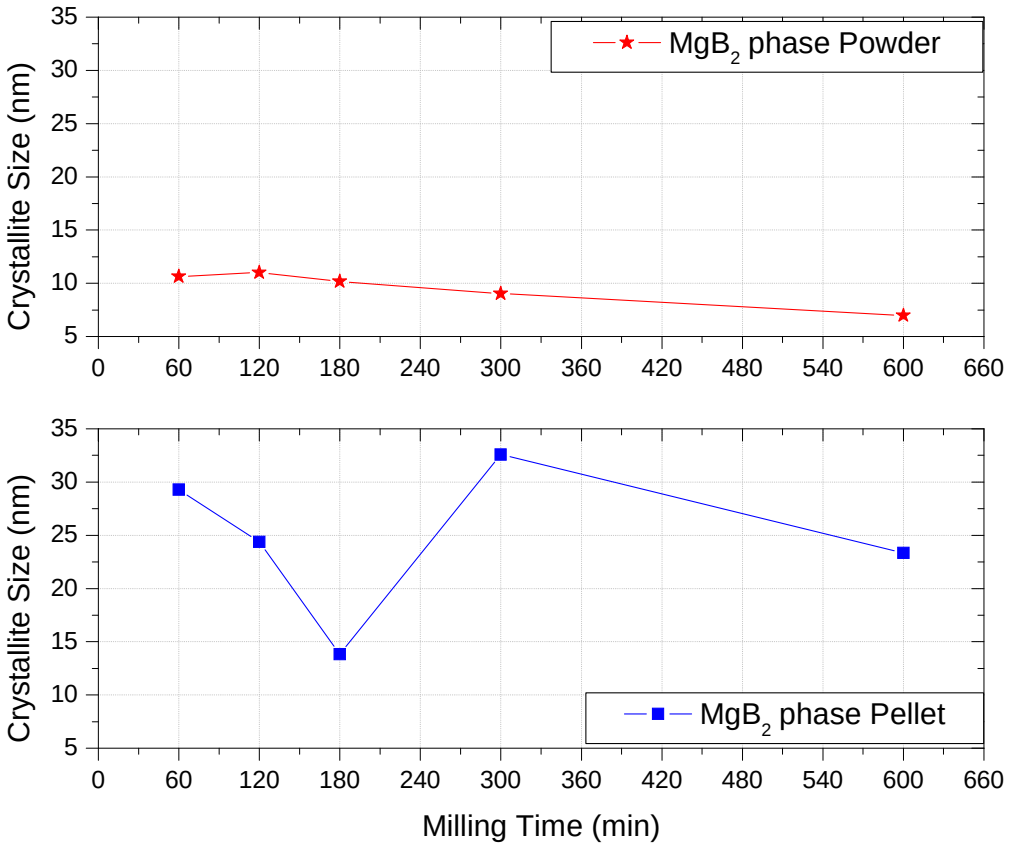

Figure 7.8. The crystallite size change of MgB_2 phase as with milling time in the powder and pellet forms.

Figure 7.9 showed that the HIP process influenced the internal strain associated with the CrB_2 phase in the powdered state. Apart from the 180 min ball milled material, the HIP process tended to reduce the strain from their values in the powdered states. This could be explained from the fact that after ball milling the samples were in metastable states with a high strain caused by the high energy imparted in the milling process which caused a change in the structure and introduce disorder in the material. After the HIP process the metastable state changed to a more stable state with high temperature which caused the reorganizing of the defect structure and subsequently decrease in the average strain.

The average strain generated during the ball milling decreased after the HIP process which was definitely associated with the effect of the heat treatment and the pressure.

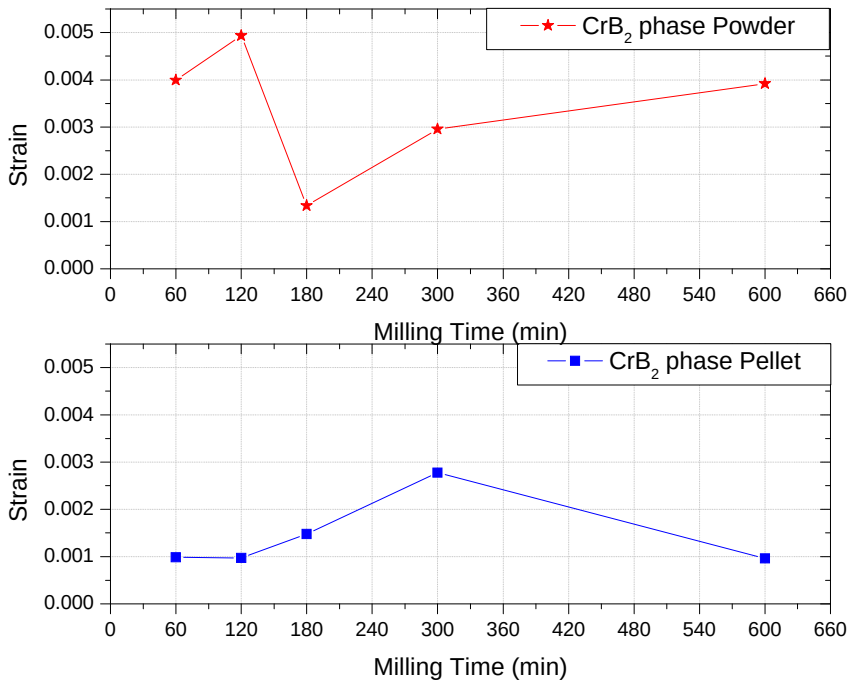

Figure 7.9. Comparison of the average strain of CrB_2 phase in the powder and pellet forms.

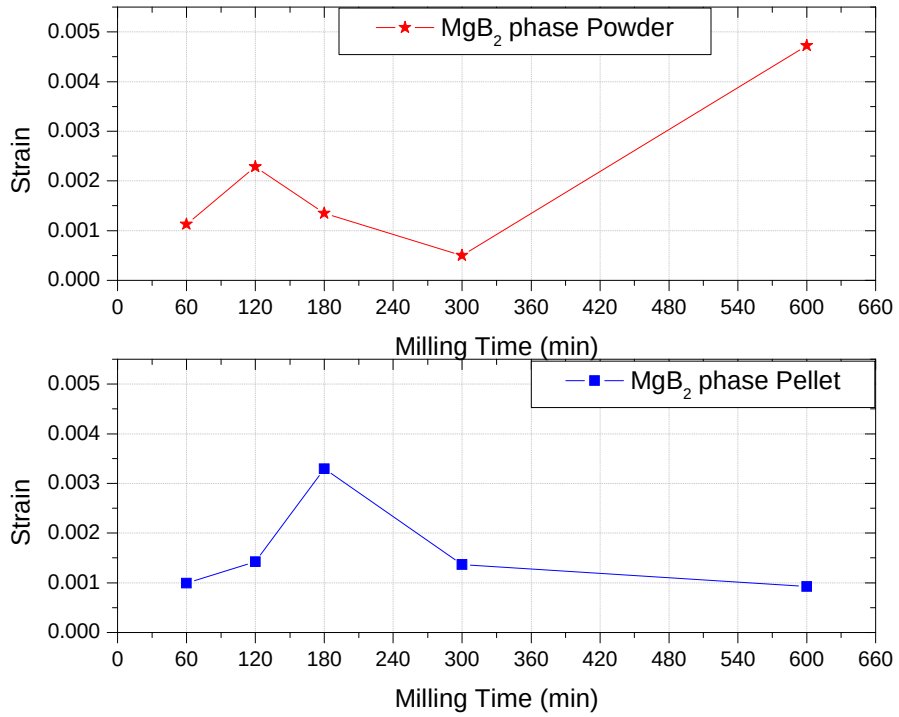

Figure 7.10. Comparison of the average strain of MgB_2 phase in the powder and pellet forms.

The variation of lattice parameter a–axis and c-axis of MgB_2 phase as a function of milling time is shown in **Figure 7.11.** There was an initial decreasing in both lattice parameters, from 0 to 60 min of milling time, however the change in c parameter was higher that the decrease in the a parameter, in 120 and 300 min the change in the lattice parameters was similar for both compounds and for 300 min and 600 min the c parameter increased and was higher than the a parameter. These changes in the lattice parameters could be associated with the strain caused during the milling process, however could also represent a change in the structure due to the introduction of the Cr element into the Mg-layer.

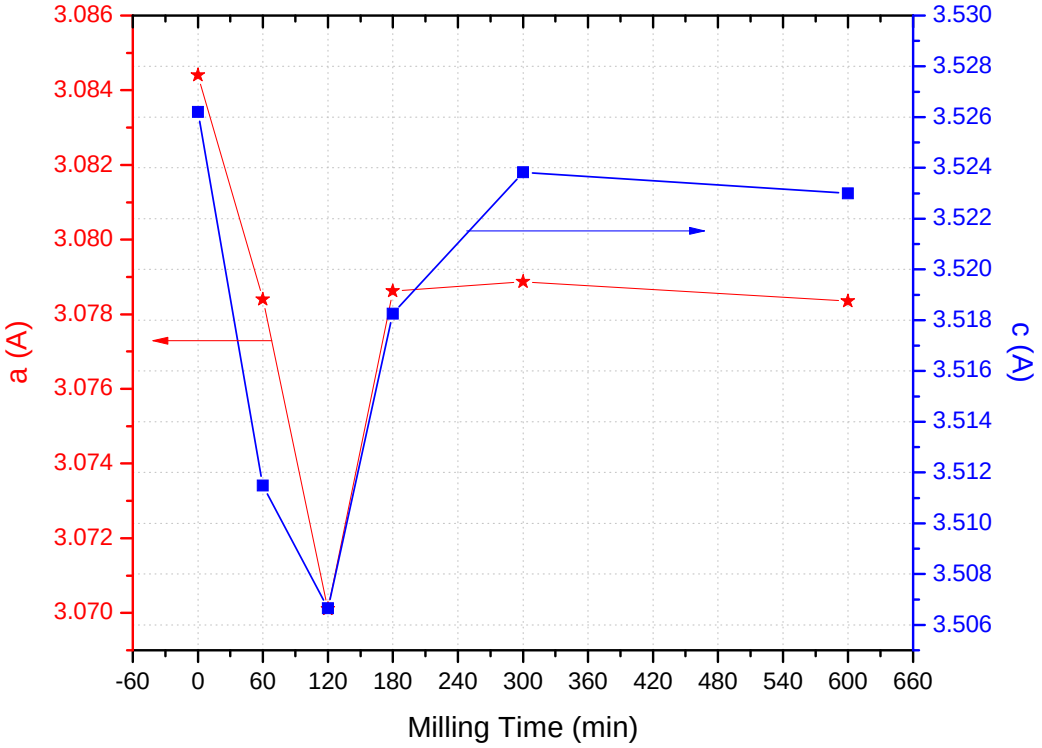

Figure 7.11. Lattice parameter variation in MgB_2 phase as a function of milling time.

Zhang *et al.* [55] reported a decrease in the c-axis lattice parameter for MgB_2 - 5 at.% Cr which is observed in **Figure 7.12,** the reduction in the c-axis lattices parameter was related with the introduction of Cr into the Mg-layer. The radius of Mg^{2+} and Cr^{3+} are similar which did not alter

the a-axis, however due to the higher valence of Cr, there are more electrons transferred for Cr than for Mg. Therefore, the Coulomb interaction between the B-layer and the Mg-layer was stronger which caused the reduction of the c-axis. Then for MgB_2 - 5 at.% Cr material there was an introduction of Cr in Mg-layer.

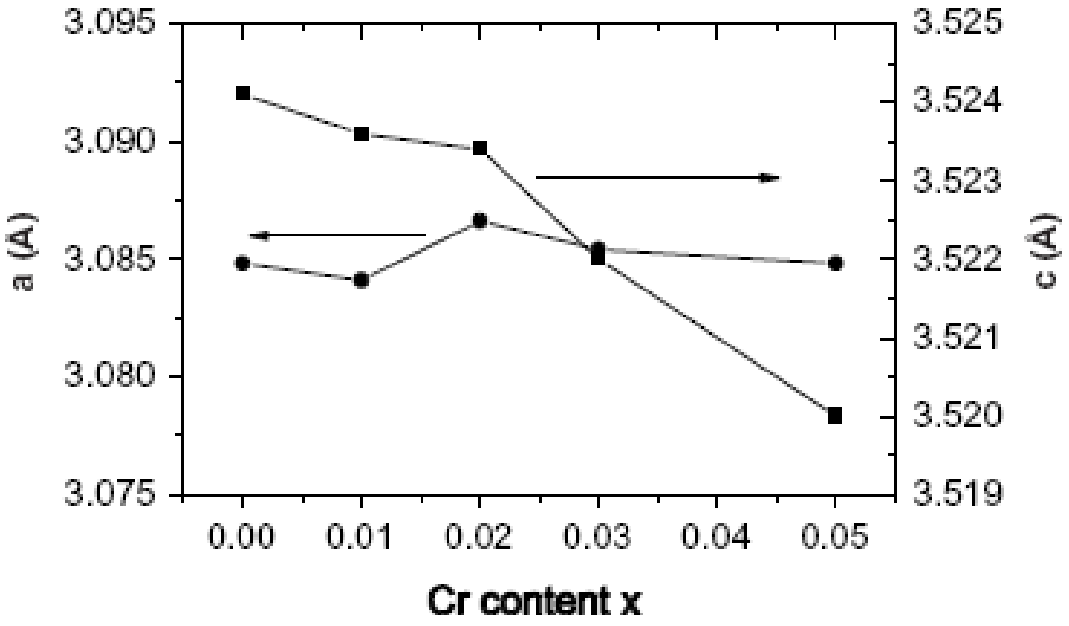

Figure 7.12. Variation of the lattice parameters of a-axis and c-axis with Cr content in $Mg_{1\_x}Cr_xB_2$ [55].

Table 7.I. Composition, lattice parameters, crystallite size and strain of CrB_2 5 at.% material in powder ball milled at different milling times.

CrB_2 5 at.% Powder Material							
Sample	**Compound**	**Composition (wt. %)**	**Lattice Parameters**			**Crystallite Size (nm)**	**Strain**
			a(Å)	**c(Å)**	**c/a**		
60 min	CrB_2	3.3	2.964036	3.044445	1.027128	9.87	0.003990
	MgB_2	74.5	3.081651	3.521249	1.14265	10.65	0.001127
	MgO	6.0	4.206283	4.206283	1	7.18	0.004687
	B	16.2	4.881540	12.47000	2.554522	3.66	0.013485
120 min	CrB_2	3.7	2.969224	3.036519		8.83	0.004936
	MgB_2	71.6	3.081871	3.517849	1.141465	11.01	0.002284
	MgO	7.5	4.208533	4.208533	1	2.90	0.008888
	B	17.1	4.838771	12.51904	2.587235	3.60	0.013495
	WC	0.2	2.89929	2.839672	0.979437	18.12	0.002031
180 min	CrB_2	3.2	2.970593	3.033670	1.021234	11.62	0.001334
	MgB_2	62.4	3.082691	3.523657	1.143046	10.16	0.001347
	MgO	6.5	4.212037	4.212037	1	3.53	0.008378
	B	27.5	4.812755	12.47000	2.591032	2.97	0.009436
	WC	0.5	2.904692	2.837057	0.976715	14.52	0.002414
300 min	CrB_2	2.9	2.962077	3.061938	1.033713	11.72	0.002958
	MgB_2	64.5	3.082293	3.519125	1.141723	9.03	0.000497
	MgO	5.0	4.209420	4.209420	1	8.58	0.003870
	B	27.0	4.880893	12.47401	2.555682	3.05	0.002769
	WC	0.5	2.903591	2.837014	0.977071	13.75	0.002904
600 min	CrB_2	3.6	2.970213	3.042728	1.024414	8.87	0.003916
	MgB_2	62.6	3.083006	3.519418	1.141554	6.98	0.004727
	MgO	7.2	4.216851	4.216851	1	3.97	0.006866
	B	25.8	4.844964	12.59618	2.59985	2.98	0.009894
	WC	0.8	2.899837	2.842857	0.980351	14.70	0.001610

Table 7.II. Composition, lattice parameters, crystallite size and strain of CrB_2 5 at.% material in pellet ball milled at different milling times.

Cr B_2 5 at.% Pellet Material							
Sample	**Compound**	**Composition (wt. %)**	**Lattice Parameters**			**Crystallite Size (nm)**	**Strain**
			a(Å)	**c(Å)**	**c/a**		
MgB_2 raw unmilled HIP*	MgB_2	92.2	3.0844	3.5262	1.143237	73.03	0.001098
	MgO	7.8	4.2242	-		19.47	0.001600
MgB_2 undoped premilled HIP	MgB_2	79.2	3.085226	3.526575	1.143052	32.76	0.001316
	MgO	17.5	4.215603	-		3.77	0.009647
	B	3.2	4.932873	12.57649	2.549526	5.10	0.006819
60 min	CrB_2	0.9	2.970714	3.062918	1.031038	122.45	0.000987
	MgB_2	87.6	3.078398	3.511484	1.140686	29.29	0.000992
	MgO	9.0	4.211503	4.211503	1	60.97	0.000698
	B	2.5	4.810000	12.47000	2.592516	2.98	0.009278
120 min	CrB_2	2.1	2.969204	3.064858	1.032215	32.64	0.000975
	MgB_2	50.5	3.070107	3.506652	1.142192	24.40	0.001421
	MgO	8.0	4.211648	4.211648	1	36.96	0.001207
	B	39.3	4.893470	12.54600	2.563825	3.59	0.013689
180 min	CrB_2	1.2	2.961864	3.070378	1.036637	61.99	0.001480
	MgB_2	59.8	3.078619	3.518255	1.142803	13.85	0.003294
	MgO	6.3	4.215812	4.215812	1	58.53	0.000738
	B	32.8	4.877848	12.47000	2.556455	2.98	0.009886
300 min	CrB_2	1.6	2.974630	3.056249	1.027438	63.32	0.002777
	MgB_2	50.3	3.078869	3.523830	1.144521	32.59	0.001367
	MgO	9.1	4.214777	4.214777	1	67.0	0.002853
	B	39.1	4.810000	12.47000	2.592516	4.32	0.007597
600 min	CrB_2	1.1	2.969500	3.065743	1.032411	89.52	0.000963
	MgB_2	50.5	3.078352	3.522989	1.14444	23.34	0.000921
	MgO	14.7	4.218801	4.218801	1	10.8	0.002814
	B	33.8	4.810000	12.47057	2.592634	7.37	0.006766

7.3. Superconducting Properties: Resistivity Measurements

The superconducting properties of MgB_2 - CrB_2 5 at.% doped material were characterized using the resistivity measurement. The effect of the milling time on the critical temperature (T_c) and critical magnetic field (Hc_2) were studied as while the Rowell theory [39, 40] was also carried out in order to determine some parameters such as the grain connectivity, the resistivity and the scattering in the material.

Table 7.III showed the data of T_c (0 T) and Hc_2 (25 K) corresponding to the 0 T, T_c extracting and 25 K extracting of the Hc_2.

7.3.1. Critical Temperature (T_c)

T_c was measured using the 90 % criterion which has been usually applied in the literature. The T_c is the temperature at which the superconducting state is completely lost; the 90 % criterion uses the 90 % of temperature when the sample achieves a normal-state resistive behavior as the T_c reported value, to consider the uncertain caused by the magnetoresistivity and the noise in the sample that could affect the value.

Figure 7.13 shows the graph of T_c versus applied magnetic field. For small and medium fields the undoped MgB_2 had the highest T_c, showing that the critical temperature is decreased with the dopant addition for all milling times.

The T_c values for the CrB_2 5 at.% samples were between 36.9 K and 37.9 K which were lower compared with the MgB_2 undoped material with a value of 38.49 K.

Table 7.III. T_c and Hc_2 values for CrB_2 doped MgB_2 material and MgB_2 undoped sample.

Sample	T_c (K)	H_{c2} (25 K) (T)
MgB_2 Undoped	38.49	6.752
60 min	37.29	3.413
120 min	37.92	4.916
180 min	37.06	3.951
300 min	37.39	4.350
600 min	35.99	3.453

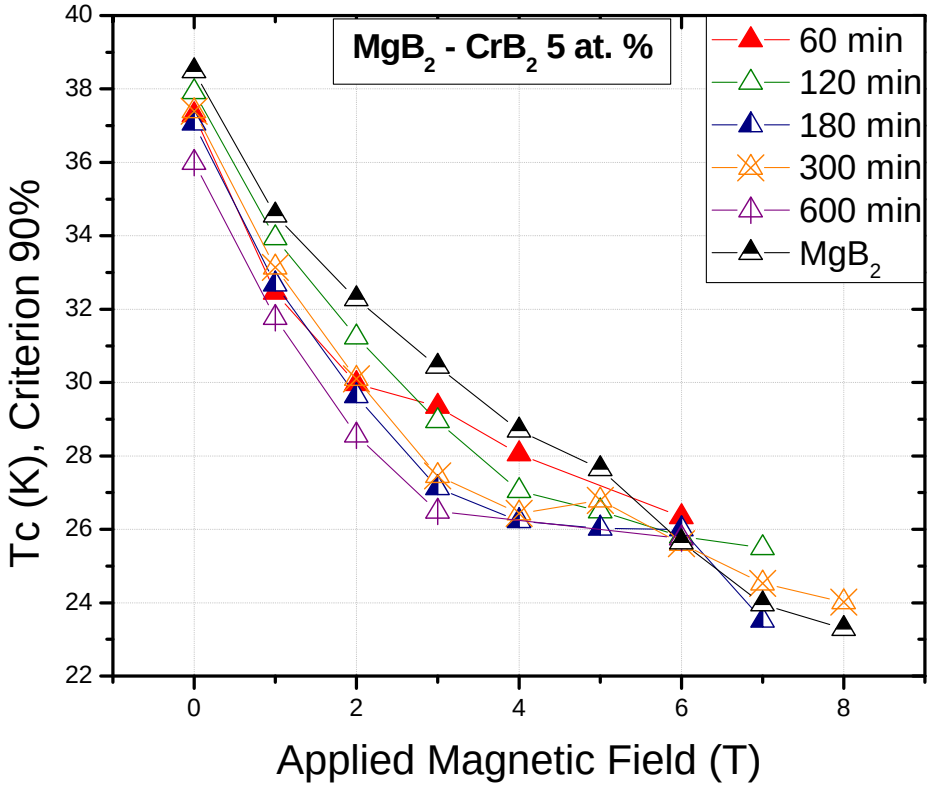

Figure 7.13. T_c Vs Applied Magnetic Field for the MgB_2 undoped and MgB_2 - 5 at.% CrB_2 doped materials.

Figure 7.14 showed he influence of the ball milling in the T_c value of the 5 at.% CrB2 doped MgB2. The highest T_c recorded corresponded to the 120 min milled material, while the minimum was for the 600 min one. In addition, the minimum value recorded was 2.5 K lower than the value for the undoped materials. The difference between the T_c value recorded for the 600 min ball mill material in comparison to the rest, did not overall pointed a clear trend, except in comparison to the 300 min milled material thast showed a decreasing tendency.

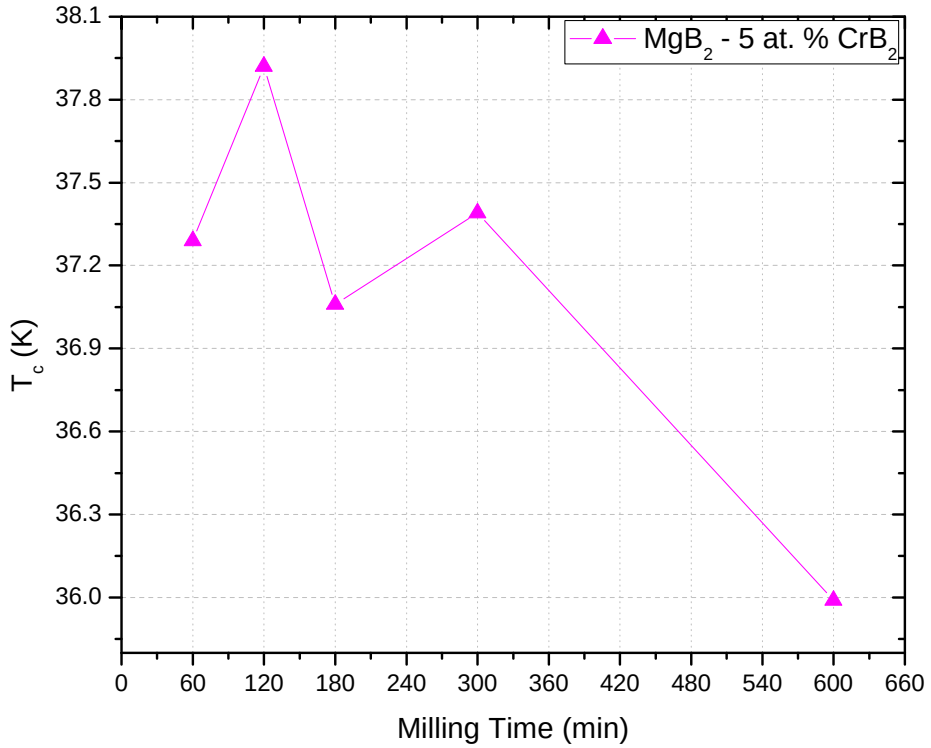

Figure 7.14. T_c Vs milling time for MgB_2 - 5 at.% CrB_2 material.

Zhang *et al.* [55] obtained in Cr doped MgB_2 a decrease in T_c from 38.2 K for the undoped sample to 35.1 K for Cr 3 at.% doped MgB_2 sample, they found that the T_c decreases quickly as the Cr doping level is less than 2at.% while for doping level higher than 2 at.% the decrease in T_c is slowly, however they did not include the T_c value for MgB_2 – 5 at.% Cr. Cr concentration dependent of T_c reported by Zhang *et al.* is shown in **Figure 7.15**. In this work the lower value in T_c was obtained for the 600 min ball milled sample with 35.99 K, similar to the reported by Zhang *et al.* [55] for the Cr 3 at.% doped MgB_2.

Zhang *et al.* [55] argued that the decreasing in T_c is related with the introduction of Cr in the Mg-layer. Hirsch *et al.* [57] reported that MgB_2 is near of the optimum level doping so that the doping with electrons will cause an underdoped which would be the reason for the decreasing in T_c.

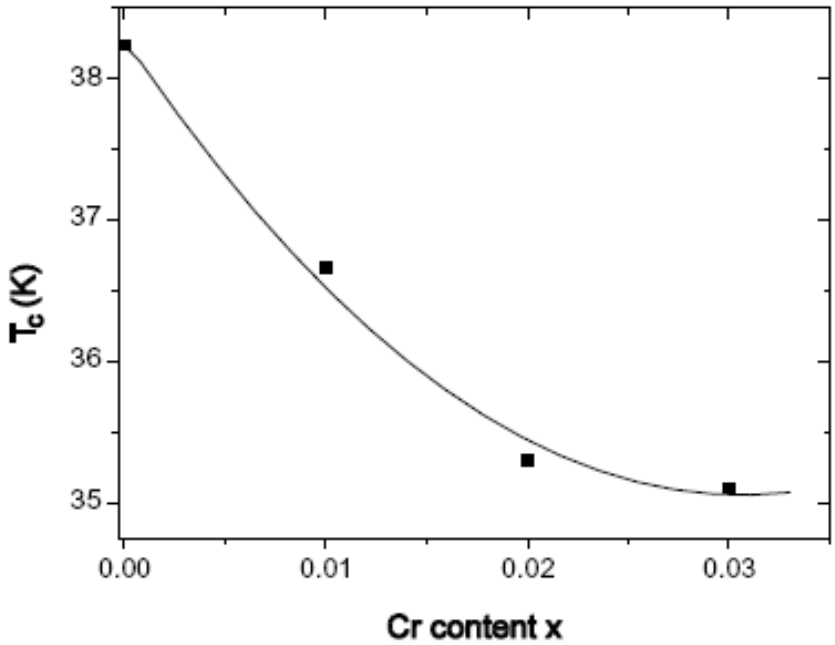

Figure 7.15. Dependence of superconducting transition temperature T_c on Cr content for $Mg_{1\_x}Cr_xB_2$ [55].

7.3.2. Critical Magnetic Field (Hc_2)

Figure 7.16 showed the graph of Hc_2 (25 K) versus temperature for the 5 at.% CrB_2 doped MgB_2 corresponding to different milling times. The overall trend observed was a decrease in Hc_2 values in comparison to the undoped MgB_2 material. For instance, the Hc_2 (20 K) for the undoped material was 9.5 T, while the 120 min ball milled doped material had a value of 7.617 T being the highest recorded for all the doped ball milled materials. The smallest value recorded for the Hc_2 (20 K) was for the 60 min ball milled material which was 5.074 T.

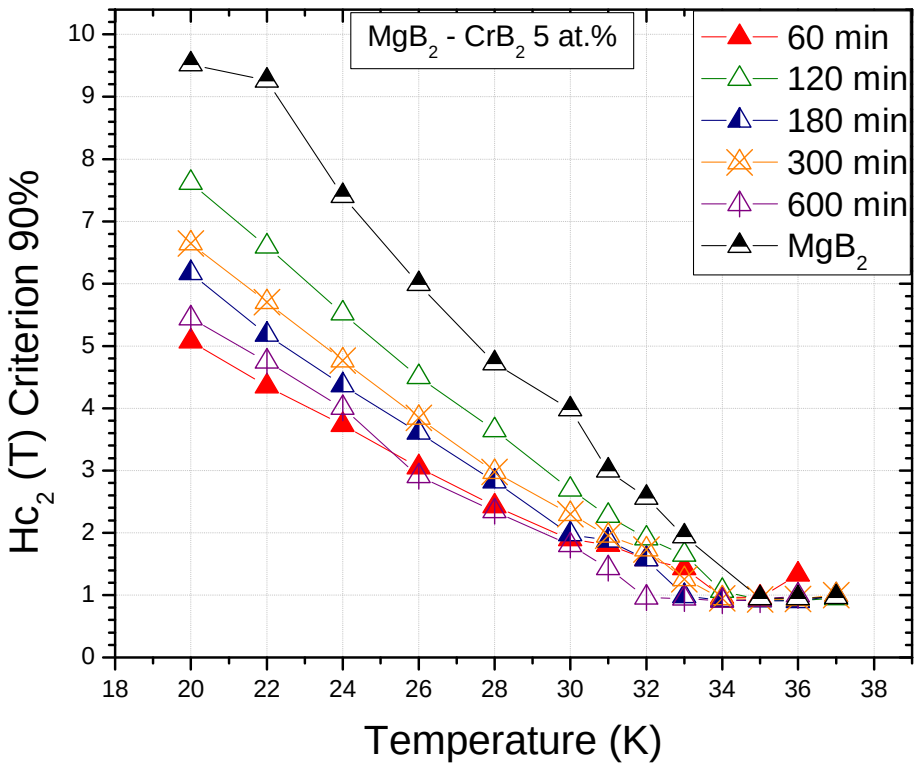

Figure 7.16. Hc_2 Vs Temperature for MgB_2 - CrB_2 5 at.% samples at different milling times.

The Hc_2 (25 K) as a function of milling time is shown in **Figure 7.17**. The highest Hc_2 (25 K) was for 120 minutes ball milled sample with a value of 4.9158 T, while the smallest value was for 60 minutes ball milled sample which had a value very close to the case of 600 minutes sample with values of 3.413 T and 3.453 T respectively.

As was the case of T_c variation shown in **Figure 7.14,** there was no clear tendency of variation of Hc_2 (25 K) as a function of milling time as shown in **Figure 7.17**.

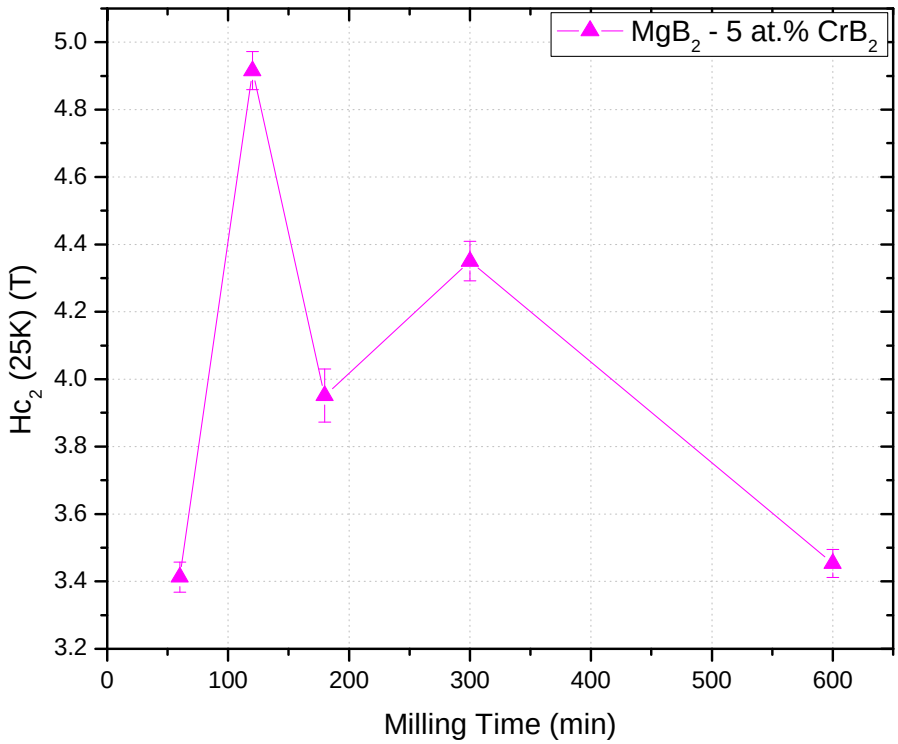

Figure 7.17. Hc_2 at 25K Vs milling time for MgB_2 - 5 at.% CrB_2.

The overall trend pointed out earlier is summarized in **Table 7.III**, displaying the critical temperature and magnetic field for the undoped and doped materials ball milled for different times. Based in the totality of the results, it is evident that CrB_2 is not a property enhancer with respect to the MgB_2 primary undoped material.

In **Table 7.III** are observed the T_c and Hc_2 values for the CrB_2 5 at.% and the MgB_2 undoped material. The results show that for CrB_2 5 at.% material there was a reduction in T_c and Hc_2 compare with the MgB_2 undoped material, which suggest that this material is not a good candidate for applications or future investigations related with the enhancement in superconducting properties by a doping process.

7.3.3. Resistivity Analysis

The analysis of the resistivity properties measurements using the Rowell theory, provides information about the connectivity in the sample, the resistivity of the well connected area and the scattering in the material.

The analysis of the resistivity properties complements the information of T_c and Hc_2 properties, and establishes important characteristics that define the viability of the material to be used in technological.

Figure 7.18 shows the resistivity behavior of the MgB_2 - CrB_2 5 at.% material compared to the MgB_2 undoped one. The resistivity of the MgB_2 - CrB_2 5 at.% material was found to be very high compared with MgB_2 undoped material. These results show that the conductivity in the interior of the sample will be affected for the high resistance and the possible cause is that CrB_2 as a dopant do not connect the material adequately.

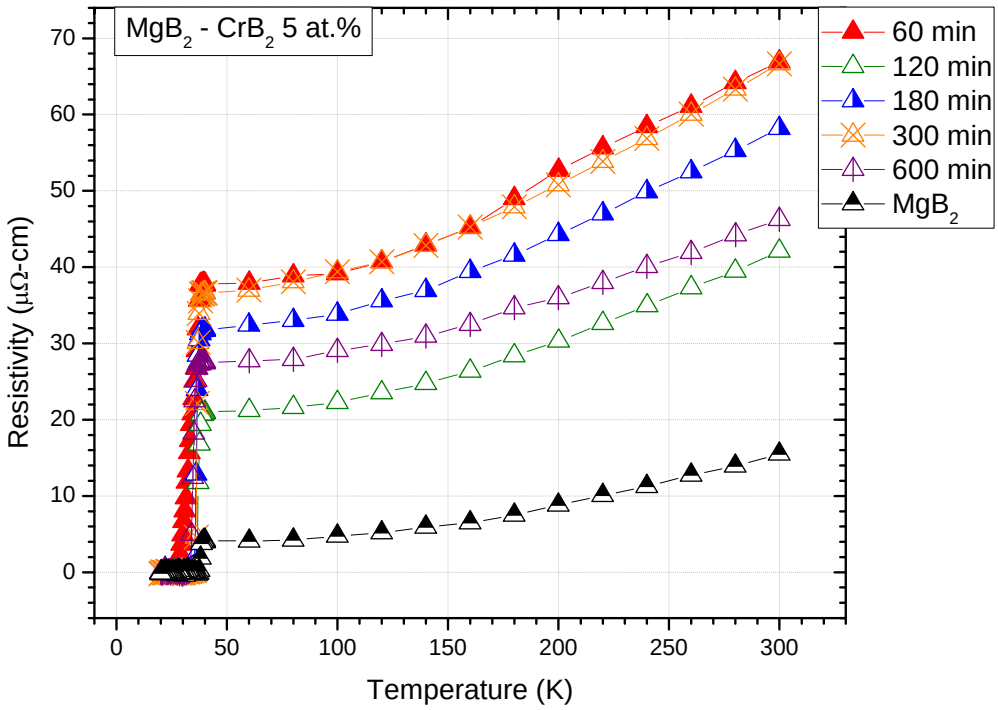

Figure 7.18. Resistivity Vs Temperature for MgB_2 - CrB_2 5 at.% ball milled at different times

Analyzing the crystallite size in the pellet material shown in **Table 7.II**, the CrB_2 crystallites are much bigger than the MgB_2 ones and considering that the CrB_2 phase has a higher resistivity than the MgB_2 one, this could indicate that there is a lower current going through the CrB_2 crystallites and that the big CrB_2 crystallites could cause a higher electron scattering, which could affect also the Hc_2 property in the MgB_2 – CrB_2 5 at.% material.

Zhang *et al.* [55] reported the increase of resistivity with the increase of Cr content for Cr doped MgB_2. **Figure 7.19** shows the resistivity ρ versus temperature for different Cr contents in Cr doped MgB_2 materials. The increase of resistivity with the Cr doping was related by Zhang *et al.* [55] with the introduction of Cr in Mg-layer which caused the decrease of chare carrier concentration, and also the decrease in T_c.

The resistivity increase in MgB_2 – 5 at.% Cr material with the introduction of Cr in Mg-layer showed in **Figure 7.19** for Zhang *et al.* has a similar trend to the observed in **Figure 7.18** found in this research. The T_c decrease and the variation in lattice parameter observed for the MgB_2 – 5 at.% CrB_2 material, could indicate that Mg substitution with Cr element was occurred for this material and that the Hc_2 reduction was a result of the increase in resistivity and the dopant process.

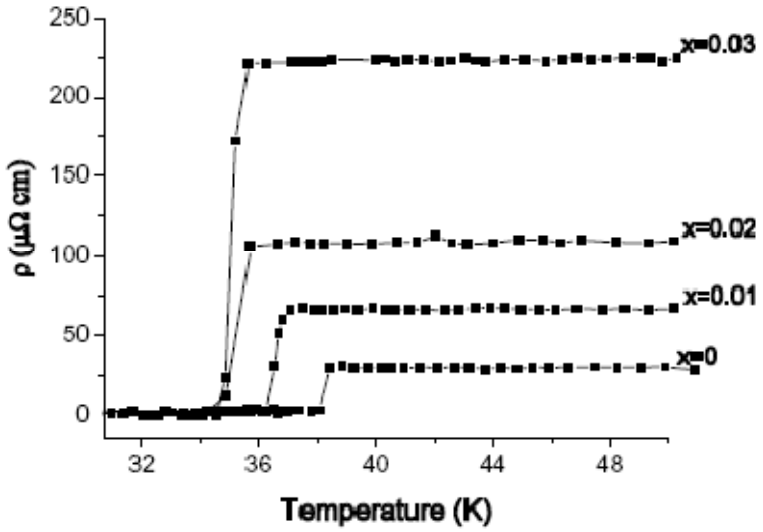

Figure 7.19. Temperature dependence of the resistivity for Cr doped MgB_2 with different Cr content [55]

Table 7.IV shows the values for the Residual Resistivity Ratio (RRR), the active area fraction (A_F) and the adjusted resistivity (ρ_A) for the CrB_2 5 at.% material.

The RRR is an indicator of the scattering in the sample; it is consider a high scattering for values in RRR close to 1, the scattering is smaller for values higher than 1. The non-superconducting second phases and the impurities could cause the electron scattering in the material.

The A_F represents the percentage of the area connected in the sample. A very well connected sample will have a value very close to 1. A porous sample is identified as a non-well-connected material. The space between grains or weak link at grain boundaries reduces the cross section carrying current and then A_F will affect directly J_c.

The ρ_A parameter represents the resistivity of the well connected area in the sample. If A_F represents the percentage of the well connected area, ρ_A represents the resistivity of that area. The A_F value is related with the porous and spaces between the grains that don't transport current. Those porous are really spaces which cannot be consider as material, when those spaces are included in the measure of the transversal area which transports current, it generates an increasing in the value of the resistivity. ρ_A is the resistivity of the sample without including those spaces between grains and then is consider the real resistivity.

Table 7.IV. Resistivity measurements for CrB_2 5 at.% ball milled at different times samples.

Sample	**ρ_{300K} (μΩ.cm)**	**ρ_{40K} (μΩ.cm)**	**RRR (ρ_{300K}/ ρ_{40K})**	**$\rho_{300K} - \rho_{40K}$ (μΩ.cm)**	**A_F $\left(\frac{\rho_{ideal}}{\rho_{(300K)} - \rho_{(40K)}}\right)$**	**ρ_A (40K) (μΩ.cm)**
MgB_2 undoped	15.48	4.01	3.86	11.48	0.64	2.55
60 min	66.91	37.66	1.78	29.26	0.25	9.40
120 min	42.11	20.92	2.01	21.19	0.34	7.21
180 min	58.19	31.76	1.83	26.43	0.28	8.77
300 min	66.68	36.69	1.82	29.99	0.24	8.93
600 min	46.28	27.48	1.68	18.80	0.39	10.67

The A_F values for the MgB_2 - CrB_2 5 at.% doped sample irrespective of milling times were smaller than 0.4 which indicates that the samples have a connected area smaller than 40 %. **Figure 7.20** shows the A_F parameter as a function of the milling times. For the MgB_2 - CrB_2 5

at.% material, the highest values in A_F were at 600 min and 120 min, however the trend for the A_F parameter as a function of milling time is not very clear.

Figure 7.21 shows the graph of Hc_2 versus A_F, however it was not possible establish the relation between the A_F parameter and Hc_2, because the critical magnetic field changes randomly with the increase of A_F. This behavior could indicate that the Hc_2 property does not dependent directly of A_F and because of its relation with connectivity and the current transport is a parameter more associated with the critical current density J_c.

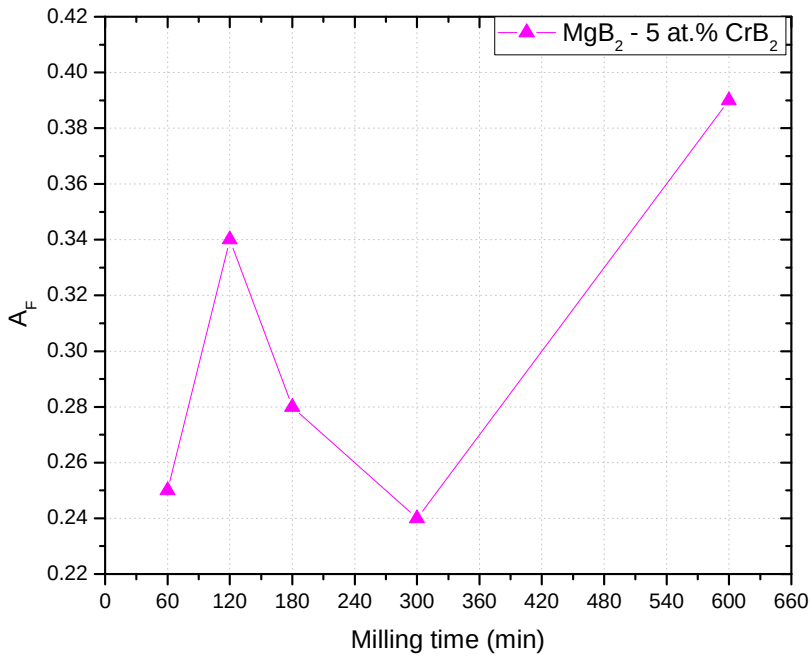

Figure 7.20. A_F Vs milling time for MgB_2 – 5 at.% CrB_2 material.

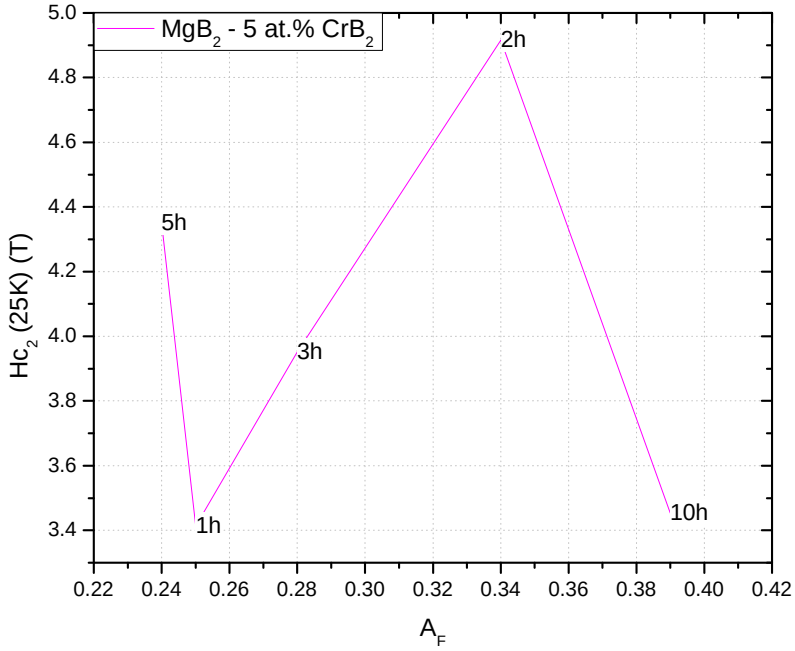

Figure 7.21. Hc_2 (25 K) Vs A_F for MgB_2 - 5 at.% CrB_2 doped material for different milling times

Figure 7.22 shows the ρ_A values in function of the milling time, the 600 min ball milled sample had the highest value for ρ_A, which indicates that even though this is the best connected sample, in agreement with the results observed in A_F, also presents the highest resistivity. These results indicates that in general the MgB_2 - CrB_2 5 at.% material did not show a good behavior in the resistivity parameters, by exhibiting a high resistivity with values between 7.21 and 10.67 μΩ.cm and low connectivity with values between 0.24 and 0.39 which correspond to values much lower than de 50% of connectivity.

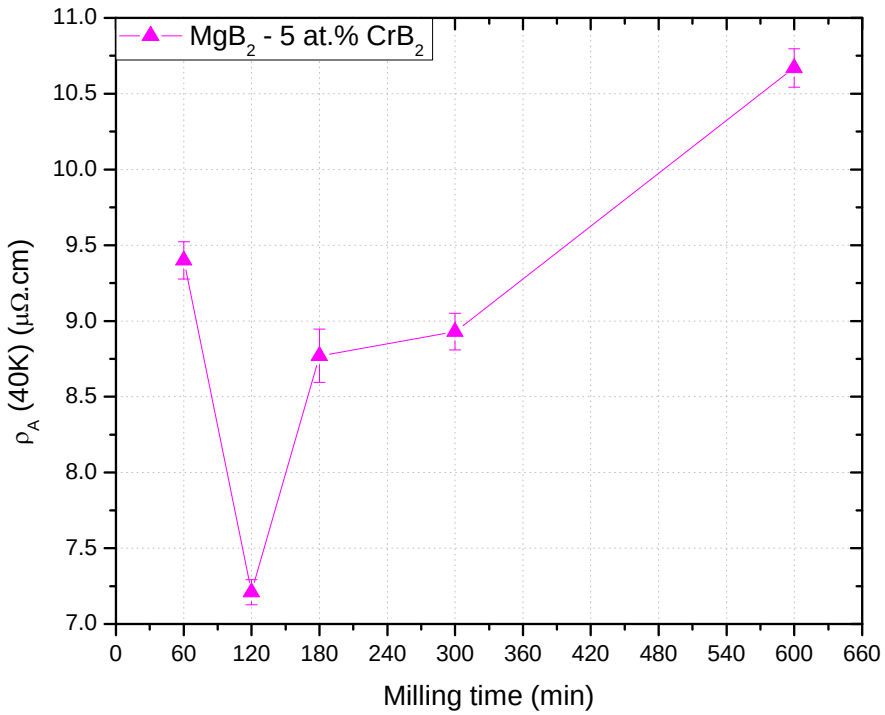

Figure 7.22. ρ_A Vs milling time for MgB_2 - 5 at.% CrB_2 doped material.

The relation of Hc_2 with ρ_A is shown in **Figure 7.23**. The general behavior observed between both parameters is that Hc_2 decreases while ρ_A increases, however this tendency was not constant for all values. The theoretical behavior of Hc_2 with ρ_A in a single band superconductor is proportional, however the presence of two superconducting bands in MgB_2 makes this relation more complicated [58, 59] and in practice could be unreliable.

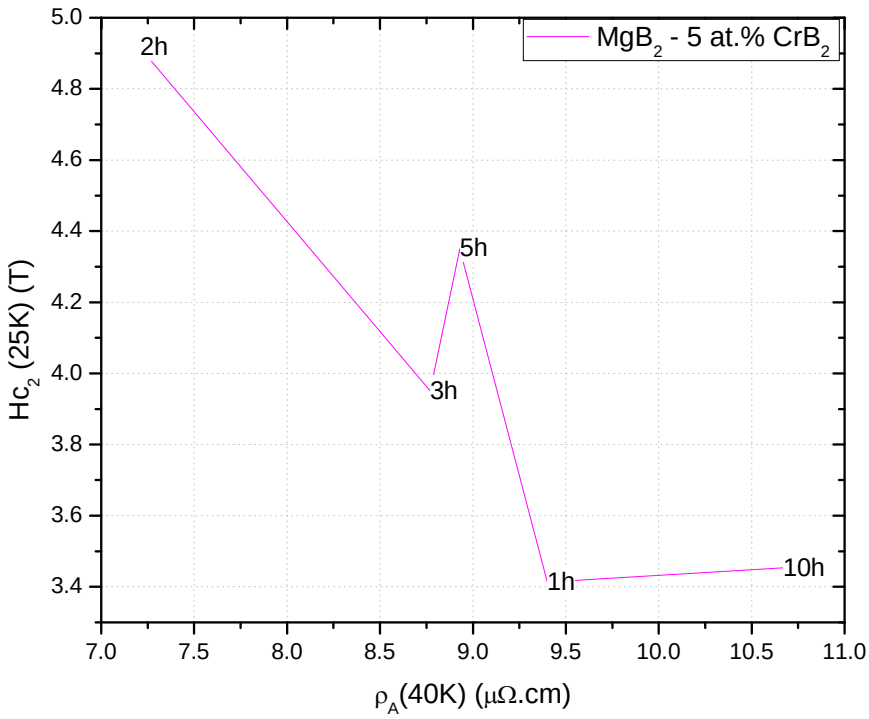

Figure 7.23. Hc_2 Vs ρ_A for MgB_2 - 5 at.% CrB_2 doped material.

The relation of RRR with the increase of milling time is observed in **Figure 7.24**. Between 120 minutes and 600 minutes is perceived a decreasing tendency in RRR with the increasing in milling time. The low values in RRR indicate high scattering in the material. For the MgB_2 – CrB_2 5 at.% the scattering is higher with the increasing in milling time, although the 60 min sample had a small value in RRR and then high scattering, which corresponds to a behavior out of the pattern.

The increase in Hc_2 for higher RRR is observed in **Figure 7.25**. The general relation observed is the increasing in Hc_2 for low scattering (high RRR), if RRR represents the scattering for compositional and microstructural defects, these results could indicate that the decreasing in Hc_2 with the decreasing in RRR could be the result of high level contamination with Fe, MgO, Si and C materials, some of the acting as non- superconducting phases destroying the superconducting state.

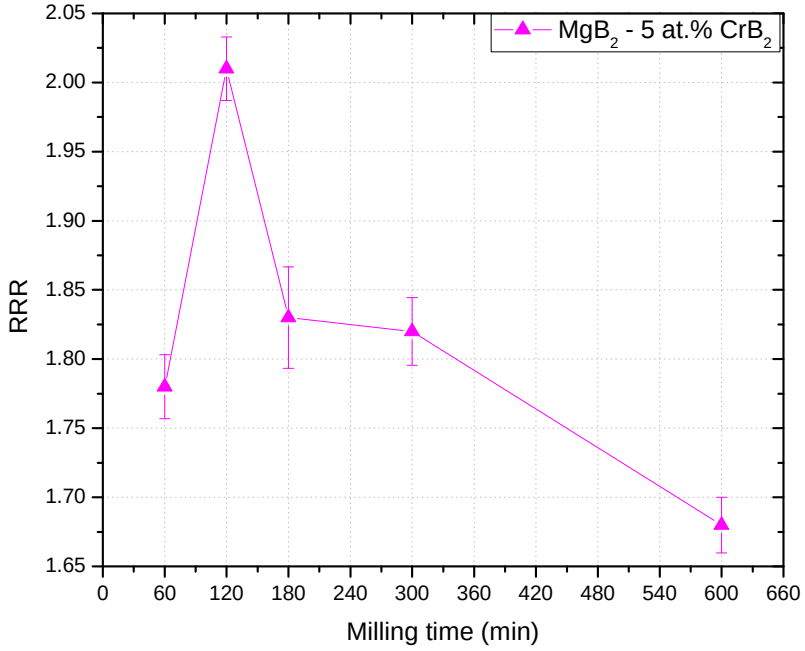

Figure 7.24. RRR Vs milling time for MgB_2 - 5 at.% CrB_2 doped material.

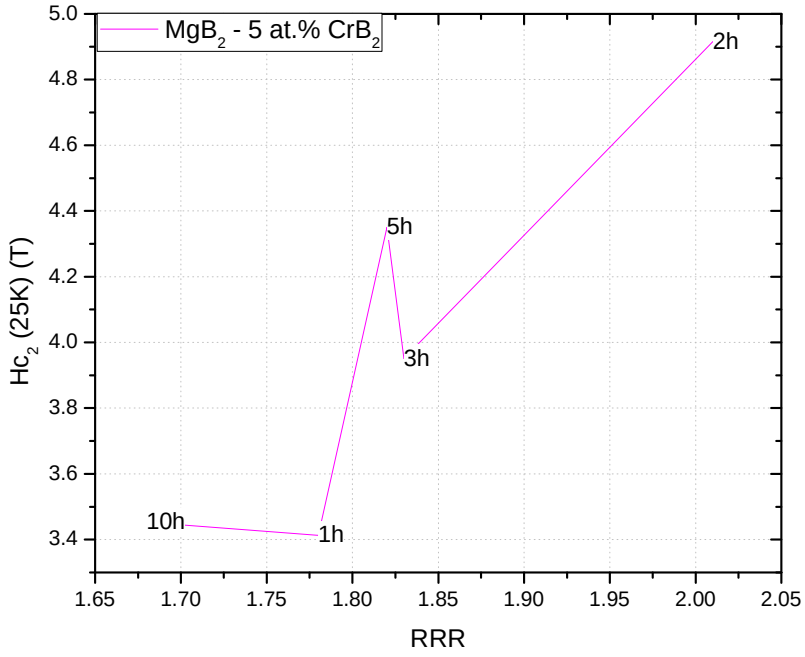

Figure 7.25. Hc_2 (25 K) Vs RRR for MgB_2 - CrB_2 5 at.% doped material.

The results presented in this chapter for MgB_2 - CrB_2 5 at.% doped material showed high crystallite size for CrB_2 phase material after HIP, low values in the superconducting properties T_c and Hc_2 and high resistivity compare with MgB_2 undoped sample. The general results showed that CrB_2 compound is not a good material to be used as dopant for MgB_2, specifically in 5 at.% implementing the HEBM technique. The structural and superconducting properties obtained for this dopant had values which could not enhance the MgB_2 undoped material and that are lower compare with other dopants reported before, which suggest the no viability of this material for applications or advances studies.

Zhang *et al.* [55] studied the Cr doped MgB_2 material with Cr concentration between 1 at.% and 5 at.%, the results showed that the crystal size increased with Cr doping concentration increase, the normal state resistivity increased with the increase of Cr content, and T_c decreased from 38.2 K for the undoped MgB_2 to 35.1 K for Cr 3 at.% doped MgB_2. They suggested that the charge transfer between the Mg-layer and the B-layer caused the decrease of the charge carrier concentration and induces the decrease in T_c and the increase in the normal state resistivity. Similar results were observed in this research, which could suggest the Cr introduction in the Mg-layer, and subsequently the reduction in T_c, increase in resistivity and decrease in Hc_2.

8. Comparison in Structural and Superconducting Properties for TaB_2, TiB_2, NbB_2 and CrB_2 doped MgB_2

In this thesis four diborides as dopants for the MgB_2 material were studied, notably TaB_2, TiB_2, NbB_2 and CrB_2. Both the dopants MeB_2 as well as the base material MgB_2 were premilled for two hours before mixing, after which the premilled materials were mixed to achieve an overall composition of MeB_2 at 5 at.% with MgB_2 at 95 at.%, where Me represents Ta, Ti, Nb and Cr. After the materials were mixed, they were further milled at different times and subsequently characterized to determine the structural and superconducting properties.

This chapter aim to compare the results of the structural and superconducting properties of the four dopants discussed independently in the previous chapters and to establish the advantage and disadvantage of each of them. This would help to determine their future viability for properties enhancement and hence basis for further studies.

8.1. Structural Properties

The XRD technique was used to determine the composition, crystallite size, strain, and lattice parameters for each sample after ball milling and after the HIP processes.

The results presented in the precedent chapters showed that after the HIP process the crystallite size increased for both the MeB_2 and the MgB_2 phases; however in some cases the crystallite size for the MeB_2 phase had higher values than for the MgB_2 phase. For TaB_2, TiB_2 and CrB_2 dopants, the crystallite size was higher in general for the MeB_2 phase than for the MgB_2 phase, while for the NbB_2 dopant the MgB_2 phase had higher crystallite size compared with the MeB_2 phase. **Table 8.I** shows the values for the MeB_2 materials after the HIP process.

The smallest crystallite size in pellet for MgB_2 phase between the dopants was for the TaB_2 5 at.%, which had values between 2.96 nm and 20.48 nm, while the TaB_2 phase had values between 15.89 and 99.76 nm. The crystallite size values for MgB_2 phase for the pellet samples are shown in **Table 8.II**.

Table 8.I. Crystallite Size for MeB_2 phase after the HIP process.

Crystallite Size (nm) for MeB_2 Phase Pellet Sample				
Milling Time	**TaB_2 5 at.% - MgB_2 95 at.%**	**TiB_2 5 at.% - MgB_2 95 at.%**	**NbB_2 5 at.% - MgB_2 95 at.%**	**CrB_2 5 at.% - MgB_2 95 at.%**
60	99.76	29.52	31.13	122.45
120	43.39	26.92	21.43	32.64
180	19.36	43.29	16.69	61.99
300	15.89	60.84	13.6	63.32
600	52.29	-	15.72	89.52

Table 8.II. Crystallite Size for MgB_2 phase after the HIP process.

Crystallite Size (nm) for MgB_2 Phase Pellet Samples				
Milling Time	**TaB_2 5 at.%- MgB2 95 at.%**	**TiB_2 5 at.%- MgB2 95 at.%**	**NbB_2 5 at.%- MgB_2 95 at.%**	**CrB_2 5 at.%- MgB_2 95 at.%**
60	3.56	24.35	61.58	29.29
120	2.96	30.78	22.59	24.4
180	10.4	39.7	20.35	13.85
300	20.48	30.85	26.68	32.59
600	6.22	-	34.83	23.34

Figure 8.1 shows the crystallite size for the MeB_2 phase after the HIP process. In the 60 min ball milled material the crystallite size for CrB_2 was the highest followed by TaB_2 phase. For the 120 minutes ball milled material the crystallite size of the dopants were close, while the tendency observed in crystallite size for all dopants between 60 min and 120 min was to decrease. In addition, the tendency in crystallite size for all dopants between 300 min and 600 min was to increase.

In general the NbB_2 phase had the smallest crystallite size between 13.6 and 31.1 nm, followed by TaB_2, while the crystallite size for CrB_2 phase was the highest in all milling times except for 120 min, with values between 32.6 and 122.4 nm.

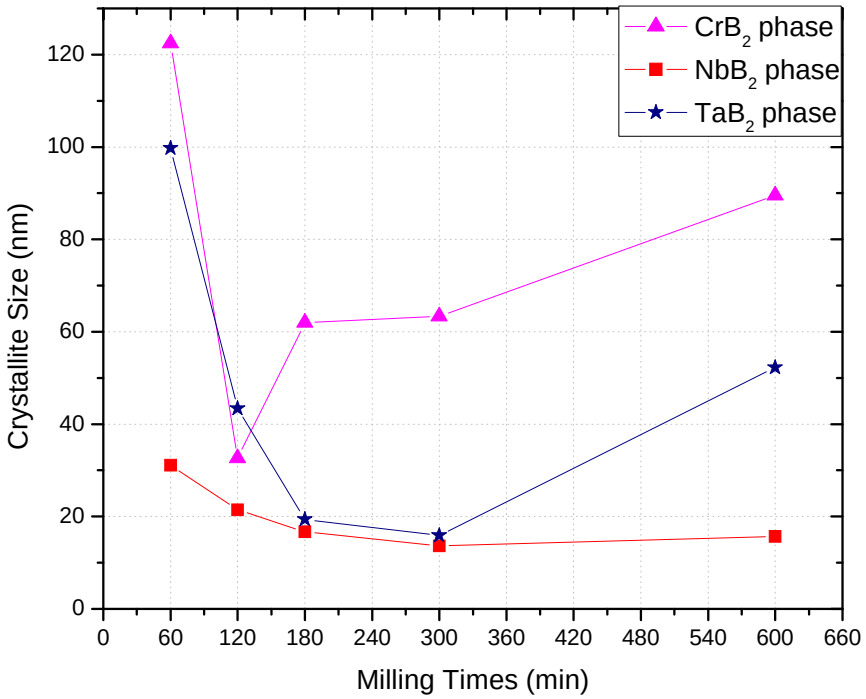

Figure 8.1. Crystallite size evolution of the MeB_2 phase for the dopant material with ball milling.

In **Figure 8.2** is observed the crystallite size for the MgB_2 phase of the doped materials. The smallest crystallite sizes were for MgB_2 - 5 at.%TaB_2 material with values between 2.96 and 20.48 nm, while the highest crystallite size at 60, 180 and 600 min corresponded to CrB_2 and for 120 and 300 min pertained to NbB_2.

Grain size growth with the heat treatment have been reported before for MgB_2 doped with different compounds [36, 34, 56], however Senkowicz [34] observed fine grains between 20 and 30 nm without evidence of a drastic increase in grain size for a HIP temperature of 1000°C, he

explained that the probably reason for that was the disperse of the second phases which retarding grain growth.

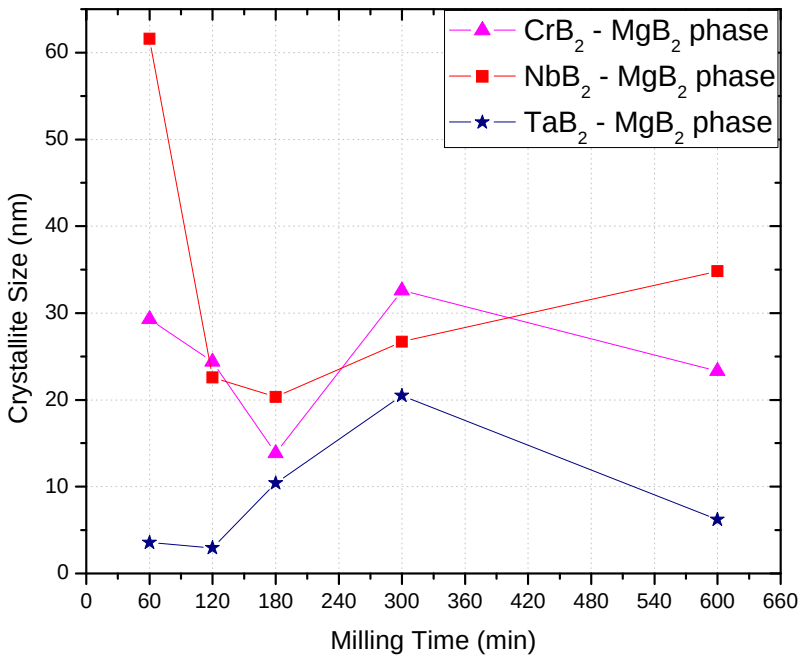

Figure 8.2. Crystallite size evolution of the MgB_2 phase for the dopant material with ball milling.

The strain for the MeB_2 phases as a function of milling time after the HIP process is shown in **Figure 8.3**. The highest strain was for the NbB_2 dopant except for the 120 min ball milled material. The strain in TaB_2 material had a tendency to increase between 60 min and 120 min, found the highest value in strain for this dopant at 120 min of milling time, then the strain decreases following a similar tendency that was exhibited by the CrB_2 doped MgB_2 between 180 min and 600 min of milling time.

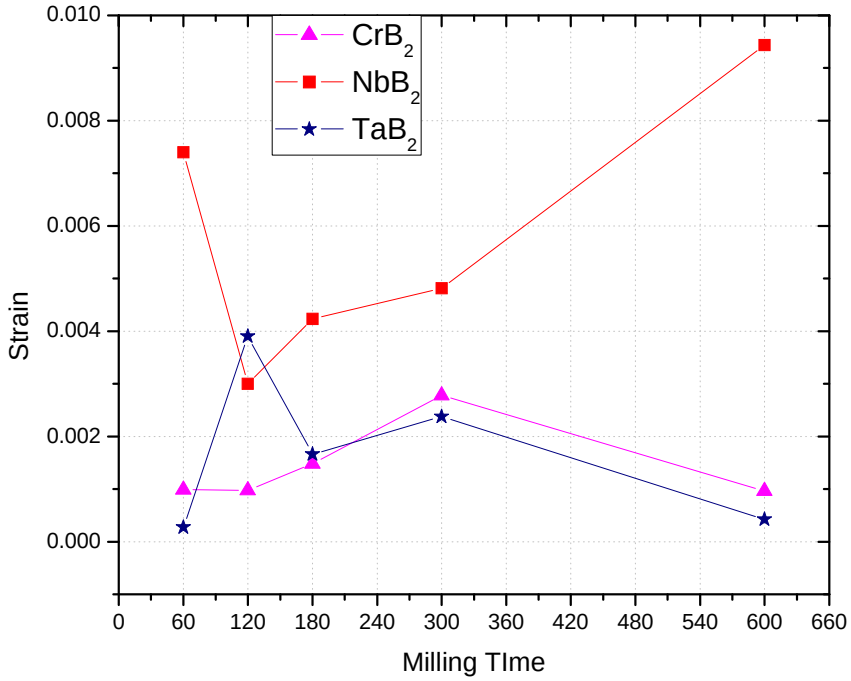

Figure 8.3. Strain for MeB_2 phase for the doped materials in function of milling time.

8.2. Superconducting Properties

The critical temperature (T_c) and critical magnetic field (Hc_2) for the MgB_2 doped MeB_2 at 5 at.% were analyzed. The reported T_c value for MgB_2 undoped is 39 K, however the material with some contaminations by oxygen or other elements or compounds can lead to decrease of T_c value, in addition to some syntheses processes as well. Senkowicz *et al.* [32] reported decreased in T_c as result of increased contact with air for MgB_2 bulk in pellet.

The T_c as a function of the applied magnetic field for the 60 minutes samples doped with MeB_2 at 5 at.% material are shown in **Figure 8.4**, together with the undoped MgB_2 material used as reference for comparison. The graph showed that the T_c at 0 T has similar values for NbB_2, TiB_2, TaB_2 and MgB_2 except for the CrB_2 which presented a smaller value.

With increasing applied magnetic field, the T_c property for the TaB_2 material showed the highest values among the dopant materials and displayed a better behavior compared with the undoped MgB_2 material. The NbB_2 and TiB_2 materials had close values to that of the TaB_2, which all together showed better behavior than the undoped MgB_2 material. The CrB_2 doped MgB_2 displayed in most of the fields the smallest T_c values.

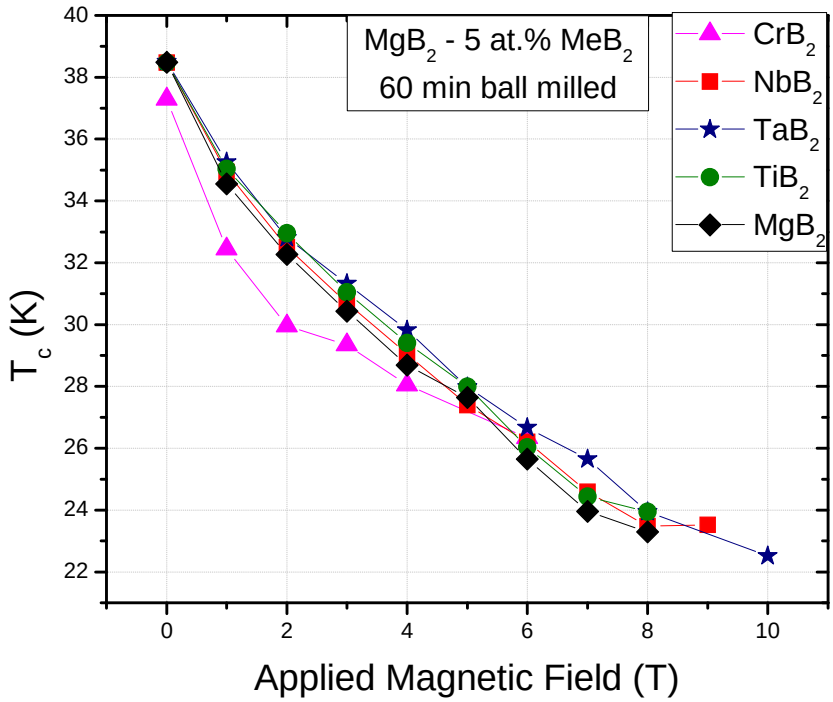

Figure 8.4. T_c of MeB_2 5 at.% doped samples in function of the applied magnetic field.

Figure 8.5 shows the T_c for the four MgB_2–MeB_2 doped materials at different milling times. TaB_2 doped MgB_2 had the highest T_c among the doped samples in the milling time range of 60 min to 300 min, corresponding to 38.51 K and 38.47 K. The TiB_2 material had the second highest value in T_c, from 38.49 K to 38.46 K in the same range than TaB_2, while NbB_2 had the third T_c values, from 38.47 K and 38.19 K, between 60 min and 300 min. Consistently all the MgB_2 - MeB_2 doped materials displayed decrease of T_c for the 10 hours ball milling, with the CrB_2 doped one at the bottom of the list as shown in Figure 5.

Analyzing the Hc_2 and T_c properties in each band it has been found that the σ band has a higher temperature and a higher Hc_2 than the π band, which opens the possibility to control both T_c and Hc_2 by the properties of the σ band, exploring different mechanisms to alter the properties, improving Hc_2 (T) without significant T_c reduction [34].

The results found in this study did not show a considerable decreased in T_c for TaB_2, NbB_2 and TiB_2 doped MgB_2 between 60 and 300 min ball milled material. It is possible that with the dopant material, the composition of the phases and some of the additional phases introduced in the material as Si, O and C, there was a control of the σ band properties, increasing Hc_2 without decreasing T_c, however, in MgB_2 – 5 at.% CrB_2 this results were different which could be related with the additional contaminations found as Fe.

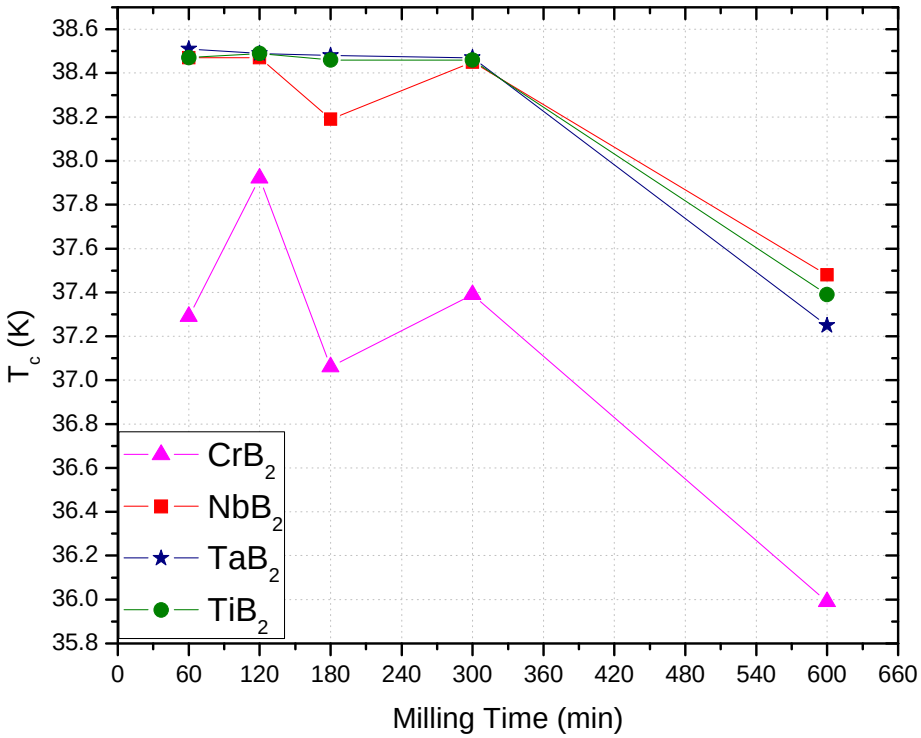

Figure 8.5. Comparison of the T_c values of MgB_2 – 5 at.% MeB_2 doped materials as a function of milling times.

Table 8.III. Comparison of T_c for the different MgB_2 – 5 at.% doped MeB_2 materials as a function of ball milling times. Me: Ta, Ti, Nb, and Cr.

T_c (K) for MeB_2 5 at.% Samples				
Milling Time	**TaB_2**	**TiB_2**	**NbB_2**	**CrB_2**
60	38.51	38.47	38.47	37.29
120	38.49	38.49	38.47	37.92
180	38.48	38.46	38.19	37.06
300	38.47	38.46	38.45	37.39
600	37.25	37.39	37.48	35.99

The plot of Hc_2 variation in 60 min ball milled MgB_2 – 5 at.% MeB_2 materials are shown in **Figure 8.6**. The plots in **Figure 8.6** showed that the 5 at.% TaB_2 doped MgB_2 showed the highest Hc_2 value at 20 K matched closely by the 5 at.% TiB_2 and NbB_2 homologue materials. The 5 at.% CrB_2 doped MgB_2 displayed a much smaller value for Hc_2 at 20 K, and in all temperatures ranges in the superconductive state. In general, except or the CrB_2 doped materials, the other materials exhibited comparable result.

Figure 8.7 shows the values for Hc_2 at 25 K in the four dopants for different milling times. The highest Hc_2 (25 K) value registered between all the dopants was for TaB_2 5 at.% at 180 min, the second value also correspond to TaB_2 at 60 min ball milled. The Hc_2 values for NbB_2 and TiB_2 doped samples were very similar; the values in Hc_2 between 60 min and 300 min were in the range of 6.8320 T and 6.4374 T. The CrB_2 doped samples have the smallest values between the doped materials with values between 4.9158 T and 3.4131 T. The 600 min ball milled sample had the smallest values for the TaB_2, TiB_2 and NbB_2 5 at.% doped samples. The totality of the Hc_2 measurement carried out at 25 K for the four doped materials as a function of milling time are summarized in **Table 8.III**.

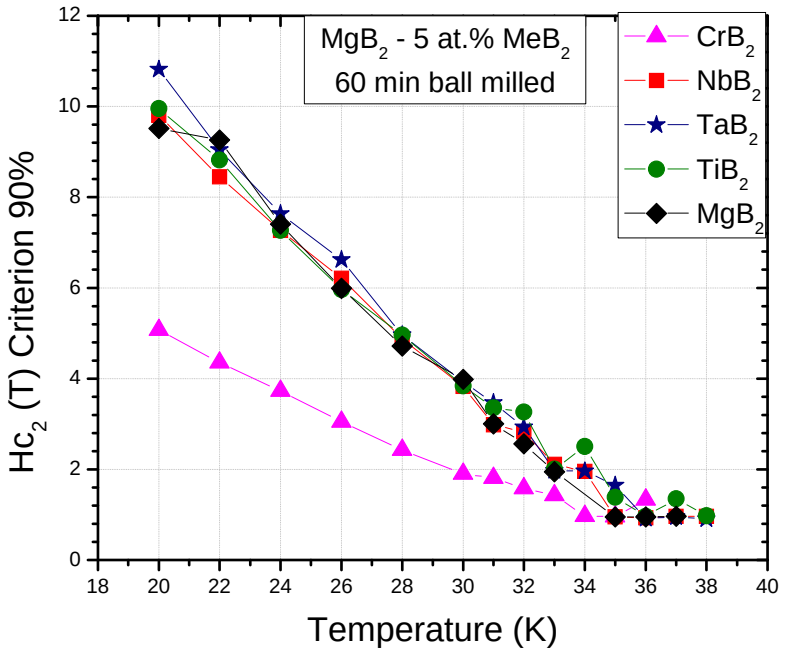

Figure 8.6. Hc_2 of MeB_2 5 at.% doped samples in function of the temperature.

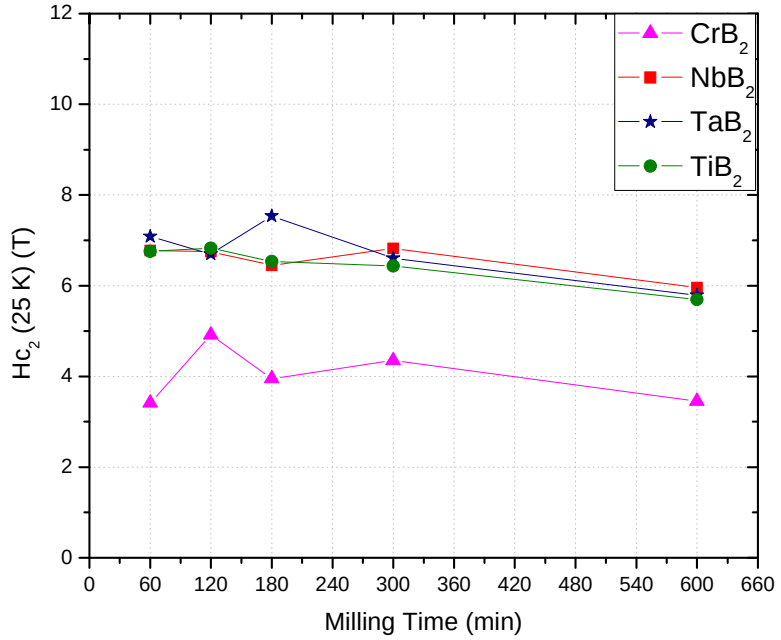

Figure 8.7. Hc_2 (25 K) of MeB_2 5 at.% doped samples at different milling times.

Table 8.IV. Hc_2 of doped MeB_2 (Me = Ta, Ti, Nb and Cr) – MgB_2 materials as a function of ball milling time after HIP process

Hc_2 (25 K) (T) for MeB_2 5 at.% Samples				
Milling Time	**TaB_2**	**TiB_2**	**NbB_2**	**CrB_2**
60	7.0874	6.7539	6.775	3.4131
120	6.7012	6.832	6.7476	4.9158
180	7.539	6.5365	6.4458	3.9513
300	6.6062	6.4374	6.8193	4.3502
600	5.7895	5.6924	5.9583	3.4532

The resistivities of the doped materials corresponding to the 60 min ball milled time are shown in **Figure 8.8**. It is observed that the smallest resistivity recorded was for the NbB_2 doped material, followed by resistivities values for the TiB_2 material, TaB_2 and the CrB_2 at 5 at.% in increasing order respectively, as revealed in **Figure 8.8**.

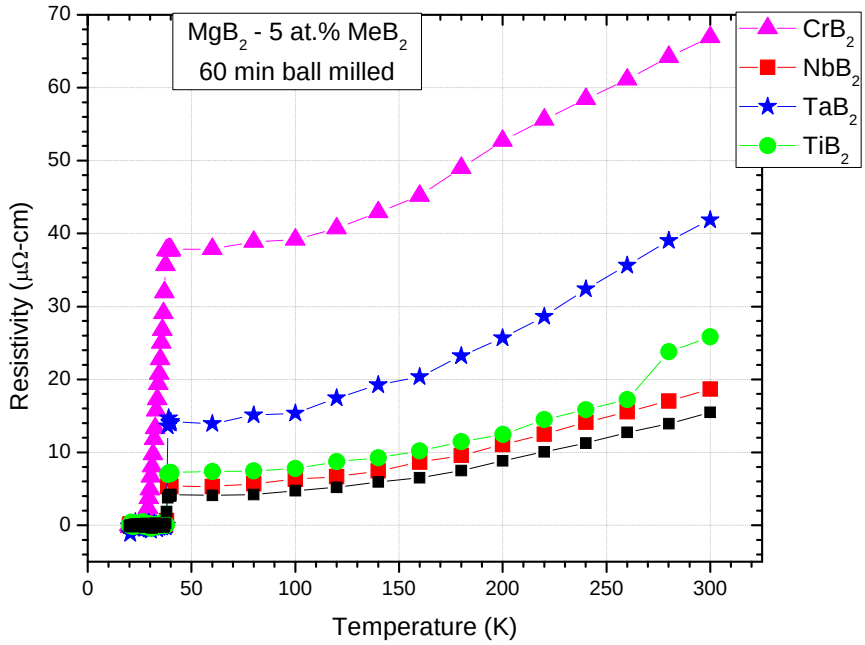

Figure 8.8. Resistivity of MeB_2 5 at.% doped MgB_2 samples in function of the temperature.

The residual resistivity ratio (RRR) for the MeB_2 materials at different milling times are collectively shown in **Figure 8.9**. The low RRR parameter indicates high electron scattering in the sample from compositional and microstructural sources; the compositional source could be directly related with additional non-superconducting phases such as MgO and the microstructural source could be associated with changes in the microstructure caused by lattice defects as such strain. The RRR graph shows higher values in RRR for TaB_2, TiB_2 and NbB_2 doped samples indicating less electron scattering for these materials, while CrB_2 doped samples have smaller values that are more proximate to 1 which indicate high electron scattering, the low results in Hc_2, T_c and RRR could be related with the contamination phases found for CrB_2 such as MgO, Si, Fe and C; these non-superconducting phases can be related to the decreasing in T_c as reported by Senkowicz and Perez [32, 34, 36], also for a high quantity of contaminations, it would be higher penetration of flux and then the rupture of the superconducting state at low field decreasing Hc_2, moreover as was indicated before the compositional sources can decrease the RRR values.

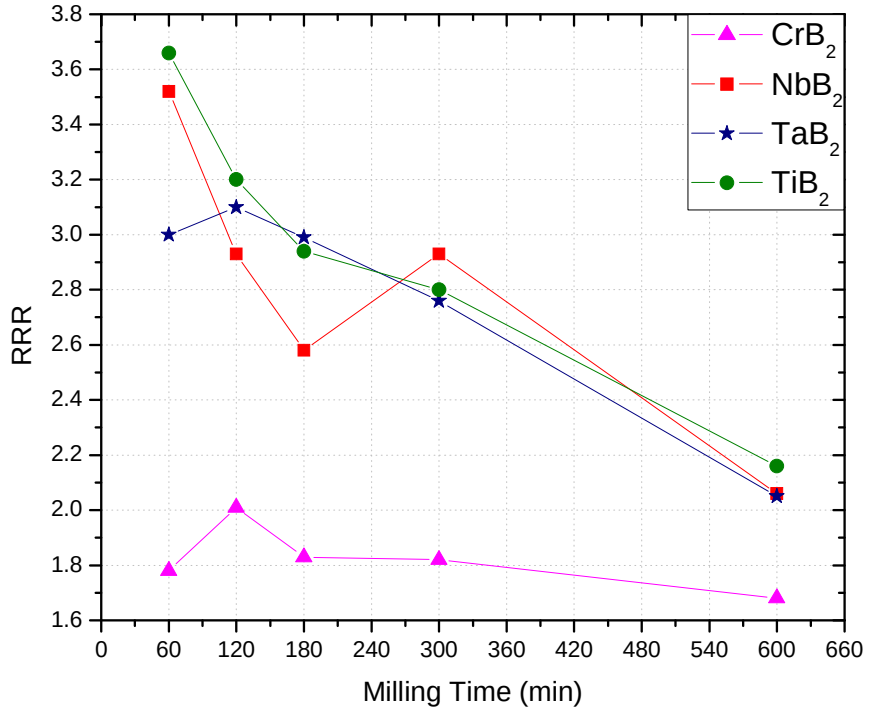

Figure 8.9. RRR Vs Milling time of MeB_2 5 at.% doped MgB_2 samples

The comparison between the MeB_2 doped samples at 5 at.% level showed that the TaB_2 5 at.% is a good prospective to be used as dopant for MgB_2 because had important properties as high Hc_2 (25 K) at 180 min of milling time (7.5390 T) and at 60 min of milling time (7.0874 T) increasing the Hc_2 (25 K) obtained for the MgB_2 undoped material (6.7518 T). The value of T_c remained in the same than the MgB_2 undoped and did not decrease with the doped process as has been reported before with other dopants as C, ZrB_2, SiC [35, 34, 56], moreover the crystallite sizes obtained with the ball milled process were smaller than for other materials, which could generate a good connectivity in the sample to improve the current flux.

The TiB_2 doped MgB_2 (at 5 at.%) did not significantly change the Hc_2 (25 K) value in comparison to the undoped base material. The 60 min and 120 min ball milled TiB_2 (5 at.%) dopped material yielded Hc_2 (25 K) values of 6.754 T and 6.832 T respectively in comparison to the 6.752 T value of the undopped material. The value recorded for NbB_2 (5 at.%) doped MgB_2 was highest for the 60 min ball milled material at 6.775 T. As for the T_c for the 60 min ball milled material (i.e., 5 at.% NbB_2), the value was 38.47 K compared to 38.49 K for the undopped MgB_2.

The TiB_2 and NbB_2 5 at.% materials although did not cause a decrease in T_c and causes an increase in the Hc_2 (25 K) values, did not lead to a bigger increase in Hc_2 compared with the values of MgB_2 undoped material. Due to these observations it would be necessary to conduct further studies on these dopant materials by varying the composition, and also the ball milling times in order to determine optimal dopant level and milling times for enhanced superconductivity properties. CrB_2 exhibited smaller Hc_2, T_c and RRR values compared to the other dopants and to the MgB_2 undoped material. These results suggest that doping with CrB_2 at 5 at.% level is not good choice for enhancing the MgB_2 properties by doping.

9. Conclusions

The High Energy Ball Milling technique reduced the grain size in TaB_2 5 at.%, TiB_2 5 at.%, NbB_2 5 at.% and CrB_2 5 at.% materials until values less than 10 nm, moreover increased the structural defects which is perceived in the lattice parameters changes and in the increasing of the strain.

Hot Isostatic Press process applied to the powder material forms a good quality pellet due to the effect of the pressure, reorganizes the structure, decreasing the strain for the effect of the temperature and increases the particle size until values between 13 nm and 120 nm.

In the XRD analysis of the powder samples were observed the initial phases introduced; MgB_2 and MeB_2, however additional phases were found, between them MgO and B; the MgO phase was the result of the reaction between the Mg and O, the O element was introduced in the sample during the ball milling process and the Mg and B elements emerge in the sample as a result of the MgB_2 decomposition during the ball milling. In the XRD analysis of the pellet sample was detected an increase in the B and MgO quantity for some samples compared with the powder samples, which suggests that during the HIP process was also occurred the decomposition of the MgB_2 phase, but it was in less proportion than the occurred during the HEBM process.

In the XRD analysis of the pelletized samples were observed additional phases of the ones found in the powder material, in most of the samples were detected the presence of Si and in the CrB_2 samples were observed C and Fe. The C, Si and Fe elements could be introduce in the sample in one of the steps between the synthesis and samples preparation for characterization, in this processes there were many steps that were made outside of the glove box in which the contamination could ingress in the sample; between the synthesis processes are the CIP, the tube cutting, the welding, and the HIP, while in the sample preparation for characterization are the processes of cutting, grinding and cleaning.

The TaB_2 5 at.% samples had the higher Hc_2 (25 K) value for the 180 min ball milled sample (7.5390 T), and the second Hc_2 (25 K) value for 60 min ball milled sample (7.0874 T); these samples presented an increase in Hc_2 (25 K) with respect to the MgB_2 undoped sample which had a value of 6.7518 T. The T_c found for the TaB_2 5 at.% 180 min and 60 min ball milled samples were 38.48 K and 38.51 K respectively, these values remain very close to the T_c of the

MgB_2 undoped sample (38.49 K). The results in Hc_2 and T_c for the TaB_2 5 at.% samples are higher than the values in MgB_2 doped with C reported by Senkowicz who obtain Hc_2 (25 K) values between 6.2 T and 7.375 T for milled samples at different times and using different percentage of dopant. [26], moreover the T_c values for the Senkowicz samples reported before were between 32 K and 36.2 K, with a T_c value of 32.74 K for the sample with the higher Hc_2, which can be considered a higher decrease in T_c compared with the theoretical value for MgB_2 of 39 K. Moreover, the TaB_2 5 at.% material milled at 180 min and 60 min had values in RRR of 2.99 and 3.00 respectively; indicating that these samples had low electron scattering. The results exposed before show that TaB_2 5 at.% samples milled at 60 min and 180 min can be considered viable materials for applications because have high Hc_2 values without decreasing T_c and also high RRR values.

The TiB_2 5 at.% samples milled at 60 min and 120 min had values in Hc_2 (25 K) of 6.754 T and 6.832 T respectively, which were higher than the Hc_2 (25 K) for the MgB_2 undoped material (6.752 T). The T_c for the same samples were 38.47 K and 38.49 K respectively which could be considered invariable with respect to T_c of the MgB_2 undoped material (38.49 K). The RRR for these samples were 3.66 and 3.20. The values in Hc_2, T_c and RRR suggest that this material could be a good candidate for applications; however the increase in Hc_2 was not so higher compare to the undoped material whence that a deeper study based in the properties analyzed here and other properties as J_c could be convenient to determine the viability of this material for applications.

The NbB_2 5 at.% samples had values in Hc_2 (25 K), T_c and RRR very similar to the MgB_2 undoped material which did not show a big range in the benefit of the dopant material combined with HEBM technique to be applied in the MgB_2 compound.

For the CrB_2 5 at.% material was found Hc_2 (25 K), T_c and RRR values smaller than the MgB_2 undoped material and than the other doped samples, for which this material cannot be considered a good material to de used as dopant for the MgB_2 compound.

9.1. Suggestions for Future Works

For the HEBM technique should be used in the balls and the jars, materials with low tendency of degeneration down the application of high impacts over their surfaces, in this way it could avoid the contamination of the sample caused by the materials detachment.

During the synthesis there are many steps which are practiced outside the glove box, the entrance of oxygen and other contaminations is more probable when the exposition time is increased. Some steps as the ball milling process, the vacuum effected to the tube with the CIP sample and the tube cutting should be made inside the glove box. These precautions could help to reduce the contamination found in the sample.

The welding of the tube takes a considerable time, and even though the end of the tube was flat to avoid the entrance of oxygen, the elapsed time while the welding is effected, makes difficult the completely isolation of the sample and in this way the entrance of contamination. The cutting and welding of the tube should be simultaneous process made for a specialized tool build for this propose.

In the pellet samples was detected a change in the color and texture of the material in the inside region, this change could be occasioned for a reaction between the sample and the tube during the heat treatment, for which could be recommended to use a material with a high temperature decomposition and that did not react with the sample compounds, to cover the sample and eliminate the possibility of reaction between the tube and the sample.

References

[1] Marouchkine, A.: (2004), "*Room Temperature Superconductor*". Cambridge: Cambridge International Science Publishing.

[2] Seeber, B.: (1998), "*Handbook of applied superconductivity*". London: IOP Publishing.

[3] Cooper, L. N.: (1956), "Bound Electron Pairs in a Degenerate Fermi Gas". *Phys. Rev.*, 104 (4), 1189 – 1190.

[4] Bardeen, J., Cooper, L. N., & Schrieffer, J. R.: (1957), "Microscopic Theory of Superconductivity". *Phys. Rev.*, 106, 162-164.

[5] Myers, H. P.: (2002), "*Introductory Solid State Physics*". London: Taylor & Francis.

[6] Akimitsu, J.: (2001), "*Symposium on Transition Metal Oxides*". *(Sendai, Japan, 10 January 2001).*

[7] Krabbes, G., Fuchs, G., Canders, W.-R., May, H., & Palka, R.: (2006), "*High Temperature Superconductor Bulk Material*". Weinheim: Wiley-VCH.

[8] Rodrigues Junior, D.: (2007), "*Improvement of Intragranular and Intergranular Pinning in MgB_2 Superconductors by Mechanical Alloying with AlB_2-Type Compounds*". Unpublished post-doctoral dissertation, University of São Paulo, Lorena, Brasil.

[9] Buzea, C., & Yamashita, T.: (2001), "Review of the superconducting properties MgB_2". *Supercond. Sci. Technol.*, *14*, 115-146.

[10] Hinks, D. G., Claus, H., & Jorgensen, J. D.: (2001), "The complex nature of superconductivity in MgB_2 as revealed by the reduced total isotope effect". *Nature,* 411**,** 457.

[11] Bud'ko, S. L., Lapertot, G., Petrovic, C., Cunningham, C. E., Anderson, N. & Canfield, P. C.: (2001), "Boron isotope effect in superconducting MgB_2". *Phys. Rev. Lett.,* 86, 1877.

[12] Bud'ko, S. L., Kogan, V. G., & Canfield, P. C.: (2001), "Determination of superconducting anisotropy from magnetization data on random powders as applied to $LuNi_2B_2C$, YNi_2B_2C and MgB_2". *Preprint cond-mat/*0106577.

[13] Grant, P.: (2001), "Rehersals for prime time". *Nature,* 411**,** 532.

[14] Kortus, J., Mazin, I. I., Belashchenko, K. D., Antropov, V. P., & Boyer, L. L.: (2006), "Superconductivity of Metallic Boron in MgB_2". *Condense Matter/ 0101446 v2*.

[15] Rowell, J. M.: (2003), "The widely variable resistivity of MgB_2 samples". *Supercond Sci Technol.,* 16, R17-R27.

[16] Canfield, P. C., Finnemore, D. K., Bud'ko, S. L., Ostenson, J. E., Lapertot, G., Cunningham C. E., & Petrovic, C.: (2001), "Superconductivity in dense MgB_2 wires". *Phys. Rev. Lett.*, 86 (11), 2423-2426.

[17] Cimberle, M. R., Novak, M., Manfrinetti, P., & Palenzona, A.: (2002), "Magnetic characterization of sintered MgB_2 samples: effect of the substitution or doping with Li, Al and Si". *Supercond. Sci. Technol.,* 15, 43-47.

[18] Kazakov, S. M., Angst, M., Karpinski, J., Fita, I. M., & Puzniak, R.: (2001), "Substitution effect of Zn and Cu in MgB_2 on T_c and structure". *Solid State Communications*, 119, 1-5.

[19] Moritomo, Y., & Xu, S.: (2001), "Effects of transition metal doping in MgB_2 superconductor". *Preprint cond-mat/*0104568.

[20] Takenobu, T., Itoh, T., Chi, D. H., Prassides, K., & Iwasa, Y.: (2001), "Intralayer carbon substitution in the MgB_2 superconductor". *Phys. Rev. B,* 64 (13), 134513.

[21] Li, J. Q., Li, L., Liu, F. M., Dong, C., Xiang, J. Y., & Zhao, Z. X.: (2001), "Superconductivity and aluminum ordering in $Mg_{1-x}Al_xB_2$". *Preprint cond-mat/*0104320.

[22] Toulemonde, P., Musolino, N., Suo, H. L., & Flukiger, R.: (2002), "Superconductivity in high-pressure synthesized pure and doped MgB_2 compounds". *Journal of superconductivity,* 15 (6), 613-619 .

[23] Li, W. X., Li, Y., Zhu, M. Y., Chen, R. H., Dou, S. X., Qin, M. J., Xu, X., & Yao, P.: (2007), "Effect of magnetic field processing on the microstructure of micronsize Zn doped MgB_2". *Physica C: Superconductivity,* 460–462, 310–311.

[24] Mehl, M. J., Papaconstantopoulos, D. A., & Singh, D. J.: (2008), "Effects of C, Cu and Be Substitutions in Superconducting MgB_2". *Phys. Rev. B,* 64 (14), 140509.

[25] Awana, V. P. S., Vajpayee, A., Mudgel, M., Rawat, R., Acharya, S., Kishan, H., Takayama-Muromachi, E., Narlikar, A.V., & Felner, I.: (2007), "Role of Carbon in Enhancing the Performance of MgB_2 Superconductor". *Physica. C. Superconductivity,* 467, 67-72.

[26] Senkowicz, B. J., Mungall, R. J., Zhu, Y., Jiang, J., Voyles, P. M., Hellstrom, E. E., & Larbalestier, D. C.: (2008), "Nanoscale grains, high irreversibility field, and large critical current density as a function of high energy ball milling time in C-doped magnesium diboride". *Supercond. Sci. Technol*., 21, 035009.

[27] Dou, S. X., Scherbakova, O., Yeoh, W. K., Kim, J. H., Soltanian, S., Wang, X. L., Senatore, C., Fulkiger, R., Dhalle, M., Husnjak, O., & Babic, E.: (2007), "Mechanism of Enhancement in Electromagnetic Properties of MgB_2 by Nano SiC Doping". *Phys. Rev. Lett.*, 98 (9)**,** 097002.

[28] Dou, S. X., Yeoh, W. K., Shcherbakova, O., Wexler, D., Zhong, Y. L., Ren, M., Munroe, P., Chen, S. K., Tan, K. S., Glowacki, B. A., & MacManus-Driscoll, J. L.: (2006), "Alignment of Carbon Nanotube Additives for Improved Performance of Magnesium Diboride Superconductors". *Adv. Mater.* 18, 758

[29] Cheng, C. H., Yang, Y., Munroe, P., & Zhao, Y.: (2007), "Comparison between nano-diamond and carbon nanotube doping effects on critical current density and flux pinning in MgB_2". *Superconductor Science and Technology,* 20 (3), 296-301.

[30] Vajpayee, A., Huhtinen, H., Awana, V. P. S., Gupta, A., Rawat, R., Lalla, N. P., Kishan, H., Laiho R., Felner, I., & Narlikar, A.V.: (2007), "The effect of nano-diamond additives on the enhancement of critical current density and related performance of bulk MgB_2". *Superconductor Science and Technology* 20 (9), S155.

[31] Ribeiro, R. A., Bud'ko, S.L., Petrovic, C., & Canfield, P.C.: (2003), "Effects of boron purity, Mg stoichiometry and carbon substitution on properties of polycrystalline MgB_2". *Physica C,* 385, 16–23.

[32] Senkowicz, B. J., Pérez Moyet, R., Mungall, R. J., Hedstrom, J., Uwakweh, O. N. C., Hellstrom, E. E., & Larbalestier, D. C.: (2006), "Atmospheric conditions and their effect on ball-milled magnesium diboride". *Supercond. Sci. Technol.,* 19, 1173-1177.

[33] Karpinski, J., Zhigadlo, N.D., Katrych, S., Puzniak, R., Rogacki, K., & Gonnelli, R.: (2007), "Single crystals of MgB_2: Synthesis, substitutions and properties". *Physica C,* 456, 3–13.

[34] Senkowicz, B. J.: (2007), "*Optimizing Critical Current Density through Composition and Microstructure in Mechanically Alloyed Magnesium Diboride*". Unpublished doctoral dissertation, University of Wisconsin, Madison.

[35] Bhatia, M., Sumption, M. D., Collings, E. W., & Dregia, S.: (2005), "Increases in the Irreversibility Field and the Upper Critical Field of Bulk MgB_2 by ZrB_2 Addition". *Applied Physics Letters,* 87 (4), 042505.

[36] Pérez Moyet, R.: (2008), "*Study of properties enhancement of Magnesium Diboride (MgB_2) by TaB_2 doping via High Energy Ball Milling*". Unpublished master's thesis, University of Puerto Rico, Mayaguez.

[37] Schaffer, J. P., Saxena, A., Antolovich, S. D., Sanders Jr, T. H., & Warner, S. B.: (1999), "*The Science and Design of Engineering Materials* (2nd ed.)". Boston: McGraw-Hill.

[38] Schultz, L.: (1988), "Formation of amorphous metals by mechanical alloying". *Materials Science and Engineering*, 97, 15-23.

[39] Fan, Z. Y., Hinks, D. G., Newman, N., & Rowell, J. M.: (2001), "Experimental study of MgB_2 decomposition". *Applied Physics Letters*, 79 (1), 16, 87.

[40] Rowell, J. M., Xu, S. Y., Zeng, X. H., Pogrebnyakov, A. V., Li, Q., Xi, X. X., Redwing, J. M., Tian, W., & Pan, X.: (2003), "Critical current density and resistivity of MgB_2 films". *Applied Physics Letters,* 83 (1)**,** 102.

[41] Eisterer, M., Emhofer, J., Sorta, S., Zehetmayer, M., & Weber, H. W.: (2009), "Connectivity and Critical Currents in Polycrystalline MgB_2". *Supercond. Sci. Technol.,* 22, 034016.

[42] Serquis, A., Zhu, Y. T., Peterson, E. J., Coulter, J. Y., Peterson, D. E., & Mueller, F. M.: (2001), "Effect of lattice strain and defects on the superconductivity of MgB_2". *Applied Physics Letters*, 79 (26), 4399.

[43] Qian, Z., Yongchang, L., Qingzhi, S., Zongqing, M., & Zhiming, G.: (2009), "Characteristic and synthesis mechanism of MgB_2 nanoparticles in solid-state reactive sintering". *Journal of Alloys and Compounds,* 470 (1-2), 443–447.

[44] Zhu, Y., Wu, L., Volkov, V., Li, Q., Gu, G., Moodenbaugh, A. R., Malac, M., Suenaga, M., & Tranquada, J.: (2001), "Microstructure and structural defects in MgB_2 superconductor". *Physica C*, 356 (4), 239-253.

[45] Gasparov, V. A., Sidorov, N. S., Zever'kova, I. I., & Kulakov, M. P.: (2001), "Electron transport in diborides: Observation of superconductivity in ZrB_2". *J. Exp. Theor. Phys. Lett.*, 73 (10), 532-535.

[46] Kaczorowski, D., Zaleski, A. J., Zogal, O. J., & Klamut, J.: (2001), "Incipient superconductivity in TaB_2". *Cond-mat/*0103571.

[47] Leyarovska, L., & Leyarovski, E.: (1979), "A search for superconductivity below 1 K in transition metal borides". *J. Less-Common Met.*, 67, 249 -255.

[48] Kotegawa, H., Ishida, K., Kitaoka, Y., Muranaka, T., Takagiwa, H., & Akimitsu, J.: (2005), "Evidence for strong-coupling s-wave superconductivity in MgB_2: ^{11}B-NMR study of MgB_2 and the related materials". *Physica C: Superconductivity,* 378-381 (1), 25-32.

[49] Schriber, J. E., Overmeyer, D. L., Morosin, B., Venturini, E. L., Baughman, R., Emin, D., Klesnar, H., & Aselage, T.: (1992), "Pressure dependence of the superconducting transition temperature in single-crystal NbB_x (x near 2) with T_c = 9.4 K". *Phys. Rev. B Condensed Matter,* 45 (18), 10787-10788.

[50] Hulm, J. K., & Mathias, B. T.: (1951), "New Superconducting Borides and Nitrides". *Phys. Rev.,* 82 (2), 273-274.

[51] Zeigler, W. T., & Young R. A.: (1953), "Studies of Compounds for Superconductivity". *Phys. Rev.*, 90, 115-119.

[52] Mudgela, M., Awana, V. P. S., Bhalla, G. L., & Kishan, H.: (2008), "Superconductivity of non-stoichiometric intermetallic compound NbB_2". *Solid State Communications,* 147 (11-12), 439-442.

[53] Rogacki, K., Oganisian, K., Sulkowski, C., Zhigadlo, N., Katrych, S., & Karpinski, J.: (2008), "Transport properties of MgB_2 single crystals doped with electrons and holes". *Journal of Physics and Chemistry of Solids*, 69 (12), 3202– 3204.

[54] Serebryakova, T. I., Ponomarenko, V. A., Karasev, A. I., Shemanin, V. I., & Marek, É. V.: (1980), "Magnesium diboride and its application in synthesis reactions of cubic boron nitride". *Powder Metallurgy and Metal Ceramics*, 10 (11), 791-792.

[55] Zhang, H., Zhao, J., & Shi, L.: (2005), "The charge transfer induced by Cr doping in MgB_2". *Physica C*, 424, 79–84.

[56] Matsumoto, A., Kumakura, H., Kitaguchi, H., Senkowicz, B. J., Jewell, M. C., Hellstrom, E. E., Zhu, Y., Voyles, P. M., & Larbalestier, D. C.: (2006), "Evaluation of connectivity, flux pinning, and upper critical field contributions to the critical current density of bulk pure and SiC-alloyed MgB_2". *Appl. Phys. Lett.,* 89**,** 132508.

[57] Hirsch, J.E.: (2001), "Hole Superconductivity in MgB_2: a high T_c cuprate without Cu". *Phys. Lett. A*, 282 (6), 392-398.

[58] Gurevich, A.: (2003), "Enhancement of the upper critical field by nonmagnetic impurities in dirty two-gap superconductors". *Physical Review B,* 67, 184515.

[59] Gurevich, A.: (2007), "Limits of the upper critical field in dirty two-gap superconductors". *Physica C: Superconductivity,* 456, 160.

[60] Ibach, H. & Luth, H.: (1995), "*Solid-State Physics* (2nd ed.)". Aachen, Germany: Springer-Verlag.

[61] Evetts, J.: (1992), "*Concise Encyclopedia of Magnetic and Superconducting Materials*". Oxford: Elsevier Publishers.

[62] Gurevich, A.: (2003), "Lectures in superconductivity given to students at University of Wisconsin – Madison".

[63] Bean, C. P.: (1962), "Magnetization of hard superconductors". *Phys. Rev. Lett.,* 8, 250-253.
[64] Awana, V. P. S., Vajpayee, A., Mudgel, M., & Kishan, H.: (2008), "Physical Property Characterization of Bulk MgB_2 Superconductor". *The European physical journal. B, Condensed matter physics*, 62 (3), 281-294.